Investigation of Robustness and Dynamic Behaviour of G1/S Checkpoint/DNA-damage Signal Transduction Pathway based on Mathematical Modelling and a Novel Neural Network Approach

---

A thesis
submitted in partial fulfilment
of the requirements for the Degree of
Doctor of Philosophy
in Computational Systems Biology

at
Lincoln University
by
Hong Ling

Lincoln University
2011

Abstract of a thesis submitted in partial fulfilment of the requirements for the Degree of Doctor of Philosophy

Investigation of Robustness and Dynamic Behaviour of G1/S Checkpoint/DNA-damage Signal Transduction Pathway based on Mathematical Modelling and a Novel Neural Network Approach

by

Hong Ling

The control of cell cycle checkpoints in cell cycle regulation is an extremely important function in living organisms. Mutation of the checkpoint regulators can cause gene or chromosome instability, which eventually results in different types of human cancers or cell apoptosis (death). A critical task in biological and medical research is to gain a thorough understanding of the mechanisms and dynamics of checkpoints in cell cycle regulation. In this thesis, a combined approach of mathematical modelling, computational simulations, analytical techniques and an artificial neural network (ANN) has been used to obtain deeper insights into the robustness and dynamic behaviour of the G1/S transition, as well as the DNA-damage signal transduction pathway and the p53-Mdm2 oscillation systems.

The first part of this thesis focuses on mathematically representing the cellular processes involved in detecting DNA-damage in cells, and their repair mechanisms, during cell division. This study uses a novel mathematical model of the G1/S transition that involves the DNA-damage signal transduction pathway, as published in 2008 by Iwamoto et al. [2008]. We develop a new analytical approach which includes: a choice of biomarkers (peak time of E2F and CycE), local and global sensitivity analysis, Type II error and mathematical definitions of biological robustness, to investigate the dynamic behaviour and robustness of biomarkers in the G1/S checkpoint in response to various levels of parameter perturbations and different DNA-damage intensities. More specifically, we concentrate on investigating the probability of accurately distinguishing healthy cells from defective cells in the G1/S transition. The results revealed from the model simulation, in terms of percentages of damaged cells passing

as healthy cells, were in good agreement with very recent experimental findings and observations.

The mathematical simulation outcomes from the first part, with corroboration from the phenomenon that the damaged cells are caught not in the pre-tumor stage but in the pre-malignant tissue where a non-invasive tumour is formed through activation of cellular senescence (another form of cell death), gives us the inspiration to develop new research questions. In the second part of this thesis, we are interested in whether the proposed G1/S model can highlight cellular senescence and so formulated scenarios, based on currently established biology, for lowering the threshold for senescence to enable cells to catch damaged cells before they reach the pre-malignant stage and evaluate the model's efficacy and outcome in this respect. Our analysis showed that cellular senescence can be highlighted through investigating the probability of DNA-damaged cells passing the G1/S checkpoint while lowering the critical trigger – CDK2 (Cyclin dependent kinase 2). We then analysed the relationship between CDK2 and its corresponding CKIs (CDK inhibitory proteins) in order to find other effective ways to bring forward cellular senescence. Finally, we validated the robustness of CDK2 for lowering the bar for cellular senescence.

The final part of the thesis introduces a novel ANN approach for modelling regulatory pathways. The developed ANN model is a new recurrent neural network which exactly represented the interactions among molecules in a pathway and its internal parameters are the corresponding kinetic parameters. Importantly, the proposed method solves the perennial problem of parameter estimation in differential equation based models by simply evolving the parameter values iteratively based on data. We applied the ANN model to simulate the p53-Mdm2 oscillation system with negative feedback and investigate the robustness of this system. Results from the ANN and corresponding ordinary differential equation based models published in 2006 by Geva-Zatorsky [2006] were then compared. By means of simulations, we showed that the proposed network can successfully represent the behaviour of the p53-Mdm2 oscillation system and solve the parameter estimation problem with 100% accuracy. Furthermore, we also investigated the robustness of the p53-Mdm2 system using the trained network, in the presence of various levels of parameter perturbation, to gain a greater understanding of the inner workings of the p53-Mdm2 system and the results revealed robustness and stability of the system and sensitivity to parameters.

In summary, the success of this research demonstrated the value of mathematical models and artificial neural networks for interpreting experimental observations, gaining novel insights into the dynamic behaviour of the G1/S checkpoint integrating the DNA-damage signal transduction pathway and the p53-Mdm2 oscillation system. In particular, the demonstration of the value of neural networks for estimating unknown kinetic parameters from data is a significant contribution of the thesis along with the analysis of the developed neural networks to investigate the robustness of the studied system. Furthermore, the thesis extended the mathematical model to elucidate a possible way, through understanding cellular senescence, for developing an effective cancer treatment.

Keywords: Artifical neural network, biomarkers, cell cycle, cell cycle checkpoints, cell cycle regulation, cell division, chemical kinetic equations, cellular senescence, DNA-damage signal transduction pathway, G1/S checkpoint pathway, nonlinear ordinary differential equations, p53-Mdm2 oscillation system, parameter sensitivity analysis, recurrent neural networks, biological robustness, Type II error

Acknowledgements

First and foremost, I must acknowledge and express my heartfelt thanks to my supervisors, Associate Professor Sandhya Samarasinghe and Professor Don Kulasiri, for their encouragement, support and guidance in all aspects of my research. They guided me not only in carrying out this research, but also in expanding my abilities and horizons that helped me become a mature and independent researcher.

Prof. Kulasiri's C-fACS (Centre for Advanced Computational Solutions) team is full of wonderful people who helped me in different ways. In particular, I would like to thank Zhongkun Zhou for his friendship when I began my graduate study and also Yao He for his continued sharing of ideas and discussions as well as his encouragement when I was in trouble. I have been fortunate to have worked with all of you.

I would like to sincerely thank Caitriona Cameron for her workshops and useful advice in improving my English writing skills significantly and also Christine Maauga for improving my English speaking skills. Sincere thanks to Mark Anderson and Yanbo Deng for fixing my computer and network problems with endless patience.

I would like to express my appreciation to Lincoln University for providing the generous Lincoln University Doctoral Scholarship during my three years of study.

I would also like to acknowledge my aunt and uncle for their encouragement and support, especially to my aunt, Lorna Xiaole Liu, who plays a very significant role in my education and my life.

Finally, I sincerely thank my parents for their constant love, dedication and encouragement throughout my study and life. And special thanks to my husband, Hao Li, for his never-ending love, understanding and inspiration that kept me going all these years.

Table of Contents

List of Tables

List of Figures

Abbreviations

P53-binding protein 1 (53BP1)
Artificial Neural Networks (ANNs)
Anaphase promoting complex/cyclosome (APC/C)
Ataxia-telangiectasia mutated (ATM)
Ataxia-telangiectasia and rad3-related (ATR)
Breast cancer protein 1 (BRCA1)
Budding uninhibited in benzimidazole (Bub)
Cyclin (Cyc)
Cyclin-dependent kinase (CDK)
CDK inhibitory protein (CKI)
DNA-damage signal (DDS)
Deoxyribonucleic acid (DNA)
Double-stranded breaks (DSBs)
E2 promoting binding factor (E2F)
Global sensitivity analysis (GSA)
Hydroxyurea (HU)
Ratio of half-life and mean period (HoMP)
Local sensitivity analysis (LSA)
Mediator of checkpoint signalling 1 (MDC1)
Mitosis (M)
Mitotic arrest defective (Mad)
Mitotic checkpoint complex (MCC)
MRE11-RAD50-NBS1 (MRN)
Ordinary differential equations (ODEs)
Peak time (PT)
Phosphoinosititide 3-kinase related kinases (PIKKs)
Probability (β)
Quiescence (G0)
Rad9, Rad1 and Hus1(9-1-1)
Receptor associated protein 80 (RAP80)
Recurrent Neural Networks (RNNs)
Retinoblastoma (Rb)
Replication factor (RPA)
Replication factor C (RFC)
Standard set of kinetic parameters (SKP)
Single strand DNA (ssDNA)
Synthesis (S)
Ubiquitininteraction motifs (UIM)

Chapter 1: Introduction

1.1 Systems Biology

Systems biology is an interdisciplinary field concerned with a system-level understanding of biological processes [Aderem, 2005; Ge et al., 2003, Heath and Kavraki, 2009; Ideker et al., 2001; Kitano, 2002; Oltvai and Barabasi, 2002]. The field is found upon taking an integrative approach that combines mathematical modelling and extensive computational analysis with experimental techniques to understand the functioning of complex biological systems as a whole instead of the individual components. For instance, systems biology offers an opportunity to quantitatively understand the characteristics of molecular (genetic, metabolic and signalling) pathways by investigating the inter-relationships (organization/structure) and inter-actions (dynamics/behaviour) of genes, enzymes, proteins and metabolites [Kitano, 2002; Wolkenhauer, 2001].

The idea of applying systems theory to biological sciences started as early as the 1940s with the introduction of cybernetics, which focuses on the analysis of control and communication in animals and machines [Trewavas, 2006; Wiener, 1948]. Since then, system-level understanding of biological systems has become a recurrent theme in biological science. For example, Ludwig von Bertalanffy [1950] proposed general and organismal systems theory in an attempt to establish a general theory of systems, and Mihajlo Mesarovic [1968] developed further ideas for combining systems theory and biological science. However, most work before the 20th century only described and analyzed biological systems at the physiological level mainly due to limitations of knowledge and theories in molecular biology. Remarkable progress in molecular biology[1], particularly in genome sequencing and high-throughput measurement techniques, makes it possible to collect comprehensive data sets on system performance and gain more useful information on the underlying molecules. A unique feature of modern systems biology is that it is distinguished from the previous attempts in that it connects system-level theory to molecular-level knowledge. There are three main issues within systems biology: (1) to generate quantitative high-throughput measurements for

[1] Molecular biology is the study of biology at a molecular level. This field focuses on investigations of macromolecules and the macromolecular mechanisms involved in life processes, such as structural and functional genomics, the structure and function of proteins and nucleic acids.

collecting comprehensive data sets on system performance and extracting the information, (2) to understand the structures of the systems and the interactions among molecules, and (3) to develop mathematical models based on the experimental data collected and an understanding of system structures.

Robustness is one of the fundamental and ubiquitously observed characteristics of biological systems. Investigating the mechanisms and principles underlying the robustness of biological systems plays an essential part in gaining a deeper understanding of biological complexity at the system level. In general, robustness is defined as a property that allows a system to maintain its functionality or characteristic behaviour in the face of internal perturbations (such as mutations), external perturbations (such as environmental variations) as well as other uncertainties (such as stochastic fluctuations in the abundance of the chemical species involved and their corresponding biochemical reactions) [Kitano et al., 2004, 2004a, b; Kitano, 2007; Kitano and Oda, 2006; Stelling et al., 2004]. More precisely, robustness allows a system to change its structure, components and states in response to perturbations or conditions of uncertainty, while the specific functionalities of the system remain unchanged. Therefore, robustness is a broader concept than stability and homeostasis[2], and robustness in subsystems is essential for homeostasis of the whole system [Stelling et al., 2004]. The measurement of robustness of biological systems based on mathematical models focuses on the investigation of a system's characteristics that maintain one or more of its functions (the model's output) under the effects of perturbations in the kinetic parameters involved as well as the effects of molecular noise on the cellular behaviours involved. Therefore, this underlines that the analysis of robustness in complex biological systems mainly involves the definition of a system, its function and the related perturbations.

1.2 Mathematical Modelling in Cell Cycle Regulation

The cell cycle is the process that achieves cell growth, DNA replication, chromosome segregation and cell division in mammalian cells. The purpose of cell cycle regulation is to make two daughter cells that have exactly the same characteristics as their parents [Stein and Pardee, 2004]. Cell cycle regulation mediates the proliferation, differentiation, apoptosis (cell death) and other important intra-cellular processes through a complex set of distinct molecular

[2] Homeostasis is one of the most remarkable properties of a system that regulates its internal environment and maintains the system in a stable, constant condition.

networks associated with cell cycle checkpoints that are regarded as surveillance and quality control mechanisms in the cell cycle [Tessema et al., 2004]. The main responsibilities of the checkpoints are to ensure faithful genome DNA replication as well as to protect, conserve and maintain the fidelity of the genome for cell growth through the control of a series of biochemical reactions among multiple proteins, genes and their mRNAs [Kohn, 1998]. Therefore, the control of checkpoints in cell cycle regulation is an extremely important function in living organisms. For example, cancer can be regarded as a product of a malfunction in cell cycle regulation, such that the defective and abnormal cells malignantly proliferate promoting the accumulation of mutations in the human body. Mutations usually happen in proto-oncogenes and tumour suppressor-genes that are very important in controlling the checkpoints in cell cycle regulation; and there is a strong relationship between cell cycle regulation and human cancer [Dickson and Schwartz, 2009; Enders et al., 2010; Foster, 2008; Giordano and Galderisi, 2010; Hartwell and Kastan, 1994; Lapenna and Giordano, 2009; Malumbres and Barbacid, 2009; Molinari, 2000; Poehlman and Roessner, 2010; Vermeulen et al., 2003].

Because cancer is strongly associated with loss of control over the cell cycle regulation system, investigation of the mechanisms and functions of cell cycle regulation has become the critical focus of biological and medical research during the past decades [Hanahanand and Weinberg, 2000]. More importantly, a detailed understanding of the mechanisms and functions underlying checkpoint pathways, tumour growth, DNA damage repair, intercellular signalling and other processes involved in the cell cycle regulation plays a significant role in the diagnosis, treatment and prognosis of human cancer. However, the following three aspects make the cell cycle regulatory system complicated: (1) there are a large number of enzymes and proteins involved in cell cycles regulation; (2) there are a large number of interactions between enzymes and proteins; and (3) there are many different ways to promote the interaction between enzymes and proteins, performing the stimulatory, inhibitory or other modulating functions. The enormous complexity of cell cycle regulation makes it difficult to study and analyze the characteristics of roles and functions of genes, enzymes and proteins using only *in vitro* experiments. Thus, the systems biology approach, including both experimental and computational components working in conjunction, would help us to understand the complex biological regulatory systems.

The mathematical principles for cell cycle regulation models are applied to one of two biochemical domains: gene regulatory networks and protein-protein interaction networks. With regard to gene regulatory networks, the models mainly focus on the interactions between genes and proteins on a genetic level. The dominant phenomenon in gene regulatory networks is molecular binding, polymerization and degradation. In terms of the protein-protein networks, the models concentrate on the interaction between proteins and enzymatic reactions represented in the protein-protein interaction or regulatory network. In fact, cell cycle regulation mainly depends on the interactions of proteins and enzymes and their modification through their phosphorylation and dephosphorylation by kinases and phosphates, respectively. Therefore, most mathematical models for cell cycle regulation are based on protein-protein networks. For the successful application of mathematical modelling to cell cycle regulation, the following questions will be answered: what is the system in question and what is the system's environment? How can we model the system, its structure and inputs and which mathematical techniques should be used for the model? What do we expect to observe and what insights do we expect from the application of the model? Which type of methods should we use for the analysis and validation of the model? How can we most effectively obtain experimental evidence to support new hypotheses?

The mathematical models of cell cycle regulation heavily use nonlinear ordinary differential equations (ODEs) which describe the reaction rates of interactions between molecular species in the system according to chemical kinetic theory [Fuss et al., 2005; Heath, 2009; Tyson et al., 1996; Tyson et al. 2002]. In general, ODEs are mathematical equations which represent changes in concentration of all molecular species in cell cycle regulation over time. The ODE models of cell cycle regulation were first developed for frog eggs by Borisuk [1998], and then expanded to budding yeast [Chen et al., 2000], and finally generalized to eukaryotes in 2006 [Csikasz-Nagy, 2006]. The advantages of ODEs are: (i) ODEs have deep mathematical roots that are used to analyze and understand a system and its properties, particularly system robustness, and (ii) ODEs can be solved by using many software packages, such as Matlab® and Mathematica®. However, the difficulties associated with ODEs are: (i) the lack of experimentally determined parameters reduces the accuracy of the ODE models, and (ii) ODEs ignore the randomness and noise found in biological systems, which may play an important role in understanding and investigating their function [Blake et al., 2003; Raser and O'Shea, 2004].

1.3 Motivation for the Study

This thesis starts with a biological-level understanding of the cell cycle and cell cycle regulation. Most previous molecular cell biology researchers have focused on cell growth and proliferation, their regulatory mechanisms and their response to certain intracellular or extracellular conditions, which provided important information for the diagnosis, treatment and prognosis of cancer. Due to the complexity of cell cycle regulation, as discussed in section 1.2, mathematical modelling and computational simulations are developed to gain a detailed understanding of the mechanisms underlying cell cycle and related processes. However, there is still a need for fundamental knowledge from both molecular cell biology and systems biology research about cell cycle regulation. We aim to outline the essential information available through asking three questions:

(a) How does the complex network of regulatory enzymes and cellular components control cell cycle regulation, particularly cell cycle checkpoints?

(b) How are mathematical models developed to investigate the dynamic behaviour and biological robustness of cell cycle checkpoints?

(c) What existing models of cell cycle checkpoints have been used to study their mechanisms and functions?

We address these questions by reviewing the existing literature using the keywords "cell cycle regulation, cell cycle checkpoints, mathematical models, systems biology"; details relevant to this are shown in Chapter 2.

According to a review of the literature about cell cycle checkpoints, we find that the G1/S checkpoint takes more responsibility for the disruption of the stability of cell cycle than other checkpoints [Iwamoto et al., 2008; Malumbres and Carnero, 2003]. Therefore, we choose to investigate the G1/S cell-cycle checkpoint pathway incorporating the DNA-damage signal transduction pathway in cell division.

The primary objective of this thesis is to mathematically represent cellular processes involved in detecting DNA-damage in cells during cell division, in particular, in the G1/S transition, to understand how cells respond to DNA-damage situations in order to shed light on the dynamic behaviour and biological robustness of the G1/S checkpoint.

This primary objective is accomplished by using a novel mathematical model of the G1/S checkpoint pathway integrating the DNA-damage signal transduction pathway which was published in 2008 by Iwamoto et al. [2008]. The original authors mainly focused on the influence of the change in value of the chemical species in the proposed model at a steady-state in response to changes in the value of individual kinetic parameters (more related information is presented in Chapter 3). We start our investigation by identifying the following three challenging questions:

(1) What are the major indicators for the proper function of the G1/S checkpoint pathway involving DNA-damage signal that are in a biologically meaningful manner?

(2) How does the model investigate the robustness and the behaviours of the G1/S checkpoint under parameter perturbations with or without DNA-damage?

To address the above two questions, we identify the peak times (PTs) of two key proteins (E2F and CycE) as *in silico* biomarkers, based on the currently established biological theory. Then, we introduce an analytical approach including parameter sensitivity analysis (local and global), Type II error and mathematical definitions of biological robustness to investigate the dynamic behaviour and the robustness of these two critical proteins in the G1/S checkpoint in the presence of various levels of parameter perturbations under different levels and different DNA-damage intensities. More specially, we are interested in analyzing the probability (β) of a DNA-damaged cell passing as a healthy cell in the G1/S transition. Work related to this is discussed in Chapter 4.

(3) Do the model simulation results qualitatively support the experimental findings and the biological theory?

We validate our simulation results, in terms of percentages of damaged cells that pass the G1/S checkpoint that agree very well with the good agreement with very recent experimental findings showing that a large number of damaged cells undergo proliferation without being caught at DNA-damage checkpoints [Collado and Serrano, 2010; Serrano, 2010]. Chapter 5 covers the simulation results obtained from the analytical approach developed. The work related to this principal objective has been published in Biosystems with the article entitled "Robustness of G1/S checkpoint pathways in cell cycle regulation based on probability of DNA-damaged cells passing as healthy cells" [Ling et al., 2010].

The second objective of this thesis is inspired by the mathematical simulation outcomes from the primary objective with the corroboration of the phenomenon that cellular senescence[3] (premature cell death), as played out, lies in the strategy used by cells to initially allow a considerable proportion of cells carrying oncogenes[4] to pass through the cell cycle, at any given time, as there are probably millions of cells that are oncogenically primed and catching all these initially would be an exhausting task for a cell [Collado and Serrano, 2010; Serrano, 2010].

The second objective of this thesis involves exploring and probing the model of the G1/S checkpoint pathway involving DNA-damage signal to further investigate how cancer prone cells can be identified. In particular, it is tested if the model can highlight how the senescence bar can be effectively lowered to catch cancer prone cells earlier than in the usual senescence.

This objective is achieved from a good understanding of cellular senescence to identify the critical factor (Cyclin-dependent kinase 2-CDK2 inhibition) in the G1/S checkpoint pathway that lowers the bar for triggering senescence in cancerous cells based on experimental findings, which helps us to formulate scenarios for the proposed model to highlight cellular senescence. We aim to provide valuable findings that biologists and clinicians may find useful to validate experimentally the actual efficacy of these targets for treating cancer. Given these observations, challenging questions are identified:

(4) How does the mathematical model highlight cellular senescence in response to a lowering of the critical point - CDK2 inhibition?

(5) Are there any other effective ways to bring forward cellular senescence through model analysis?

To address the above two questions，we calculate the values of β for a DNA-damaged cell passing a G1/S checkpoint using the same analytical approach and parameter set as our earlier study by reducing CDK2 levels for two DNA-damage situations. The model will highlight cellular senescence depending on whether β decreases with decreasing levels of CDK2 or not. We then interrogate the model to investigate the relationship between CDK2 and CDK

[3] Cellular senescence is considered to be an irreversible state of cell cycle arrest whereby a normal cell loses the ability to divide and promote cell proliferation.
[4] Oncogenes are genes that have the potential contribution to cause cancer. In general, oncogenes are mutations of normal cellular genes.

inhibitory proteins (CKIs) under different DNA-damage situations in search of alternative approaches to lowering the cellular senescence bar through these relationships by exploring the most effective means of bringing cellular senescence forward.

(6) How robust is cellular senescence triggered by lowering the bar through reduced CDK2?

We investigate the robustness of CDK2 on lowering the bar for cellular senescence through two different approaches: (i) analysing the values of β for different thresholds of PTs for the previously chosen two biomarkers under the given parameter perturbation regimes and under different DNA-damage situations in response to different reduced CDK2 levels, and (ii) analysing the robustness of CDK2 in triggering cellular senescence based on our mathematical definition of biological robustness. The details of both approaches for investigating the robustness are shown in the context of achieving the primary purpose of this thesis. The work related to this specific objective is presented in Chapter 6.

As mentioned in section 1.2, one weakness of the ODE models is parameter estimation, which plays a significant role in the accuracy of the models in representing real biological systems. This leads to the development of another purpose of this thesis.

The third objective of this thesis involves how an artificial neural network (ANN) technique is implemented to deal with the "parameter estimation" problem in the ODE models for biological systems and investigate the dynamic behaviour and robustness of the system based on the analytical results from the proposed ANN model.

This objective can be accomplished by using mathematical models of the p53-Mdm2 oscillation system, as proposed by Geva-Zatorsky et al. [2006], for developing the ANN models. The original ODE models have successfully captured the observed oscillations and variability in the p53-Mdm2 system in response to DNA damage caused by gamma irradiation. We start our study by answering the following three questions:

(7) How do we develop ANN models to represent the exact behaviour and interactions in the p53-Mdm2 oscillation system?

ANNs can be viewed as mathematical models to simulate natural and biological systems on the basis of mimicking the information processing methods in the human brain. Development

of an ANN model for the p53 system gives most attention to the following three factors: the number of neurons needed, the structure of the network and the learning algorithm.

(8) How do we validate the proposed ANN models with high levels of accuracy?

We use two different methods to validate the proposed ANN models: (i) compare the model parameters with previously reported parameter values, and (ii) compare the temporal behaviour of p53 and Mdm2 with that generated from ODE-based models.

(9) What is used as a measure to investigate the robustness of the p53-Mdm2 oscillation system in the presence of various levels of perturbations in the model parameters?

According to studies on investigating the robustness of circadian rhythms, the ratio of the half-life of the correlation divided by the mean period can be used as a measure of robustness of the oscillation system [Baras, 1997; Baras, et al., 1990; Gonze et al., 2002]. Thus, we used this approach to analyze the robustness of the p53-Mdm2 oscillation system in response to various model parameter perturbations. The details of this work are presented in Chapter 7.

1.4 Overview of the Chapters

This thesis comprises eight chapters.

In the current chapter, an introduction is provided to systems biology, cell cycle regulation and mathematical modelling of cell cycle regulations, and the motivation for the thesis.

Chapter two provides biological and mathematical background knowledge, ANN techniques as well as mathematical definition of robustness that are useful for later chapters. It also includes a detailed historic summary of the development of the mathematical modelling for the G1/S transition.

In Chapter three, a detailed background of the molecular components and interactions in the G1/S checkpoint pathway that integrates the DNA-damage signal transduction pathway is given, followed by a complete description of the proposed mathematical model for G1/S transition including the DNA-damage signal pathway, based on Iwamoto et al.'s [2008] model as well as the biochemical meaning of kinetic parameters, the initial conditions and the parameter values for the G1/S model.

In Chapter four, we define a new analytical approach to investigate robustness and dynamic behaviour of chemical species in G1/S transition in response to DNA-damage situations. This analytical approach (which includes local sensitivity analysis, global sensitivity analysis, Type II error and the mathematical definition of robustness) mainly focuses on the investigation of the dynamic response of a limited number of key proteins (biomarkers) in the G1/S checkpoint pathway in the presence of various levels of perturbations in the kinetic parameters under different DNA-damage conditions.

Chapter five presents the results and an analysis of the numerical simulations of the behaviour of the chosen biomarkers of the G1/S checkpoint pathway under various levels of parameter perturbations in response to different DNA-damage situations and draws relevant conclusions based on the revealed results from the *in silico* experiments.

In Chapter six, we use the proposed mathematical model of the G1/S checkpoint to highlight cellular senescence under DNA-damage situations and explore the potential possibility of lowering the bar for triggering cellular senescence in cells, for catching damage prone cells earlier than normal senescence, based on the model's analytical results. More importantly, we investigate the robustness of CDK2 in triggering cellular senescence.

In Chapter seven, the ANN technique is used to solve the parameter estimation problem in the ODE models of the p53-Mdm2 oscillation system. The trained ANNs are used to study and analyze the dynamic characteristics and robustness of the p53-Mdm2 oscillation system.

Finally, in Chapter eight, a retrospective look at the overall implications of this work, as well as the contribution of the thesis and direction for future research, is provided.

Chapter 2: Background and Literature Review

This chapter provides the necessary background information for the research. It covers the fundamental biological concepts and theories of cell cycles, cell division and cell cycle checkpoints, the primary mathematical concepts of modelling the cell cycle checkpoint pathway (for example, chemical kinetic theory and the Hill function), as well as a comprehensive review of the developed mathematical models of cell cycle regulation, particularly for modelling the mammalian G1/S cell cycle phase transition.

2.1 Overview

There is a very strong relationship between cell cycle checkpoints and human diseases, such as various cancers [Dickson and Schwartz, 2009; Enders et al., 2010; Foster, 2008; Giordano and Galderisi, 2010; Hartwell and Kastan, 1994; Lapenna and Giordano, 2009; Malumbres and Barbacid, 2009; Molinari, 2000; Poehlman and Roessner, 2010; Vermeulen et al., 2003]. The main function of checkpoints is the protection, conservation and maintenance of cell growth and development. However, mutation of these checkpoint regulators causes gene or chromosome instability as well as further losses of proliferation, which eventually cause diverse types of cancer or apoptosis. Furthermore, mutations of tumour suppressor genes controlling the cell cycle checkpoints cause oncogenic propagation resulting in the development of tumour cells [Morgan, 2007; Murray and Hunt, 1993; Petersen et al., 2010; Stein and Pardee, 2004]. As a result, it is necessary to have a thorough understanding of the whole cell cycle regulation system, which makes a significant contribution to the diagnosis, treatment and prognosis of human cancer. Moreover, there are some difficulties in studying and analyzing cell cycle regulation using real experiments, for example, in the analysis of complex interactions between various proteins and enzymes. Due to the limitations of experimental research on cell cycle regulation, more and more mathematical models have become powerful tools to analyze and understand the complex behaviour of cell cycle regulation [Fuss et al., 2005; Klipp and Liebermeister, 2006].

2.2 Biological Concepts

2.2.1 Cell Cycle and Cell Division

Before designing and developing a mathematical model, it is essential to answer this question: what is the logical formulation of a mathematical model for cell cycle regulation? Consequently, the current focus is to learn and understand some fundamental concepts and theories about cell cycle, cell division and cell cycle checkpoints. There are some excellent books on some of these topics: Murray and Hunt [1993] give an excellent introduction to cell cycle and its control; Stein and Pardee [2004] provide a wealth of information on cell cycle, growth control as well as their significant role in human cancer development, Pierce [2005] describes a wide panoramic view of genes, DNA and chromosomes, and Morgan [2007] provides a clear, concise and easily accessible guidebook with an in-depth description of all the essential aspects of cell cycle and cell division.

2.2.1.1 Cell Cycle

The cell cycle, which is also called cell-division cycle, means that a series of events; for instance, cell growth, DNA replication, chromosomes segregation and cell division, occur in human cells in order to replicate or duplicate themselves [Murray and Hunt, 1993; Stein and Pardee, 2004]. There are two fundamental parts in a cell cycle: interphase and mitosis. Interphase is the major part of the cell cycle. The functional characteristic of the interphase is to complete DNA replication and accumulate enough nutrients for mitosis, while the function of the mitotic phase is to divide a cell into two distinct daughter cells in order to finish the process of nuclear division (karyokinese) as well as cytoplasmic division (cytokinesis). Figure 2-1 shows an overview of the cell cycle.

The interphase consists of three steps: G1 phase, S phase and G2 phase, which indicates that the whole cell cycle has four distinct phases. After the mitotic phase, the daughter cells enter the interphase of a new cell cycle. This marks the mitotic phase as the signal for the end of the previous cell cycle and the beginning of the current cell cycle. The first phase of interphase is G1, which mainly synthesizes of various enzymes for DNA replication in the S phase. Then the cell enters the S phase (called DNA synthesis phase) the most important part of the cell cycle. The reason is that DNA synthesis happens in this phase. When DNA synthesis is

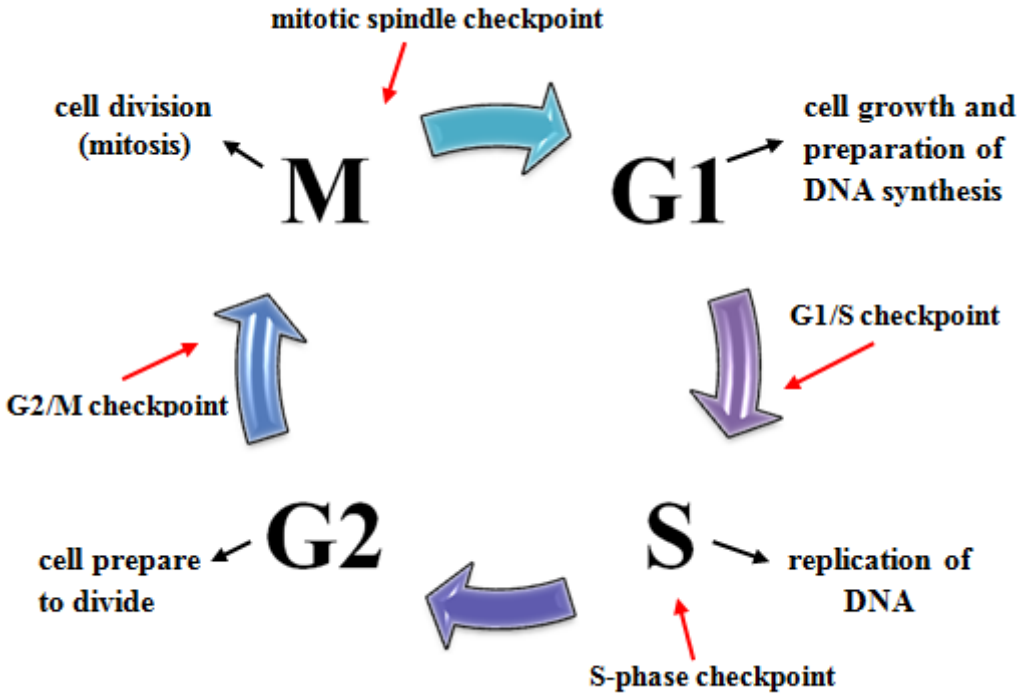

Figure 2-1 An overview of cell cycle. The cell cycle, or cell-division cycle, is the well-ordered sequence of events that occur in human cells for their division and replication. The events of the cell cycle include G1 phase (cell growth and preparation of DNA synthesis), S phase (precise replication of DNA), G2 phase (further cell growth and prepraration for cell division) and M phase (cell division- mitosis). There are multiple cell cycle checkpoints, which are localized in each phase of the cell cycle. The main responsibility of these checkpoints is to ensure the fidelity of cell division.

complete, each chromosome is replicated, which means that it has two sister chromatids. Furthermore, these two sister chromatids remain attached to each other through kinetochores. After the S phase, the cell enters the G2 phase, which prepares it for cell division. The remarkable change in the G2 phase is the organization of microtubules through the synthesis of many significant proteins. The aim of this is to prepare for mitosis. Finally, the cell enters the mitotic phase marking the end of the current cell cycle [Morgan, 2007; Murray and Hunt, 1993; Stein and Pardee, 2004].

2.2.1.2 Cell Division

Cell division is considered as the division of a parent cell into two daughter cells. In general, there are two different types of cell division: mitosis and meiosis [Freeman, 2002]. Mitosis is a process which separates the duplicated chromosomes of the parent cells into two identical daughter cells. This means that the two daughter cells have the same number of chromosomes as the parent cell and they can divide again. In meiosis, the daughter cells have only half the number of chromosomes so they cannot divide until fertilization. The focus of the following discussion is on the process of mitosis. There are four stages involved in the process of mitosis: prophase, metaphase, anaphase and telophase [Cooper, 2000; Pierce, 2005; Zimmerman and Ebrary, 2004]. A schematic depiction of the stages of mitosis is displayed in Figure 2-2.

The sign of mitosis entry is a period called prophase. During prophase, the chromatid becomes condensed in order to form chromosomes. Each chromosome has a pair of sister chromatids joined at the centromere. This means that the number of chromosomes is equal to the number of centromeres. The nuclear envelope then breaks down and the nucleolus disappears. The centrioles start to move to opposite poles of the cell and the mitotic spindles (which are also called microtubules) are formed by the protein fibres between them. The second stage of mitosis is called the metaphase. It contains two sub-stages: prometaphase and metaphase. In the early stage-prometaphase the spindle fibres attach to the chromosomes at the centromeres creating kinetochores. Meanwhile, some mitotic spindle microtubules form an attachment to the kinetochores to make a connection between the centromeres and the centrioles, and then the chromosomes begin to move, marking the progression to metaphase. During this phase, the chromosomes attached to microtubules align in the middle plane of the cell. The next stage of mitosis is anaphase stage for the separation of the sister chromatids. The centromeres are divided in order to create sister chromosomes instead of a pair of

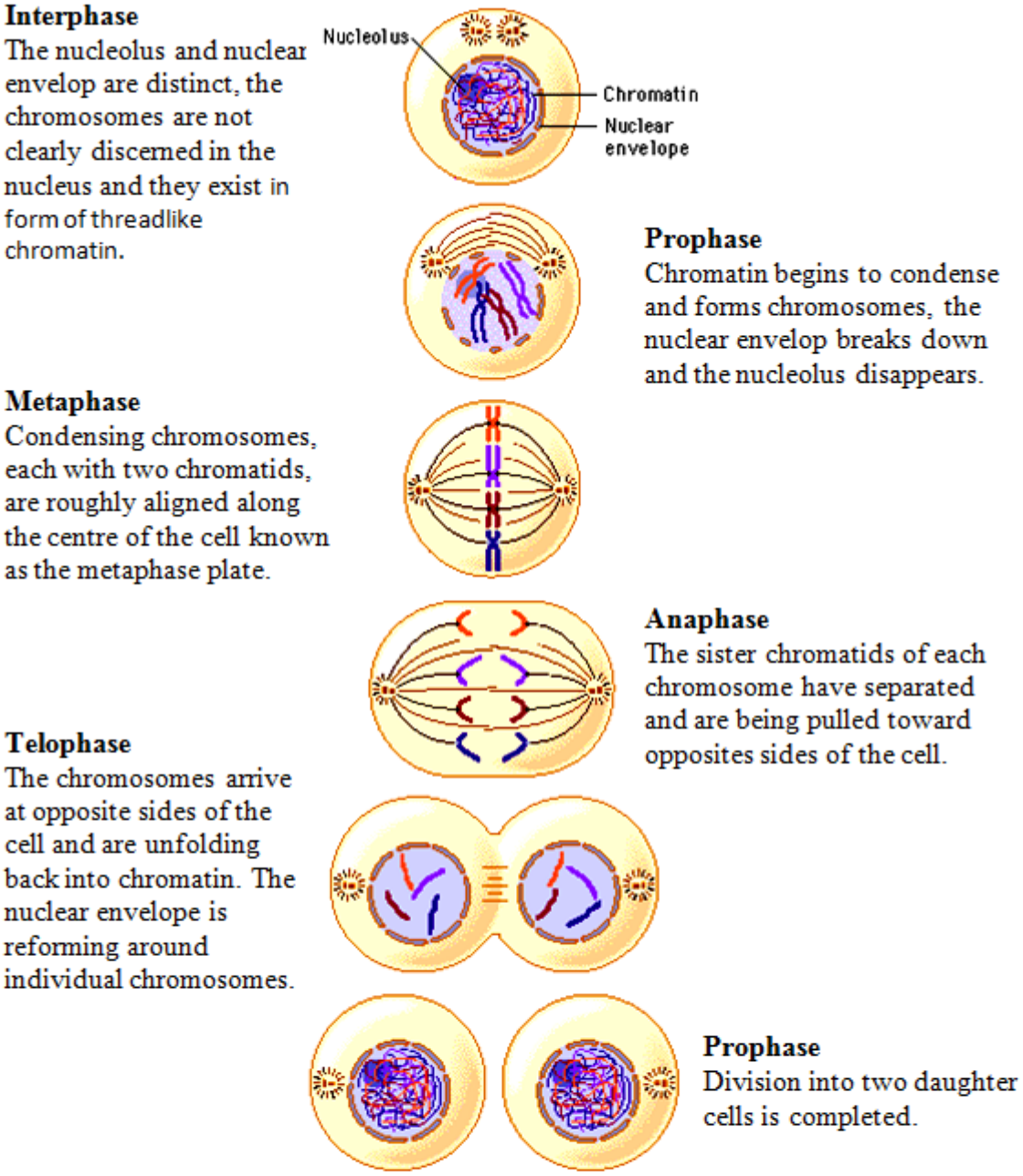

	A brief definition
Chromatin	Mass of genetic material composed of DNA and proteins that condense to form chromosomes
Chromatid	One of the two identical copies of a replicated chromosome
Centromere	A region on a chromosome that joins two sister chromatids
Centriole	A cylindrical structure that can be found near the cell nucleus

Figure 2-2 Schematic depiction of the stages of mitosis.

Source:http://www.maph49.galeon.com/mitosis/stages1.gif

attached sister chromatids. Furthermore, the created sister chromosomes are pulled apart by the spindle apparatus and move to opposite poles of the cell. The fourth stage, telophase, is entered when the chromosomes arrive at the opposite poles of the cell and the daughter nuclei form. After that, the nucleoli reappear inside the daughter nuclei, the new nuclear envelops forms around the daughter nuclei and the chromosomes decondense in the daughter cells and become invisible. In addition, the mitotic spindles disappear and cytokinesis starts, completing cell division. The main purpose of cytokinesis is the division of the cytoplasm through cleavage marking the completed separation of the daughter nuclei. Thus, one single cell has been divided into two daughter cells with the exact same genetic information as the parent cells. The created daughter cells will enter interphase for the beginning of the new cell cycle.

2.2.2 Cell Cycle Checkpoints

Cell cycle checkpoints are regarded as surveillance and quality control mechanisms in the cell cycle. They are localized in each phase of the cell cycle. Their purpose is to decide whether the cell can move into the next phase of the cell cycle based on an error-free completion of the previous phase in the cell cycle. As a result, the main responsibility of these checkpoints is to ensure faithful genome DNA replication as well as to protect, conserve and maintain the fidelity of the genome for the progeny cells [Giordano and Galderisi, 2010; Morgan, 2007; Nyberg et al., 2002; Stein and Pardee, 2004].

There are three main checkpoints in the cell cycle: the mitotic spindle checkpoint, the S phase replication checkpoint and the multifaceted DNA damage checkpoint. All three checkpoints have their own particular structural characteristics and functionalities in the cell cycle. The responsibility of the mitotic spindle checkpoint is to ensure that the chromosomes are segregated accurately at the mitotic plate in order to prevent instability of the chromosomes. The S phase replication checkpoint is to successfully achieve the faithful replication of DNA at the S plate. Furthermore, the multifaceted DNA damage checkpoint senses various information about DNA damage and arrest cell cycle progression and facilitate the DNA repair pathway. In fact, the multifaceted DNA damage checkpoint plays the most important role in ensuring the fidelity of cell division. According to cell cycle processes, there are three main DNA damage checkpoints: the G1/S checkpoint; the S phase checkpoint and the G2/M

checkpoint. The following sections present more detailed information about cell cycle checkpoints, particularly the DNA damage checkpoints.

2.2.2.1 Mitotic Spindle Checkpoint

The mitotic spindle checkpoint is a regulatory mechanism that ensures the proper alignment of chromosomes entering the anaphase stage and exiting the mitosis [Skibbens and Hieter, 1998; Stein and Pardee, 2004; Zacharie and Nasmyth, 1999]. The mitotic spindle checkpoint is composed of different types of proteins, such as, the MAD (mitotic arrest defective) and BUB (budding uninhibited in benzimidazole) families, and is also called the mitotic checkpoint complex (MCC) [Sudakin et al., 2001]. There are three significant duties for the MCC. First, the MCC is a sensor of misaligned chromosomes in the mitosis plate. Second, the MCC is a signal transducer which relays signals from the sensors. Third, the MCC is an inhibitor which must effectively monitor cell cycle progression according to the information relayed from the signal transducer. If the chromosomes are improperly attached to the mitotic spindle fibre (for instance, the mitotic spindle fibres only attach to one side of the centromere), the MCC has to block mitotic progression until there is accurate attachment between kinetochores and opposite spindle poles by the mitotic spindle fibres [Rieder et al., 1995].

Based on the above information, the MCC has the ability to control the progression of mitosis as well as exit from mitosis through regulating the activity of the anaphase by promoting complex/cyclosome (APC/C) [Harper et al., 2002; Zacharie and Nasmyth, 1999]. How does the spindle checkpoint inhibit these two mitotic aspects of the cell cycle? There are two important mitotic pathways regulated by the ubiquitin ligase APC/C: the mitotic metaphase-to-anaphase transition and the mitotic exit transition. In terms of the mitotic metaphase-to-anaphase transition, the responsibility of APC/C is to initialize the anaphase through the destruction of the securin protein PDS1 by CDC20 in order to inhibit the activity of the separin protein, ESP1. The reason is that ESP1 plays an essential role in promoting sister-chromatid separation and mitotic metaphase-to-anaphase transition. For the progression of mitosis to enter the new cell cycle, the target of APC/C is to degrade the complex of CyclinB (CycB) and cyclin-dependent kinase (CDK, i.e. CDC2/CDK1) through CDH1/HCT1 [Gardner and Burke, 2000; Musacchio and Hardwick, 2002].

2.2.2.2 The S-phase Replication Checkpoint

The S phase replication checkpoint plays an important role in monitoring the progression of a cell through the S-phase and ensuring the fidelity of DNA duplication. When the cell undergoes DNA replication stress, the main function of the replication checkpoint is to block DNA synthesis for the maintenance of the integrity of the existing replication fork as well as provide enough time for the rearrangement of the defective replication forks [Branzi and Foiani, 2007; Sogo et al., 2002]. In general, the activation of the replication checkpoint is regulated by hydroxyurea (HU), which is regarded as a ribonucleotide reductase inhibitor, which eventually results in the replication forks stalling due to a lack of nucleotide precursors. Furthermore, there are three main drownstream events in the cell cycle when the replication checkpoint is activated by HU: a) mitotic chromosome segregation would be delayed unless the chromosomal replication is accurately completed; b) stabilization of structural replication intermediaries is achieved through controlling the activation of the replication fork elongation, re-initiation and recombination. However, all these events may result in resolved intermediates and increased chromosomal instability; c) there is an induction in the expression of genes that makes a significant contribution to recovery, such as ribonucleotide reductase [Desany et al.,1998; Kelly and Brown, 2000; Stein and Pardee, 2004; Yarbro, 1992]. According to literature on the replication and DNA damage checkpoints, it can be seen that the replication checkpoints have common architectural features with the DNA damage checkpoint, such as the phosphoinositide 3-kinase related kinases (PIKKs) involved in the DNA damage response as well as in the replication checkpoint. Therefore, more details on the replication pathway will be discussed in the DNA damage checkpoint section.

2.2.2.3 Multifaceted DNA Damage Checkpoints

A multifaceted DNA damage checkpoint is used to recognize and respond to information on DNA damage and abnormal DNA structures through arresting cell cycle progression, and then facilitating the DNA repair pathway. During the cell cycle process, there are three main DNA damage checkpoints with their own function: the G1/S checkpoint, the S-phase checkpoint and the G2/M checkpoint. The G1/S checkpoint is used to detect DNA damage before the cell progresses into S-phase. The purpose of this is to delay entry into S for DNA damage repair and provide an accurate genome for the initiation of DNA replication. The S-phase checkpoint provides an opportunity to replicate a defect-free genome through repair mechanisms. Likewise, the G2/M checkpoint is used to detect damage of the newly

synthesized DNA before entry into mitosis, which ensures error-free chromosomal substrates for chromosome segregation.

The DNA damage checkpoint pathway involves three main components: DNA damage sensor, signal transducer and signal effector. In general, when DNA damage happens under various endogenous and exogenous factors, the damage can be recognized by the sensor proteins which initiate a biochemical cascade of activity. The DNA damage signal can then be amplified and propagated by transducer protein kinases from the sensor to the downstream control mechanism. Finally, the effector proteins, the downstream targets of the transducer protein kinases, are identified and regulated in order to transiently slow cells progression through the cell cycle. The purpose of this is to provide enough time for DNA damage repair and recovery and maintain genomic integrity and chromosome stability [Liu et al., 2006; Nyberg et al., 2002].

2.2.2.3.1 Sensing DNA Damage and Signal Transduction

The first step in the DNA damage checkpoint pathway is marked by the initiation of the activation of PIKKs like ATM (ataxia-telangiectasia mutated) and ATR (ataxia-telangiectasia and rad3-related). In general, ATM mainly responds to DNA double-stranded breaks (DSBs), the most important form of DNA damage. DSBs indicate that the base pair and the chromatin structure of two complementary strands of DNA is not strong enough to combine for a long time. This means that two complementary strands are simultaneously separated from each other at the DNA damage sites. Likewise, ATR focuses on all types of DNA damage, such as abnormal DNA structures and single strand DNA brake. Furthermore, ATR play an important role in the response to the stalled replication forks in DNA replication and synthesis [Nyberg, 2002].

How does the activated ATM/ATR efficiently propagate DNA damage signals to the downstream control mechanism? The main focus of this section is on the discussion of the interaction among checkpoint proteins in response to a DSB situation in order to efficiently amplify the initial DNA damage signal. DSBs are originally recognized by a tri-protein complex Mre11-Rad50-Nbs1 (MRN complex), then the MRN complex recruits to and activates ATM at the DNA damage site. Furthermore, ATM can be also activated by changes in higher order chromatin structures. The recruitment and activation of ATM phosphorylates

various early downstream target substrates; for instance, MDC1 (mediator of checkpoint signalling 1), H2AX (which is a variant of H2A, a major core histone in nucleosomes), BRCA1 (Breast cancer protein1) and 53BP1 (the checkpoint adapter protein, p53-binding protein 1). In terms of MDC1, it is localized to the DNA damage site for quick response to DNA damage, and then it has a direct interaction with γ-H2AX, which is to phosphorylate histone H2AX by ATM at the serine139 through its BRCT domain. With the recruitment of ATM molecules or limiting H2AX dephosphorylation at DNA damage site, MDC1 can further amplify the histone H2AX phosphorylation signal. Eventually, more and more DNA repair factors, such as BRCA1 and 53BP1 are recruited and accumulated in a significant numbers at the DNA damage site. Furthermore, H2AX and H2A ubiquitination play another key role in regulating and facilitating the recruitment and accumulation of DNA repair factors at the DSB site. Accumulation of the local ubiquitinations of H2AX and H2A mainly depends on the ring-finger protein, RNF8, associated with UBC13 as well as the complex E2 and E3 at the damage site. The phosphorylated RNF8 in its FHA domain can bind with MDC1 and directly recognize signals for the ubiquitininteraction motifs (UIM) of RAP80 (receptor associated protein 80) by promoting further addition of ubiquitin chains. The recruitment and accumulation of BRCA1 is mainly dependent on the combination of ABRA1, RAP80 and the BRCT domain of BRCA1 at the DNA damage site [Srivastava et al., 2008]. In addition, the activated ATM/ATR promotes the phosphorylation of their effector kinases, Chk2/Chk1, which results in different effects on the cell cycle transition in different phases in order to achieve a delay in cell cycle progression.

2.2.2.3.2 G1/S Checkpoint

The G1/S checkpoint mediates cell cycle progression from G1 to S by regulating the complex of CycE and CDK2, which is called CycE/CDK2 [Beck et al., 2010; Ohtsubo et al., 1995]. This is achieved by the stabilization and activation of p53 and the phosphorylation of Cdc25A. Figure 2-3 shows how the G1/S checkpoint regulates the activity of CycE/CDK2 to block cell cycle progression into S-phase. In Figure 2-3, it can be seen that there are two pathways to control the activation of CycE/CDK2. One is controlled by p53 through p21 and the other is dominated by Cdc25A.

After DNA damage, the activated ATM/ATR can directly phosphorylate p53 at serine 15 (Ser^{15}). Meanwhile, ATM/ATR also activates Chk2/Chk1 by phosphorylating them at

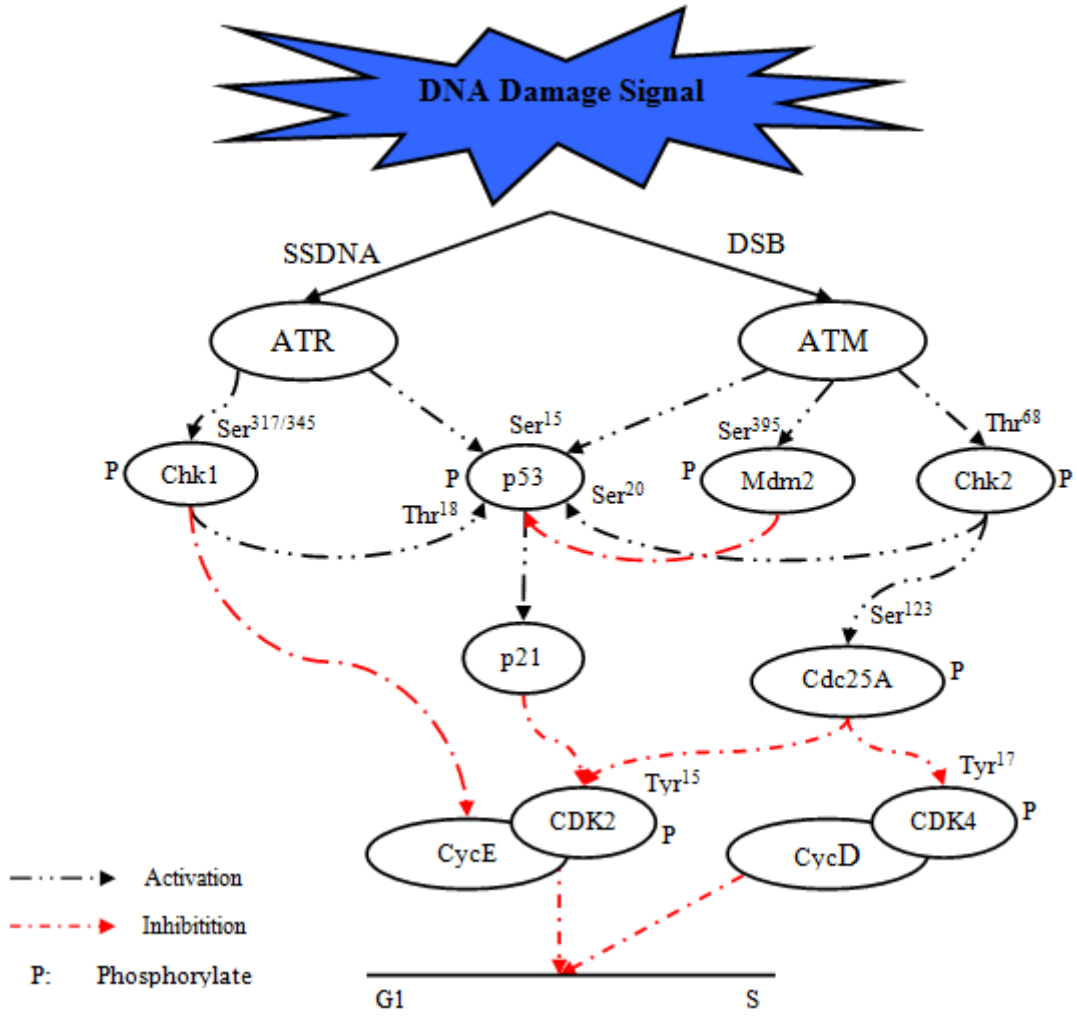

Figure 2-3 Schematic depiction of how the G1/S checkpoint delays cell progression into S by regulating the activation of the CycE/CDK2 complex. The figure only shows the key proteins involved in regulating the activation of CycE/CDK2 in repsonse to DNA-damage situations.

threonine 68 (Thr^{68}) and serine 317/345 ($Ser^{317/345}$), respectively. These activations of Chk2/Chk1 can also lead to the phosphorylation of p53 at serine 20 (Ser^{20}) and threonine 18 (Thr^{18}). In addition, the phosphorylated Mdm2 at serine 395 (Ser^{395}) makes a significant contribution to the stability and activity of p53 because the phosphorylated Mdm2, as the ubiquitin ligase, has already lost its ability to ubiquitinlate and degrade p53. As a result, the stability and activity of p53 leads to the transcription of p21 with its inhibitory signals on the CycE/CDK2 complex. Eventually, the inhibition of CycE/CDK2 delays G1/S transition [Bartek and Lukas, 2001; Beck et al., 2010; Liu et al., 2006; Nyberg et al., 2002].

Moreover, the increased Chk2 activity phosphorylated by ATM can result in the phosphorylation of Cdc25A at serine 123 (Ser^{123}), which promotes its ubiquitin-dependent degradation. The loss of Cdc25A inhibits the phosphorylation of CDK2 on tyrosine 15 (Tyr^{15}), thus blocking its connection with CycE, an essential step for the S-phase progression. Furthermore, the degradation of Cdc25A also promotes its inhibition in phosphorylation of CDK4 at tyrosine 17 (Tyr^{17}), which means that CDK4 does not combine with CycD. All these signals mark a transient delay in the S-phase entry in order to provide enough time for DNA damage repair and accurate cell cycle progression [Boutros et al., 2006; Mailand et al., 2000].

2.2.2.3.3 S-phase Checkpoint

In regard to the S-phase checkpoint, there are two checkpoint pathways in the S-phase: a DNA replication checkpoint and an intra-S-phase checkpoint. The main function of the DNA replication checkpoint is to maintain the stability of the replication forks by repairing DSB and removing replication blockages. In general, this checkpoint can be activated by blocking replication forks collapses. The intra-S-phase checkpoint is mainly used to inhibit the initiation of DNA replication by blocking the firing of uninitiated DNA replication origins [Liu et al., 2006; Petermann and Caldecott, 2006]. In response to these blocks of the replication forks, the ATR/Chk1 pathway plays an important role in maintaining the accurate replication fork progression in the S-phase (see Figure 2-4).

The blocking of replication forks results in the uncoupling of DNA polymerase (Pol) and helicase as well as long stretches of single strand DNA (ssDNA), which increases the accumulation of the ssDNA-binding replication factor (RPA) on chromatin [Walter and Newport, 2000]. Meanwhile, the ATR/Chk1 pathway is activated by the complex MRN

which generates RPA-coated ssDNA at DSBs. This signal promotes interaction between ATR and ATRIP and recruitment of ATR/ATRIP to RPA-coated ssDNA [Dart et al., 2004; Petermann and Caldecott, 2006; Zou and Elledge, 2003]. The activated ATR then phosphorylates the effector kinase, Chk1, at $Ser^{317/345}$ as an important component of the S-phase pathway, and the following replication and checkpoint proteins also provide an efficient environment to phosphorylate Chk1 by ATR:

1. After replication is blocked, the accumulation of replication proteins like RPA and Pol on the chromatin promotes the phosphorylation of Chk1 by ATR [Lupardus et al., 1998];
2. After replication is blocked, the accumulation of the replication helicase complex, MCM2-7, on the DNA helicase is phosphorylated by ATR and also requires Chk1 phosphorylation. Furthermore, there is an interaction among MCM7, a complex of ATR/ATRIP and Rad17. Rad17 is part of replication factor C (RFC) with its function of loading PCNA (the complex of Rad9, Rad1 and Hus1 and this complex is called 9-1-1) onto chromatin for normal replication. As a result, RPA accumulates Rad17 onto ssDNA and then Rad17 recruits the 9-1-1 complex, which eventually leads to the loading of 9-1-1 complex onto the DNA template [Dang et al., 2005; Kobayashi et al., 2004; Zou et al., 2002];
3. In response to replication blocks, checkpoint proteins, such as TopBP1 and Claspin, increase the phosphorylation of Chk1. TopBP1 is used to initiate DNA replication and regulate the activity of the checkpoint, while Claspin can connect with ATR in order to activate the interaction between Claspin and Chk1 [Chini and Chen, 2003; Kim et al., 2005].

Based on the above information, Chk1 is efficiently phosphorylated through ATR. This results in its disconnection from chromatin. The phosphorylated Chk1 then promotes the activity of Cdc25A in order to delay progression through S by inhibiting the activity of CDK2 without association with CycA (CycA/CDK2) [Karlsson-Rosenthal and Millar, 2006; Sanchez et al., 1997]. Moreover, the inhibitory phosphorylation of CDK2 also suppresses the loading of Cdc45 at the beginning of replication to achieve inhibition of the initiation of DNA replication. The reason is that the loading of Cdc45 at the origin can promote its association with RPA, and then Pol, on the chromatin at the beginning of DNA replication [Andreassen et al., 2006; Walter and Newport, 2000].

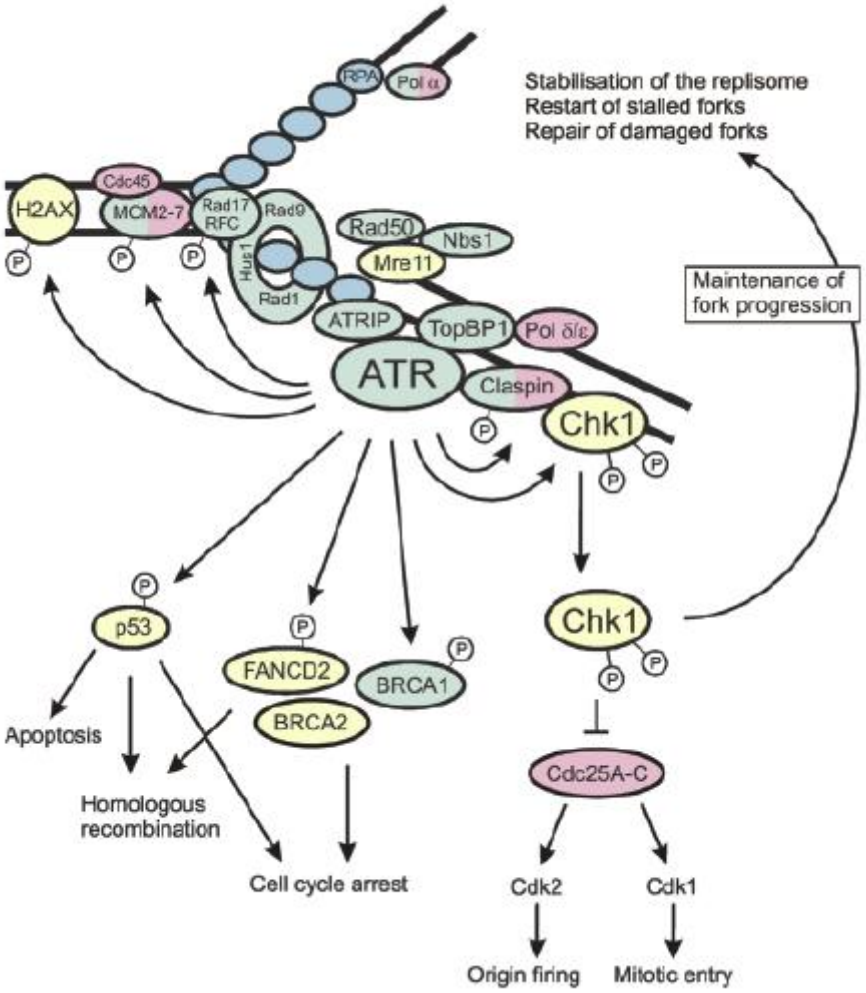

Figure 2-4 The ATR/Chk1 pathway in response to DNA damage and stalled replication forks block the S-phase (Acknowledgement: This figure is Figure 2-4 in Petermann and Caldecott [2006]).

2.2.2.3.4 The G2/M Checkpoint

The G2/M checkpoint mediates cell cycle progression from G2 to M by regulating a complex of CycB and CDK1 (CDC2), which is called CycB/CDC2. In fact, CDC2 must be phosphorylated at Thr^{161} or be dephosphorylated at Tyr^{15} or Thr^{14} to promote the association with CycB for the progression into mitosis [Arellano and Moreno, 1997; Smits and Medema, 2001; Stein and Pardee, 2004; Wu et al., 2010]. Figure 2-5 shows how the G2/M checkpoint primarily functions to block CycB/CDC2 activity in order to delay the entry into mitosis. In Figure 2-5, there are various parallel pathways to regulate CDC2 activity including the regulation of Cdc25C, the kinases Wee1/Mik1 for blocking of CDC2 function, and other related proteins.

In terms of the regulation of Cdc25C, DNA damage results in the activation of four different downstream kinases in order to block Cdc25c from dephosphorylating CDC2 at Tyr^{15} or Thr^{14} and preventing the mitotic progression:

1. The activated ATR promotes the activation of Chk1 by phosphorylating it at $Ser^{317/345}$, and then Chk1 phosphorylates Cdc25C at Ser^{216} to promote its binding with 14-3-3. This complex prevents the dephosphorylation of CDC2 at Tyr^{15} and Thr^{14} by the Cdc25 C, thus blocking the binding of CycB and CDC2 [Gutierrez et al., 2010; Peng et al., 1997; Sanchez et al., 1997];

2. The activated ATM phosphorylates Chk2 at Thr^{68}, thus resulting in the phosphorylation of Cdc25C at Ser^{216}, inhibiting its activation and function of dephosphorylating CDC2 [Gutierrez et al., 2010; Matsuoka et al., 1998];

3. Plk3 is regarded as a regulator of Cdc25C in the G2/M checkpoint pathway. It has the same functionality as Chk1/2 in inhibiting the activity of Cdc25C. When DNA damage happens, Plk3 activated by ATM can facilitate the phosphorylation of Cdc25C at Ser^{216} to achieve an inhibitory function [Gutierrez et al., 2010; Xie et al., 2001];

4. Another protein, Plk1, plays an important role in promoting the progression into mitosis by phosphorylating Cdc25C to activate its function of dephosphorylating CDC2. However, the activated ATM/ATR phosphorylates Plk1, which inhibits its function to activate Cdc25C and block the binding of the CycB/CDC2 complex resulting in a

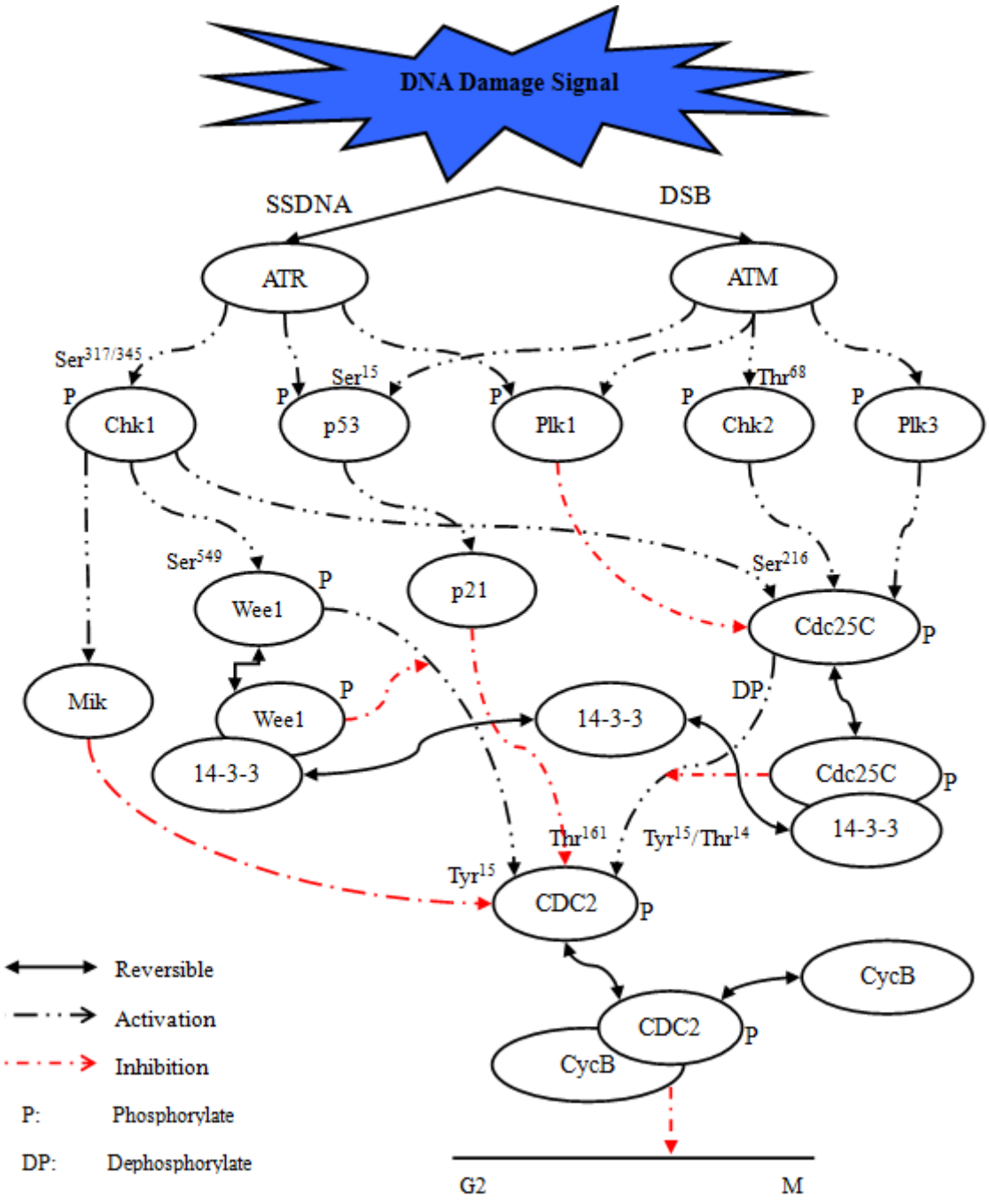

Figure 2-5 Schematic depiction of how the G2/M checkpoint delays cell progression into M by regulating the activation of the CycB/CDC2 complex.

decrease in CycB/CDC2 activity [Gutierrez et al., 2010; Smits et al., 2000; Van Vugt et al., 2001].

In addition, there are other proteins which play a significant part in transiently blocking G2/M transition. For instance; during DNA damage, ATM/ATR phosphorylates p53 on Ser^{15}, which promotes the activation of p21 in order to inhibit the phosphorylation of CDC2 on Thr^{161} through the activated p21. As a result, CDC2 loses its ability to combine with CycB and eventually results in the blocking of entry to mitosis [Nyberg et al., 2002; Smits and Medema, 2001]. Furthermore, the phosphorylation of Wee1 on Ser^{549} as well as Mik by Chk1 facilitate the activation of phorphorylation on Try^{15} of CDC2. The purpose is to keep the complex of CycB/CDC2 in the inactive state and provide enough time for DNA repair and accurate cell cycle progression [Nyberg et al., 2002; Stein and Pardee, 2004; Wu et al., 2010].

2.3 Mathematical Concepts

2.3.1 Importance of Mathematical Modelling

According to the above analysis of cell cycle checkpoints, it can be seen that they are very complex, involving a huge number of proteins and enzymes as well as various interactions between proteins and enzymes under different environments. This makes it difficult to deeply study and understand the characterisation and interaction of these complicated cell cycle checkpoints pathways from only *in vitro* and/or *in vivo* experiments. Therefore, increasingly mathematical models and computational simulation techniques have become more important in investigating the mechanisms and functions of cell cycle checkpoint pathways and analysing the complex and dynamic behaviour of cell cycle checkpoint pathways. In general, there are multifaceted objectives for mathematical models in cell cycle checkpoint pathways. The first objective is to validate the current knowledge by comparing model predictions with experimental data. When discrepancies are found in these types of comparisons, our knowledge of the underlying networks can be systematically expanded [Covert and Palsson, 2002]. The second objective is to study and investigate the inner workings of cell cycle checkpoint pathways, which are not accessible through biological experiments [Fuss et al., 2005; Pritchard and Kell, 2002]. The third objective is to suggest some novel biological

experiments for testing the model's hypothesis by reproducing the expected observations from the developed models [Klipp and Liebermerister, 2006; Yuh et al., 2001]. The fourth objective is to predict and design the most effective products based on the model's predictions [Arkin, 2001]. For instance, the implementation of mathematical model predictions on targeted tumour therapy makes a significant contribution to selecting anti-cancer drugs and reducing the overall costs of the therapy [Robert et al., 2004].

2.3.2 The Steps in Modelling Cell Cycle Checkpoints

In general, there are three essential steps in modelling cell cycle checkpoint pathways: model design, model analysis and model validation (see Figure 2-6). The following section contains more details of each step in developing a mathematical model for cell cycle checkpoint pathways.

- **Model Design**

Designing the model is the most important step in mathematical modelling. The objective of this step is to decide the logical formulation of a mathematical model for the part of the cell cycle checkpoints under investigation. This is because the mathematical model should describe behaviour of important aspects of cell cycle checkpoints reflecting a deep understanding of the real cell cycle process. It involves decisions on which cell cycle checkpoint pathway should be modelled, which types of biochemical reactions are involved in the protein-protein interaction networks for regulating activity of the simulated checkpoint and what initial conditions should be used to activate the simulated checkpoint signal pathways. Once these three factors are decided, the assumptions for the developed mathematical model, variables, quantities and interaction relationships between variables of the developed mathematical model are then decided.

- **Model Analysis**

The model analysis step focuses on the study of the dynamic behaviour of the simulated cell cycle regulations under different conditions using computational techniques. The purpose of this step is to make the developed mathematical model promote an understanding of the inner workings of cell cycle checkpoints and provide insights into real biological processes or systems. Furthermore, the analytical results also provide opportunities for researchers to

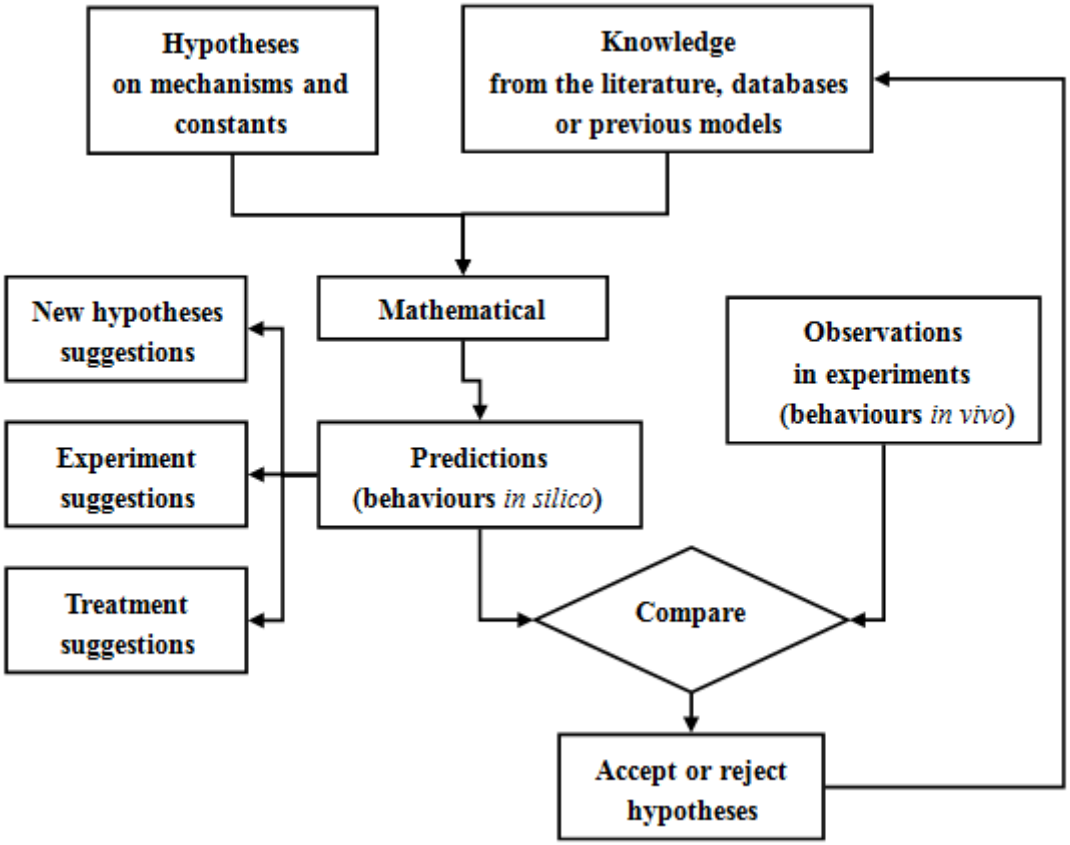

Figure 2-6 The workflow of the mathematical model for cell cycle checkpoints.

intelligently select and explore real experiments in order to reduce experimental time and costs.

The model analysis step is usually divided into two parts: the model parameter analysis and the model behaviour analysis. The model parameter analysis involves decisions on parameterisation and initialisation of the model, including all kinetic parameters (protein interaction rates or binding rates) and the initial conditions. Once these factors are specified, the mathematical model developed can be solved by numerical integration, and then used to concentrate on the analysis of model behaviour. The reason is that results from the model represent the corresponding behaviour of the simulated biological processes or systems. In fact, the developed mathematical models are mainly used to analyze and study the dynamic behaviour of a system in response to quantitative changes of the parameters in the mathematical model. Therefore, the investigation of qualitative changes in dynamic behaviour of a system in the presence of parameter variations is called bifurcation analysis. There are two main implications of the bifurcation analysis theory for cell cycle modelling: multistability analysis and sensitivity analysis [Strogaz, 2000]. Multistability means that there are more than one stable state in a system within a range of parameters. Multistability is an important property in controlling cell cycle progression and it involves a hysteretic switch to prevent cells from returning to the previous phase after the progression is completed. In the mathematical model, multistability analysis under kinetic parameter variations makes a significant contribution to the understanding of mechanisms underlying the cell cycle checkpoints [Novak and Tyson, 2003; Novak and Tyson, 2004]. Sensitivity analysis focuses on the role of individual parameters in the model, how individual parameters affect the whole model and how all these kinetic parameters simultaneously regulate the whole model. This involves the analysis of proteins included in the cell cycle checkpoints as well as their behaviour and effect in controlling the behaviour of cell cycle checkpoints.

- **Model Validation**

The model validation step compares the behaviour and data obtained from a computational simulation of the developed model with data generated from analogous experiments with the real cell cycle process or based on existing knowledge. For mathematical models, there are a series of hypotheses used in the models. Observations obtained from real biological experiments are used as evidence to ascertain whether the model's hypotheses should be rejected or not. Moreover, real experimental observations can also suggest some novel

hypothesis in order to optimize the existing mathematical models. For example, a hypothetical kinase (Xic1 as a stoichiometric inhibitor of the complex CycE/CDK2) was added into the kinase model developed by Ciliberto et al. [2003] in order to reproduce the behaviour observed in real biological experiments. In Ciliberto et al.s' [2003] model, they assumed that Xic1 can bind to all forms of CycE/CDK2 for inhibiting its activity. Furthermore, Xic1 bound to CycE/CDK2 was also used for the steady degradation of CycE. Based on these assumptions, the model simulation was consistent with experimental evidence that the degradation of CycE was a few hours after the degradation of Xic1 [Ciliberto et al., 2003].

2.3.3 Mathematical Structure of the Cell Cycle Checkpoint Models

Most mathematical models for simulating the cell cycle checkpoint pathways are based on chemical kinetic theory involving interactions of linked reactions among proteins and enzymes in the cell cycle checkpoint pathways. The purpose of this is to show the dynamic behaviour of the reactive components. A set of mathematical equations are used to describe the reaction rates which represent the change of concentration of all participating chemical species in the pathway per unit time. A number of kinds of rate laws exist to describe different types of reaction mechanisms. The most common ones are the Mass-action rate law [Waage, 1864], the Michaels-Menten rate law [Michaelis and Menten, 1913] and the Hill rate law [Hill, 1910].

Suppose the cell cycle checkpoint pathway consists of n chemical species $x_1, x_2, \ldots x_n$ participating in the reactions. In its most general form, the rate of the ith reaction (v_i) can be written as a function (f_i) of concentration (also denoted x_i) of all participating chemical species:

$$v_i = f_i(x_1, x_2, \ldots x_n) \tag{2-1}$$

The rate laws are used to decide the actual format of v_i in the simulated pathway.

2.3.3.1 Mass-Action Kinetics

The law of mass action describes the relationship between the rates of chemical reactions and the molecular concentration of the reacting substances in typical elementary reactions with

only one transition state/ mechanistic step [Waage, 1864]. This states that the rate of the chemical reaction at a spatially homogeneous medium is directly proportional to the product of the effective concentrations of the participating molecules. For a simple reaction like

$$aA + bB \xrightarrow{k} cC \ , \tag{2-2}$$

A and B are reactants, C is the product, a, b and c are the number of molecules, and k is the rate constant of the reaction. Thus, according to the law of mass action, the rate of this reaction can be written as

$$v = k[A]^a[B]^b , \tag{2-3}$$

where v is the rate of the reaction and the square brackets "[]" are concentrations. Once v is solved, we can use a set of ODEs to describe the change of concentration of all participating species in the system:

$$\frac{d[A]}{dt} = -av \ , \tag{2-4}$$

$$\frac{d[B]}{dt} = -bv \ , \tag{2-5}$$

$$\frac{d[c]}{dt} = cv \ . \tag{2-6}$$

The powers a and b of the concentrations of the reactants are the kinetic orders of the reactants A and B, respectively, which reflect the stoichiometry of the reaction. The overall order of this reaction is the sum of a and b.

The mass action rate law is only valid for elementary reactions with a single mechanistic step. In fact, most chemical reactions occur with the formation of intermediaries and/or through parallel reaction pathways and can be represented as a set of elementary reactions.

2.3.3.2 Michaelis-Menten Kinetics

In contrast to the mass action rate law, Michaelis-Menten kinetics are used to approximately describe the properties of enzyme-catalysed reactions that play an important role in biochemical systems [Michaelis and Menten, 1913]. Here, we consider an enzyme reaction as

$$S + E \underset{k_2}{\overset{k_1}{\rightleftarrows}} ES \xrightarrow{k_3} P + E\,, \tag{2-7}$$

where S is a substrate, P is a product, E is an enzymes or a catalyse, ES is a substrate-bound enzyme or the intermediate complex and k_1, k_2, k_3 are rate constants. Based on the mass action rate law, the rates of change of concentration of S, E, ES and P can be written as:

$$\frac{d[S]}{dt} = k_2[ES] - k_1[S][E]\,, \tag{2-8}$$

$$\frac{d[E]}{dt} = (k_2 + k_3)[ES] - k_1[S][E]\ , \tag{2-9}$$

$$\frac{d[ES]}{dt} = k_1[S][E] - (k_2 + k_3)[ES]\ , \tag{2-10}$$

$$\frac{d[P]}{dt} = k_3[ES]\ . \tag{2-11}$$

There are two key assumptions for the Michaelis-Menten Kinetics. The first key assumption is that the change of the concentration of the enzyme-substrate complex (ES) is much slower than those of the product (P) and the substrate (S). This assumption is also called quasi-steady-state assumption. It indicates that the concentration of ES remains constant or the rate of the change of [ES] is equal to zero

$$\frac{d[ES]}{dt} = k_1[S][E] - (k_2 + k_3)[ES] = 0\,. \tag{2-12}$$

Therefore,

$$[ES] = \frac{1}{K_M}[S][E], \text{ where } K_M = \frac{k_2 + k_3}{k_1}, \tag{2-13}$$

where K_M is called the Michaelis-Menten constant.

The second key assumption is that the total enzyme concentration $[E_T]$ remains constant and it is the sum of the concentrations of the free (unbound) enzyme E and the substrate-bound enzyme ES over time. The total enzyme concentration can be written as

$$[E_T] = [E] + [ES] \ . \tag{2-14}$$

Substituting Eq.(2-14) into Eq.(2-13), we obtain an expression for [ES]

$$[ES] = \frac{([E_T] - [ES])[S]}{K_M} \Rightarrow [ES] = [E_T]\frac{[S]}{[S] + K_M} \ . \tag{2-15}$$

By combining Eq.(2-11) and Eq.(2-15), the rate $v = \frac{d[P]}{dt}$ for the product P can be written as

$$v = \frac{d[P]}{dt} = k_3[ES] = k_3[E_T]\frac{[S]}{K_M + [S]}, \text{ or}$$

$$v = v_{\max}\frac{[S]}{K_M + [S]}, \text{ where } v_{\max} = k_3[E_T] \tag{2-16}$$

where $v_{\max}$ is the maximum reaction rate when all the enzyme molecules are in the form of the enzyme-substrate complex, ES at the substrate saturation. K_M is the Michaelis-Menten constant, as defined in Eq.(2-13). Eq.(2-16) is called the Michaelis-Menten equation, which shows that the rate of the product is hyperbolic with respect to the substrate concentration.

There are some limitations of Michaelis-Menten kinetics. First, it is only achieved when these two key assumptions are satisfied. In particular, the quasi-steady-state assumption is not reached in many biochemical or cellular processes. In fact, the change of enzyme-substrate complex [ES] can be very small but not equal to zero. Secondly, Michaelis-Menten kinetics are appropriate for simple situations without intermediate/ product inhibition and allostericity/cooperativity in the system.

2.3.3.3 Hill Kinetics

Although Michaelis-Menten kinetics take a predominant part in analysing enzyme kinetics, they cannot appropriately describe the complex cell cycle checkpoint pathways because these pathways exist with many intermediates/product inhibition and allostericity/cooperativity in interactions of linked reactions among proteins and enzymes. Therefore, Hill-type functions

are introduced as a simple, convenient and useful way to simulate the activation and inhibition/repression phenomena in these pathways.

In biochemistry, the Hill function is widely used to describe equilibrium binding in ligand-receptor interactions. It was first formulated by A.V. Hill [1910] to describe how oxygen binds to a hemoglobin. The Hill function also provides a possible way to model the activation and inhibition in complex systems. In general, sigmoidal functions are used to formulate the Hill function for the rate (v) of the activation and inhibition/repression as

$$v = f([x]) = \frac{\beta [x]^n}{K^n + [x]^n} \quad \text{for activation,} \tag{2-17}$$

$$\text{and } v = f([x]) = \frac{\beta}{1 + \left(\frac{[x]}{K}\right)^n} \quad \text{for inhibition/repression,} \tag{2-18}$$

where β is the maximum expression level of the promoted activity. n is the Hill coefficient describing cooperativity. K denotes the half –saturation constant (i.e., the concentration of x occupies half of activation or inhibition), and is commonly known as the dissociation constant. When n is equal to 1, the Hill function has the same format as the Michaelis-Menten equation (Eq. (2-16)), which describes a noncooperative reaction. When n is larger than 1, the effect of the cooperativity can be observed based on the properties of the cooperative reaction, such as activation (positively cooperative reaction) or inhibition/repression (negatively cooperative reaction).

For better understanding of the effect of the Hill coefficient, n, on the cooperativeness of the binding of the receptor protein with its ligands, we plotted the Hill function ($v = f([x])$) for activation and inhibition/repression against increased levels of [x], from 0 to 5, for four different n values: 1 (no cooperativity reaction), 2, 5 and 20 (the last three 'n's involve cooperativity reactions), respectively (Figure 2-7). For simplicity, values of β and K are equal to 1. According to Figure 2-7, it is clear that the rate of activation (v) (Hill function) reaches its maximum/minimum under the activation/ inhibition situations, respectively, much more rapidly with the increase of n, which indicates that the Hill curve becomes more sensitive to the increasing n. In particular, the Hill curve is like an on-off switch when n becomes very large.

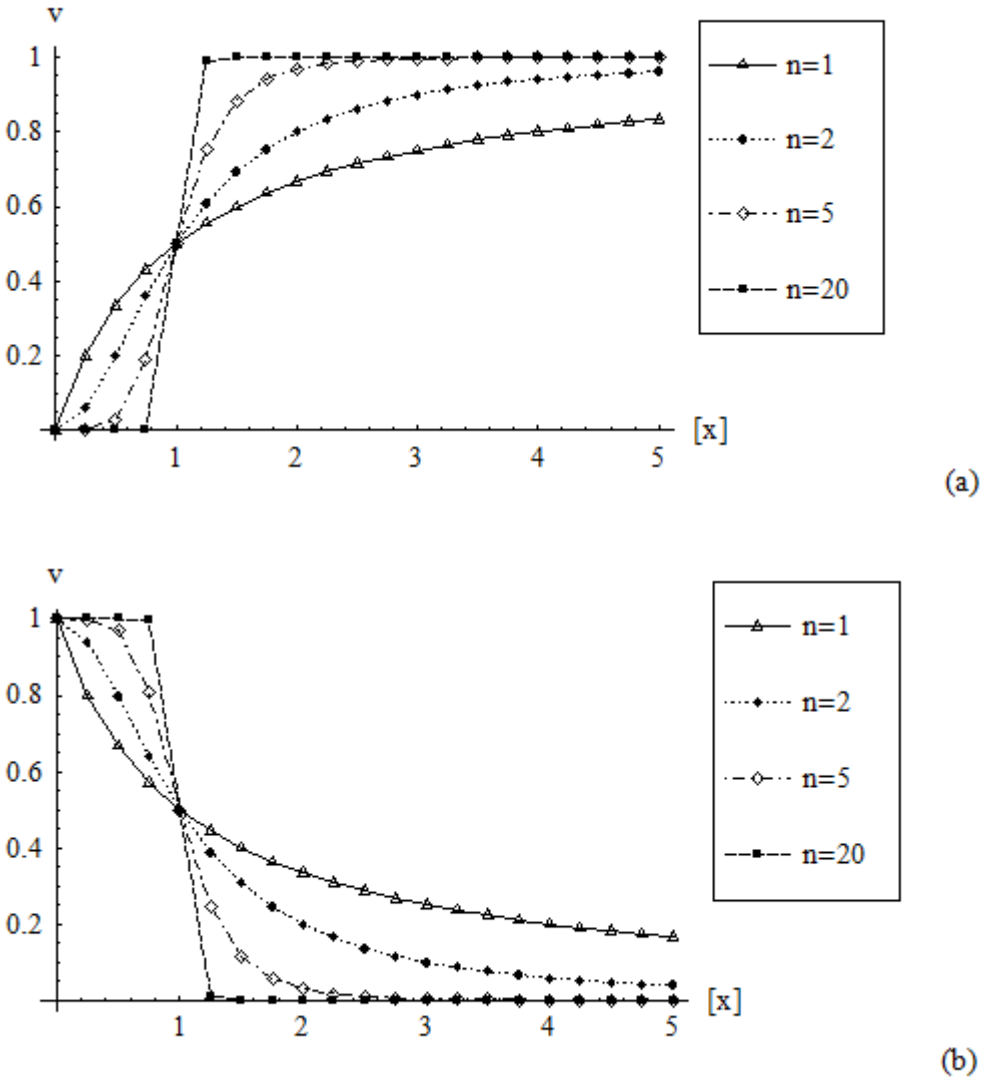

Figure 2-7 The effect of the Hill coefficient (n=1, 2, 5 and 20) on the Hill curve: (a) Hill functions for activation (positively cooperative reactions), and (b) Hill functions for inhibition/repression (negatively cooperative reactions).

2.3.4 Existing Models of Cell Cycle Checkpoints

Over the last decade, there have been several successful mathematical models developed for cell cycle checkpoints in the mammalian cell cycle regulation, particularly for the G1/S checkpoint. Most of these models are quantitative and describe the system to represent interactions among proteins and reproduce experimental observations. They provide enough evidence that mathematical models can simulate and explain the complex behaviour of the cell cycle as well as provide important insights into the inner workings of these cell cycle checkpoints. The simulation of the G1/S cell cycle phase transition started in 1995 and was based on the simple protein-protein network involving CycE, CDK2, the retinoblastoma gene product (Rb) and the transcription factor, E2F [Hatzimanikatis, 1995]. With time, mathematical models became more and more complicated because some significant factors needed to be taken into account, such as CycD, CDK4/6, CDK inhibitory proteins (p21, p27 and p16), the DNA-damage signal pathway and so on. For instance, Iwamoto et al. [2008] developed a complex mathematical model involving all essential proteins which control G1/S progression as well as proteins which include the DNA-damage signal transduction pathway. This made the mathematical model more comprehensive and powerful for exploring the potential behaviour of the whole G1/S transition pathway under DNA-damage situations. More details on the role of these proteins, such as Rb, E2F, CycD and CDK2, in the G1/S transition will be discussed in Chapter 3. Table 2-1 summarises the advantages and disadvantages of these existing mathematical models for the mammalian G1/S cell cycle phase transition.

2.4 Artificial Neural Networks

ANNs (ANNs) are considered a massively parallel-distributed information processing system that has similar characteristics to biological neural networks of the human brain to store, analyze and use experiential information and knowledge [Haykin, 1994]. ANNs have a high capability in approximating input-output mappings that are complex and nonlinear to arbitrary degrees of precision [Samarasinghe, 2006]. Typically, an ANN consists of computing elements called neurons and their connections depicted by ‘weights’ that are the internal parameters of the network. The incremental learning approaches used in ANNs make it possible for them to approximate all internal parameters iteratively and ANNs solve some

Table 2-1 Advantages and disadvantages of the past mathematical models for modelling the mammalian G1/S cell cycle transition.

Source for the developed mathematical model	Advantages	Disadvantages
A mathematical model for the G1/S transition of the mammalian cell cycle [Hatzimanikatis et. al., 1995]	• Displays successfully real experimental observations, particularly in studying the effects of the CycE synthesis rate and the total E2F concentration on the appearance or not, of oscillatory solutions • Suggests strategies for rational manipulation of the cell cycle through bifurcation analysis • Considers the effects of the cell growth causing dilution of intracellular species	• Simulates a very simple protein-protein networks just involving CycE, CDK2, Rb and E2F • Lacks the effects of cyclin dependent kinase inhibitors (CKIs) • Lacks the effects of cell volume in combination with the regulatory network
A mathematical model of regulation of the G1 phase of Rb+/+ and Rb-/- mouse embryonic fibroblasts and an osteosarcoma cell line [Obeyesekere et al., 1997]	• Displays the excellent agreement with current experimental observations in terms of how the activity of CycE/CDK2 responds to both Rb concentration and growth factors • Compares differences between normal cells, transformed cells and Rb-deficient cells • Involves more species to make the model a little bit complex • Makes specific predictions for further experiments	• A simplified version of the G1 phase of the cell cycle compared with a real situation • Ignores the crucial component of $p27^{kip1}$ and the phosphatise Cdc25A • Lacks an investigation of the cell cycle behaviour under unsaturated conditions • Lacks the effects of the growth factors on cyclin D synthesis
Functional capabilities of molecular network components controlling the mammalian G1/S cell cycle phase transition [Kohn, 1998]	• Provides functional insights useful for the interpretation of experiments and for guidance of experimental inquiry through a quasi-evolutionary sequence of simulations of hypothetical primordial systems (which starts with the simplest plausible functional system and adds functionality step by step in order to simulate the complexity of the mammalian G1/S cell cycle phase transition) • Provides a new approach involving unambiguous reaction diagrams, a convenient computer simulation method and a quasi-evolutionary method	• Ignores the functional characteristics of several factors, such as Rb phosphorylated at different sites has different properties • Ignores components of the network such as cdk inhibitor, $p27^{kip1}$ and the phosphatise Cdc25A • Focuses on the important functional core to keep the network simple • Lacks information on the relevant rate constants

	• Suggests some new functional concepts of relationship between Rb, E2f and cyclin-dependent kinase activities	• Lacks details in the simulated reaction network • Limitations in the distribution of regulatory molecules within the cell
The kinetic origins of the restriction point in the mammalian cell cycle [Aguda &Tang,1999]	• Develops a detailed model mechanism for the G1/S transition in the mammalian cell cycle, which takes the effects of cdk inhibitor, $p27^{kip1}$ and Cdc25A into account • Reproduces real experiments in terms of the relationship between the activity of CycE/CDK2 and the level of $p27^{kip1}$ as well as the relationship between the activity of CycE/CDK2 and the Rb pathway • Suggests the core mechanism involving the coupled phosphorylation- dephosphorylation (PD) cycles between CycE/CDK2 and Cdc25A	• Ignores the incorporation of signal transduction systems for G1/S transition • Ignores the participation of CycA • Lacks the effects of $p16^{INK4a}$ in the activities of E2F and CycE/CDK2 • Difficult to define the actual rate expression for individual processes as well as the rate parameters
A mathematical description of regulation of the G1-S transition of the mammalian cell cycle [Hatzimanikatis et. al., 1999]	• Optimizes the preliminary model in 1995, such as considering effects of a Cyc/CDK complex inhibitor and the change of cell volume with time • Replicates a significant number of experiments in the laboratory • Provides a solid foundation for further mathematical study of cell-cycle control and related areas	• A simple protein-protein network although the model adds a CycE/CDK2 complex inhibitor to the previous model
A model of cell cycle behaviour dominated by kinetics of a pathway stimulated by growth factors [Obeyesekere et al.,1999]	• Optimizes the previous model developed in 1997, such as, analysing effects of the growth factors on CycD under saturated or unsaturated growth factors • Reproduces the existing experiments on the effect of growth factors on cell cycle behaviour under saturated and unsaturated conditions • Gives some interesting predictions on the effect of growth factors in signal transduction pathway (leading to CycD synthesis) in the cell cycle • Suggests a new treatment plan for diseases governed by immortal cells	• Lacks enough data to approximate the values of parameters in the mathematical model, particularly for the efficiencies for the production of CycD and CycE

Kinetics behaviour of G1-to-S cell cycle phase transition model, [Tashima et al., 2003]	• Based on the detailed mathematical model developed by Aguda and Tang [1999] but focuses on individual molecules through changing their corresponding parameters • Analyzes the dynamics of G1/S transition by means of the adjustment of individual parameters in the model • Proves some important results from Aguda and Tang model	• Difficulty in interpreting model's results in terms of biological knowledge
Regulation of the mammalian cell cycle; a model of the G1-to- S transition [Qu et al., 2003]	• Divides the whole complicated G1/S transition regulatory network into individual simplified signal modules, and then reintroduces them into the full model in order to deeply analyze their dynamic properties as well as to decide their individual roles and their combined effects in the whole regulation network • Provides a wide degree of flexibility for the model to reproduce experimental observations and interpret the system's dynamics • Simulates interactions among components of the model based on biologically realistic schemes not on phenomenological representations	• Lacks experimental support to define parameters in the model • Ignores other regulatory interactions, such as Wee1 phosphorylated by activated CDK • Neglects nonuniform and dynamic distribution of proteins in the model
A model for restriction point control of the mammalian cell cycle [Novak & Tyson, 2004]	• Considers the interactions between cell growth and the dynamics of the CDK regulatory system • Compares the CDK-regulatory system in yeast and mammalian cells • Analyzes subtle interplays between two attributes of mammalian cell cycle: "sizer" and "timer" functions • Studies mutants of components in mammalian cell cycle, such as Rb, CycE	• Does not use additional signal transduction pathways to regulate proliferation in response to internal and external cues • Does not add the complicated details representing realistic cell cycle machinery and physiological circumstances
Simulation for detailed mathematical model of G1-to-S cell cycle phase transition [Tashima et al., 2004]	• Optimizes their previous model, developed in 2003, by adding CycA into the model and analyzes the effects of CycA activities • Provides some useful information for solving developmental mechanisms of cancer • Has an excellent agreement with the related experimental observations and biological knowledge	• Ignores the effects of the phosphatise Cdc25A and DNA damage signal transduction • Ignores some important components of the network, such as p53 and Mdm2

Mathematical modelling of G1/S Phase in the cell cycle with involving the p53/Mdm2 Network [Iwamoto et al., 2006]	• Adds DNA damage signal by p53/Mdm2 network into the previous mathematical model developed by Tashima et al. in 2004 • Confirms the dynamics of the influence of DNA damage signal on checkpoint pathways • Compares time courses of some chemical species under the normal process and under a DNA-damage situation	• Does not verify the effect of the intensity of DNA damage signal on the dynamics of E2F • Does not confirm the relationship between the intensity of DNA damage signal and the dynamics of these components: p16, p21 and p27
A system biology dynamical model of mammalian G1 cell cycle progression [Haberichter et al., 2007]	• Analyzes dynamic mechanisms of mammalian G1 cell cycle progression under constant growth factors • Simulates accurately the observed physiological data, kinetics and transitions • Compares differences between normal cells and tumour cells in a constant environment • Provides a foundation for the development of therapeutics	• Does not explicitly incorporate kinases and phosphatases which regulate cdk activation into the model, such as Cdc25A • Lacks enough information to estimate precise values of the parameters
Prediction of key factor controlling G1/S phase in the mammalian cell cycle using system analysis [Tashima et al., 2008]	• Agrees with the related experimental observations and biological knowledge • Identifies the predominant factors that affect G1/S phase transition in the cell cycle • Incorporates the behaviour of CycA into the mathematical modelling of the G1/S checkpoint • Has a precise understanding of the mechanisms regulating the dynamics of the G1/S phase transition	• Does not take DNA damage signal transduction pathway into account • Needs further study on sensitivity analysis and stability of the proposed model for the G1/S phase transition
Mathematical modelling and sensitivity analysis of G1/S phase in the cell cycle including the DNA-damage signal transduction pathway [Iwamoto et al., 2008]	• Integrates the G1/S checkpoint with DNA damage signal transduction pathway • Evaluates the influence of the non-linear dynamics of DNA damage signal • Identifies the predominant factors in G1/S phase in response to different levels of DNA damage signal • Analyzes the stability of the G/S transition without and with DNA damage situations	• Does not consider effective and compensating factors for the transformation from normal to damaged cells • Lacks the consideration of the DNA-damage repair process

Robustness of G1/S checkpoint pathways in cell cycle regulation based on probability of DNA-damaged cells passing as healthy cells [Ling et al., 2010]	• Detects DNA-damage in cells and their repair mechanisms during cell division to understand how cells are replicated for gaining deeper understanding of conditions that cause cancer, characterised by uncontrolled cell proliferation • Investigates the robustness of two critical proteins (E2F and CycE) of G1/S checkpoint in the presence of various levels of parameter perturbations under different levels of DNA-damage intensities by analysing the probability of a DNA-damage cell passing as a healthy cell in the G1/S transition • Validates the model simulation results through comparing them with the experimental findings and the biological theory	• Lacks the consideration of DNA-damage repair pathway • Does not make a connection between different intensities of DNA-damage signal in the model and the actual DNA-damage caused by different doses of UV-irradiation
Mathematical modelling of cell cycle regulation in response to DNA damage: exploring mechanisms of cell-fate determination [Iwamoto et al., 2011]	• Integrates the G1/S model with the G2/M model in response to DNA damage signal transduction pathway • Validates several numerically simulated time course levels of individual biochemical species • Evaluates the effect of different intensities of DNA damage on cell cycle arrest • Analyzes which cells determine an appropriate cell fate, making a useful contribution to developing novel therapeutic systems for tumour tissues	• Does not analyze in detail the relationship between p53 oscillation and the induction of cell apoptosis

problems that cannot be solved analytically by most mathematical models. With the development of neural networks, ANNs have become increasingly popular in many disciplines as a problem solving tool. More importantly, implementations of ANNs that have been successfully demonstrated in a variety of fields fall into a few simple categories [Maren et al., 1990; Hassoun, 1995].

Classification/Pattern Classification: Medical and disease diagnosis, character recognition, speech recognition, signature verification, spectra identification, classification of plant and animal species, blood cell classification and printed circuit board inspection etc.

Forecasting/Prediction: Stock market predictions, economic predictions, weather forecasting, prediction of disease spread, prediction of properties and behaviour of biological materials, Forecasting inflows into rivers and lakes, electricity load forecasting, chemical reaction products and environmental risk assessment etc.

Modelling: Engine idle-speed control, system control, process control, robot control, modelling land use change, signal compression, dynamic systems simulation and so on.

However, very limited work has been done to investigate the capability of neural networks to directly learn and represent interaction reactions among proteins in biological networks. In this research we focus on developing and implementing new recurrent neural networks (RNNs) to directly represent chemical reactions in a simple biological network (p53-Mmd2 oscillation system) as well as analyze and understand the internal workings among proteins involved in this biological network. In the following section, we discuss the fundamentals of ANNs, such as the basic idea behind RNNs, and more details on RNN development for this project will be described in a later chapter. A more general description of ANNs can be found in Maren et al., [1990], Hertz et al., [1991], Hagan et al., [1995], Hassoun [1995], Rojas [1996], Samarasinghe [2006] and many others.

2.4.1 Recurrent Neural Networks (RNNs)

RNNs became an important focus of neural network research during the 1990's. A recurrent neural network can be considered as a class of network which has recurrent connections that unite to form a directed cycle (this means that network outputs create feedback loops/connections into the network as additional inputs) as well as delay elements [Fausett,

1994, Haykin, 1999]. The purpose of RNNs is to learn and exhibit the dynamic temporal behaviour of a system based on the present activity of the system, which is continuously fed back into the network to create the internal state of the network as its internal memory, and that the network should then use this internal memory to generate the next activity of the system. Therefore, RNNs are usually used to study and simulate nonlinear or linear dynamical systems.

2.4.2 Recurrent Neural Networks Representing Chemical Kinetic Equations

According to the discussion of mathematical modelling of chemical kinetic equations in Section 2.3.3, non-linear or linear ODEs are used to represent chemical kinetic theory involving interactions of linked reactions in a biological network. In general, numerical techniques, instead of the analytical techniques, are used to solve these ODEs to understand the dynamic behaviour of the system: the next task of the system is to generate the summation of the current activity of the system and change the system over time, using the following equation

$$\begin{aligned} &\frac{dx_i}{dt} = \frac{x_i(t+1) - x_i(t)}{dt} = f_i(x_1, x_2, \ldots x_n) \Rightarrow x_i(t+1) - x_i(t) = \int_{\Delta t} f_i(x_1, x_2, \ldots x_n)\, dt \\ &\Rightarrow x_i(t+1) = x_i(t) + \int_{\Delta t} f_i(x_1, x_2, \ldots x_n)\, dt \end{aligned} \tag{2-19}$$

where $f(x_1, x_2, \ldots x_n)$ is the function which describes the rate of change of the i^{th} participating chemical species in the biological network. When dt becomes very small, from Taylor series expansion disregarding higher order terms, Eq. (2-19) for $dt \approx \Delta t$ can be rewritten as

$$x_i(t+1) = x_i(t) + f_i(x_1, x_2, \ldots x_n)\, dt = x_i(t) + f_i(x_1, x_2, \ldots x_n)\, \Delta t \ . \tag{2-20}$$

This characteristic of the numerical solution of ordinary differential equation techniques can be directly applied to a continuous-time recurrent neural network (RNN). More importantly, parameter estimation is the most difficult part of developing mathematical models for biological systems. Once an RNN is implemented to simulate chemical kinetic equations of a biological system, parameter estimation will become much easier and more feasible due to the

incremental learning approaches used in RNNs. There are some successful examples which demonstrate the application of RNNs to solve nonlinear projection equations in engineering. For instance, Kennedy and Chua [1988] developed a neural network for solving nonlinear programming problems based on the Kuhn-Tucker optimality conditions. Xia and Wang [1998] and Tao et al. [2001] also developed a two-layer neural network for solving nonlinear convex programming problems, indicating that the network can be globally convergent to an exact solution under a Lipschitz continuity condition and a strictly convex condition.

2.5 Mathematical Formulation of Biological Robustness

Although an abundance of research reports have been published on the role of robustness in multifactorial human disease [Gibson, 2009; Kitano, 2004b] and complex biological systems [Carlson and Doyle, 2002; Kitano 2004a], a mathematical foundation giving a unified perspective on biological robustness is still lacking. Kitano [2007] discussed the need for a complete mathematical formulation of biological robustness, and a mathematical theory. According to the concept of robustness, it can be defined as the ability of a system to maintain one or more of its functions under diverse perturbations. Therefore, the mathematical definition of robustness (R) of the system (s) may be written as a function (a) against a set of perturbations (P) as

$$R^s_{a,P} = \int_P \psi(p) D^s_a(p) dp, \tag{2-21}$$

where the function $\psi(p)$ is the probability for a particular perturbation 'p' to occur, and this should be equal when all perturbations occur with equal probability. The function $D(p)$ is used to evaluate the system performance under a particular perturbation p, and P is the whole perturbation space. In terms of the evaluation function, $D(p)$, it measures whether the system can maintain its function or performance against a perturbation and to what degree.
$D(p)$ can be defined as:

$$D^s_a(p) = \begin{cases} 0, & p \in A \subset P \\ f_a(p) / f_a(0), & p \in P \cup p \notin A \end{cases}, \tag{2-22}$$

where A is a set of perturbations when the system fails to maintain its functions, which means that $D(p)$ is equal to zero when a function cannot meet a defined requirement /criteria under

a particular perturbation. Otherwise, $D(p)$ has a relative viability for a function under a certain perturbation compared with the non-perturbed state. For example, the production of the critical protein in a system has decreased to 80% under a particular perturbation against its production under non-perturbed conditions, which indicates that D(p) is equal to 0.8 for this specific perturbation.

This mathematical definition of biological robustness concentrates on the stability and maintenance of the system's function in response to diverse perturbations. However, robustness is a broader concept than stability and homeostasis. Therefore, more work is required to establish a mature theory of robustness by taking these factors into account; for example, phase transition and instability as an approach to achieve robustness, heterogeneity and the structured nature of biological systems, and the evolution of biological systems.

Chapter 3: A Mathematical Model of G1/S Transition Including the DNA-damage Signal Transduction Pathway

In the following four chapters, the biological system under investigation is G1/S transition incorporating the DNA-damage signal transduction pathway, which is responsible for maintaining the stability of the cell cycle. Therefore, understanding the interaction between DNA-damage signal transduction and the G1/S checkpoint is a critical issue that affects the basis of life sciences. However, it is difficult to understand the interactions in this complicated biochemical network (the G1/S checkpoint) involving DNA-damage signals just from *in vitro* experiments; hence, we study a mechanistic mathematical model of the system and implement computational simulations for various levels of perturbations in the kinetic parameters of the model, followed by a systematic study and analysis of the model's outcomes. The purpose is to study and explore the complex characterisation of G1/S transition. This chapter provides: first, a detailed background of the molecular components and interactions in the system; and secondly, a description of the mathematical model developed by Iwamoto et al. [2008] for G1/S transition including the DNA-damage signal. In Chapter 4, we define an analytical approach to investigate the robustness of G1/S transition in response to DNA-damage situations. In Chapter 5, we analyze and discuss results of a series of simulations and draw relevant conclusions. In Chapter 6, we study model's ability to shed light on cellular senescence based on the results obtained from the mathematical simulation of the G1/S checkpoint through adjusting the corresponding kinetic parameters in the model.

3.1 Biological Background of the G1/S Checkpoint Pathway and the DNA-damage Signal Transduction Pathway

The cell cycle checkpoint pathways and the DNA-damage signal transduction pathway regulate the cell cycle in response to various endogenous and exogenous factors, which may directly or indirectly damage the components of genomic DNA [Dasika et al., 1999]. When normal cells undergo chemical or physical stresses resulting in DNA damage, the DNA-

damage signal transduction pathway senses and propagates the "damage" signal to the cell cycle. Once the cell cycle recognizes the damage signal, the cell cycle checkpoints block cell cycle progression and provide sufficient time for the DNA repair mechanisms to complete their tasks successfully [Geva-Zatorsky et al., 2006; Iwamoto et al., 2008]. There are two approaches to blocking cell cycle progression in response to a DNA-damage signal: one depends on the activation of p53 and the other depends on the phosphorylation of Cdc25A, as discussed in Chapter 2. This study focuses on the former approach and the whole process is divided into the following five steps: (1) the DNA-damage signal activates the tumour suppressor protein, p53, because its (p53's) negative feedback loop with Mdm2 cannot effectively and strictly control its stability, (2) the activated p53 sequentially promotes the activity of Mdm2 and p21, (3) p21, as a CDK inhibitor, binds to the binary complexes of Cyc/CDK, which play an important role in the cell cycle checkpoint pathway and control cell cycle progression, (4) the trimeric complex, p21/Cyc/CDK, inhibits the activity of Cyc/CDK leading to a blockage of cell cycle progression, and (5) p53 can also trigger the DNA-damage repair pathway or the apoptosis pathway by activating their cellular mechanisms. [Avkin et al., 2006; Fridman and Lowe, 2003; Harris and Levine, 2005; Haupt et al., 2003; Shu et al., 2007]. When the cell cycle checkpoint pathway loses the ability to sense the DNA-damage signal, the defective and abnormal genome of a cell can pass through the cell cycle progression to future cellular generations. Thus, the disruption of the mediation between the cell cycle checkpoint pathway and the DNA-damage signal transduction pathway can make the genome unstable and predispose normal cells to malignant transformation, which eventually causes various diseases, in particular, human cancers.

As discussed in Chapter 2, there are several cell cycle checkpoints with their own mechanisms to control cell cycle progression, for instance, G1/S, G2/M and G0[5]/G1 phase transition. These checkpoints have their own responsibility in the cell cycle: the G1/S checkpoint is used to control the initiation of DNA replication, the G2/M checkpoint is used to trigger mitosis and the G0/G1 checkpoint is used to sense the proliferation signal [Dasika et al., 1999; Hartwell and Kastan, 1994; Ikeda et al., 1996; Iliakis et al., 2003; Mckay et al., 2000; Stelling et al. 2004]. A cell generally stays in the G0 phase for a long time before it moves to G1. The reason for this is to accumulate nutrients and growth factors as well as propagate the proliferation signal for cell development [Iliakis et al., 2003; Molinari, 2000]. Furthermore,

[5] G0 phase is also called quiescence which means that the cell enter into a resting state, where the cell continues with its biological function but does not go through the rest of the cell cycle. The cell enters the G0 phase mainly due to a lack of growth factors or nutrients.

some important proteins, such as p27, CycD/CDK4/6 and p27/CycE/CDK2, in cell cycle regulation have already been accumulated in cells at this stage. After sensing the proliferation signal, cells enter the G1 phase and prepare for the initiation of DNA replication. Here, DNA is checked for any damage and the disruption of the G1/S checkpoint leading to non-recognition of the damage-signal can cause further problems to cell cycle progression. The G1/S phase checkpoint controls cell cycle progression into S phase. In the event of no DNA-damage, transition is initiated through the release of E2F (The E2 promoter provides a direct assay for E2F transcription activating function [Helin, 1998]) that involves the preparation of important proteins that allow for the passage into S phase as well as DNA replication [Dyson, 1998; Ikeda et al. 1996; Leone et al., 1999; Ohtani, 1999; Ohtani et al., 1995]. In the event of DNA-damage, this process is halted until the damage is repaired or the cell undergoes senescence or apoptosis [Bartek and Lukas, 2001a, b]. There are two questions to be answered: one is how the involved proteins regulate the cell cycle progression from G1 to S; the other is what the cell does in response to a DNA-damage signal. The following section provides more details in response to the above questions.

3.1.1 What Happens in the Absence of DNA-damage?

In the absence of a DNA-damage signal, cells usually stay in a quiescent (G0) state for a long time. As previously mentioned in Section 3.1, the purpose of this is to accumulate nutrients and growth factors as well as to propagate the proliferation signal. Once the proliferation signal is sensed in the early G1 phase, it triggers the synthesis of CycD increasing its concentration (See Figure 3-1). The CycD produced binds to CDK4 or CDK6 to form the complexes of CycD/CDK4 and CycD/CDK6, keeping them in an activated state (In this study, CycD/CDK4/CDK6 is used to represent these two complex proteins, CycD/CDK4 and CycD/CDK6, because they have quite similar physiological functions). There are two functions attributed to the CycD/CDK4/CDK6 complex: one function is to initiate the phosphorylation of Rb bound to E2F to obtain the hypophosphorylated form (Rb-PP/E2F) and the other function is to keep CycE/CDK2 in active form by (i) competing with CycE/CDK2 for binding with free p27 to form the complex p27/CycD/CDK4/6 and by (ii) sequestering p27 from p27/CycE/CDK2 [Obaya and Sedivy, 2002]. The activated form of CycE/CDK2-P results in further hypophosphorylation of Rb-pp/E2F, promotes the dissociation of Rb-PPPP and E2F, and releases the activating E2F. The increase in level of free E2F promotes the synthesis of CycE in the mid to late G1 phase, which facilitates the association between CycE

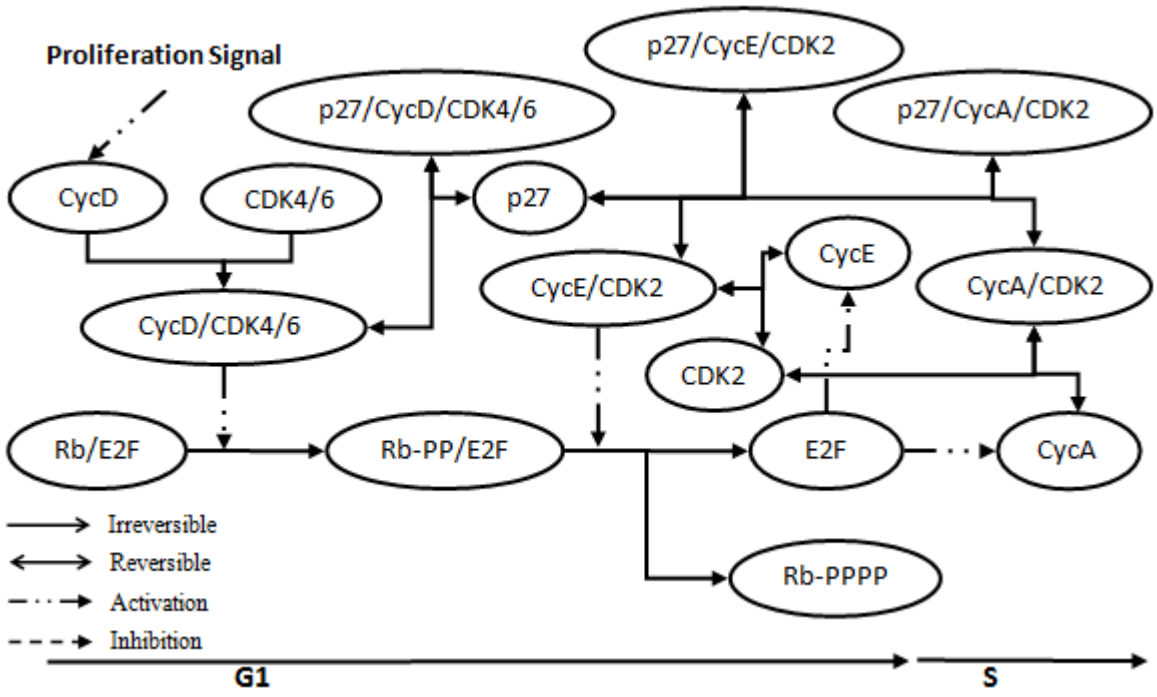

Figure 3-1 Simplified representation of the main protein interactions occurring in G1 phase andG 1/S transition in the absence of a DNA-damage signal.

and CDK2 to form more of the complex CycE/CDK2. This results in increases in E2F activity and establishes a positive feedback loop between E2F and CycE; increased levels of E2F and CycE let the cell pass the G1/S transition and trigger S phase initiation [Hiebert et al., 1992]. The degradation of CycD occurs in the mid-G1 phase which promotes the release of p27 bound to the complex CycD/CDK4/6. Furthermore, free-p27 is redistributed to the new complexes, such as CycE/CDK2 or CycA/CDK2. Although p27 can inhibit the activity of CycE/CDK2 or CycA/CDK2, the large amount of activated CycE/CDK2 can initiate p27 degradation by phosphorylating it at threonine when p27 binds to CycE/CDK2 [Coqueret, 2003]. This is why there is a significant degradation of p27 at the end of G1 due to the accumulation of CycE/CDK2 in the cell. E2F subsequently promotes CycA expression at the G1/S transition with a significant increase in the S phase. CycA is an important protein in the transition through the S phase as well as DNA replication [Obaya and Sedivy, 2002]. In S phase, the synthesized CycA also binds to CDK2 to form the complex CycA/CDK2. Once CycA/CDK2 is activated, it drives a negative feedback loop to inhibit the activity of E2F by phosphorylating E2F for its degradation. In addition, Rb-PPPP is dephosphorylated into Rb and E2F rebinds to Rb when the cell completes the G1/S transition progression. The purpose is to inhibit E2F activity and keep it in an inactivated form (Rb/E2F) in the S phase.

3.1.2 What Happens When DNA Is Damaged?

How do cells regulate the cell cycle transition from G1 to S in response to a DNA-damage signal? There are two different processes to remove DNA-damage from the cell cycle: a reversible form of cell cycle arrest/a state of temporary cell cycle arrest (DNA-damage repair) and an irreversible form of cell cycle arrest/a state of permanent cell cycle arrest (such as cellular senescence or apoptosis). As mentioned in Section 3.1, p53 plays an important role in response to the DNA-damage signal and to maintain the fidelity of the cell genome. In the normal cell cycle, a negative feedback loop between p53 and Mdm2 keeps p53 at a low and stable steady-state concentration through inhibiting p53 activity and enhancing the p53 degradation rate [Barak et al., 1993; Haupt et al., 1997; Kubbutat et al., 1997; Wu et al., 1993]. However, this negative feedback loop cannot effectively and strictly control the level of p53 when DNA-damage happens (see Figure 3-2). The accumulation of p53 in the nucleus leads to the arrest of cell cycle progression, repair of DNA damage or cellular senescence/apoptosis if repair is impossible. Depending on the different levels of DNA-damage, p53 has different functions in the cell cycle [Ciliberto et al., 2005; Geva-Zatorsky et al., 2006; Harris and

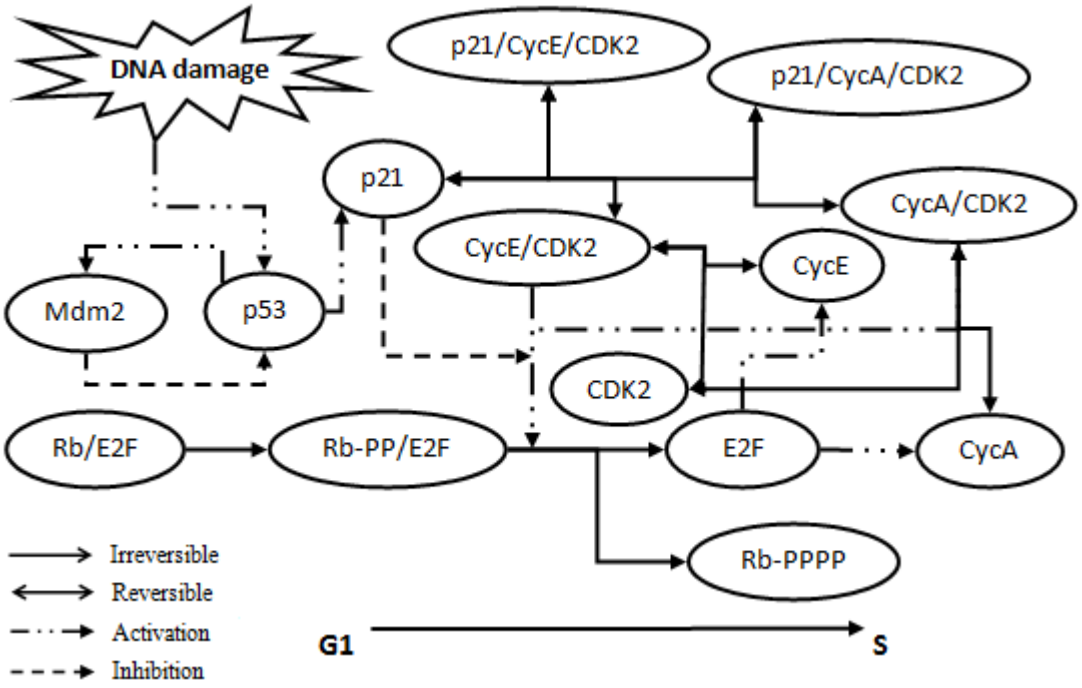

Figure 3-2 Diagram of key regulators in G1/S transition in response to DNA damage.

Levine, 2005; Lahav et al., 2004; Li and Ho, 1998]. In terms of low DNA-damage, the DNA-damage signal promotes the activation of p53. The activated p53 promotes the transcription and synthesis of p21. The increased p21 binds to CycE/CDK2-P and CycA/CDK2-P to form p21/CycE/CDK2-P and p21/CycA/CDK2-P in order to inhibit their activation. As a result, Rb-PP/E2F cannot be further hypophosphorylated due to the loss of CycE/CDK2-P and CycA/CDK2-P, which inhibit the release of E2F and, consequently, synthesis of CycE and CycA, which are essential steps in the progression to the S phase [Dulic et al. 1994]. This temporarily blocks cell cycle progression and activates the cell cycle repair pathway in order to provide enough time for cells to repair DNA damage. With the removal of DNA-damage, the negative feedback loop of p53 and Mdm2 is fully restored and p53 returns to a low level. The decrease in p53 reduces the level of p21, which releases the complexes of CycE/CDK2-P and CycA/CDK2-P and makes the cell cycle return to the normal condition. With regard to high DNA-damage, p53 activated by the DNA-damage signal triggers the apoptosis pathway instead of DNA-damage repair pathway. In this case, the level of p21 is not as high as in the low-level DNA-damage case. The reason is that most p53 is used to activate the apoptosis pathway [Fridman and Lowe, 2003; Harris and Levine, 2005; Haupt et al. 2003; Li and Ho, 1998].

Combining these two situations together, the completed structure of the G1/S checkpoint pathway integrating the DNA-damage signal transduction pathway is shown in Figure 3-3. According to Figure 3-3, it can be seen that the whole process in the G1/S transition is very complex, which contains a large number of interactions among many chemical species involved in the G1/S transition as well as the DNA-damage signal pathway.

3.2 Description of the Mathematical Model

A range of mathematical models have been proposed for the G1/S checkpoint pathway and the DNA-damage signal transduction pathway over the last twenty years (details of these models are in Chapter 2). However, most of these models study and analyze these two pathways individually. Only a few mathematical models concentrate on the dynamic behaviour of G1/S in response to the DNA-damage signal [Iwamoto et al. 2006; Iwamoto et al. 2008].

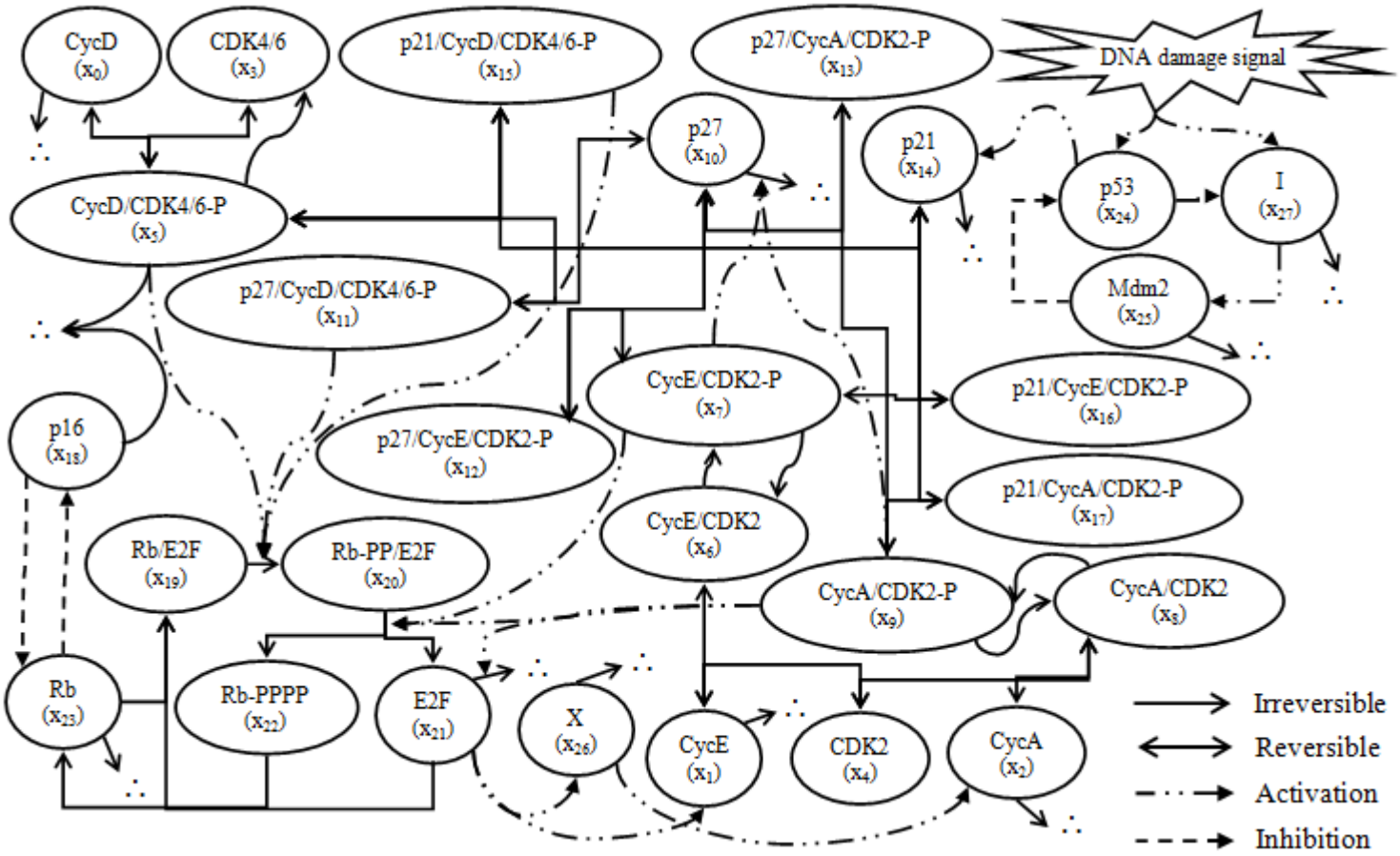

Figure 3-3 Schematic diagram of the structure of the G1/S checkpoint involving the DNA damage signal traduction pathway [Ling et al., 2010].

The latest mathematical model of the G1/S phase transition, published in 2008 by Iwamoto et al. [2008], simulates the G1/S phase transition involving the DNA-damage signal transduction pathway based on the biological finding that effectively combine Tashima et al.'s [2004] G1/S phase transition model and Lev Bar-Or et al.'s [2000] DNA damage signal transduction model. Tashima et al. [2004] focus on the chemical interactions among the biochemical species of the G1/S transition and their dynamic behaviour, while Lev Bar-Or's model [2000] focuses on the dynamic behaviour of the DNA signal transduction mechanism, which is mainly based on the damped oscillation of p53 and Mdm2. Iwamoto et al. [2008] mainly analyze the dynamic behaviour of the key proteins, such as E2F, CycE, CycA, p21, p53, Mdm2, in the G1/S phase transition in response to three different levels of DNA-damage (no DNA-damage, low DNA-damage and high DNA-damage). Furthermore, they identify what the predominant kinetic parameters are in the G1/S transition under different DNA-damage levels based on a local sensitivity analysis. The purpose is to develop a measure and a criterion to evaluate the variation of chemical species with respect to the perturbations in each kinetic parameter. Variation is defined as a change in the steady-state value of each chemical species divided by the change of a particular parameter. The focus of this sensitivity analysis is to count the number of chemical species with variations larger than 0.1 or less than -0.1 corresponding to the changes in model parameters. If the changes in kinetic parameters affect a larger number of steady-state chemical species, they are defined as predominant factors in the G1/S transition phase in the cell cycle. Meanwhile, Iwamoto et al. [2008] also analyzed changes in peak time of E2F in response to the different values of the specific kinetic parameter, k5, which corresponds to the synthesis of CycE promoted by E2F.

Iwamoto et al.s' model -hereafter simply referred to as the G1/S model- has 28 ODEs based on the mass balances with 75 kinetic parameters, which displays the interactions among the chemical species in the G1/S phase transition integrating the DNA-damage signal transduction pathway (see Figure 3-3). Michaelis-Menten and Hill kinetics are used to simulate the inhibiting effects of proteins in the G1/S model. Moreover, each ODE describes the time course of concentration for the corresponding chemical species. Now we take the protein (Rb) as an example of how ODE represents the change of concentration of Rb based on the equation given below:

$$\frac{dx_{23}}{dt} = k_{56} + \frac{k_{58}}{1 + k_{59}\, x_{18}} + k_{55}\, x_{22} - (k_{57}\, x_{23} + k_{45}\, x_{21} x_{23})$$

where $x_{18}, x_{21}, x_{22}, x_{23}$ represent p16, E2F, Rb-PPPP and Rb, respectively; the biochemical meaning of parameters is shown in Table 3-2. In this equation, we use Michaelis-Menten kinetics (the second term on the right side) to express p16 inhibition of the synthesis of Rb as shown in Figure 3-3. The change of concentration of the remainder of the participating molecular species in the G1/S transition can be written in the same way as above.

The following content shows how ODEs represent chemical interations involved in the G1/S model based on small changes from Iwamoto et al.s' [2008] model. We divide the complex G1/S model (see Figure 3-3) into four sub-models: inhibition model of CDK4/6 and CDK2 by p16 and p27, activation model of CDK2 by CycE and CycA, activation model of Rb/E2F cycle and DNA-damage signal transduction pathway in the G1/S transition. Therefore, ODEs are introduced with the description of each sub-model in order to easily and deeply understand this complex G1/S checkpoint pathway in response to the DNA-damage situation. Furthermore, the sequential order ODEs for the G1/S model is shown in Appendix A. We summarise the model variables corresponding to chemical species in the G1/S phase in Table 3-1 and the biochemical meaning of these 75 parameters in Table 3-2.

We first introduce interactions involved in the inhibition model of CDK4/6 and CDK2 by p16 and p27 in the G1/S transition (see Figure 3-4). Proteins p16 and p27 are considered as CKIs in the G1/S transition, but they have different functions. P16 only binds to CycD/CDK4/6 in order to inhibit its activity through degrading CycD/CDK4/6. P27 can bind to these three complexes: CycD/CDK4/6, CycE/CDK2-P and CycA/CDK2-P to form the trimeric complex p27/CycD/CDK4/6, p27/CycE/CDK2-P and p27/CycA/CDK2-P. However, p27 only inhibits the activation of CycE/CDK2-P and CycA/CDK2-P. Moreover, both the binary complex CycE/CDK2-P and CycA/CDK2-P can promote p27 degradation. The following equations (Eqs. (3-1 to 3-8)) represent a series of chemical interactions involved in the sub-model of inhibition of CDK4/6 and CDK2 by p16 and p27:

$$\frac{dx_0}{dt} = k_1 + k_4 x_5 - (k_2 x_0 + k_3 x_0 x_3) \tag{3-1}$$

$$\frac{dx_3}{dt} = k_4 x_5 + k_{13} x_5 - (k_3 x_0 x_3) \tag{3-2}$$

$$\frac{dx_5}{dt} = k_3 x_0 x_3 + k_{19} x_{15} + k_{21} x_{11} - (k_4 x_5 + k_{13} x_5 + k_{18} x_5 x_{14} + k_{20} x_5 x_{10} + k_{44} x_5 x_{18}) \tag{3-3}$$

Table 3-1 Description of variables in the G1/S Model.

Model variables	Chemical species	Model variables	Chemical species
x_0	CycD	x_{14}	p21
x_1	CycE	x_{15}	p21/ CycD/CDK4/6
x_2	CycA	x_{16}	p21/ CycE/CDK2-P
x_3	CDK4/6	x_{17}	p21/ CycA/CDK2-P
x_4	CDK2	x_{18}	p16
x_5	CycD/CDK4/6	x_{19}	Rb/E2F
x_6	CycE/CDK2	x_{20}	Rb-PP/E2F
x_7	CycE/CDK2-P	x_{21}	E2F
x_8	CycA/CDK2	x_{22}	Rb-PPPP
x_9	CycA/CDK2-P	x_{23}	Rb
x_{10}	p27	x_{24}	p53
x_{11}	p27/ CycD/CDK4/6	x_{25}	Mdm2
x_{12}	p27/ CycE/CDK2-P	x_{26}	‘X’
x_{13}	p27/ CycA/CDK2-P	x_{27}	‘I’

Table 3-2 Biochemical meaning of the kinetic parameters of the G1/S model.

Parameter	Biochemical meaning	Parameter	Biochemical meaning
k_1	synthesis rate of CycD	k_{39}	degradation rate of p21
k_2	degradation rate of CycD	k_{40}	synthesis rate of p16
k_3	association rate of CycD/CDK4/6	k_{41}	constant as influx or precursor
k_4	dissociation rate of CycD/CDK4/6	k_{42}	rate of inhibition of synthesis p16 by Rb
k_5	synthesis rate of CycE	k_{43}	degradation rate of p16
k_6	degradation rate of CycE	k_{44}	degradation rate of p16/ CycD/CDK4/6
k_7	association rate of CycE/CDK2	k_{45}	association rate of Rb/E2F
k_8	dissociation rate of CycE/CDK2	k_{46}	phosphorylation rate of Rb/E2F to form Rb-PP/E2F through CycD/CDK4/6
k_9	synthesis rate of CycA	k_{47}	phosphorylation rate of Rb/E2F to form Rb-PP/E2F through p27/CycD/CDK4/6
k_{10}	degradation rate of CycA	k_{48}	phosphorylation rate of Rb/E2F to form Rb-PP/E2F through p21/CycD/CDK4/6
k_{11}	association rate of CycA/CDK2	k_{49}	rate of activation of E2F by CycE/CDK2-P
k_{12}	dissociation rate of CycA/CDK2	k_{50}	rate of activation of E2F by CycA/CDK2-P
k_{13}	rate of CDK4/6 production through CycD/CDK4/6	k_{51}	rate of synthesis of E2F promoted by itself
k_{14}	rate of CDK2 production through CycA/CDK2-P	k_{52}	synthesis rate of E2F
k_{15}	rate of CDK2 production through CycA/CDK2	k_{53}	degradation rate of E2F
k_{16}	rate of CDK2 production through CycE/CDK2	k_{54}	rate of E2F degradation by CycA/CDK2-P
k_{17}	rate of CDK2 production through CycE/CDK2-P	k_{55}	dephosphorylation rate of Rb-PPPP to Rb
k_{18}	association rate of p21/ CycD/CDK4/6	k_{56}	synthesis rate of Rb
k_{19}	disassociation rate of p21/ CycD/CDK4/6	k_{57}	degradation rate of Rb
k_{20}	association rate of p27/CycD/CDK4/6	k_{58}	constant as influxes or precursor
k_{21}	disassociation rate of p27/CycD/CDK4/6	k_{59}	rate of inhibition of synthesis Rb by p16
k_{22}	phosphorylation rate of CycE/CDK2 to form CycE/CDK2-P	k_{60}	synthesis rate of p53
k_{23}	dephosphorylation rate of CycE/CDK2-P to form CycE/CDK2	k_{61}	rate of synthesis of p53 through DNA-damage signal
k_{24}	association rate of p27/ CycE/CDK2-P	k_{62}	degradation rate of p53
k_{25}	disassociation rate of p27/ CycE/CDK2-P	k_{63}	synthesis rate of Mdm2
k_{26}	association rate of p21/ CycE/CDK2-P	k_{64}	degradation rate of Mdm2
k_{27}	disassociation rate of p21/ CycE/CDK2-P	k_{65}	dissociation constant in Hill function
k_{28}	phosphorylation rate of CycA/CDK2 to form CycA/CDK2-P	k_{66}	rate of synthesis of Mdm2 through ‘I’
k_{29}	dephosphorylation rate of CycA/CDK2-P to form CycA/CDK2	k_{67}	degradation rate of ‘I’
k_{30}	association rate of p27/ CycA/CDK2-P	k_{68}	synthesis rate of ‘X’
k_{31}	disassociation rate of p27/ CycA/CDK2-P	k_{69}	degradation rate of ‘X’
k_{32}	association rate of p21/ CycA/CDK2-P	k_{70}	rate of p53’s sequence-specific DNA binding activity by DNA-damage signal
k_{33}	disassociation rate of p21/ CycA/CDK2-P	k_{71}	association rate of p53 and Mdm2
k_{34}	synthesis rate of p27	k_{72}	rate of DNA-damage repair
k_{35}	rate of p27 degradation by CycE/CDK2-P	k_{73}	rate of inhibition of degradation of p53 and/or Mdm2 by DNA-damage signal
k_{36}	rate of p27 degradation by CycA/CDK2-P	k_{74}	rate of Mdm2’s ability to promote p53 degradation
k_{37}	synthesis rate of p21	k_{75}	rate of inhibition of Mdm2-mediated p53 degradation under the initial damage signal
k_{38}	rate of synthesis of p21 through p53		

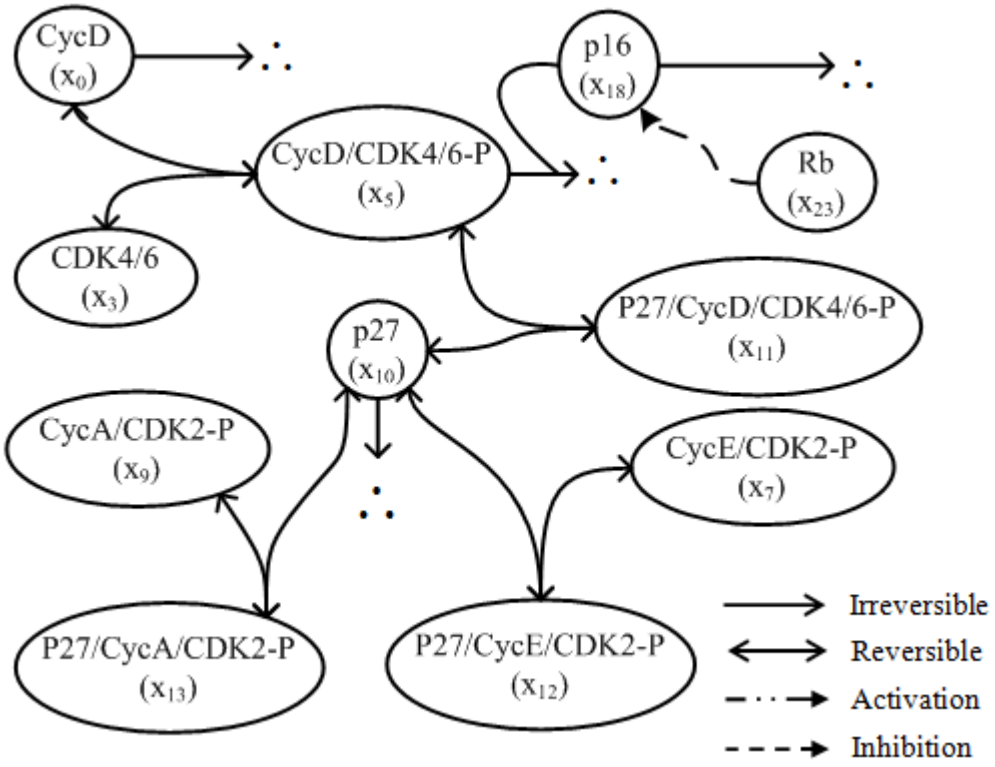

Figure 3-4 Inhibition model of CDK4/6 and CDK2 by p16 and p27 in the G1/S Model.

$$\frac{dx_{10}}{dt} = k_{34} + k_{21}\,x_{11} + k_{25}\,x_{12} + k_{31}\,x_{13} - (k_{20}\,x_5\,x_{10} + k_{24}\,x_7\,x_{10} + k_{30}\,x_9\,x_{10} + k_{35}\,x_7\,x_{10} + k_{36}\,x_9\,x_{10}) \quad (3\text{-}4)$$

$$\frac{dx_{11}}{dt} = k_{20}\,x_5\,x_{10} - k_{21}\,x_{11} \quad (3\text{-}5)$$

$$\frac{dx_{12}}{dt} = k_{24}\,x_7\,x_{10} - k_{25}\,x_{12} \quad (3\text{-}6)$$

$$\frac{dx_{13}}{dt} = k_{30}\,x_9\,x_{10} - k_{31}\,x_{13} \quad (3\text{-}7)$$

$$\frac{dx_{18}}{dt} = k_{40} + \frac{k_{41}}{1 + k_{42}\,x_{23}} - (k_{43}\,x_{18} + k_{44}\,x_5\,x_{18}) \quad (3\text{-}8)$$

For the activaction model of CDK2 by CycE and CycA in the G1/S transition (see Figure 3-5), the synthesis of CycE and CycA is promoted by the release of E2F in the later stage of G1 phase. According to the experimental finding [Braken et al., 2004], the synthesis of CycA promoted by E2F requires some other co-activator at the same time. Therefore, we introduce the intermediate protein 'X' to display this requirement in the model. The produced CycE and CycA bind to CDK2 to form the binary complex CycE/CDK2 and CycA/CDK2. Once these two binary complexes (CycE/CDK2 and CycA/CDK2) are phosphorylated, they become the activated forms to take their responsibility in cell cycle regulation. For example: CycE/CDK2-P controls cell progression into S phase while CycA/CDK2-P controls the DNA replication in the S phase. The details of ODEs for the activation model of CDK2 are shown below (Eq. (3-9 to 3-15)):

$$\frac{dx_1}{dt} = k_5\,x_{21} + k_8\,x_6 - (k_6\,x_1 + k_7\,x_1\,x_4) \quad (3\text{-}9)$$

$$\frac{dx_2}{dt} = k_9\,x_{26} + k_{12}\,x_8 - (k_{10}\,x_2 + k_{11}\,x_2\,x_4) \quad (3\text{-}10)$$

$$\frac{dx_4}{dt} = k_8\,x_6 + k_{12}\,x_8 + k_{14}\,x_9 + k_{15}\,x_8 + k_{16}\,x_6 + k_{17}\,x_7^2 - (k_7\,x_1\,x_4 + k_{11}\,x_2\,x_4) \quad (3\text{-}11)$$

$$\frac{dx_6}{dt} = k_7\,x_1\,x_4 + k_{23}\,x_7 - (k_8\,x_6 + k_{16}\,x_6 + k_{22}\,x_6\,x_7) \quad (3\text{-}12)$$

$$\frac{dx_7}{dt} = k_{22}\,x_6\,x_7 + k_{25}\,x_{12} + k_{27}\,x_{16} - (k_{23}\,x_7 + k_{24}\,x_7\,x_{10} + k_{26}\,x_7\,x_4 + k_{17}\,x_7^2) \quad (3\text{-}13)$$

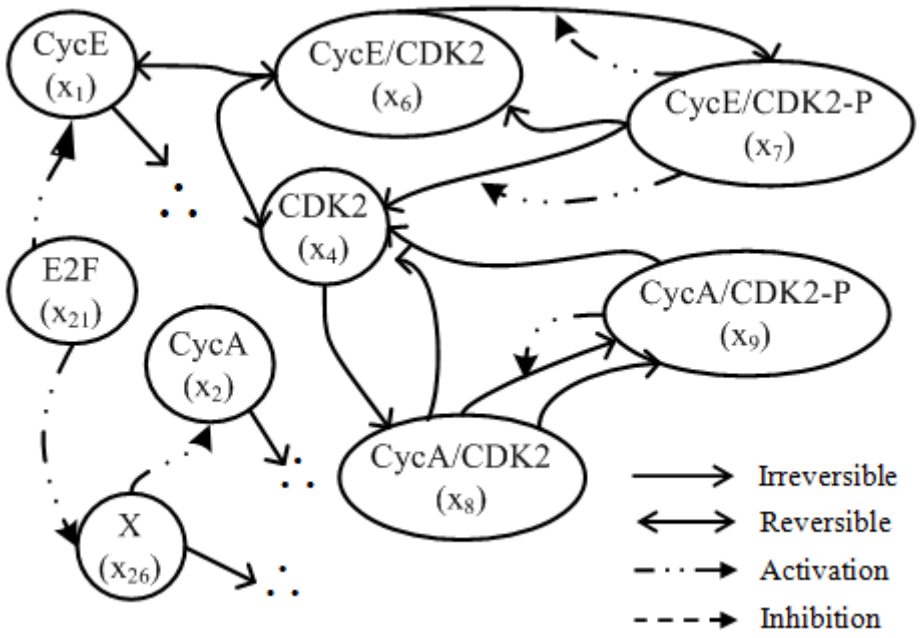

Figure 3-5 Activation model of CDK2 by CycE and CycA in the G1/S Model.

$$\frac{dx_8}{dt} = k_{11}x_2x_4 + k_{29}x_9 - (k_{12}x_8 + k_{15}x_8 + k_{28}x_8x_9) \quad (3\text{-}14)$$

$$\frac{dx_9}{dt} = k_{28}x_8x_9 + k_{31}x_{13} + k_{33}x_{17} - (k_{14}x_9 + k_{29}x_9 + k_{30}x_9x_{10} + k_{32}x_9x_{14}) \quad (3\text{-}15)$$

In the activation model of Rb/E2F cycle in the G1/S transition (see Figure 3-6), E2F is released through disassociation from E2F/Rb as follows: CycD/CDK4/6 and its related complexes (such as p27/ CycD/CDK4/6 and p21/CycD/CDK4/6) initiate the phosphorylation of Rb bound to E2F to obtain the hypophosphorylated form (Rb-PP/E2F). Furthermore, Rb-PP/E2F can be further phosphorylated by the activated CycE/CDK2-P and CycA/CDK2-P in order to promote the dissociation of Rb-PPPP and E2F. The release of E2F promotes the synthesis of CycE, CycA and itself. However, the activated CycA/CDK2-P triggers the degradation of E2F to inhibit its activation. Once the cell enters the S phase, Rb-PPPP is dephosphorylated to Rb which rebinds to E2F to form the complex Rb/E2F. The following equations (Eqs. (3-16 to 3-20)) represent the chemical interactions in the activation model of Rb/E2F cycle:

$$\frac{dx_{19}}{dt} = k_{45}x_{21}x_{23} - (k_{46}x_5x_{19} + k_{47}x_{11}x_{19} + k_{48}x_{15}x_{19}) \quad (3\text{-}16)$$

$$\frac{dx_{20}}{dt} = k_{46}x_5x_{19} + k_{47}x_{11}x_{19} + k_{48}x_{15}x_{19} - (k_{49}x_7x_{20} + k_{50}x_9x_{20}) \quad (3\text{-}17)$$

$$\frac{dx_{21}}{dt} = k_{52} + k_{51}x_{21} + k_{49}x_7x_{20} + k_{50}x_9x_{20} - (k_{53}x_{21} + k_{45}x_{21}x_{23} + k_{54}x_9x_{21}) \quad (3\text{-}18)$$

$$\frac{dx_{22}}{dt} = k_{49}x_7x_{20} + k_{50}x_9x_{20} - k_{55}x_{22} \quad (3\text{-}19)$$

$$\frac{dx_{23}}{dt} = k_{56} + \frac{k_{58}}{1 + k_{59}x_{18}} + k_{55}x_{22} - (k_{57}x_{23} + k_{45}x_{21}x_{23}) \quad (3\text{-}20)$$

For the model of DNA-Damage signal transduction pathway in the G1/S transition (see Figure 3-7), the damaged signal activates p53 which breaks the negative feedback loop between p53 and Mdm2, making the negative feedback loop ineffective in strictly controlling the level of p53. The synthesis of p53 promotes the production of the interminate ‘I’, an unknown mechanism leading to a possible delay between the activation of p53 and the induction of Mdm2. The increased ‘I’ triggers the synthesis of Mdm2 but the synthesis of

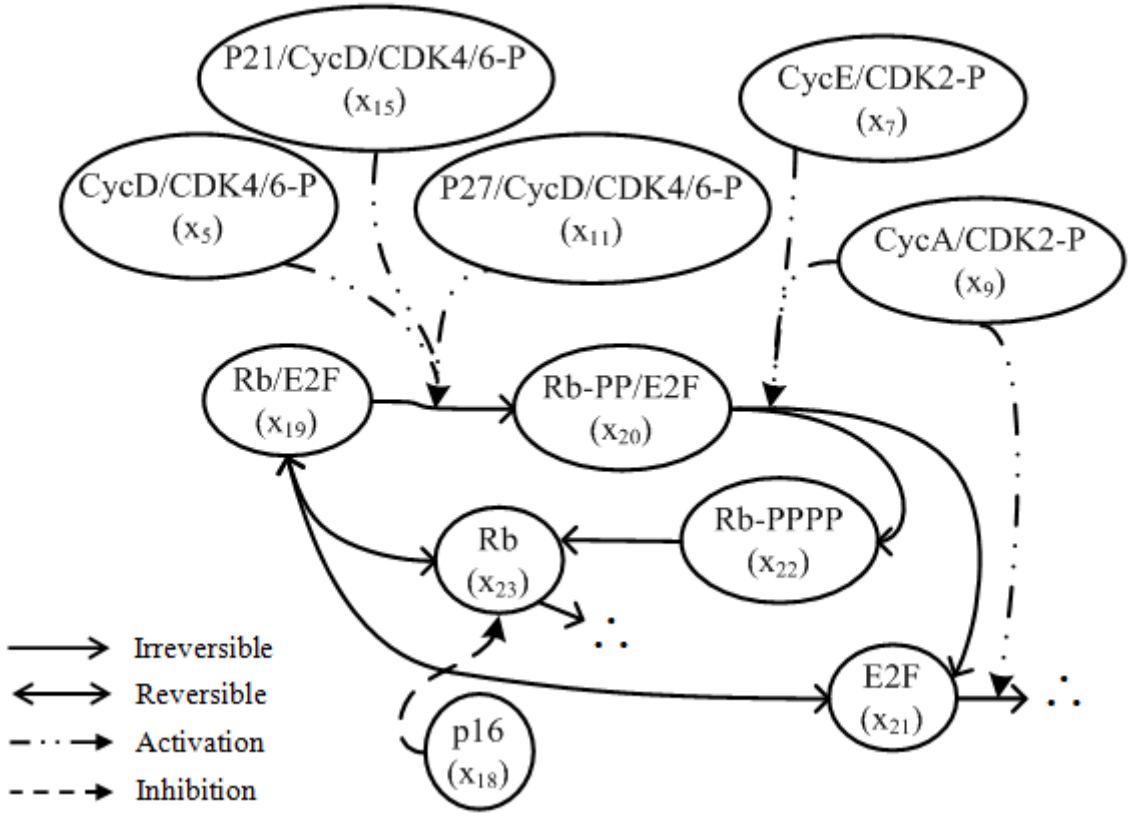

Figure 3-6 Activation model of Rb/E2F cycle in the G1/S Model.

Mdm2 inhibits the synthesis of 'I' as well as the activation of p53 through its (p53's) degradation. In addition, p53 can promote the synthesis of p21 as one of the key CKIs to inhibit the activation of CycE/CDK2-P and CycA/CDK2-P through binding to these two complex proteins. The purpose of this binding is to delay cell progression and provide enough time for DNA-damage repair. The p21 also binds to CycD/CDK4/6 without inhibiting the activation of this binary complex. The details of ODEs for the DNA-damage signal transduction pathway model are shown below (Eqs. (3-21 to 3-28)):

$$\frac{dx_{14}}{dt} = k_{37} + k_{19}\,x_{15} + k_{27}\,x_{16} + k_{33}\,x_{17} + k_{38}\,x_{24} - (k_{39}\,x_{14} + k_{18}\,x_5\,x_{14} + k_{26}\,x_7\,x_{14} + k_{32}\,x_9\,x_{14}) \tag{3-21}$$

$$\frac{dx_{15}}{dt} = k_{18}\,x_5\,x_{14} - k_{19}\,x_{15} \tag{3-22}$$

$$\frac{dx_{16}}{dt} = k_{26}\,x_7\,x_{14} - k_{27}\,x_{16} \tag{3-23}$$

$$\frac{dx_{17}}{dt} = k_{32}\,x_9\,x_{14} - k_{33}\,x_{17} \tag{3-24}$$

$$\frac{dx_{24}}{dt} = k_{60} + k_{61}\,signal - (degradation\,x_{24}\,x_{25} + k_{62}\,x_{24}) \tag{3-25}$$

$$\frac{dx_{25}}{dt} = k_{63} + \frac{k_{66}\,x_{27}^9}{k_{65}^9 + x_{27}^9} - k_{64}\,x_{25} \tag{3-26}$$

$$\frac{dx_{26}}{dt} = k_{68}\,x_{21} - k_{69}\,x_{26} \tag{3-27}$$

$$\frac{dx_{27}}{dt} = \frac{k_{70}\,x_{24}\,signal}{1 + k_{71}\,x_{24}x_{25}} - k_{67}\,x_{27} \tag{3-28}$$

The following two equations represent the kinetics of the signal for p53 activation (Eq. (3-29)) and the strength of Mdm2's ability to inhibit the activation of p53 by promoting the degradation of p53 (Eq. (3-30)),

$$signal = DDS \times \exp(-k_{72}\,t) \tag{3-29}$$

$$degradation = k_{74} - k_{73}(signal - DDS \times \exp(-k_{75}\,t)) \tag{3-30}$$

where DDS is the initial intensity of the DNA-damage signal. In this case, the value of DDS is quantitatively defined as follows: 0 for no DNA-damage (normal situation), 0.003 for low

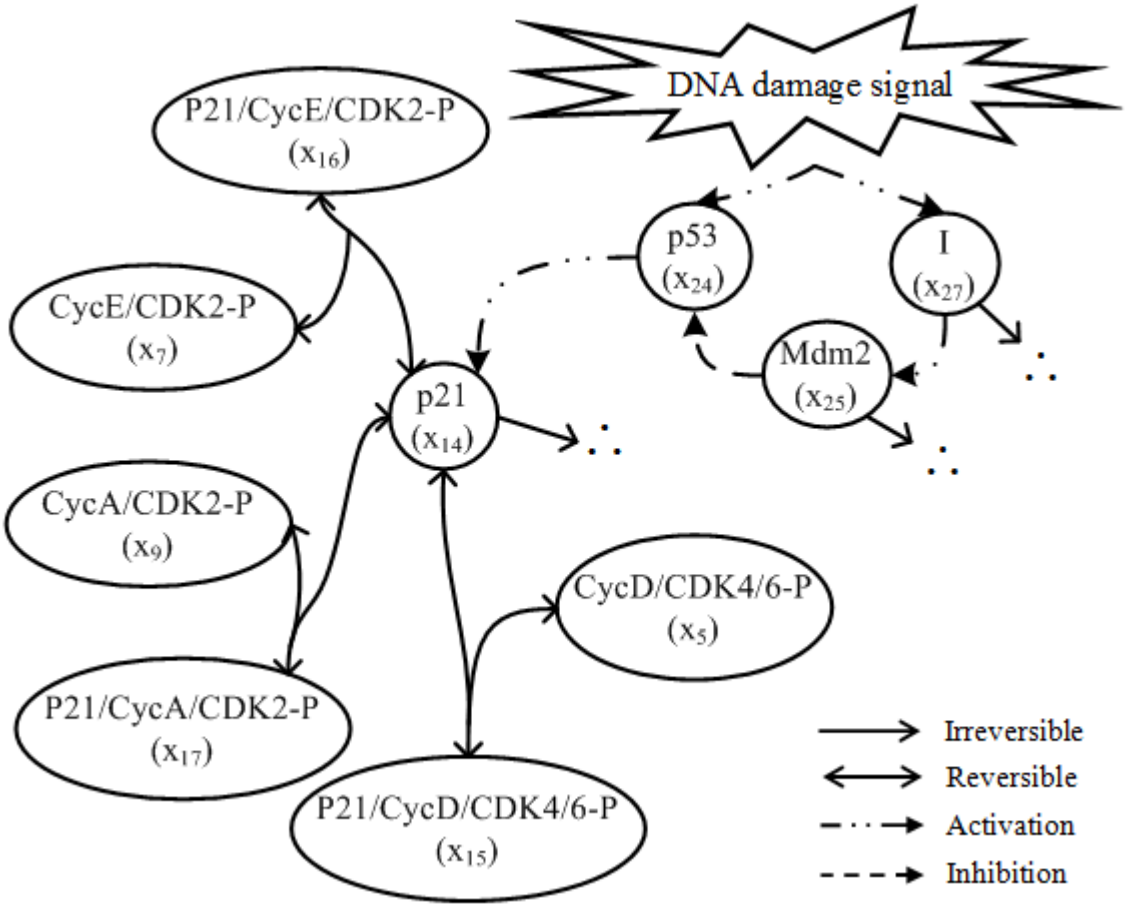

Figure 3-7 DNA-damage signal transduction pathway sub-model in the G1/S model

DNA-damage and 0.005 for high DNA-damage. In terms of the signal denoted in Eq. (3-29), the complex process involved in subsequent resolution of the damage signal by cellular mechanisms of DNA damage repair is represented by a constant parameter k_{72} in order to keep the model as simple as possible. Therefore, we ignore the complex reactions involved in cellular mechanisms of DNA-damage repair in the real biology. In addition, the values of these 75 parameters and initial values of the model's variables are tabulated in Tables 3-3 and 3-4, respectively [Iwamoto et al., 2008]. In this research, "NDSolve" in Mathematica® is used to find a numerical solution to 28 ODEs and generate the dynamic behaviour of chemical species in the G1/S phase.

3.3 Summary

In this chapter, we provided a detailed background of the molecular components and interactions in the G1/S checkpoint pathway and the DNA-damage signal transduction pathway as well as a summary of the mathematical model for the G1/S transition involving the DNA-damage signal that will be the basis for this study.

In terms of biological background of the G1/S transition, we described what happens among the molecular components in the G1/S transition under no DNA-damage and DNA-damage situations. In the absence of a DNA-damage signal, CycD/CDK4/6 initiates phosphorylation of Rb in the early G1 phase. It prepares for the realse of E2F at the G1/S transition. In the late G1 phase, CycE/CDK2 completes the further phosphorylation of Rb to release more E2F in order to let the cell pass the G1/S transition and promote S phase initiation. When DNA-damage happens, p53 is activated and promotes the transcription and synthesis of p21. Furthermore, p21 can bind to CycE/CDK2 to inhibit the activation of this complex. As a result, the cell progression is temporarily blocked due to the uncompleted progress in the further phosphorylation of Rb for releasing E2F by CycE/CDK2.

For the mathematical model of the G1/S transition, we gave a detailed summary of ODEs, the biochemical meaning of kinetic parameters, the initial conditions and the parameter values for the G1/S model. These factors can help us to understand the meaning of the G1/S model. More importantly, the G1/S model can be effectively used to investigate the robustness and dynamical behaviour of the G1/S transition in response to a DNA-damage signal.

Table 3-3 Kinetic parameter values for the G1/S model.

Parameter	Value	Parameter	Value	Parameter	Value
k_1	5×10^{-3}	k_{26}	2.25×10^{-2}	k_{51}	5×10^{-8}
k_2	5×10^{-4}	k_{27}	1.75×10^{-4}	k_{52}	5×10^{-7}
k_3	5×10^{-3}	k_{28}	1.9×10^{-2}	k_{53}	5×10^{-5}
k_4	2.5×10^{-3}	k_{29}	5×10^{-4}	k_{54}	1×10^{-2}
k_5	7.5×10^{-2}	k_{30}	2.5×10^{-3}	k_{55}	5×10^{-8}
k_6	2.5×10^{-3}	k_{31}	1.75×10^{-4}	k_{56}	5×10^{-5}
k_7	1.25×10^{-3}	k_{32}	2.5×10^{-3}	k_{57}	5×10^{-3}
k_8	2.5×10^{-4}	k_{33}	1.75×10^{-4}	k_{58}	5×10^{-5}
k_9	8×10^{-4}	k_{34}	5×10^{-8}	k_{59}	5×10^{-4}
k_{10}	5×10^{-4}	k_{35}	1×10^{-2}	k_{60}	1×10^{-4}
k_{11}	1×10^{-3}	k_{36}	1.5×10^{-3}	k_{61}	1.5
k_{12}	2×10^{-4}	k_{37}	5×10^{-5}	k_{62}	1×10^{-3}
k_{13}	5×10^{-4}	k_{38}	1×10^{-2}	k_{63}	9.4×10^{-4}
k_{14}	5×10^{-4}	k_{39}	5×10^{-3}	k_{64}	2×10^{-2}
k_{15}	5×10^{-4}	k_{40}	2×10^{-3}	k_{65}	9.5
k_{16}	5×10^{-4}	k_{41}	5×10^{-5}	k_{66}	10
k_{17}	2×10^{-3}	k_{42}	1×10^{-4}	k_{67}	5×10^{-3}
k_{18}	5×10^{-4}	k_{43}	5×10^{-4}	k_{68}	5×10^{-2}
k_{19}	5×10^{-3}	k_{44}	5×10^{-4}	k_{69}	8×10^{-4}
k_{20}	5×10^{-4}	k_{45}	5×10^{-5}	k_{70}	6
k_{21}	5×10^{-5}	k_{46}	2.5×10^{-3}	k_{71}	4×10^{-3}
k_{22}	2.5×10^{-2}	k_{47}	2.5×10^{-3}	k_{72}	1×10^{-8}
k_{23}	1.75×10^{-3}	k_{48}	2.5×10^{-3}	k_{73}	7.72×10^{-1}
k_{24}	2.25×10^{-2}	k_{49}	4×10^{-2}	k_{74}	5.56×10^{-2}
k_{25}	1.75×10^{-4}	k_{50}	2.5×10^{-3}	k_{75}	2×10^{-2}

Table 3-4 Initial conditions of the variables in the G1/S model.

Chemical Species	Initial Value	Chemical Species	Initial Value
x_0	3×10^{-2}	x_{14}	0
x_1	1×10^{-3}	x_{15}	0
x_2	4×10^{-5}	x_{16}	0
x_3	5	x_{17}	0
x_4	13.5	x_{18}	1×10^{-3}
x_5	2	x_{19}	1.95
x_6	1×10^{-3}	x_{20}	1×10^{-3}
x_7	1×10^{-3}	x_{21}	0
x_8	4×10^{-4}	x_{22}	1×10^{-2}
x_9	1×10^{-4}	x_{23}	5×10^{-2}
x_{10}	6.3	x_{24}	2.65×10^{-2}
x_{11}	1×10^{-3}	x_{25}	2.35×10^{-4}
x_{12}	1	x_{26}	1×10^{-4}
x_{13}	1×10^{-4}	x_{27}	0

Chapter 4: Computational Methods of Investigation

Robustness of biochemical pathways is crucial to the very existence of healthy cells, and the concept of robustness of living organisms has been discussed in many papers (see Kitano [2007] and Stelling et al. [2004], for example). We define robustness accordingly, as an emergent systemic property related to the ability of a system to sustain functionality amidst internal and external perturbations and uncertainties. Robustness is a broader concept than stability and homeostasis and the robustness of subsystems is essential for homeostasis of the whole system [Kitano, 2007]. Therefore, any investigation into the complex checkpoint pathways as a subsystem for systemic robustness begins with the identification of a performance measure(s) and a limited number of key proteins (biomarkers), as major indicators of the proper functioning of the system, in a biologically meaningful manner. We need to develop measures of performance for the system, which can be monitored as functions of the biomarkers selected. By perturbing the kinetic parameter space associated with the biomarkers and investigating the effects on the performance measures give us information on the robustness of the system. However, this approach is very difficult to implement *in vivo* or *in vitro*, justifying the use of mathematical models for the purpose. In this chapter, we focus on how to develop such an approach based on a mathematical model of the G1/S checkpoint pathway; more specifically, we identify two key biomarkers characterising the G1/S checkpoint. Then, we compute the probability (β) of a DNA–damaged cell passing as a healthy cell in the G1/S phase transition, and define 1-β as a performance measure associated with the G1/S checkpoint pathway, and investigate the β of the G1/S transition in the presence of various levels of perturbations in the key kinetic parameters associated with the model.

4.1 Choice of Biomarkers for G1/S Transition

In general, a biomarker is considered as an indicator of a biological state. Its characteristic is that it can be objectively detected and measured as an indicator of normal biological processes. In regard to the G1/S cell cycle phase transition involving the DNA-damage signal transduction pathway, E2F and CycE are used as our *in silico* biomarkers to analyze the G1/S transition pathway, particularly the peak times (PTs) of E2F and CycE. There are very good reasons, in addition to the ones mentioned in Chapter 3, for choosing the transcription factor

E2F. During the G1/S transition, the target of the activated E2F is to control the regulatory elements of the cell cycle (for example, two critical G1/S gene products are the G1/S Cyclin E, and the S Cyclin, CycA) for the completion of the G1/S progression, as well as to control essential components of the DNA replication machinery (such as dihydrofolate reductase, thymidine kinase and DNA polymerase alpha) involved in the initiation of DNA replication [Iliakis et al., 2003; Obaya & Sedivy, 2002; Ohtani, 1999; Ohtani et al. 1995]. In fact, the activation of E2F is directly regulated by the activity of Rb and indirectly regulated through the action of cyclins and their dependent kinases at the G1/S transition. The accumulation of E2F and CycE activity could be a critical event for making the decision on whether the cells enter into S phase or not [Lukas et al. 1996; Ohtani, 1999; Ohtani et al. 1995]. Taking the DNA-damage signal into account, the oscillation of p53 is an important indicator for the DNA-damage signal; however, p53 is not a significant factor for deciding whether a cell passes the G1/S transition or not. In fact, the p53 activated through the DNA-damage signal can promote the accumulation of p21 as one of the CDK inhibitors, resulting in the arrest of cell cycle progression. With the repair of DNA-damage, a cell re-enters the normal cell cycle progression, as before. However, delay due to repair of DNA-damage causes delays on these chemical species leading to delays in their peak times compared to healthy cells [Iliakis et al., 2003]. Appendix B shows these delays in the behaviour of the key proteins (E2F, CycE, p53, p21 and CycA) in G1/S transition revealed from the mathematical model under different DNA damage situations. The reason for showing the behaviour of CycA is to validate the model results with the experimental findings and the related information will be dicussed in Chapter 5.

4.2 Analytical Method for Investigating the Dynamic Behaviour of G1/S Transition

We have chosen predominant chemical species, such as E2F, CycE and p53, in the G1/S phase under different levels of DNA-damage as *in silico* biomarkers, and the PTs of E2F and CycE as two significant time-based measures to monitor the status of the system under different DNA-damage situations, such as no DNA-damage, low-level DNA-damage and high-level DNA-damage. The release of additional E2F can sequentially promote the synthesis of CycE, CycA and itself, which are essential proteins for the progression to S phase [Ikeda et al., 1996], while the PT of E2F signifies that the cell passes through the restriction point and prepares for the initiation of DNA replication; the PT of CycE usually occurs at the

G1/S transition and CycE is down regulated during the S phase [Keyomarsi and Herliczek, 1997; Reed, 1997]. Local sensitivity analysis (LSA) is used to decide which kinetic parameters are the most significant to the selected key proteins in the G1/S phase under different DNA-damage conditions; global sensitivity analysis (GSA) is used to analyze how these selected significant kinetic parameters from LSA simultaneously regulate these key proteins in the G1/S phase transition under different DNA-damage conditions. Based on the results of GSA, statistical hypothesis testing with Type II error was used to compute β (the probability of a damaged cell passing as a healthy cell). The β will indicate not only the robustness of the checkpoint pathway model but also will lead to biologically meaningful interpretations of the results of the model.

4.2.1 Local Sensitivity Analysis

In LSA, only one kinetic parameter can be varied at a time within a predefined range (the range for all 75 kinetic parameters is from 50% to 150% at 10% intervals, with 100% as the standard condition), and the following criterion was used to evaluate the significance of the changed kinetic parameter (variation):

$$Variation = \frac{(t_{\mathbf{new}}^{\mathbf{max}} - t_{\mathbf{standard}}^{\mathbf{max}}) / t_{\mathbf{standard}}^{\mathbf{max}}}{(k_{\mathbf{new}} - k_{\mathbf{standard}}) / k_{\mathbf{standard}}}, \tag{4-1}$$

where $k_{\mathbf{standard}}$ is the value of the kinetic parameter under the standard conditions, $t_{\mathbf{standard}}^{\mathbf{max}}$ is the value of PT of the protein of interest, employing the standard set of kinetic parameters (SKP), $k_{\mathbf{new}}$ represents the changed value of the kinetic parameter from SKP and $t_{\mathbf{new}}^{\mathbf{max}}$ represents the PT of the protein of interest corresponding to the changed kinetic parameter. The values of SKP are based on the published mathematical model for the G1/S transition in 2008 [Iwamoto et al., 2008]. This study concentrates on the magnitude of *Variation* regardless of whether the variation is positive or negative because high *Variations* indicate significant influence on the protein of interest.

4.2.2 Global Sensitivity Analysis

GSA provides information of the change of output in response to simultaneous variations in parameters. In real biochemical systems, rate constants of biochemical reactions *in vivo* seem to simultaneously vary based on the external environment [Stelling et al., 2004; Rand, 2008]. The characteristic of dependence of biochemical reactions on their rate constants indicates that GSA is suitable and appropriate for sensitivity analysis of biochemical systems and reactions [Rand, 2008]. In this investigation, the whole process of GSA is divided into three main steps:

1. According to the analytical results of LSA, we appropriately choose the most significant kinetic parameters relevant to each of the interested chemical species. We then define the ranges for them to be varied simultaneously while keeping the remaining kinetic parameters constant under the standard conditions. For instance, the number of the most significant kinetic parameters for PT of E2F is 10 under no DNA-damage (normal or healthy cells). Thus, we simultaneously change these 10 parameters in a range and keep the remaining 65 parameters at their SKP levels. The range of the selected parameters is divided into four different levels: reference values $\pm 10\%$; reference values $\pm 20\%$; reference values $\pm 30\%$ and reference values $\pm 50\%$. For example, reference values $\pm 10\%$ means that the parameters are examined within 10% variations of their reference values.

2. We randomly generate samples of parameter vectors for the most sensitive parameters in the defined levels of the range. For an individual range under each individual DNA-damage situation (damage conditions or no damage), 3000 parameter vectors are generated and each parameter vector contains the values for the selected most significant parameters affecting a protein. For instance, if we investigate the change in PT of E2F in response to simultaneous variations in its most significant 10 parameters within a range of $\pm 10\%$ under no DNA damage, each parameters vector contains 10 elements displaying the values for the corresponding significant parameters randomly drawn within the $\pm 10\%$ range. In order to guarantee that each individual parameter can be evenly distributed in the defined range, as well as to ensure that the generated sample parameter vectors are representative of the real variability, Latin Hypercube Sampling (LHS) is used to generate samples of random parameter vectors [McKay et al,. 2000].

3. Once the 3000 sample parameter vectors are generated from LHS, we run the model and record PTs of the *in silico* biomarkers in order to calculate the frequency distribution and then to estimate the corresponding probability density function (PDF) using the Gaussian density function (In this case, we checked several difference density functions, such as Gaussian, Gamma, Beta, Exponential and Lognormal density functions. Results indicate that Gaussian density function is the most suitable for our study). Gaussian density function can be characterised completely by the mean and standard deviation.

4.2.3 Evaluation of β: Statistical Hypothesis Testing with Type II Error

Statistical hypothesis testing is used to determine whether an observed experiment provides conclusive evidence to accept a proposition (which is called a null hypothesis). A Type II error (β) is committed when a researcher fails to reject a null hypothesis that is false. In this investigation, a Type II error indicates the probability that a cell is considered healthy when, in reality, it is affected and damaged. In general, β is used to represent the probability of committing a Type II error, while the power $(1-\beta)$ of the test represents the probability of not committing a Type II error (i.e. damaged cells are declared damaged) [Black, 2007]. There are three main steps in determining the probability of a Type II error (see Figure 4-1):

1. We need to determine the critical value t_{hc} to accurately distinguish healthy cells based on the PDF under no DNA-damage situation. In testing the null hypothesis, this value is used as the boundary to separate the non-rejection region from the rejection region. We accept the null hypothesis when the PT is less than or equal to the critical value, t_{hc}, and rejects the null hypothesis when PT exceeds t_{hc}. The standardized critical value of healthy cells is based on Eq.(4-2):

$$Z_0 = \frac{t_{hc} - \mu_{hc}}{\sigma_{hc}} \tag{4-2}$$

where Z_0 is equal to 1.645 at the 5% level of significance (α), μ_{hc} is the mean and σ_{hc} is the standard deviation of the peak time of the protein of interest, estimated from the PDF of healthy cells (see Section 4.2.2).

2. After determining t_{hc}, the next step is to extend the critical value (t_{hc}) from the PDF of healthy cells to the PDF of damaged cells, which has two different scenarios: low-level DNA-damage and high-level DNA-damage. The purpose of this is to calculate the standard variate Z_1 based on Eq.(4-3) for determining the probability of a Type II error,

$$Z_1 = \frac{t_{hc} - \mu_{dc}}{\sigma_{dc}} \tag{4-3}$$

where μ_{dc} is the mean and σ_{dc} is the standard deviation estimated from the PDF of the damaged cells under different damage levels.

3. The probability of committing a Type II error, β, is the area to the left side of t_{hc} in the PDF of damaged cells (or less than or equal to Z_1 in the standard PDF of damaged cells with zero mean and unit standard deviation) (see Figure 4-1). This probability also indicates how often a cell is considered as healthy when, in fact, it is defective and damaged. This also indicates the proportion of damaged cells passing through the cell cycle as healthy cells.

4.3 Mathematical Definition of Robustness

According to Eq. (2-21), we define the robustness of our system under different perturbations as follows:

$$R = \sum_i \chi(\Delta p_i)(1-\beta_i)|\Delta p_i|, \tag{4-4}$$

where R is robustness of the system (the larger the R, the more robust of the system). $\chi(\Delta p_i)$ is the probability of a particular perturbation occurrence. More importantly, all perturations for the system occur with equal probability. $1-\beta_i$ is used to evaluate the performance measure under a particular perturbation p_i. In this research, it measures whether the G1/S checkpoint does not allow damaged cells passing it as healthy cells against diverse perturbations. For example, there is 30% damaged cells passing the G1/S transition as healthy

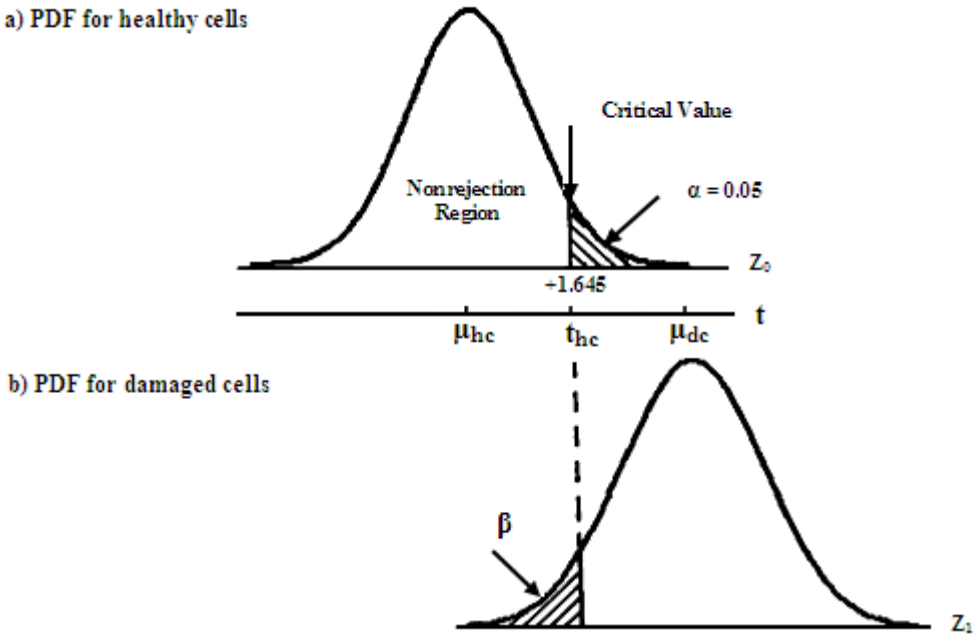

Figure 4-1 Calculating Type II error based on PDF of healthy cells and damaged cells.

cells under a particular parameter perturbation, which indicates that the G1/S checkpoint can only accurately distinguish 70% damaged cells not passing this checkpoint as healthy cells against this particular parameter perturbation. p_i is a perturbation of the i^{th} significant biomarker variable. In our case, we have two biomarker variables -- CycE and E2F (meaning that i is equal to two) -- whose PTs are perturbed. For each biomarker, the total number of perturbations for the system is based on the number of PT perturbations as well as parameter perturbations. The Δp_i represents the difference in PT between the standard and perturbed values of SKP for the i^{th} significant biomarker variable. The Δp_i is obtained for several perturbation occurrences (parameter conditions) for the calculation of robustness.

4.4 Summary

We have presented in this chapter the general framework of computational methods for investigating the robustness and dynamical behavior of G1/S transition in response to DNA-damage situations. We started with the definition of biomarkers (E2F and CycE) in the G1/S checkpoint pathway, and then discussed details of the analytical approach, which includes LSA, GSA, Type II error and the mathematical definition of robustness. The next chapter will make use of this method and apply it to the G1/S checkpoint pathway in detail.

Chapter 5: Robustness and Dynamical Behaviour of G1/S Transition: Analysis, Results and Discussion

As discussed in Chapter 4, an analytical approach has been developed to investigate the robustness and the dynamic behaviours of the G1/S checkpoint pathway. This chapter first shows results from the parameter sensitivity analysis, to identify the significant kinetic parameters associated with the *in silico* biomarkers, based on the mathematical model of the G1/S checkpoint pathway with different levels of DNA-damage. Then, the robustness of the G1/S checkpoint pathway with or without DNA-damage is defined, based on the probability (β) of DNA-damaged cells passing as healthy cells in the presence of various levels of perturbations in the key kinetic parameters of the *in silico* biomarkers associated with the mathematical model. Finally, this chapter also discusses the results from the model and validates the results in comparison with the currently established biology as well as some experimental findings.

5.1 Most Significant Parameters of Biomarkers Revealed by LSA

The six heat maps in Figure 5-1 show results revealed by LSA under three different DNA-damage levels. Figure 5-1 (a) shows the influence of the variations of the 75 kinetic parameters on the peak time of E2F, while Figure 5-1 (b) illustrates results of the PT for CycE. Each heat map contains values for all 75 parameters over the whole parameter range. All parameter are changed within the $\pm 50\%$ range of SKP at 10% intervals. Therefore, there are 10 values corresponding to each parameter, and each heat map contains 750 (75×10) small squares. The blue colour in the heat map indicates higher variation and the higher significance of the kinetic parameters for the PTs of the biomarkers whereas the white colour indicates lower values of variation and less or no significance of the kinetic parameters for PTs. In this study, we only focused on the magnitude of *Variation* as mentioned in Section 4.2.1. Thus, the white colour in the heat map indicates that the absolute value of *Variation is* less than 0.01. Table 5-1 summarizes the most significant kinetic parameters for PTs of the two chosen biomarkers (E2F and CycE) under normal (no damage) and two different DNA-

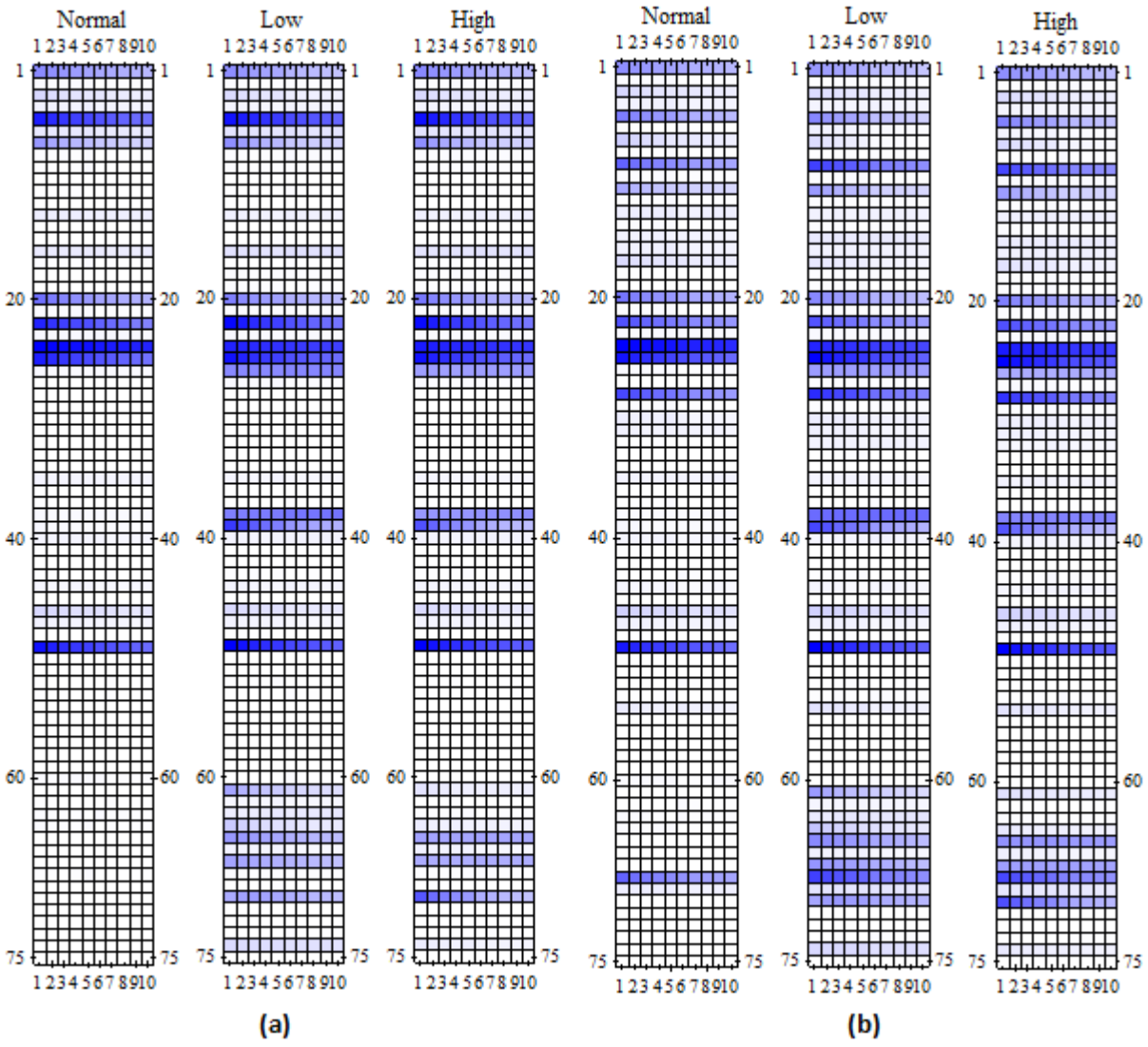

Figure 5-1 Local parameter sensitivity for biomarkers in the G1/S phase transition involving DNA-damage signal transduction pathway: (a) influence of 75 kinetic parameters on PT of E2F; (b) influence of 75 kinetic parameters on PT of CycE (each heat map contains values for all 75 parameters in the defined parameter range from 50% to 150% of SKP at 10% interverals. There are 10 values for each parameter so each heat map has 750 small squares (75×10 **). The numbers (1 to 10) in each heat map indicate the individual parameter change range, for example, 1 means 50% of SKP and 10 means 150% of SKP).**

Table 5-1 The most significant kinetic parameters for PTs of the *in silico* biomarkers (E2F and CycE) revealed by LSA under three different DNA-damage situations. The bottom Venn diagram shows the relationship of the most significant kinetic parameter under no damage and two different DNA-damage situations.

DNA-damage Level	The most significant kinetic parameters	
	PT of E2F	PT of CycE
Normal (No DNA-damage)	k24, k49, k25, k5, k22, k20, k1, k7	k24, k25, k49, k28 k22, k9, k68, k20, k5, k1
Low-Level DNA-damage	k24, k49, k5, k22, k25, k39, k38, k20, k26, k1, k7, k65, k67, k70, k61	k49, k25, k24, k28, k9, k68, k39, k22, k38, k5, k20, k65, k26, k67, k1, k61, k11
High-Level DNA-damage	k24, k49, k5, k25, k22, k39, k70, k20, k1, k7, k38, k26, k65, k67	k24, k49, k25, k28, k9, k68, k22, k70, k39, k20, k5, k38, k1, k65, k67, k11

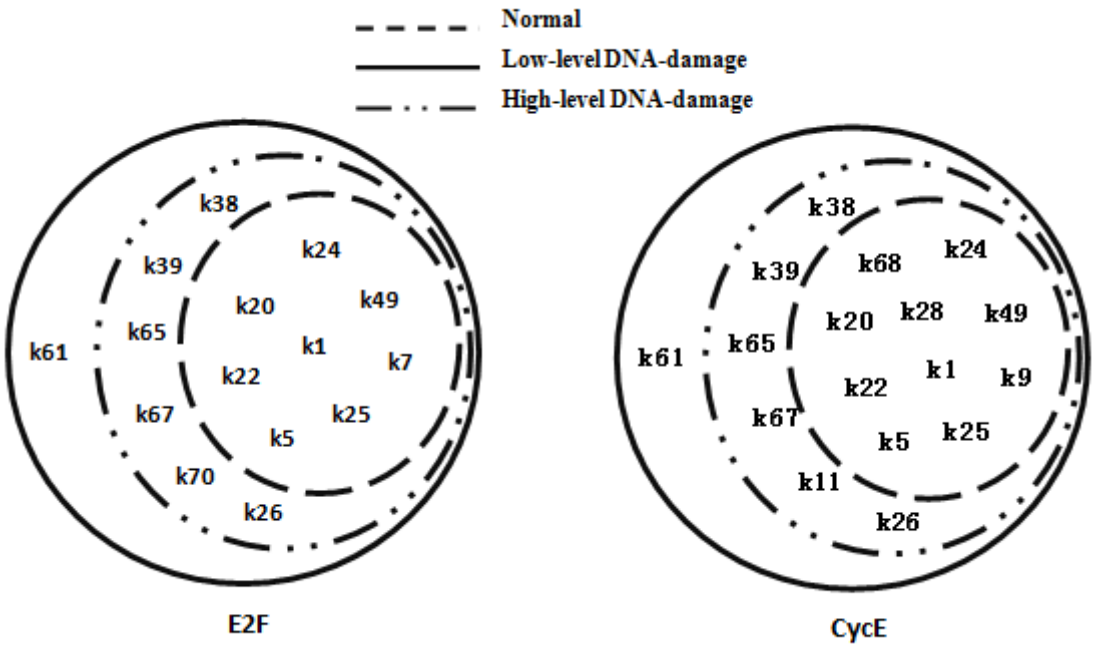

damage situations.

In terms of normal cells (no DNA-damage), the kinetic parameter k24 (association rate of the p27/CycE/CDK2-P complex) has the most critical influence on the PT of E2F, followed by k49 (rate of activation of E2F by CycE/CDK2-P), k25 (dissociation rate of the p27/CycE/CDK2-P complex), k5 (synthesis rate of CycE), k22 (rate of activation of CycE/CDK2-P or phosphorylation rate of CycE/CDK2 to form CycE/CDK2-P), k20 (association rate of p27/CycD/CDK4/6-P), k1(synthesis rate of CycD) and k7 (association rate of CycE/CDK2). For the PT of CycE in normal cells, k24 remains the most important kinetic parameter, followed by k25, k49, k28 (rate of activation of CycA/CDK2-P), k22, k9 (synthesis rate of CycA), k68 (synthesis rate of the intermediary 'X', which achieves the observed delay in PT between CycE and CycA (see Appendix B)), k20, k5 and k1.

According to the above results, it can be seen that the reversible reaction between p27 and CycE/CDK2-P (which corresponds to kinetic parameters k24 and k25) is a critical process in controlling the concentration of E2F, which qualitatively supports the experimental findings: p27-related reactions are important to maintain the stability of the G1/S transition [Bloom and Pagano, 2003; Obaya and Sedivy, 2002; Sherr and Roberts, 1999]. For example, when the rate of association between p27 and CycE/CDK2-P (k24) becomes faster than that of the dissociation of the p27/CycE/CDK2-P complex (k25), this indicates that more free CycE/CDK2-P could bind to p27 resulting in the inhibition of CycE/CDK2-P activity. Once the activity of CycE/CDK2-P is inhibited, it causes a delay in the release of E2F and disrupts the G1/S progression. In contrast, when k25 becomes faster than k24, it shows that the dissociation of the p27/CycE/CDK2-P complex results in the release of more CycE/CDK2-P than the level obtained from using SKP in cells, which promotes the release of E2F through phosphorylating Rb as well as the G1/S progression. Therefore, data analysis reveals that p27 and CycE/CDK2-P are essential to control the activity of E2F in the G1/S phase transition. This is why the remaining significant parameters mostly relate to p27 and CycE/CDK2-P.

The most significant kinetic parameters for PTs of E2F and CycE under low-level and high-level DNA-damage situations are shown in Table 5-1, the results indicate that there are 15 and 14 significant parameters for PT of E2F under the low-level and high-level DNA-damage, respectively. For the PT of CycE under these two different DNA-damage conditions, the

number of the most significant parameters is 17 and 16, respectively. Compared to the normal cell cycle progression, the number of the most significant kinetic parameters has increased for both biomarkers under DNA-damage situations. However, the most significant kinetic parameters for normal cells still remain at the two different DNA-damage levels.

The increase in kinetic parameters for the DNA-damage situation is mainly related to p21 as well as the negative feedback loop between p53 and Mdm2, such as k26 (association rate of p21/CycE/CDK2-P), k38 (rate of synthesis of p21 through p53), k39 (degradation rate of p21), k61 (synthesis rate of p53 through the DNA-damage signal), k65 (dissociation constant in the Hill function), k67 (degradation rate of the intermediary 'I', which is an unknown mechanism leading to a possible discrepancy between the activation of p53 and the induction of Mdm2) and k70 (rate of the sequence-specific DNA binding activity of p53 caused by DNA-damage signal [Lev Bar-Or et al. 2000]). Thus, in response to DNA damage, p53 is activated by the DNA-damage signal. The activated p53 promotes the synthesis of p21 that plays a critical role in inhibiting the activity of CycE/CDK2-P, which results in delay in the release of E2F and retards the cell cycle progression into the S phase. This observation is in good agreement with the experimental findings [Dulic et al. 1994].

As mentioned in Chapter 3, p53 has different functions for the low-level and high-level DNA-damage. Therefore, we further investigate the influence of the kinetic parameters related to p21 (k26, k38 and k39) on PTs of E2F and CycE for these two different intensities of DNA-damage (see Figure 5-2). According to results shown in Figure 5-2, the kinetic parameters related to p21 become a little less sensitive to the high-level DNA-damage than to the low-level DNA-damage. Although the values of *variation* for these three kinetic parameters do not look very different for the low- and the high-levels of DNA-damage (Figure 5-2), there is a 19 to 25% decrease in the rate of *variation* for these three kinetic parameters for the high-level DNA-damage compared to the low-level DNA-damage. This result is in good agreement with the experimental findings and the biological theory that the synthesis of p21 is mainly enhanced and induced after the low-level DNA-damage [Li and Ho, 1998]. Its purpose is to induce cell cycle arrest and provide enough time for DNA repair before reactivating the cell cycle progression. For the high-level DNA-damage, the apoptosis pathway is triggered to maintain the fidelity of the genome of cells [Ciliberto et al., 2005; Geva-Zatorsky et al., 2006; Lahav, 2004; Li and Ho, 1998]; therefore, high levels of p21, as needed in the low-level DNA-damage, are not required. According to the results obtained from the mathematical

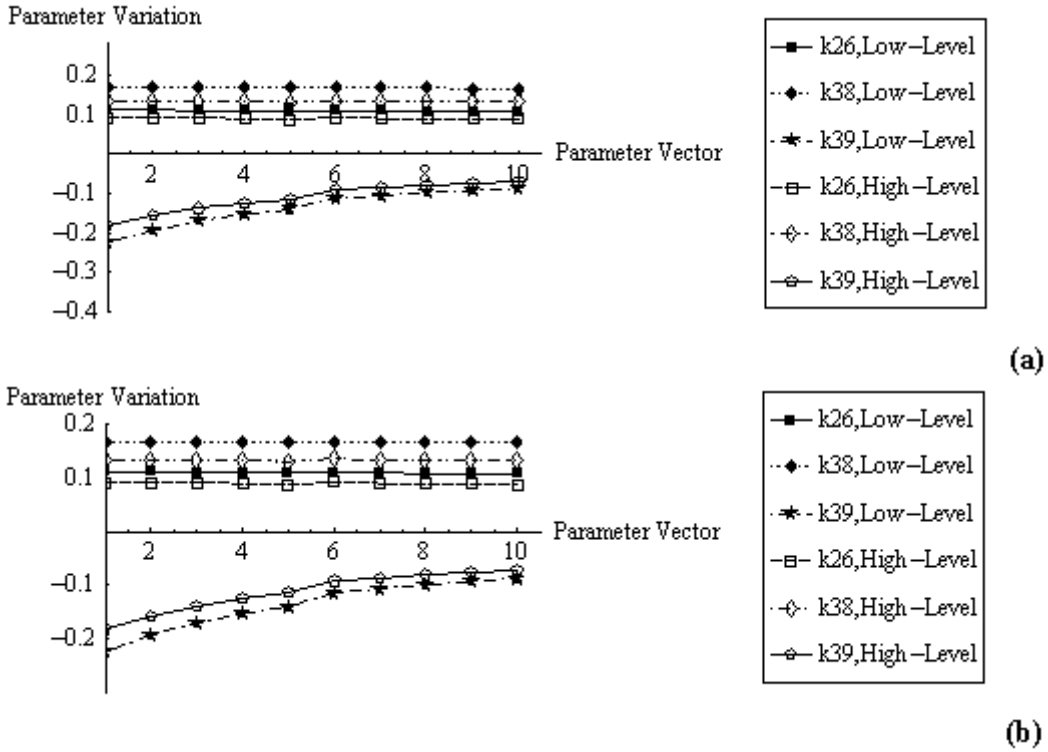

Figure 5-2 The influence of the kinetic parameters related to p21 on *in silico* biomarkers in the G1/S phase transition involving the DNA-damage signal transduction pathway: (a) *influence on PT of E2F*; (b) *influence on PT of CycE* (the vertical axes display the variation in the kinetic parameter related to p21, the horizontal axes shows the parameter vector (one parameter change range, such as 50% of SKP, is regarded as one parameter vector. There are 10 parameter vectors corresponding to the defined range, from 50% to 150% of SKP at 10% intervals, and the legend displays the related kinetic parameters under two different DNA-damage conditions).

model, the maximum level of p21 for the low- and high-levels of DNA-damage, based on the SKP, are 1.856 and 1.488, respectively. This indicates that there is a significant decrease (nearly 20%) in the maximum level of p21 for the high-level DNA-damage compared to the low-level DNA-damage.

According to results revealed from the LSA of the developed mathematicalmodel, it can be seen that the developed model reveals the cell cycle arrest in response to DNA-damage situations as well as the slight difference in the behaviour of p21 with the low-level and high-level DNA-damage. This means that it is possible to analyze the effects of different intensities of DNA-damage on G1/S transition based on the developed mathematical model.

5.2 Analysis of Type II Error Based on GSA

In this section, significant parameters obtained from LSA for E2F and CycE are varied simultaneously to study the effect on PTs. Figure 5-3 illustrates the PDF of PT for E2F with no DNA-damage and low DNA-damage under the four defined levels of the 8 and 15 significant parameters: reference values $\pm 10\%$; reference values $\pm 20\%$; reference values $\pm 30\%$ and reference values $\pm 50\%$, respectively. The PDF of PT of E2F with no DNA-damage and high DNA-damage situation is displayed in Figure 5-4. In Figures 5-3 and 5-4, the red line is the critical value in testing the null hypothesis, which is used as the boundary separating the non-rejection region from the rejection region in the PDF of PT for E2F with no DNA-damage.

For the PDF with no DNA- damage, the area left of the red line is the non-rejection region while the area right of it is the rejection region. We focus on the area in the PDF of PT for E2F with the low-level and high-level DNA-damage, which falls within the non-rejection region of normal cells. Furthermore, this area represents the probability of committing a Type II error, β. According to Figures 5-3 and 5-4, it can be seen that the value of β increases with the level of parameter range. Moreover, the value of β with the high-level DNA-damage is slightly larger than that for the low-level DNA-damage for the same level of parameter change (the differences in probability, based on the PDF of PT for E2F between the low-level and high-level DNA-damage for the four levels of ascending parameter change, are 0.025, 0.147, 0.113 and 0.05, respectively (see Table 5-2)).

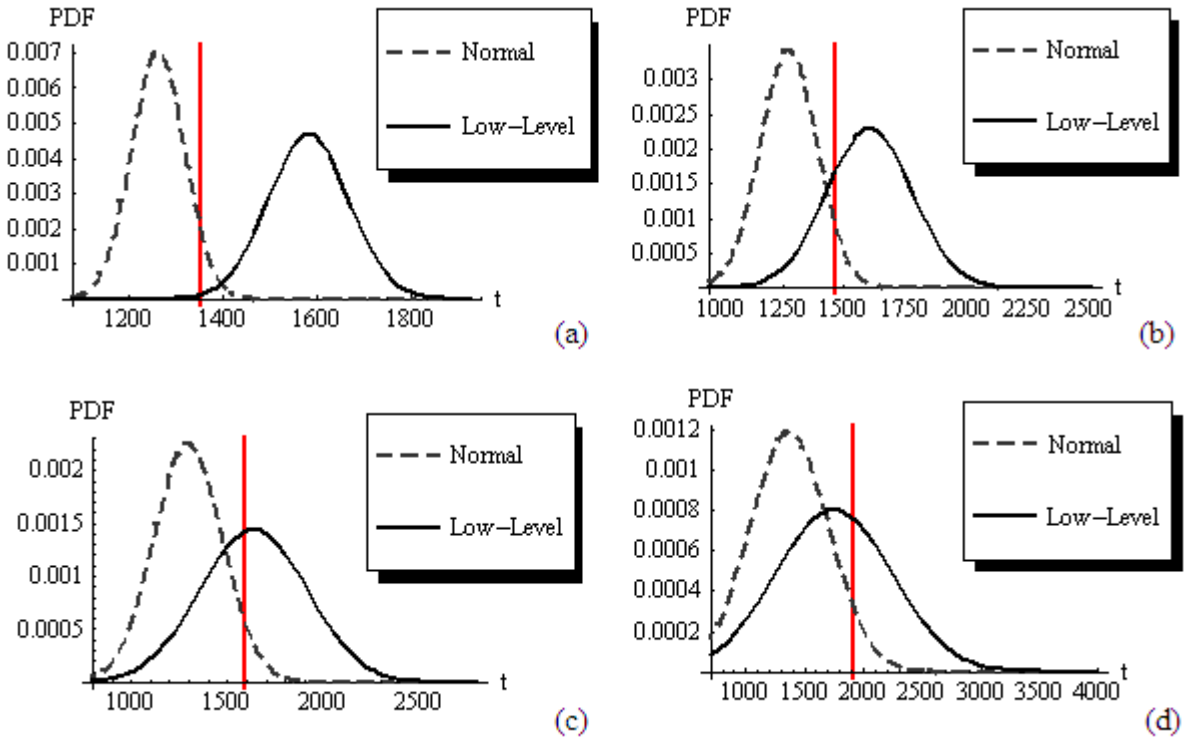

Figure 5-3 The PDF of PT for E2F with no DNA-damage (normal or healthy cells) and the low-level DNA-damage under the four defined levels of parameter range: (a) reference values $\pm 10\%$, (b) reference values $\pm 20\%$, (c) reference values $\pm 30\%$, and (d) reference values $\pm 50\%$.

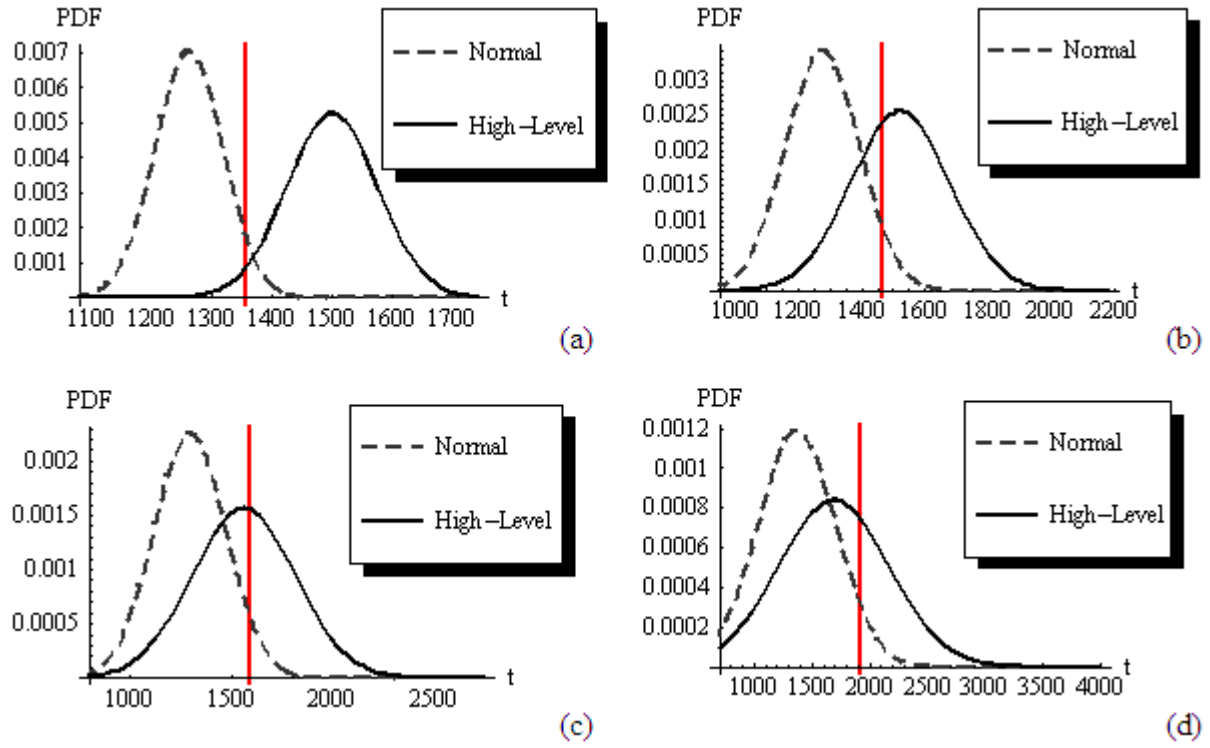

Figure 5-4 The PDF of PT for E2F with no DNA-damage (normal or healthy cells) and the high-level DNA-damage under the four defined levels of parameter range: (a) reference values $\pm 10\%$, (b) reference values $\pm 20\%$, (c) reference values $\pm 30\%$, and (d) reference values $\pm 50\%$.

Table 5-2 The probability of committing a Type II error (β) based on the PDF of the PTs for E2F and CycE in response to simultaneous variations of the most sensitive parameters under different DNA-damage situations (The β could indicate how often a cell is wrongly considered as healthy when, in fact, it is defective and damaged).

Parameter range	β (probability of a damaged cell passing as a healthy cell)			
	Low-level DNA-damage		High-level DNA-damage	
	E2F	CycE	E2F	CycE
Reference values ±10%	0.004	0.001	0.029	0.01
Reference values ±20%	0.218	0.147	0.365	0.272
Reference values ±30%	0.429	0.386	0.542	0.504
Reference values ±50%	0.639	0.574	0.689	0.658

Figures 5-5 and 5-6 show the PDF of PT for CycE with no DNA-damage and DNA-damage situations (the low-level and high-level DNA-damage, respectively) under the same parameter ranges. According to the results from the behaviour of CycE, there is the same trend as for the behaviour of E2F. This indicates that the probability of committing a Type II error, β, increases when the level of parameter range increases. Furthermore, the probability of damaged cells passing as healthy cells under the high-level DNA-damage is a little larger than that under the low-level DNA-damage. The differences in β, calculated on the PDF of PT for CycE for these two different DNA-damage situations for the four parameter perturbation levels, are 0.009, 0.125, 0.118 and 0.084, respectively (see Table 5-2). In these figures, the horizontal axes show PT of the chosen biomarker in terms of timesteps. According to the experimental findings reported by Ohtsubo et al. [1995], the time lag between the expression of CycE and CycA in normal cells is about 9.5 hours. We also analysed the PT of CycA (see Appendix B) from our model to calculate model-time to real-time, and validate the observed PTs. In our model, there are about 1250 timesteps between the PTs of CycE and CycA under no DNA-damage situation. Thus, one hour in real time might correspond to 131.6 time steps in the developed model. Based on results revealed by the proposed model for no DNA-damage condition, this indicates that the PTs for CycE and CycA are calculated as 12.3 hours and 21.82 hours real time, respectively. These PTs for CycE and CycA have a good agreement with experimental observations in Ohtsubo et al. [1995] where CycE and CycA reach their peak levels at 12-16 hours and 20-24 hours, respectively, after the initiation of G1 progression.

A summary of the probability of committing a Type II error based on the PDF of PT for E2F and CycE, in response to simultaneous variations of the most sensitive parameters, is shown in Table 5-2. The reason for the investigation of PTs of the chosen biomarkers under different ranges of parameter values is that living cells display heterogeneity; moreover, even the same cell can show completely different properties under different external environmental conditions. By changing parameters, we study the behaviour of a realistic cell population. As shown in Table 5-2, the value of β based on E2F is very low when the parameters are examined within the range of $\pm 10\%$. It seems that we can accurately distinguish healthy cells from defective/damaged cells when simultaneous parameter variations are within a range of $\pm 10\%$. For the change of parameter within a range of $\pm 20\%$, the value of β for E2F is 0.218 for the low-level DNA-damage and 0.365 for the high-level DNA-damage, respectively. This indicates that there is a low risk of wrongly identifying damaged cells as

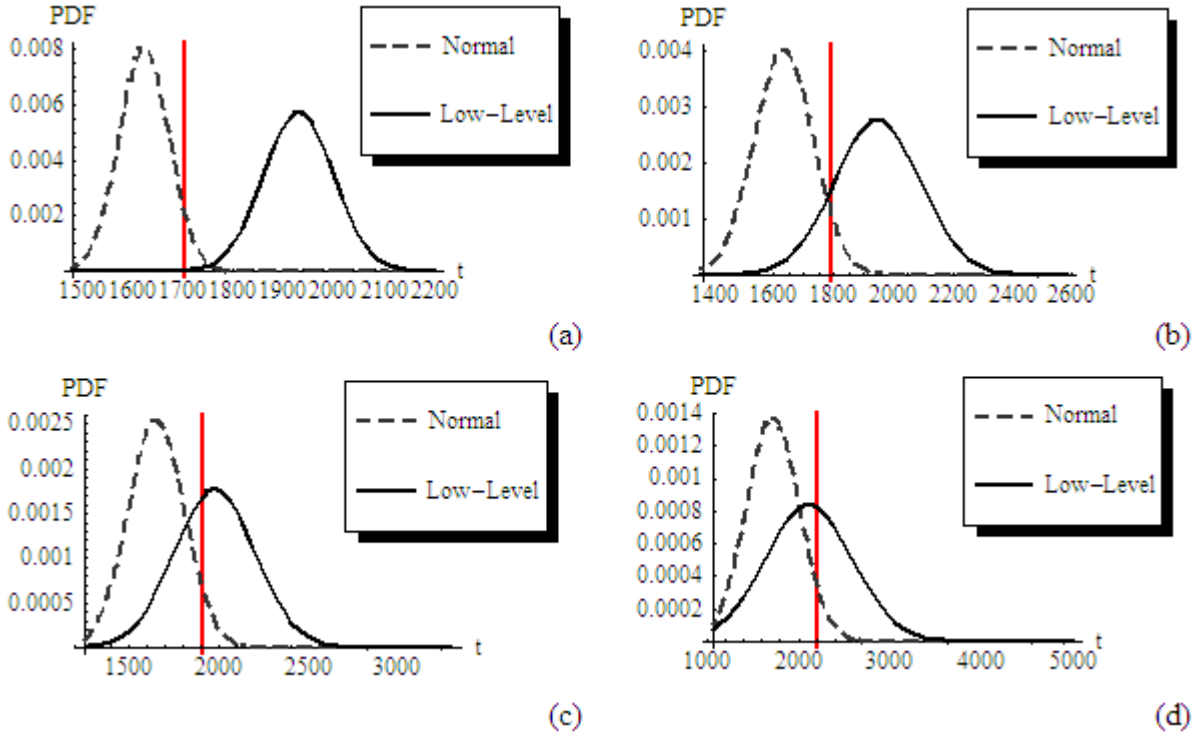

Figure 5-5 The PDF of PT for CycE with no DNA-damage (normal or healthy cells) and the low-level DNA-damage under the four defined levels of parameter range: (a) reference values $\pm 10\%$, (b) reference values $\pm 20\%$, (c) reference values $\pm 30\%$, and (d) reference values $\pm 50\%$.

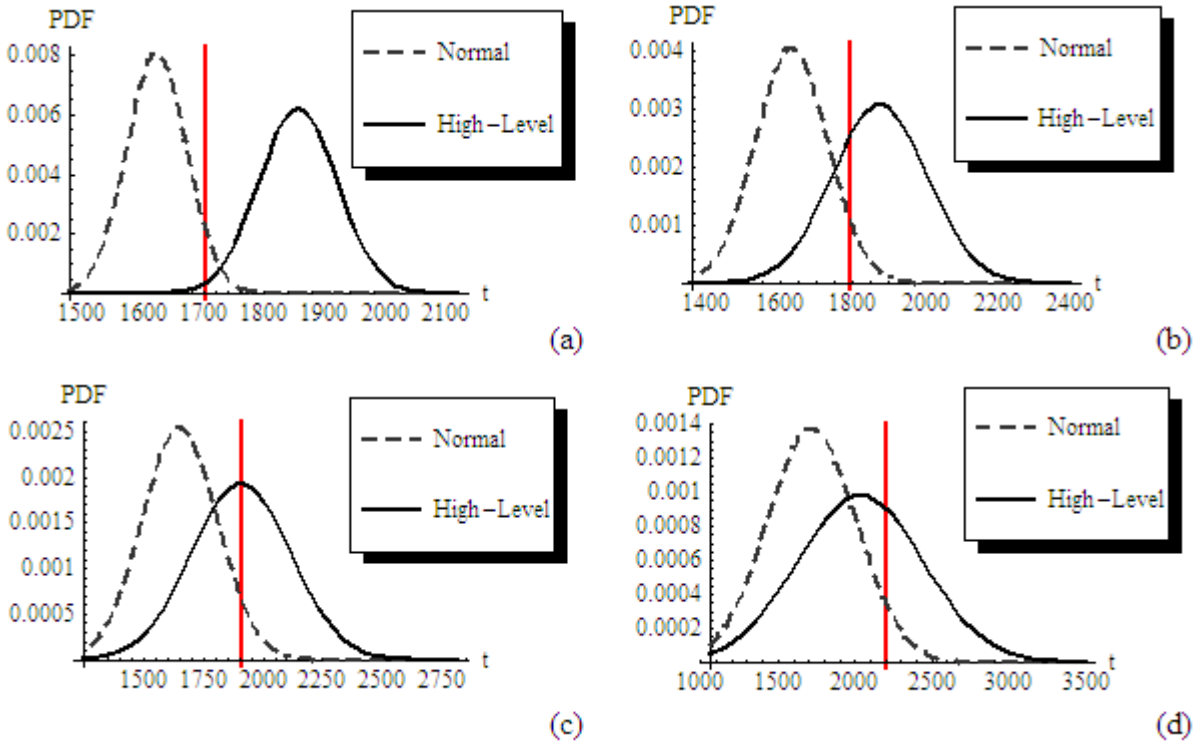

Figure 5-6 The PDF of PT for CycE with no DNA-damage (normal or healthy cells) and the high-level DNA-damage under the four defined levels of parameter range: (a) reference values $\pm 10\%$, (b) reference values $\pm 20\%$, (c) reference values $\pm 30\%$, and (d) reference values $\pm 50\%$.

healthy and letting the defective and abnormal genome of cells pass through the cell cycle progression to future cellular generations, which can potentially result in cancer. However, when the level of change in parameters exceeds $\pm 20\%$ the results reveal that it is very difficult to distinguish between normal cells and defective cells because β ranges from 0.429 to 0.689. For the healthy cell, the overexpression or underexpression of some significant chemical species due to the large variation in significant parameters have a significant influence on the PTs of E2F and CycE in the G1/S transition. For instance, the overexpressions of CycE can accelerate E2F accumulation as well as entry into S phase while the underexpession of CycE can delay E2F accumulation as well as S phase entry. Therefore, the range of PTs for E2F becomes much larger for the larger variation in parameters. In addition, the same situation also happens for the DNA-damage conditions, which results in more overlapping of PDFs of PTs under normal and DNA-damage conditions and indicates that β becomes large with the increase of parameter ranges.

Table 5-2 also shows the value of β based on the PDF of the PT for CycE under different DNA damage conditions. The β based on the PDF of the PT for CycE is a little smaller ($\Delta\beta$ in the range of 0.003 and 0.065) for the two damage levels than that based on PT of E2F except in the range of $\pm 20\%$. With regard to the range of $\pm 20\%$, differences in the probability based on the PTs of these two proteins under two different DNA-damage levels are 0.071 and 0.093, respectively. However, there is a good agreement between the two biomarkers in terms of a large percentage of damaged cells that pass the G1/S checkpoint when the variation of parameters equals or exceeds $\pm 30\%$.

We also evaluated the probability of committing a Type II error based on the PDF of the PTs for E2F and CycE in response to simultaneous variations in all the 75 parameters under different DNA-damage situations as shown in Table 5-3. Comparison of results from these two different sample parameter vectors reveals that the values of β based on the PDF of the PTs of E2F and CycE are quite similar to each other. This indicates that simultaneous variations of the most significant kinetic parameters play an important role in influencing the behaviour of the PTs of E2F and CycE and simultaneous variations in the kinetic parameters that are not relevant to E2F and CycE have less or no significance for PTs. As a result, all sample parameter vectors in GSA for all our investigations are generated based on the most sensitive parameters to calculate the probability of committing a Type II error (β).

Table 5-3 The probability of committing a Type II error (β) based on the PDF of the PTs for E2F and CycE in response to simultaneous variations of all 75 parameters under different DNA-damage situations (The β could indicate how often a cell is wrongly considered as healthy when, in fact, it is defective and damaged).

Parameter range	β (probability of a damaged cell passing as a healthy cell)			
	Low-level DNA-damage		High-level DNA-damage	
	E2F	CycE	E2F	CycE
Reference values ±10%	0.004	0.001	0.029	0.01
Reference values ±20%	0.22	0.164	0.362	0.3
Reference values ±30%	0.433	0.388	0.546	0.507
Reference values ±50%	0.623	0.568	0.682	0.633

From what has been discussed above, the simulation results indicate that the probability of a damaged cell wrongly passing as a healthy cell becomes much larger (more than 0.38) when the level of parameter change exceeds ±20%. Thus, over 38% of cells with DNA-damage pass as normal cells is a very large percentage. However, this finding has support by the experimental observation. It is estimated that each gene in an organism is mutated once in 20,000 cells [Vijg and Dollé, 2002]. Considering that an organism consists of trillions of cells, there are probably millions of cells that are oncogenically primed at any given time. These dangerous cells are disposed of through apoptosis and cellular senescence. Cellular senescence is a robust inhibition of cell proliferation in response to oncogenic stress such as DNA damage. However, Collado and Serrano [2010] state that this irreversible process happens not in the pre-tumoral stage (initial proliferation of cells carrying oncogenes) but in the pre-malignant tissue where a non-invasive tumour is formed. This shows that a large number of damaged cells undergo proliferation without being caught at DNA damage checkpoints. Our simulation results, in terms of a large percentage of damaged cells that pass the G1/S checkpoint, agree with this finding.

5.3 Robustness of the G1/S Checkpoint Pathway

5.3.1 Analysis of Robustness with Respect to Different Thresholds of Biomarkers

In general, the PTs of proteins are the focus of most research studies. This can be used as an indicator robustness of the G1/S checkpoint. Specifically, it can be proposed that if the G1/S pathway is resistant to variations in PT (within limits) of key proteins, then it is robust in managing the cell entry into S. Therefore, we perturbed PT within a range in an effort to quantify the robustness of G1/S checkpoint. Specifically, we calculate the values of β for four different thresholds of PT for the two biomarkers (E2F and CycE) under the given parameter perturbation regimes for different DNA-damage situations. Table 5-4 shows the value of β based on the PDF of E2F under different DNA-damage conditions for four different thresholds; for example, PT-20%, PT-10%, PT+10% and PT+20%, respectively. It can be seen that the results from different thresholds are quite similar to each other and also agree with the findings based on the PDF of PT (orignal) for E2F. Table 5-5 displays the value of β based on the PDF for CycE four different thresholds of PT under different DNA-

Table 5-4 The probability of committing a Type II error (β) based on the PDF of four different thresholds of PT, such as, PT-20%, PT-10%, PT+10% and PT+20%, using the behaviour of E2F under different DNA-damage conditions (The β indicates how often a cell is wrongly considered as healthy when, in fact, it is defective and damaged).

Parameter range	β (probability of a damaged cell passing as a healthy cell)									
	Low-level DNA-damage					High-level DNA-damage				
	PT-20%	PT-10%	PT	PT+10%	PT+20%	PT-20%	PT-10%	PT	PT+10%	PT+20%
Reference Values ± 10%	0.0041	0.0039	0.004	0.004	0.004	0.03	0.029	0.029	0.03	0.029
Reference Values ± 20%	0.219	0.218	0.218	0.219	0.219	0.365	0.367	0.365	0.366	0.365
Reference Values ± 30%	0.428	0.430	0.429	0.455	0.431	0.541	0.543	0.542	0.543	0.543
Reference Values ± 50%	0.638	0.639	0.639	0.639	0.639	0.689	0.689	0.689	0.689	0.689

Table 5-5 The probability of committing a Type II error (β) based on the PDF of four different thresholds of PT, such as, PT-20%, PT-10%, PT+10% and PT+20%, based on the behaviour of CycE under different DNA-damage conditions (The β indicates how often a cell is wrongly considered as healthy when, in fact, it is defective and damaged).

Parameter range	β (probability of a damaged cell passing as a healthy cell)									
	Low-level DNA-damage					High-level DNA-damage				
	PT-20%	PT-10%	PT	PT+10%	PT+20%	PT-20%	PT-10%	PT	PT+10%	PT+20%
Reference Values ± 10%	0.001	0.001	0.001	0.0003	0.0006	0.0096	0.009	0.01	0.009	0.0095
Reference Values ± 20%	0.15	0.15	0.147	0.15	0.15	0.276	0.276	0.272	0.277	0.274
Reference Values ± 30%	0.387	0.386	0.386	0.384	0.385	0.505	0.506	0.504	0.5	0.505
Reference Values ± 50%	0.575	0.575	0.574	0.574	0.574	0.658	0.658	0.658	0.657	0.658

damage conditions. Results revealed that the probabilities of committing a Type II error are exactly same for different thresholds for the two damage conditions. According to results for the two biomarkers, it can be seen that β is not affected by the changes in PT up to $\pm 20\%$, indicating the robustness of the G1/S checkpoint in the presence of various levels of perturbations in the key kinetic parameters associated with the model.

5.3.2 Analysis of Robustness Based on its Mathematical Definition

As the changes in threshold values of the PTs would not change β_i significantly (Tables 5-4 and 5-5), we ignore the variations in PT. Therefore, we assume that the probability of a perturbation is equally likely (i.e. $\chi(\Delta p_i) = 1/\mathrm{n}$) and n represents the number of perturbations in four different thresholds of PT in response to four differen levels of variations in parameters under normal and DNA-damage situations (it means that n equals to 16). According to the mathematical definition of robustness in Section 4.3, robustness for healthy cells ($\beta = 0$ for normal cells in this case), the cells with the low-level and the high-level DNA-damage, are shown in Figure 5-7. As a result of the activation of the signalling pathways in the presence of DNA-damage to different degrees, the robustness of the G1/S checkpoint pathway decreases, as expected.

5.4 Summary

In this chapter, we demonstrated the functional influence of the most significant biochemical parameters on the PTs of the critical proteins (E2F and CycE) in the G1/S transition with different intensities of DNA-damage signals. The results from LSA verified the consistency of the analysis with the current knowledge of biology and the experimental observations, which helped us better understand the mechanism of the G1/S transition involving the DNA-damage signal.

The LSA of the model was used to clarify the influence of individual kinetic parameters in the model on the PTs of the selected two important key proteins in the G1/S transition and the response of cells to different intensities of DNA-damage. According to the LSA, kinetic parameters related to p27 (such as k24, k25 and k20) and CycE (such as k49 and k22) played

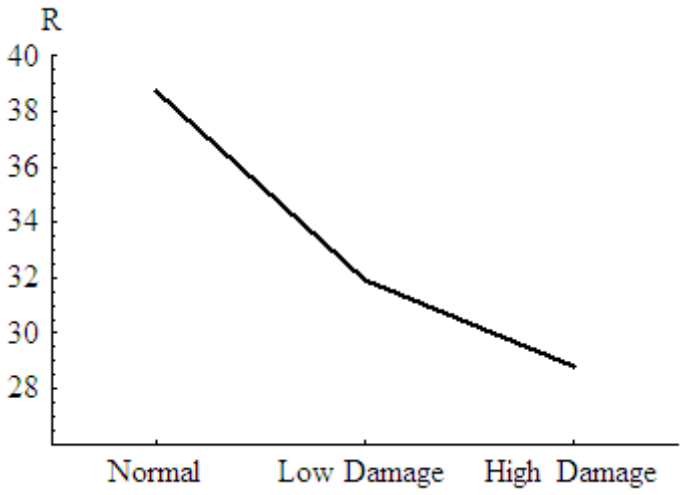

Figure 5-7 Robustness of the G1/S checkpoint pathway.

a significant role in affecting the PTs for E2F with no DNA-damage, while the influence of the PTs for CycE involved some additional kinetic parameters related to CycA (such as k28, k9 and k68). The reason for these observations was that the release of additional E2F depended mainly on the hyperphosphorylation of Rb-PP/E2F through the activation CycE/CDK2-P in the G1/S transition and p27, as CDK inhibitor, controlled the activity of CycE/CDK2. Moreover, the release of E2F promoted the synthesis of CycE and CycA.Considering the case of DNA- damage, the kinetic parameters related to p21 (such as k26, k38, and k39) and p53 (such as k61, k65 and k67) became more important than normal cells. All these parameters revealed how the DNA-damage signal was involved in the G1/S transition: once DNA-damage occurred, the DNA damage signal promoted the activation of p53, which resulted in the synthesis of p21 as a critical factor to retard cell cycle progression in the G1/S phase through binding to CycE/CDK2-P and CycA/CDK2-P and delaying the release of the activation of E2F.

The results from the GSA, based on four defined levels of parameter range, revealed that when there is a ±10% variation in parameters within the cell population, only a small percentage (less than 2.9%) of damaged cells pass as healthy cells and we can accurately distinguish most healthy cells from defective cells. However, when the variation of parameters equals or exceeds ±30%, over 38% damaged cells can pass cell cycle as normal cells. Provided that there are probably millions of cells oncogenically primed at any given time, these dangerous cells are disposed of through apoptosis and cellular senescence. However, the very recent experimental findings [Serrano, 2010] stated that the irreversible process of senescence happened not in the pre-tumoral stage but in the pre-malignant tissue where a non-invasive tumour was formed. This revealed that a large number of damaged cells undergo proliferation without being caught at DNA damage checkpoints. Our simulation results, in terms of the large percentage of damaged cells that pass the G1/S checkpoint, agreed with this possibility and opened a new avenue to continue our research with the mathematical model to explore its ability to shed light on senescence.

Chapter 6: Investigation of Cellular Senescence through The Mathematical Model of G1/S Transition

We revealed that the results obtained from the proposed model have a good agreement with the experimental findings and the biological theory based on our analytical approach in the previous chapter, indicating that the proposed model can reveal the behaviour of the G1/S phase. We also mentioned that damaged cells are caught through activation of cellular senescence in the pre-malignant tissue where a non-invasive tumour is formed. Furthermore, some current experimental evidence pointed out that the inhibition of some critical factors in the G1/S phase can lower the bar for triggering cellular senescence in cancerous cells. Therefore, it was of interest to find out whether the mathematical model can highlight cellular senescence and formulate scenarios for adjusting the threshold for senescence to evaluate its efficacy and outcomes in tems of its ability to prevent damaged cells from passing the G1/S checkpoint. In this chapter, we begin with a definition of cellular senescence. Then, we discuss how to use the mathematical model of G1/S transition to highlight cellular senescence under DNA damage situations, more specifically; we compute the probability of a DNA-damaged cell passing the G1/S phase transitions in response to lowering the threshold for senescence. Finally, we investigated the possibility of lowering the bar for triggering cellular senescence in cells based on the model's analytical results.

6.1 Cellular Senescence

Cellular senescence is considered to be an irreversible state of cell cycle arrest whereby a normal cell loses the ability to divide and promote cell proliferation. This phenomenon was first described by Hayflick and Moorhead [1961] more than five decades ago. They showed that normal cells entered an irreversible state of cell growth arrest in response to the uncontrolled proliferative capacity of normal cells. According to our current knowledge of the cell cycle, cellular senescence is a physiological mechanism employed by cells for thwarting the proliferation of cancer cells, and Serrano [2010] aptly points out that "Encouraging cancer-prone cells to senesce (before reaching pre-tumoral or pre-malignant stages) might therefore be a way to nip this disease in the bud".

Serrano [2010] states that cancer progresses in three stages beyond the healthy stage: pre-tumour, pre-malignant and malignant, where the transition from one stage to the next was generally accompanied by increased levels of senescence induced stresses. He points out that most human and mouse tumour cells, however, stop proliferating and undergo senescence at the pre-malignant stage, where a non-invasive tumour is formed, indicating that it is at this level that senescence inducing stresses reach sufficient intensity to be effective. This also suggests that once allowed through the cell cycle, many of the cells carrying oncogenes are allowed to further proliferate in the pre-tumoral stage – the first stage of tumorigenesis- with little or no senescence. Moreover, mutations that disable senescence are instrumental in the transition from oncogene-harbouring cells to the malignant stage, highlighting the importance of senescence in countering malignancy. Summarising the work of Lin et al. [2010] and Campaner et al. [2010] who elucidate the molecular mechanism of cancer associated senescence, Serrano [2010] emphasises the clinical relevance of lowering the bar for senescence in curing cancer and raises hopes for, and questions about, possibilities for doing it so that oncogenically primed cells are targeted early, before reaching the pre-malignant stage, as happens normally. Considering the prevalence of cancer today, manipulating the threshold for senescence to encourage cancer cells to senescence early can lead to better protection against cancer. Thus, a deeper understanding of the pathway to cellular senescence plays an important role in exploiting this route for effective cancer treatment.

Both Lin et al. [2010] and Campaner et al. [2010] found that the inhibition of the activity of cyclin-dependent kinases (CDKs), such as CDK4, CDK6 and CDK2, played a significant role in establishing cellular senescence in order to protect cells against cancer, particularly in inhibiting CDK2's activity as a critical factor in lowering the bar for triggering senescence in cancerous cells. All these CDKs are important proteins that mediate the initiation of the G1 phase and control the G1/S transition in the cell cycle. They also mentioned that senescence-inducing stressors inhibit the activity of CDKs by controlling their inhibitory proteins (called CDK inhibitory kinases or CKIs), which include p21, p27 and p16 [Collado et al. 2007, Malumbres & Barbcid, 2009]. Furthermore, Skp2 inhibition might be critical in lowering the bar for senescence in oncogenically primed cells based on the current studies [Serrano, 2010, Lin et al., 2010, Campaner et al., 2010]. Skp2 can mediate the degradation of some CKIs, such as p21 and p27, and Skp2 inhibition can increase the expression of CKIs in the cell cycle which results in inhibiting the activity of CDK2s.

6.2 Analytical Method for Investigating Cellular Senescence Based on the Mathematical Model

Although there is some experimental evidence pointing out that the inhibition of CDK2 or Skp2 can be the critical trigger for senescence, currently, there are no any mathematical models developed to highlight cellular senescence under DNA-damage situations. Senescence in this respect leads to an exciting question: Can a mathematical model highlight cellular senescence and formulate scenarios for adjusting the threshold for senescence to evaluate its efficacy and outcomes for controlling proliferation? This investigation is presented in the following pages.

In this study, the mathematical model developed is used to investigate the behaviour of PTs for the chosen biomarkers (E2F and CycE) of the G1/S transition in response to CDK2-deficient situations. The purpose is to confirm whether the developed model can highlight cellular senescence in response to lowering the critical point (CDK2 inhibition) for cellular senescence. We use the same method as described in Chapter 4. We keep the parameter sets in Table 5-1, only reducing CDK2 in three different levels (for example, CDK2-10%, CDK2-30% and CDK2-50%, respectively) under two DNA-damage situations (low-level and high-level DNA-damage) and calculate β of a DNA-damaged cell passing the G1/S transition. We then compare the values of β under the normal CDK2 level and low CDK2 levels. If β decreases with decreasing levels of CDK2, our model can represent the phenomenon attributed to cellular senescence and supports the hypothesis that lowering CDK2 is an effective means of promoting senescence in damaged/cancerous cells.

Next, we interrogate the model to investigate whether it represents and supports the relationship between CDK2 and CKIs: the increasing expression of CKIs is an effective way to inhibit the activity of CDK2 under senescence-inducing stressors [Lin et al., 2010, Campaner et al., 2010]. There are two different ways to validate the relationship between CDK2 and its CKIs under DNA-damage situations using the mathematical model: one is to focus on what the behaviour of CKIs, such as p16, p21 and p27, is in response to reducing CDK2 levels; the other is to focus on the behaviour of CDK2 in response to increasing the expression of its CKIs by adjusting their corresponding kinetic parameters in the mathematical model in relation to: initial condition, production rate and degradation rate. We

also study the effectiveness of simultaneously changing CDK2 and CKIs in lowering the senescence bar.

Finally, we investigate the robustness of CDK2 in lowering the bar for cellular senescence through two different approaches: one is to analyze the values of β for different thresholds, and the other is based on the mathematical definition of robustness from Section 4.3.

6.3 Analysis of the Effectiveness of CDK2 in Lowering the Bar for Cellular Senescence

Table 6-1 summarizes the probability β of damaged cells passing the G1/S checkpoint based on the PDF of the PTs for biomarker E2F under two different DNA-damage conditions for three reduced CDK2 levels: -10%, -30% and -50%, respectively. Table 6-2 displays the values of β for the three decreased CDK2 levels based on the PDF of PT for CycE under two different DNA-damage conditions. According to the results of the behaviour of E2F and CycE under reduced and normal CDK2 levels, the probability of committing a Type II error (probability of a damaged cell passing the G1/S transition) decreased with the inhibiting activity of CDK2; more importantly, there is a significant decrease in β based on the PTs for E2F and CycE when the CDK2 level is reduced to 50% of the normal level.

According to Table 5-2, under normal CDK2 level, the percentage of tumour cells passing the G1/S transition increases with the level of DNA-damage and the range of parameters, both biomarkers indicate similar trends for β. For example, when the level of DNA-damage is high, E2F and CycE indicate that 68.9% and 65.8%, respectively, of damaged cells pass the G1/S for ±50% perturbation to the key parameters. In contrast, Table 6-1 indicates that for the same damage conditions and parameter ranges, this percentage, based on E2F, can be reduced to 42.2% by decreasing the CDK2 levels by 50%. This amounts to a reduction of 38.8%. For the low-level DNA-damage, lowering CDK2 by 50% amounts to a 42.7% reduction in damaged cells passing the G1/S transition. The trend observed above is confirmed by the trends in PDF of PT for CycE in Table 6-2. Here, a 50% reduction of CDK2 level under a high-level DNA-damage situation results in a 64.59% reduction in the percentage of damaged cells passing the G1/S transition. For the low-level DNA-damage, a

Table 6-1 The probability β of a damaged cell passing the G1/S checkpoint based on the PDF of PT for E2F for three reduced CDK2 levels: CDK2-10%, CDK2-30% and CDK2-50%, under two DNA-damage conditions (The β indicates the level of activation of senescence and corresponding effect on how often a damaged cell passes G1/S).

Parameter range	β (probability of a damaged cell passing G1/S checkpoint)					
	Low-level DNA-damage			High-level DNA-damage		
	CDK2-10%	CDK2-30%	CDK2-50%	CDK2-10%	CDK2-30%	CDK2-50%
Reference values ± 10%	0.0018	0.0002	0	0.015	0.0019	0
Reference values ± 20%	0.178	0.097	0.034	0.311	0.185	0.064
Reference values ± 30%	0.39	0.287	0.159	0.5	0.389	0.229
Reference values ± 50%	0.606	0.515	0.366	0.66	0.574	0.422

Table 6-2 The probability of β of damaged cells passing the G1/S checkpoint based on the PDF of PT for CycE for three reduced CDK2 levels: -10%, -30% and -50%, under two DNA-damage conditions (The β indicates the level of activation of senescence and corresponding effect on how often a damaged cell passes G1/S) .

Parameter range	β (probability of a damaged cell passing G1/S checkpoint)					
	Low-level DNA-damage			High-level DNA-damage		
	CDK2-10%	CDK2-30%	CDK2-50%	CDK2-10%	CDK2-30%	CDK2-50%
Reference values ± 10%	0.00005	0	0	0.0013	0	0
Reference values ± 20%	0.085	0.0166	0.0032	0.172	0.033	0.0037
Reference values ± 30%	0.302	0.141	0.0453	0.411	0.202	0.059
Reference values ± 50%	0.5136	0.362	0.203	0.57	0.413	0.233

50% reduction of CDK2 produces a 64.63% reduction in the percentage of damaged cells passing the G1/S checkpoint. These results indicate the possibility that the damaged cells enter an irreversible state of cell cycle arrest, such as cellular senescence or apoptosis, in response to low CDK2 levels, which is consistent with Campaner et al. [2010] who show that mice deficient in CDK2 became more sensitized to cellular senescence under the oncogenic stress caused by the Myc oncogene or oncoprotein. Thus, our model supports the biological findings that relate CDK to senescence. More importantly, it reveals the effect of reducing CDK2 levels in terms of the reduction in the percentage of damaged cells passing the G1/S checkpoint; i.e., the effectiveness of lowering CDK2 in thwarting proliferation.

6.4 Analysis of the Effectiveness of CKIs in Lowering the Bar for Senescence

6.4.1 Behaviour of CKIs in Response to Reducing CDK2 Levels

Here, we investigate the behaviour of CKIs in response to reduced CDK2 levels, by reducing CDK2 in three different levels under two different DNA-damage conditions; for example, CDK2-10%, CDK2-30% and CDK2-50%, respectively. Analytical results show that the change of CDK2 has little or no effect on p16 and p27 at either the low-level or the high-level DNA-damage. The reason is that most p27 molecules bind to the CycD/CDK4/6 complex at the beginning of the G1 phase and only a few p27 molecules bind to the CycE/CDK2-P complex near the G1/S transition. However, variation in CDK2 has a significant effect on p21 level in these two DNA-damage situations. In the event of DNA-damage, p21 is activated by p53 which results in a dramatic effect on the concentration required to promote its binding to the CycE/CDK2-P complex for arresting cell cycle. Figure 6-1 shows the behaviour of p21 for four levels of CDK2 under the low- and high-levels of DNA-damage as well as p21's behaviour in healthy cells. It shows that the p21 level under damage conditions is much higher than that under no DNA damage (healthy cell) due to an increase in production in response to DNA damage. Furthermore, the p21 level in the high-level DNA damage is lower than that in the low-level DNA damage (20-25% difference between the maximum levels) because p53 is used to trigger the apoptosis pathway for high-level DNA damage. Under both DNA damage conditions, the effect of lowering CDK2 is initially insignificant on the p21 level, which remains constant until closer to the G1/S transition (at around 1500 time steps – about 11.36 hours- in Figure 6-1), for all four CDK2 levels. Then, the reduced CDK2

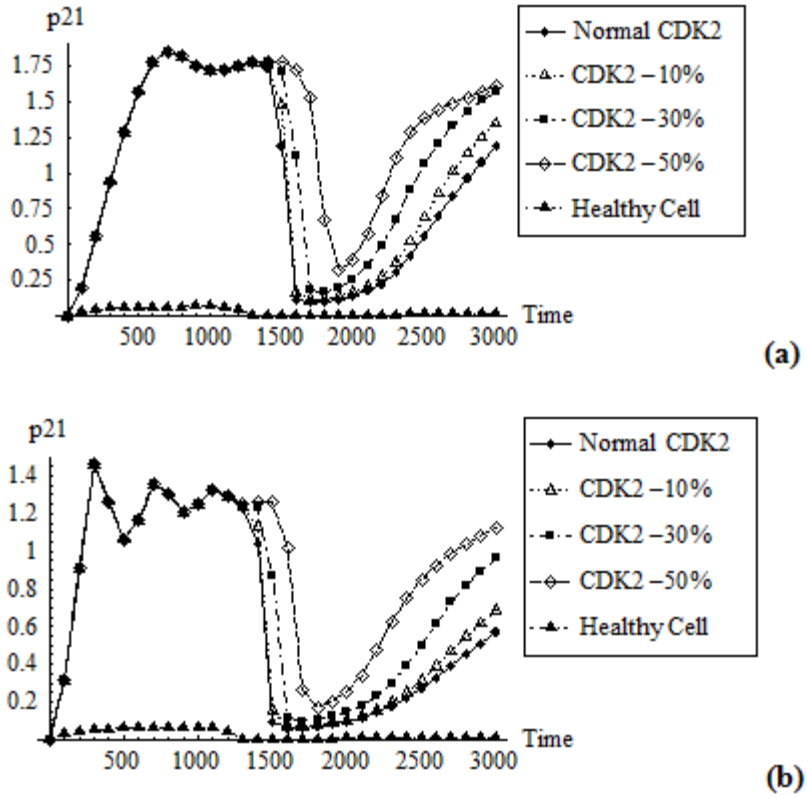

Figure 6-1 The behaviour of p21 in response to four different CDK2 levels for (a) low-level DNA-damage and (b) high-level DNA-damage (For reference purposes, p21 level for no DNA-damage under normal CDK2 level (healthy cell) is also shown in the figure). The p21 level in the high-level DNA damage is lower than that in the low-level DNA damage (20-25% difference between the maximum levels) because p53 is used to trigger the apoptosis pathway for high-level DNA damage.

level comes into effect influencing the behaviour of p21. Increasing CycE production in the cell cycle requires increasing level of CDK2 for binding to CycE to form the CycE/CDK2 complex and this complex can further associate with p21 to form the triple complex, p21/CycE/CDK2. This process results in a dramatic decrease in the p21 level; however, the p21 level increases at the end of the G1 phase because the CycE level decreases in the S phase thereby releasing more p21 in the cell cycle transition. Reducing CDK2 levels results in the production of less CycE/CDK2 to associate with p21 thereby increasing the concentration of p21. For this reason, the p21 level in the cell cycle is the highest for a 50% reduction in CDK2 levels compared to the two smaller reductions.

6.4.2 Behaviour of CDK2 in Response to Increasing Expression of its CKIs

Now we turn to investigating the behaviour of CDK2 in response to increased levels of its CKIs. First we analyze the effect of the **degradation rate of CKIs** on the CDK2 concentration by decreasing their corresponding kinetic parameters in the mathematical model. According to our model results, presented in Figure 6-2, there is an effect from adjusting the degradation rate of p21 on the variation of CDK2 for DNA-damage situations. However, variation in the degradation rate of p27 and p16 has little or no effect on CDK2 levels under these two DNA-damage conditions (not shown). Based on the study of the behaviour of CDK2 in response to the reduced degradation rate of p21, as shown in Figure 6-2, the influence of the degradation rate of p21 on CDK2 is dominant during the G1/S transition. The reason is that the concentration of CDK2 is mainly controlled by CycE in the G1/S transition. For example, at the beginning of G1 in the cell cycle of a healthy cell, the CycE level is kept at a low level which keeps CDK2 and CycE in balance. However, the concentration of CycE significantly increases during G1/S transition, which results in an imbalance between CycE and CDK2; therefore, more CDK2 is required to associate with CycE. In the DNA-damage situation, however, p21 is activated in the G1 phase and plays an important role in reducing CDK2 levels. The reason is that increased p21 binds to the CycE/CDK2 complex to inhibit E2F, which in turn inhibits CycE levels, leading to a delayed and slower production of CycE under damage conditions compared to the healthy condition. This reduces the need for as high CDK2 levels as in the healthy condition. Therefore, lower p21 degradation rates lead to higher CDK2 levels, as indicated by Figure 6-2. Higher levels of free CDK2 indicate the presence of low CycE levels giving rise to further delays in the

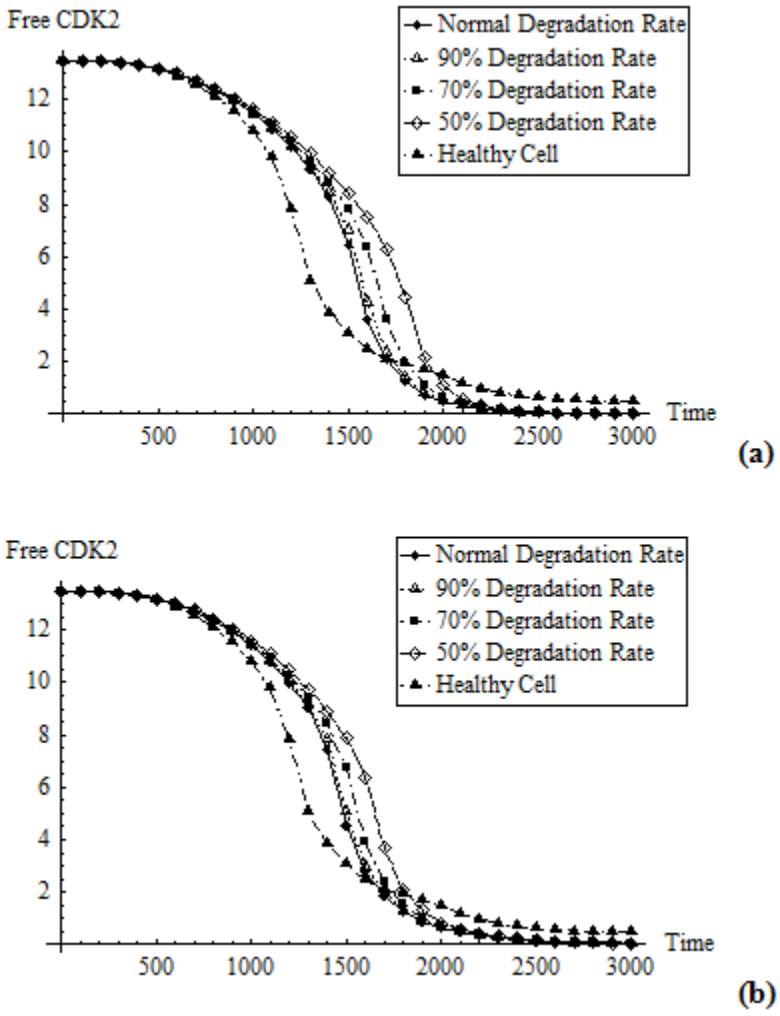

Figure 6-2 The behaviour of CDK2 in response to the variation in the degradation rate of p21 for (a) low-level DNA-damage and (b) high-level DNA-damage (For reference purposes, CDK2 level for no DNA-damage under normal degradation rate of p21 (healthy cells) is also shown in the figure).

progression of these cells through the G1/S transition. According to Figure 6-2, there is a small difference in free CDK2 levels between the low-level and high-level DNA damage conditions. Although there is a significant difference in the amount of p21 in the two different DNA-damage situations shown in Figure 6-1, only part of p21 can bind to CycE/CDK2-P or CycA/CDK2-P to control free CDK2 in cells because the increased CycE/CDK2-P and CycA/CDK2-P can promote the degradation of p27. The p27 degradation can cause the release of more free CycD/CDK4/6 which binds to p21 to form p21/CycD/CDK4/6. Therefore, CycD/CDK4/6 competes with these two complex proteins (CycE/CDK2-P and CycA/CDK2-P) to bind with p21 in cells. This is the reason for smaller difference in CDK2 levels between the two damage conditions.

Next, we focus on the effect of **production rate of CKIs** on CDK2 levels. Results revealed by the mathematical model show that the production rate of CKIs has little or no effect on the CDK2 concentration for low-level and high-level DNA damage situations (not shown). Finally, **the initial conditions of CKIs** are used to analyze their relationship to CDK2. The analytical results show that only the initial condition of p27 has a significant effect on the variation of CDK2 under DNA damage situations as shown in Figure 6-3. According to Figure 6-3, variation in the initial condition of p27 has a more significant effect on CDK2 behaviour than that caused by variation in the degradation rate of p21, as shown in Figure 6-2. The increased initial concentration of p27 makes available more free p27 for binding with the CycE/CDK-P complex to inhibit its activity after p27 associates with CycD/CDK4/6 during the G1 phase. This inhibites the activation of E2F, the critical protein in G1/S which, in turn, inhibits the accumulation of CycE required for the completion of the G1/S progression. Inhibition of CycE also decreases the rate of CDK2 in response to increased initial concentration of p27. Thus, CDK2 can be lowered by adjusting the initial conditions of p27 to trigger early senescence. Thus, analysis of the CKIs reveals that the initial level of p27 and the degradation rate of p21 affect significantly CDK2 and can be targets for lowering the senescence bar.

According to the investigation of the effect of CKIs on the behaviour of CDK2 under two different DNA-damage situations from the model's simulation, results indicates that the degradation rate of p21and the initial rate of p27 contribute to inhibiting the activation of CDK2 in cells. These results qualitatively support the experimental findings and the biological theory that p21 and p27 as cell cycle Cip/Kip inhibitors prevent cell cycle

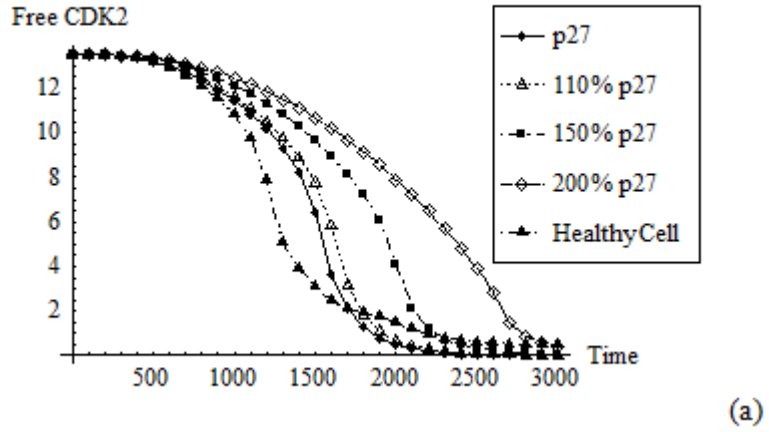

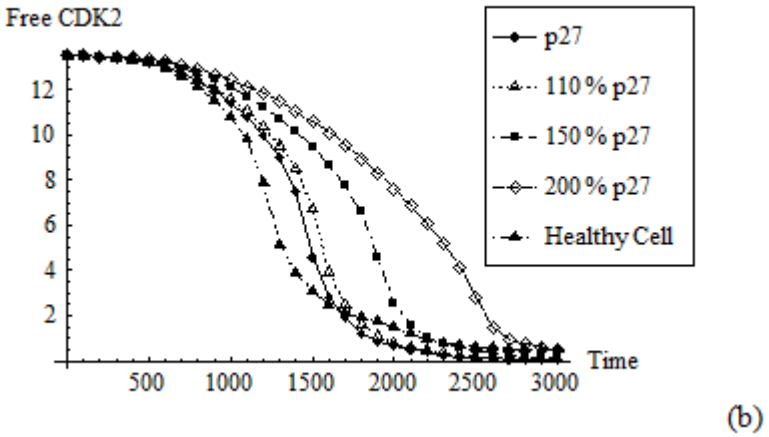

Figure 6-3 The behaviour of CDK2 in response to the variation in the initial condition of p27 for (a) low-level DNA-damage and (b) high-level DNA-damage (For reference purposes, CDK2 level for no DNA-damage under normal initial condition of p27 (healthy cells) is also shown in Figure 6-3).

progression and suppress tumour growth by inhibiting the activation of CycE/CDK2 and CycA/CDK2 to regulate the level of CDK2 in cells [Sherr and Roberts, 1999; Obaya and Sedivy, 2002; Denicourt and Dowdy, 2004]. Additionally and importantly, an advantage of the model is that it reveals the spectrum of the behaviour of CDK2 as it relates to varying levels of p21 and p27 in the whole region of G1/S transition.

6.4.3 Analysis of the Effectiveness of CKIs Alone and Simultaneous Variation of CDK2/CKIs on Lowering the Senescence Bar

Relying on the outcome of the analysis of the relationship between CDK2 and CKIs, the focus of this step in our research is to analyze the percentage of damaged cells that can be prevented from passing G1/S by further lowering the senescence threshold through regulating the CKIs and the combination of CDK2 and CKIs. The value of β, in response to individually changing CDK2 or CKIs (in our case, p21 degradation rate and p27 initial condition) based on the behaviour of E2F for a parameter range of ±30% , is shown in Figure 6-4, which reveals that the increase in the initial condition of p27 makes the most significant contribution to reducing the probability of a damaged cell passing the G1/S for two different DNA-damage situations, followed by the reduced CDK2 levels and the decreased p21 degradation rate, with the differences between the latter two being minor. Comparing the 30% change of CDK2 or CKIs with their 50% counterpart, the results show that a 50% change in CDK2 or CKIs can reduce a larger percentage of damaged cells passing G1/S. In terms of values of β based on the behaviour of CycE for parameter range ±30% (see Figure 6-5), we obtain similar results to those revealed by the behaviour of E2F, except that the reduction in CDK2 level makes a larger contribution to decreasing the percentage of damaged cells passing the G1/S checkpoint than increases in the initial condition of p27. These simulation results, in response to the effectiveness of CKIs alone, are in good agreement with the experimental findings that Skp2 inactivation that leads to oncogenic-stress-driven senescence critically depends on p27, p21 and Atf4 [Lin et al., 2010]. Lin et al. [2010] pointed out that upregulation of p27, p21 or Atf 4 contributes to promoting cellular senescence upon Skp2 inactivation. Furthermore, Lin et al. (2010) found that the concomitant upregulation of p27, p21 and Atf4 can be considered as a required powerful engine to trigger cellular senescence under the Skp2 deficiency situation. The most important advantage of modelling is that, while supporting the above biological findings, the model simulations allow us to ascertain and quantify the reduction in the

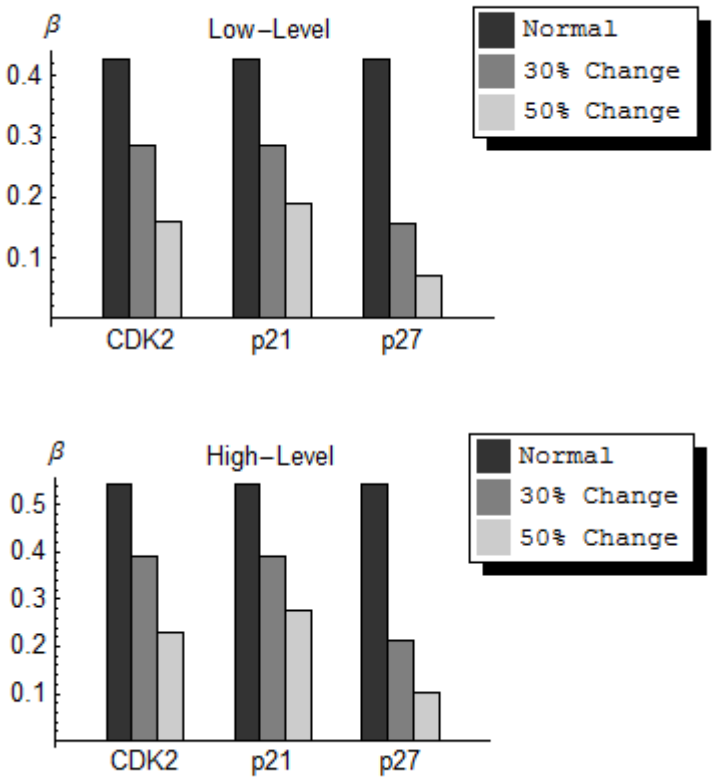

Figure 6-4 The probability β of a damaged cell passing the G1/S checkpoint in response to only changing CDK2 or CKIs (i.e. p21 degradation rate and p27 initial condition) for three different ranges of normal, 30% and 50% (i.e., CKD2 or p21 degradation rate reduced or p27 initial condition increased by 0%, 30% and 50%, respectively - using the behavior of E2F for parameter range ±30% under different DNA-damage conditions: low level DNA-damage and high level DNA-damage. Results from figure indicates that the increase in initial condition of p27 makes the most significant contribution to reducing β, followed by the reduced CDK2 levels and the decreased p21 degradation rate. Compared to 30% change, a 50% change in CDK2 or CKIs can reduce a larger percentage of damaged cells passing G1/S.

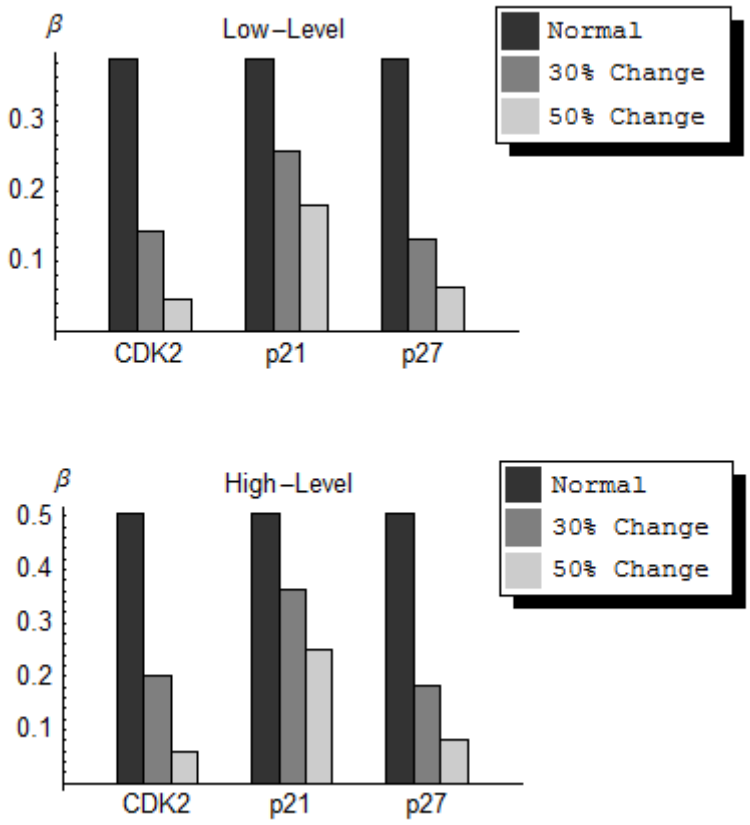

Figure 6-5 The probability β of a damaged cell passing G1/S checkpoint in response to only changing CDK2 or CKIs (i.e. p21 degradation rate and p27 initial condition) for three different ranges of normal, 30% and 50% - specifically, CKD2 or p21 degradation rate reduced or p27 initial condition increased by 0%, 30% and 50%, respectively - using the behavior of CycE for parameter range ±30% under different DNA-damage conditions: low level DNA-damage and high level DNA-damage.

percentage of damaged cell passing the G1/S checkpoint in response to different levels of CKIs.

After analysis of separately changing CDK2 or CKIs, we concentrated on the effect of the combination of CDK2 and CKIs on β for two different change ranges (30% and 50%). For example, simultaneously reducing CDK2 and p21 degradation rates as well as simultaneously reducing CDK2 and increasing p27 initial condition. Figure 6-6 displays the results of the combination of CDK2 and CKIs based on the behaviour of E2F for parameter range ±30%, which indicates that the combination of CDK2 and p27 initial condition makes a much greater reduction in the percentage of damaged cells passing G1/S than the CDK2 and p21 combination. For a 50% change to CDK2 and p27 levels, the percentage of damaged cells passing G1/S is almost equal to zero for the two different DNA-damage situations.

Probing into the G1/S checkpoint pathway can shed light into the above observations, as follows. Taking the characteristics of the G1/S pathway into account, the accumulation of E2F is regulated directly by the activity of Rb and indirectly through the action of cyclins and their dependent kinases (such as CycD/CDK4/6 to initiate the phosphorylation of Rb, CycE/CDK2-P and CycA/CDK2-P to further hypophosphorylate Rb for the release of E2F) at the G1/S transition. The reduction of CDK2 alone can decrease the concentration of CycE/CDK2-P or CycA/CDK2-P in cells to delay the release of E2F under no DNA-damage conditions. In response to CDK2-deficiency in DNA-damage situations, the synthesis of p21, triggered by the DNA-damage signal, further inhibits the activation of CycE/CDK2-P or CycA/CDK2-P and results in a further delay in the activation of E2F.

For the combination of CDK2 and p27 under DNA-damage situations, p21 is already activated by the DNA-damage signal. If the concentration of p27 is kept at the standard level, it further delays the accumulation of E2F, caused by the activated p21. If the concentration of p27 increases, more CycE/CDK2-P and CycA/CDK2-P will be associated with p27, which results in a longer delay in the accumulation of E2F. In terms of the combination of CDK2 and p21, the total concentration of p21 (which is mainly activated by DNA-damage singal) is much less (more than three times less) than that of p27 in cells. Therefore, less CycE/CDK2-P and CycA/CDK2-P are required for binding with p21 compared to p27, which makes the effect of p21 less significant than p27. This is why the combination of CDK2 and p27

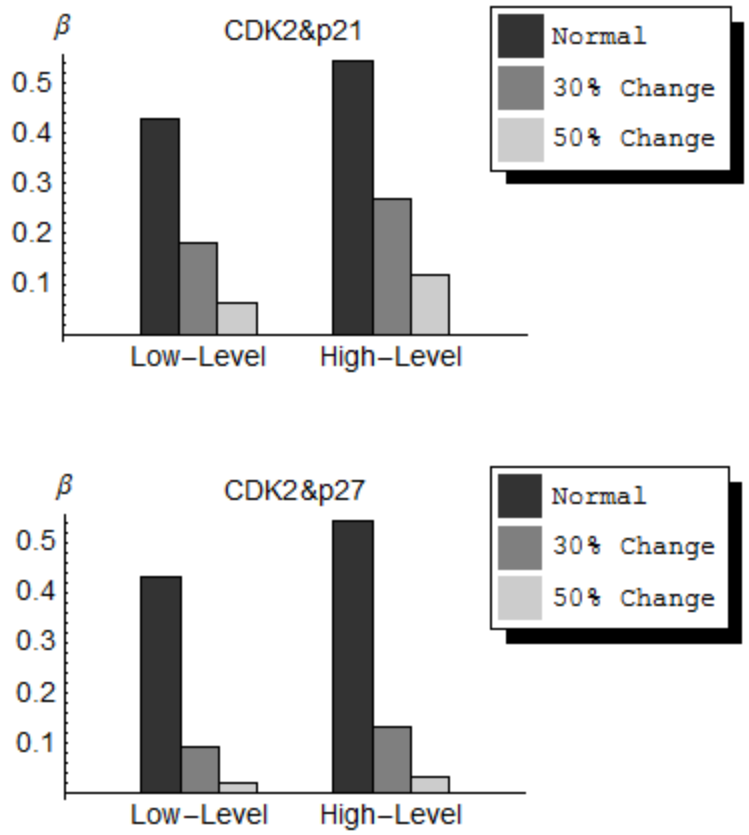

Figure 6-6 The probability β of a damaged cell passing G1/S in response to simultaneously changing CDK2 and CKIs (i.e. p21 degradation rate and p27 initial condition) for three different ranges of normal, 30% and 50% - specifically, CKD2 and p21 degradation rate both reduced by 0%, 30% and 50%, respectively, or CDK2 reduced and p27 initial condition increased by 0%, 30% and 50%, respectively- using the behaviour of E2F for the parameter range ±30% under two different DNA-damage conditions. It can be seen that the combination of CDK2 and p27 makes a much greater reduction in β than the CDK2 and p21 combination. For a 50% change of CDK2 and p27, β is almost equal to zero for both DNA-damage situations.

makes a larger contribution to reducing the percentage of damaged cells passing the G1/S transition. Thus, the combined targeting of CDK2 and key CKIs is a powerful way to lower the senescence bar. As far as we know, the combined effect CDK2 and CKIs has not been studied experimentally. Therefore, the results from our analysis suggest some novel biological experiments for validating the effectiveness of the combined targets in a practical setting. The above observed trend is confirmed by the trends in the PDF of PT for CycE in Figure 6-7. Comparison with the results revealed by the behaviour of E2F (Figure 6-6) indicates that the combination of CDK2 and CKIs has slightly larger effect on CycE than E2F.

We also investigate the values of β in response to changing CDK2 or CKIs alone as well as the combination of CDK2 and CKIs based on biomarkers for a larger parameter range of ±50% to compare with the outcome for ±30% parameter change in the previous analysis. The details of β under parameter range ±50% are shown in Appendix C. Results for the chosen biomarkers under this ±50% situation show a good agreement with results revealed under the parameter range ±30%. The only difference is that the percentage of damaged cells passing G1/S under parameter range ±50% is larger than that under parameter range ±30%. The probable reason is that the variation of parameters in ±50% range makes a more significant effect on PTs of the chosen biomarkers than that in ±30% range. All these results indicate that our model can highlight the possibility of lowering the bar for cellular senescence by regulating CDK2 levels and their corresponding significant CKIs.

6.5 Robustness of CKD2 in Triggering Cellular Senescence

6.5.1 Analysis of Robustness with Respect to Different Thresholds of Biomarkers

We also evaluated the probability (β) of damaged cells passing the G1/S checkpoint for four different thresholds of PT for the activity of the two biomarkers, E2F and CycE (PT ±10% and PT ±20%), under different DNA-damage situations in response to different reduced CDK2 levels. Table 6-3 displays the range of β values based on the PDF for the four different thresholds of PTs for E2F under different DNA-damage situations in response to different reduced CDK2 levels. According to Table 6-3, the results for the different thresholds are quite

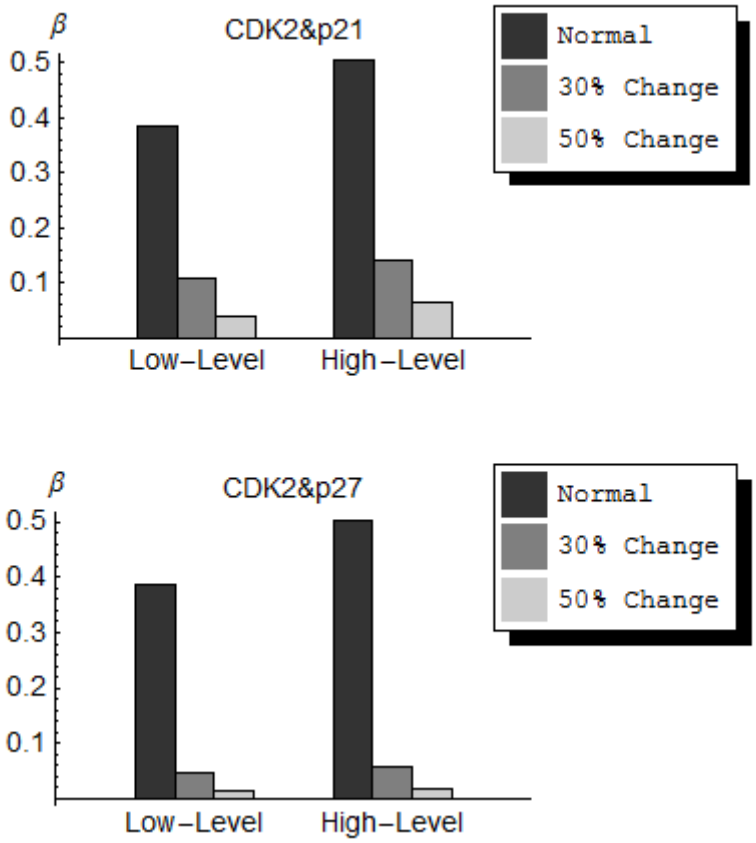

Figure 6-7 The probability β of a damage cell passing G1/S in response to simultaneously changing CDK2 and CKIs (i.e. p21 degradation rate and p27 initial condition) for three different range (normal, 30% and 50%- specifically, CKD2 and p21 degradation rate both reduced by 0%, 30% and 50%, respectively, or CDK2 reduced and p27 initial condition increased by 0%, 30% and 50%, respectively - using the behaviour of CycE for the parameter range ±30% **under two different DNA-damage conditions.**

Table 6-3 The range of the probability (β) of a damaged cell passing G1/S based on the PDF for four different thresholds of PT (PT-20%, PT-10%, PT+10% and PT+20%) for E2F under different DNA-damage conditions in response to three reduced CDK2 levels (The values corresponding to perturbed PT are shown as a range in each entry of the table).

Parameter Range	β (probability of a damaged cell passing G1/S checkpoint)					
	Low-Level DNA-damage			High-Level DNA-damage		
	CDK2-10%	CDK2-30%	CDK2-50%	CDK2-10%	CDK2-30%	CDK2-50%
Reference Values ± 10%	0.0018~0.0019	0.0002	0	0.015~0.016	0.0019~0.002	0
Reference Values ± 20%	0.178~0.18	0.097~0.098	0.035~0.037	0.311~0.312	0.185~0.186	0.064
Reference Values ± 30%	0.39	0.287~0.288	0.159	0.5	0.389~0.39	0.229~0.23
Reference Values ± 50%	0.606	0.515	0.203	0.66	0.413	0.422

similar to each other and similar to the results based on the PDF of PT for E2F in Table 6-1. As for β, for the different thresholds of PT for CycE under different DNA-damage situations and different reduced CDK2 levels, the results in Table 6-4 follow exactly the same trend asshown by E2F, that β is not affected by the perturbation in PT up to ±20%, indicating the robustness in lowering the senescence bar through reduced CDK2.

6.5.2 Analysis of Robustness Based on its Mathematical Definition

Since the changes in threshold values of PTs for the two biomarkers would not change β_i significantly, as shown in Tables 6-3 and 6-4, we ignore the variations in PT. Therefore, we assume that the probability of a perturbation is equally likely (i.e. $\chi(\Delta p_i) = 1/2$). For example, if we have a total of n perturbations, $\chi(\Delta p_i) = \frac{1}{n}$. According to the mathematical definition of the robustness of (Section 4.3), the robustness of CDK2 in triggering cellular senescence under the low-level and high-level DNA-damage situations is shown in Figure 6-8. Results in Figure 6-8 indicate that the robustness of CDK2 in triggering cellular senescence under the low-level DNA-damage situation is slightly higher than that under the high-level DNA-damage situation. This means that a system under the low-level DNA damage is more robust than the high-level DNA-damage in regard to the reduced CDK2 level triggering cellular senescence against various levels of perturbations in the key kinetic parameters associated with the model. For both DNA-damage situations, the robustness of CDK2 in triggering cellular senescence increases as expected with the reduced CDK2 levels.

6.6 Summary

We have demonstrated that the mathematical model incorporating the G1/S checkpoint pathway and DNA damage signal transduction pathway supported the possibility of lowering the bar for cellular senescence. It showed that CDK2 and its CKIs (p21 and p27) can be targets for achieving this. Specifically, by analysing the time to reach the maximum (PT) concentration of E2F and CycE, as two critical proteins in the G1/S transition, we demonstrated that lowering CDK2 levels influences the PT of these critical proteins, which we used to assess the change in the probability of a damaged cell passing the G1/S checkpoint. We then investigated the relationship between CDK2 and its CKIs for the two

Table 6-4 The range of the probability (β) of a damaged cell passing G1/S based on the PDF for four different thresholds of PT (PT-20%, PT-10%, PT+10% and PT+20%) for CycE under different DNA-damage situations in response to three reduced CDK2 levels (The values corresponding to perturbed PT are shown as a range in each entry of the table).

Parameter Range	β (probability of a damaged cell passing G1/S checkpoint)					
	Low-Level DNA-damage			High-Level DNA-damage		
	CDK2-10%	CDK2-30%	CDK2-50%	CDK2-10%	CDK2-30%	CDK2-50%
Reference Values ± 10%	0.00005	0	0	0.0013	0	0
Reference Values ± 20%	0.085~0.087	0.0166~0.0169	0.0032	0.172~0.175	0.034	0.0037~0.0038
Reference Values ± 30%	0.301~0.302	0.14~0.141	0.0453~0.0456	0.41~0.43	0.202~0.203	0.059~0.06
Reference Values ± 50%	0.5137~0.514	0.362	0.203	0.57	0.413~0.414	0.233~0.234

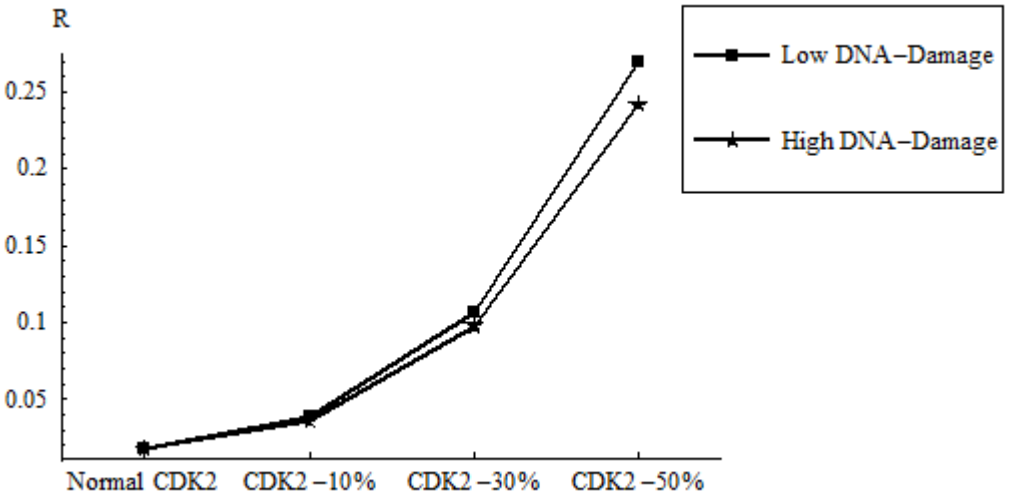

Figure 6-8 Robustness of CDK2 in triggering cellular senescence based on the probability of DNA-damaged cells passing the G1/S checkpoint.

DNA-damage signals as well as the effects of CKIs and the combination of CDK2 and CKIs on the probability of a damaged cell passing the checkpoint.

The results based on the PDF of the PTs for the chosen biomarkers (E2F and CycE) for three reduced CDK2 levels (CDK2-10%, CDK2-30% and CDK2-50%) under two DNA-damage conditions revealed that reducing CDK2 levels can reduce the percentage of damaged cells passing the G1/S checkpoint, indicating that CDK2 can be a target for lowering the threshold for senescence to bring forward the entry of damaged cells into an irreversible state of cell growth arrest and prevent the proliferation of cancerous cells. More specifically, a 50% reduction of CDK2 can cause a 65% reduction in the percentage of damaged cells passing the checkpoint. These results showed that the model can highlight the possibility of lowering the bar for cellular senescence by lowering the CDK2 level.

In the search for other effective ways to bring forward cellular senescence, the model revealed some useful relationships between CDK2 and its CKIs (in terms of production rate, degradation rate and initial conditions) under DNA-damage situations. Specifically, the results revealed that CDK2 has a strong relationship with p21 (degradation rate) and p27 (initial condition). Additionally, the model revealed a spectrum of behaviour for CDK2 in terms of varying levels of p21 and p27 through the whole region of G1/S transition. This gives us some insights into how to further trigger cellular senescence in oncogenically primed cells through targeting these key CKIs individually or in combination with lowered CDK2 levels and reduced degradation rate of p21, and/or increased initial level of p27 before cells start proliferating. Individually, p27 appeared to be more than twice as effective as p21 in resisting damaged cells passing the G1/S, based on the behaviour of both E2F and CycE. The behaviour of the two biomarkers revealed a small discrepancy in the effect of individually varying CDK2 levels in that CDK2 is slightly more effective than even p27 according to CycE, making CDK2 the most effective individual target. Nonetheless, both E2F and CycE showed that the combination of CDK2 and p27 was much more effective than that of CDK2 and p21, with a 50% change in the former arresting almost all damaged cells before they passed G1/S.

In terms of the investigation on the robustness of CDK2 in triggering cellular senescence, results of the values of β for damaged cells passing the G1/S checkpoint for four different

thresholds of PT of the two chosen biomarkers revealed that β was not affected by the changes in PT up to ±20% indicating that CDK2 activity was robust in lowering the senescence bar. According to the mathematical definition of robustness, results revealed that the robustness of CDK2 in lowering the cellular senescence bar increased with reduced CDK2 levels for both DNA-damage situations. However, the robustness of CDK2 in triggering cellular senescence under the low-level DNA-damage was slightly higher than that under the high-level DNA-damage.

The results revealed from the mathematical model were consistent with the current knowledge of biology and experimental observations, and add a detailed view of the efficacy of important targets in lowering the senescence bar. More importantly, the model investigation on the effect of a combination of CDK2 and CKIs on the percentage of damaged cells passing the G1/S transition gave us some ideas to explore a powerful and effective way to further trigger cellular senescence in oncogenically primed cells. Biologists may wish to verify these findings to validate the effectiveness of the targets in a practical setting. We hope that further analysis will help us better understand cellular senescence for exploiting its mechanisms for an effective cancer treatment by lowering its threshold.

Chapter 7: Implementation of Artificial Neural Networks for Representing the P53-Mdm2 Oscillation System

The p53 tumour suppressor protein is a critical protein in cancer studies and the p53-Mdm2 negative feedback loop constitutes the core module for most activities of p53 protein-related networks. Although there are many mathematical models (based on ODEs) to explain and analyze the oscillation phenomena in p53-Mdm2 interaction during the past decade, the common characteristic of these proposed mathematical models for the parameter estimation uses various ODE solver packages from professional software to obtain the appropriate solutions. The ANN technique has never been implemented in parameter estimation for the developed models in biological networks until now. In this chapter, the ANN technique is initially discussed for parameter estimation of four proposed mathematical models (Models III-VI published in Geva-Zatorsky et al. [2006]) for p53-Mdm2 regulation. Then, we evaluate the success of the proposed ANN model by comparing results from the networks with those from the corresponding ODE based models. Finally, we study the behaviour of the p53-Mdm2 oscillation system through the analysis of the robustness of this system (in this case, we only focus on Model VI) using the developed ANN.

7.1 Overview of the P53-Mdm2 Oscillation System

The tumour suppressor protein p53 known as the "guardian of the genome" [Vogelstein et al., 2000] plays an essential role in preserving the integrity of the genome and preventing the development of cancer through transcribing genes which induce cell cycle arrest, mediate DNA damage repair, promote cellular senescence and trigger apoptosis in response to various cellular stresses, such as DNA damage and oncogene activation [Harris and Levine, 2005; Jin and Levine, 2001; Lane, 1992; Toledo and Wahl, 2006; Vogelstein et al. 2000]. More importantly, approximately 50% of all malignancies carry a p53 mutation, and the tumours without the mutated p53 are mainly caused by the inactivated p53 function through a failure in another mechanism [Horn and Vousden, 2007]. Therefore, studies of the p53 system have

attracted the attention of many researchers in biology and life science for three decades [Bourdon et al., 2003].

In the p53 system, the E3 ubiquitin liagase Mdm2 protein is a core player in the regulation of p53. Under normal/unstressed conditions, the p53 protein is kept at low levels primarily through the negative feedback with Mdm2: p53 triggers the synthesis of Mdm2 by activating Mdm2 transcription, while Mdm2 keeps p53 at a stable steady-state concentration by inhibiting p53 activity and promoting p53 ubiquitination and degradation (See Figure 7-1(b)) [Barak et al., 1993; Haupt et al., 1997; Kubbutat et al., 1997; Wu et al., 1993]. Under various cellular stresses, the damage signal involves activation of a protein kinase, ATM, which can directly phosphorylate p53 at Ser15 [Banin et al., 1998]. The ATM also activates Chk2, which results in the phosphorylation of p53 at Ser20 [Hirao et al., 2000]. Both phosphorylated sites of p53 make a significant contribution to its activation and stability. This makes it difficult for the negative feedback loop with Mdm2 to effectively and strictly control the level of p53. The accumulation of p53 in the nucleus activates several stress response programmes which include the arrest of cell cycle progression, DNA damage repair and cellular senescence/apoptosis if repair is impossible (See Figure 7-1 (a)) [Ciliberto et al., 2005; Geva-Zatorsky et al., 2006; Harris and Levine, 2005; Lahav et al., 2004; Li and Ho, 1998]. With the complete removal of DNA-damage, the negative feedback loop of p53 and Mdm2 is fully restored and p53 returns to its low level.

In the past decade, a large number of mathematical models have been developed for explaining and investigating oscillatory behaviours in the p53-Mdm2 system. They mainly focus on the following two aspects: (i) the damped oscillatory behaviours in cell populations, and (ii) the undamped oscillatory behaviours in individual cells in response to various cellular stresses [Lev Bar-Or et al., 2000; Monk, 2003; Lahav et al., 2004; Wagner et al., 2005; Ciliberto et al., 2005; Ma et al., 2005; Geva-Zatorsky et al., 2006; Ramalingam et al., 2007; Samuel and Basile, 2007; Batchelor et al., 2008; Proxtro and Gray, 2008; Yang et al., 2009]. Almost all mathematical models are based on ODEs, which describe the change of concentration of all participating chemical species in the protein interaction network in the system. Although they can be used to study various dynamic and kinetic processes of the p53 system and provide useful insights on the inner workings of the system, there are still some limitations in the current methods and models: the most common one is parameter estimation. Most mathematical models are established based on chemical kinetic theory which describes

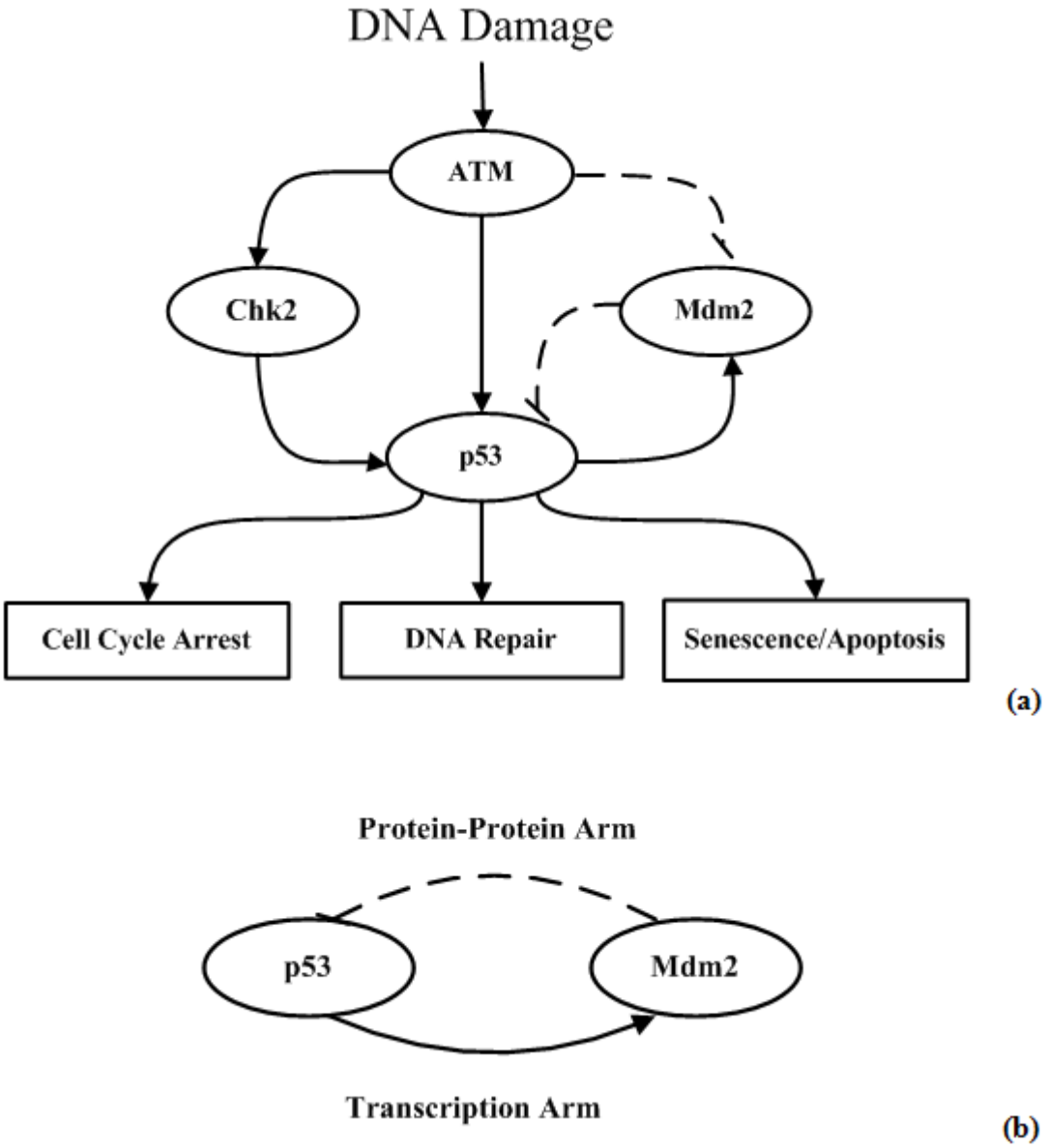

Figure 7-1 Network diagram of the p53 signalling pathway. (a) p53's response to DNA damage: in response to DNA-damage signal, ATM can directly transfer DNA-damage signal or through activating Chk2, to p53. The accumulation of p53 in the nucleus activates several stress response programmes including cell cycle arrest, DNA damage repair and cellular senescence/apoptosis; (b) p53-Mdm2 negative feedback loop: p53 is a transcription factor that promotes the synthesis of Mdm2, while Mdm2 inhibits p53 activity and promotes p53 ubiquitination and degradation.

the reaction rates of interactions in biological system. Due to the lack of kinetic parameter values from experimental measurements, the best kinetic parameter values of models are generated by minimizing the difference between simulation data and experimental data, which results in the representation of real biological systems by models without high precision. For overcoming this difficulty, Artificial Neural Network (ANN) can proposed as a feasible method. The main advantage of neural networks is precisely the accurate parameter estimation. Another important feature is ANNs ability to represent nonlinear interactions. Here, we use one of the best-characterized systems in human cells (the p53-Mdm2 oscillation system that focuses on the p53-Mdm2 negative feedback loop (See Figure 7-1 (b))) as an example to help us understand how to develop ANN to represent the four mathemtaicl models (Models III-VI) proposed by Geva-Zatorsky et al. [2006] which can generate the characteristic of oscillations that were found in the p53-Mdm2 system.

7.2 Design of Artificial Neural Networks

Artificial Neural Networks (ANNs) can be viewed as a mathematical model to simulate natural and biological systems on the basis of mimicking the information processing methods in the human brain. It is well known that ANNs are very capable of approximating input-output mappings that are complex and nonlinear to an arbitrary degree of precision [Samarasinghe, 2006]. This makes ANNs very efficient in representing the behaviour of a range of phenomena. The incremental learning approaches in ANNs make it possible for them to approximate all internal parameters iteratively. ANNs solve some complex nonlinear problems that cannot be solved analytically by most mathematical models. All these characteristics of ANN make it a feasible approach to deal with the “parameter estimation” problem in the traditional mathematical model of the p53 system. There are five types of task to simulate the p53 system using ANN as follows:

1. Understand the protein interactions involved in the p53 system;
2. Develop an ANN to represent the exact behaviour of interactions in the p53 system;
3. Estimate model parameters and compare them with previously reported parameter values;
4. Compare the temporal behaviour of p53 and Mdm2 with that generated from the ODE based model;
5. Investigate the dynamic behaviour and robustness of the ANN based p53-Mdm2 oscillation system.

The following section discusses each step in the development of ANN for the p53-Mdm2 oscillation system.

7.2.1 Understanding Interactions in the P53 System

Deriving a formal abstraction of the p53 system is a crucial step in developing an ANN model. This step requires the definition of system boundaries and the components of the system. More importantly, it is necessary to determine what types of interaction with the environment should be included. Once detailed and comprehensive information about interactions among proteins involved are incorporated into the simulated system (see Section 7.1), the next step is to develop the ANNs.

7.2.2 The Development of an ANN

In terms of developing an ANN model for the p53 system, three factors require attention: the number of neurons needed, the structure of the network and the learning algorithm.

7.2.2.1 Number of neurons needed

In general, ANNs are nonmodular which means that the number of neurons in an ANN is case dependent [Hopfield, 1982; Alon, 2003]. This number is adjusted during training until the network output converges on the actual output based on a criterion such as least square error minimization. However, the first advantage of the ANN proposed in this study is that the number of neurons is decided before network training; the number of neurons depends on the chemical species involved and their corresponding reactions in the p53 system. This means that the number of neurons in the ANN can be fixed once we understand the existing chemical reactions in the simulated system, which is the first step in developing the mathematical model for studying and capturing its essential characteristics. Thus our approach makes a point of departure from traditional neural network development by fixing the number of neurons thereby making the network an exact representation of the reactions involved in the protein network.

7.2.2.2 Structure of Neural Networks

For demonstrating how to determine the structure of the network based on the chemical reactions of the p53 system, we take one of Geva-Zatorsky et al.'s [2006] proposed models (Model V) as an example for detailed explanation. Model V consists of three differential equations (Eqs. (7-1 to 7-3) which explain the reactions between p53 (x), Mdm2 precursor (y_0) and Mdm2 (y). The details of the model variables and parameters together with their descriptions are presented in Table 7-1 and the structure of this p53-Mdm2 network is shown in Figure 7-2. According to Figure 7-2, there are two feedback loops on p53: one is a negative feedback loop to represent the effects of Mdm2 on p53; the other is a linear positive feedback loop representing an upregulating effect on p53 from the action of additional p53 system components (which are not shown in Figure 7-2). The delay between p53 and Mdm2 is due to transcription of Mdm2 and is achieved by Mdm2 precursor (y_0 such as Mdm2 mRNA) in this model.

$$\frac{dx}{dt} = \Gamma x - \alpha_{xy} xy \,, \tag{7-1}$$

$$\frac{dy_0}{dt} = \beta_y x - \alpha_0 y_0 \,, \tag{7-2}$$

$$\frac{dy}{dt} = \alpha_0 y_0 - \alpha_y y \,. \tag{7-3}$$

From the numerical treatment and finite difference method, Eqs. (7-1) to (7-3) can be transformed into:

$$x(t+1) = x(t) + \int_{\Delta t} (\Gamma x - \alpha_{xy} xy)\, dt \,, \tag{7-4}$$

$$y_0(t+1) = y_0(t) + \int_{\Delta t} (\beta_y x - \alpha_0 y_0)\, dt \,, \tag{7-5}$$

$$y(t+1) = y(t) + \int_{\Delta t} (\alpha_0 y_0 - \alpha_y y)\, dt \,. \tag{7-6}$$

According to Eq. (2-20), when dt is small enough, Eqs. (7-4) to (7-6) can be rewritten in a matrix form to represent these ODEs as

Table 7-1 Description of variables and parameters in Model V of Geva-Zatorsky et al.'s [2006] for the p53-Mdm2 oscillation system.

Model Variables and Parameters	Description
x	nuclear p53
y_0	Mdm2 precursor
y	nuclear Mdm2
Γ	linear p53 production rate
α_0	Mdm2 maturation rate
α_x	Mdm2-independent p53 degradation rate
α_y	Mdm2 degradation rate
α_{xy}	Mdm2-dependent p53 degradation rate
β_y	p53-depdendent Mdm2 production rate

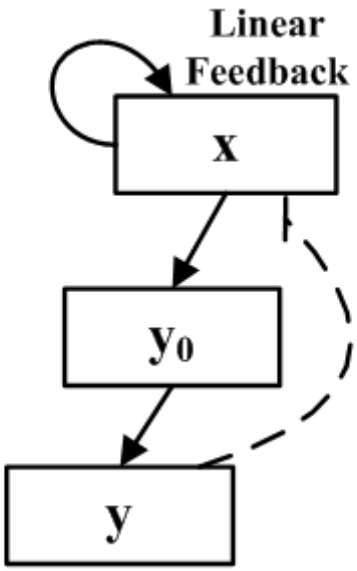

Figure 7-2 Schematic diagram to illustrate the p53-Mdm3 system for Model V.

$$\begin{bmatrix} x(t+1) \\ y_0(t+1) \\ y(t+1) \end{bmatrix} = \begin{bmatrix} x(t) \\ y_0(t) \\ y(t) \end{bmatrix} + \begin{bmatrix} \Gamma & 0 & 0 & -\alpha_{xy} \\ \beta_y & -\alpha_0 & 0 & 0 \\ 0 & \alpha_0 & -\alpha_y & 0 \end{bmatrix} \begin{bmatrix} x(t) \\ y_0(t) \\ y(t) \\ x(t)y(t) \end{bmatrix} \Delta t \,. \tag{7-7}$$

Thus, Eqs. (7-7) can be simplified as:

$$X(t+1) = X(t) + WA\Delta t \,, \tag{7-8}$$

where $X = \begin{bmatrix} x \\ y_0 \\ y \end{bmatrix}$ represents the chemical species in the p53 system, $W = \begin{bmatrix} \Gamma & 0 & 0 & -\alpha_{xy} \\ \beta_y & -\alpha_0 & 0 & 0 \\ 0 & \alpha_0 & -\alpha_y & 0 \end{bmatrix}$ represents the chemical species' related kinetic constants in the model system, and $A = \begin{bmatrix} x(t) \\ y_0(t) \\ y(t) \\ x(t)y(t) \end{bmatrix}$ represents the current state of the system resulting from the existing relationships among the chemical species in the system. The product of WA represents the change of each chemical species in the system at time t. As discussed in section 2.4.2, the activity of the system at time $t+1$ can be calculated by Eq. (2-19) as $x_i(t+1) = x_i(t) + \int_{\Delta t} f_i(x_1, x_2, \ldots x_n)dt$. When dt becomes very small, from the Taylor series expansion disregarding higher order terms, the activity of the system at $t+1$ can be considered as the linear combination of the current activity of the system and the product of the change of the system during the time increment and dt using Eq. (2-20) as $x_i(t+1) = x_i(t) + f_i(x_1, x_2, \ldots x_n)\Delta t$.

Figure 7-3 shows the architecture of the developed recurrent ANN for Model V of the p53-Mdm2 oscillation system. The model consists of four inputs (x, y_0, y, xy) and three linear neurons that receive inputs as specified in Eq. (7-8). The connections between inputs and neurons represent the relevant kinetic constants. Each neuron represents one equation in Eq. (7-7) and computes the weighted sum of inputs and products of the weighted sum and Δt. The final result is obtained by adding the neuron outputs to the initial system state. In Figure 7-3, we can find the second advantage of the proposed ANN in that the weights of ANNs

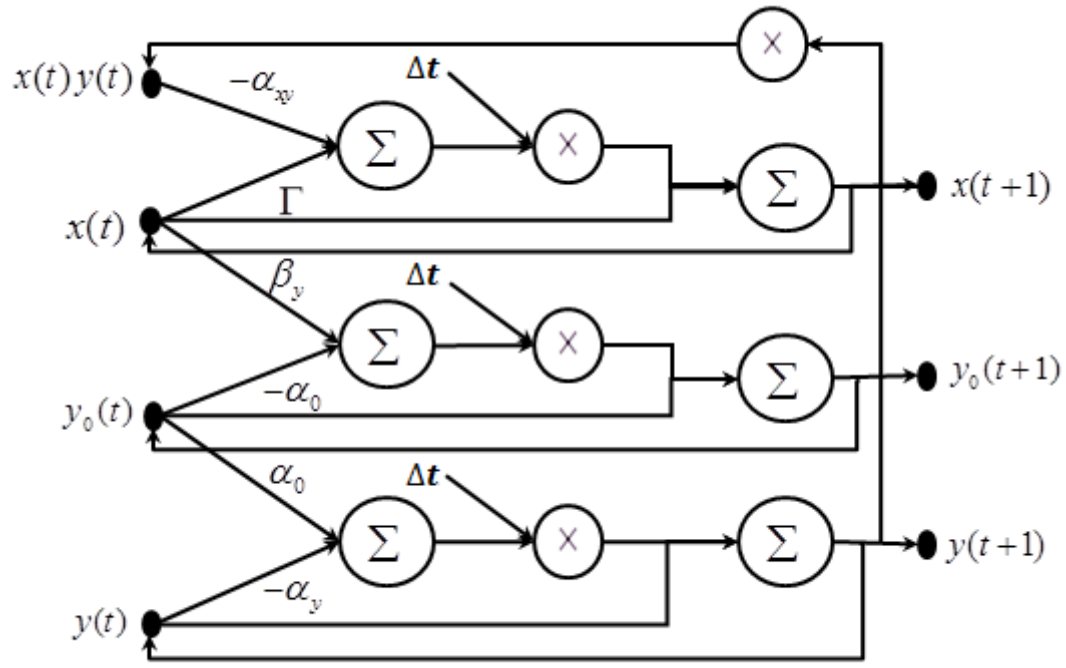

Figure 7-3 Architecture of the developed recurrent ANN for Model V of the p53-Mdm2 oscillation system given in Eq. (7-8).

represent the corresponding kinetic constants of the chemical species, indicating that the developed ANN can directly estimate the values of kinetic constants of chemical reactions in the system during training. Thus, the most difficult problem of parameter estimation in the ODE-based mathematical models of the biological system can be easily solved by the ANN technique; more importantly, the ANN represents the protein network exactly and the successfully trained ANN can be used to study and analyze the dynamic behaviour of the p53-Mdm oscillation system through adjusting the respective kinetic constants in the proposed ANN.

7.2.2.3 ANN Learning Algorithm

In a neural network, the unknowns are the weights and in our case, they depict the parameters of the system. The unknowns are estimated by showing the network inputs and corresponding outputs repeatedly and adjusting the weights incrementally using a learning algorithm. The inputs and outputs in this case are generated from the ODE version of the model (Once experimental method become more powerful, these data can directly come from experperimental measurements). These are called training vectors. Each vector contains values for the four inputs (x, y_0, y, xy) for time t and the corresponding output (x, y_0, y) for the next time step. In general, it is advisable to use simple algorithms that yield quick and accurate solution. As the studied Model V of the p53-Mdm2 system only requires a linear ANN (i.e. linear neurons), a backpropagation algorithm in batch mode is used as the learning algorithm to update the weights of the network. It basically minimizes the network's global error between the actual network outputs and their corresponding desired outputs based on gradient descent error minimisation. The network's global error (E) between its output and actual output is given by

$$E = E_1^2 + E_2^2 + \cdots + E_k^2 = \frac{1}{2NK}\sum_{j=1}^{K}\left[\sum_{i=1}^{N}\left(T_{ij} - Z_{ij}\right)^2\right], \tag{7-9}$$

where E_j represents the error of neuron j, T_{ij} and Z_{ij} are the actual output and the network output, respectively, of the j^{th} neuron for the i^{th} training vector, K is the number of neurons, and N is the total number of training vectors. Basically, error E represents the total mean square error across all the neurons in the model. The objective of learning is to minimise this error through incremental adjustment of weights.

The method of modifying a weight is the same for all weights; here we show the change to an arbitrary weight as an example. The change to a single weight w_{ji} of a connection between input i and neuron j in the neural network based on batch learning is defined as

$$\Delta w_{ji} = -\eta \sum_{p=1}^{k} \left(\frac{dE}{dw_{ji}}\right)_p , \tag{7-10}$$

where $\frac{\partial E}{\partial w_{ji}}$ is the error gradient with respect to weight w_{ji}. The η is called the learning rate with a constant value between 0 and 1, and it controls the rate of weight adjustment. k is the total number of input vectors. Thus, the new weight for the next batch (which is denoted by w_{ji}^{n+1}) can be presented as

$$w_{ji}^{n+1} = w_{ji}^{n} + \Delta w_{ji}^{n} \tag{7-11}$$

The process that propagates the error information backwards into the network and updates weights of the network is repeated until the network minimizes the global error between the actual network outputs and their corresponding desired outputs. In the learning process, the weights of the network converge on the optimum values. A particular feature of an ANN in this case is that it uses a simple first order learning algorithm based on error gradients to map accurately the required system behaviour.

7.3 Evaluating the Success of ANN Models

In this study, the focus is on the development of an ANN model to represent the mathemtaicl models proposed by Geva-Zatorsky et al. [2006]. Geva-Zatorsky et al. [2006] examined six model families to capture the observed oscillations and variability in the p53-Mdm2 system in response to DNA damage caused by gamma irradiation. We focus on four of these (Models III-VI) in this research. All four models contain a negative feedback loop between p53 and Mdm2: p53 transcriptionally activates Mdm2 and the activated Mdm2 promotes the degradation of p53. Models III-VI only focus on the chemical reactions between p53 and Mdm2. The number of parameters in Models III-V are five, six and five, respectively. However, Model VI (with six parameters) takes a checkpoint mechanism into account. It is achieved by two negative feedback loops: (i) a direct feedback loop between p53 and Mdm2, and (ii) a longer feedback loop impinging on an upstream regulator of p53 in response to the

active damge signal. The values of parameters involved in these four original models were selected by reproducing an effective average individual cell measurements of nuclear p53 and Mdm2 following gamma irradation revealed from the real experimental observations [Geva-Zatorsky et al., 2006]. The structure and mathematical details of Models III, IV and VI are shown Figure 7-4. The details of the model variables and parameters together with their description for the three models are presented in Appendix D. Figure 7-5 displays the corresponding architectures of the developed ANNs as well as the corresponding mathematical (matrix) forms to represent ODEs of Models III, IV and VI. The following section explains how we developed the ANNs and estimated the values of parameters in the mathematical models (Models III-VI) of the p53-Mdm2 oscillation system.

We first analyzed the four models (III-VI) by numerically showing their ODEs. Figure 7-6 displays the p53 and Mdm2 oscillations generated by these mathematical models. It shows that the four models can capture the oscillatory behaviour of the p53-Mdm2 feedback loop and represents four possible oscillatory reponses. The structure of ANNs has already been decided based on the ODEs of the proposed mathematical models (III-VI) representing the rate of change of concentration of all participating chemical species in the p53-Mdm2 oscillation system (See Figures 7-3 and 5).

The last step required, according to section 2.4.2, is the determination of a value for dt that is small enough. The reason for this is that the activity of the system at the time $t+1$ is calculated as in Eq. (7-7) (i.e. the linear combination of the current activity of the system ($x(t)$, $y_0(t)$, $y(t)$, $x(t)y(t)$) and the product of the changes in the system during a time increment and Δt). Based on the analysis of these four different Models III-VI as shown in Figure 7-6, we define the values of Δt as 0.002, 0.001, 0.005 and 0.002 (hours), respectively (In this case, we fixed the maximum value of dt for the four models depending on whether oscillations in p53 and Mdm2 levels generated by Eq. (7-7) have a prefect agreement with those directly generated from ODEs solutions). Once the value of Δt are fixed, the developed ANNs are trained to learn their corresponding mathematical models, while weights (directly representing the chemical kinetic parameters of reactions in the p53-Mdm2 system) are updated until each proposed network reaches global minimum error. Figures 7-7 and 7-8 illustrate the behaviour of p53 and Mdm2 obtained from the ANN along with the respective ODE solutions. According to these two figures, ANN results for p53 and Mdm2 and those from ODE solutions are in perfect agreement.

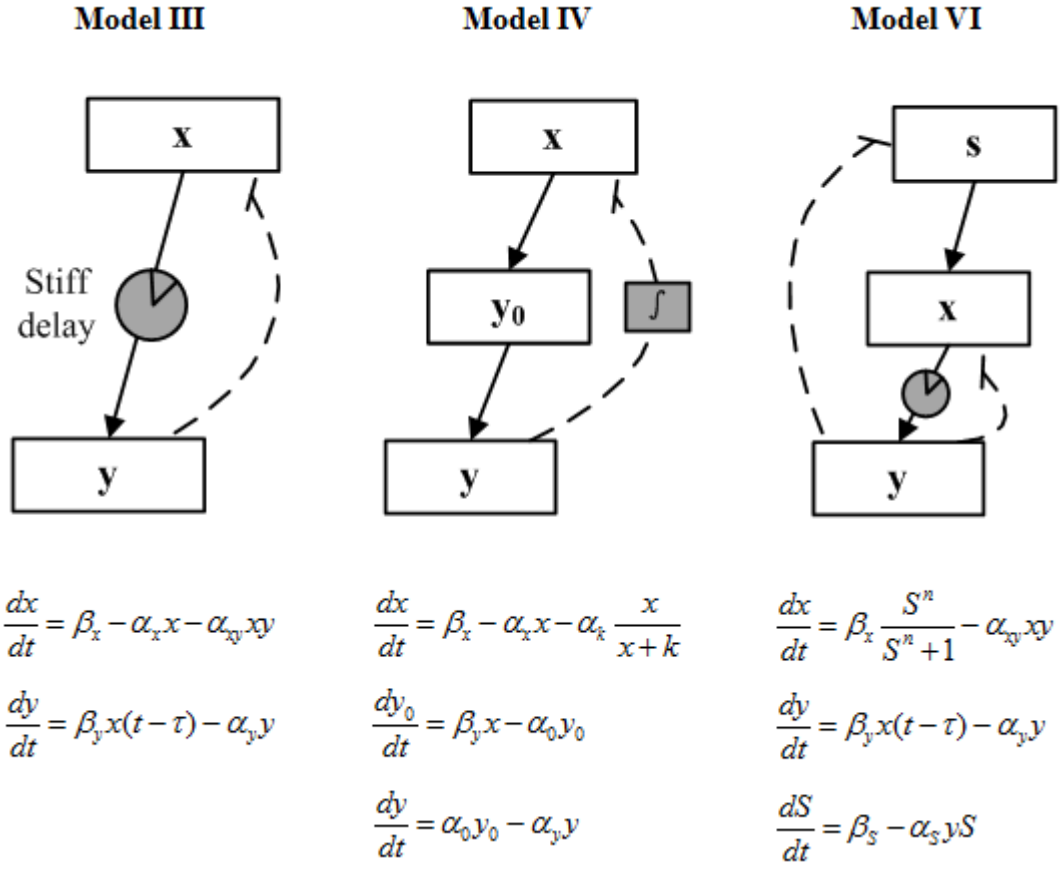

Figure 7-4 The structure and mathematical details (ODEs) of Models III, IV and VI of Geva-Zatorsky et al.'s [2006] for the p53-Mdm2 oscillation system.

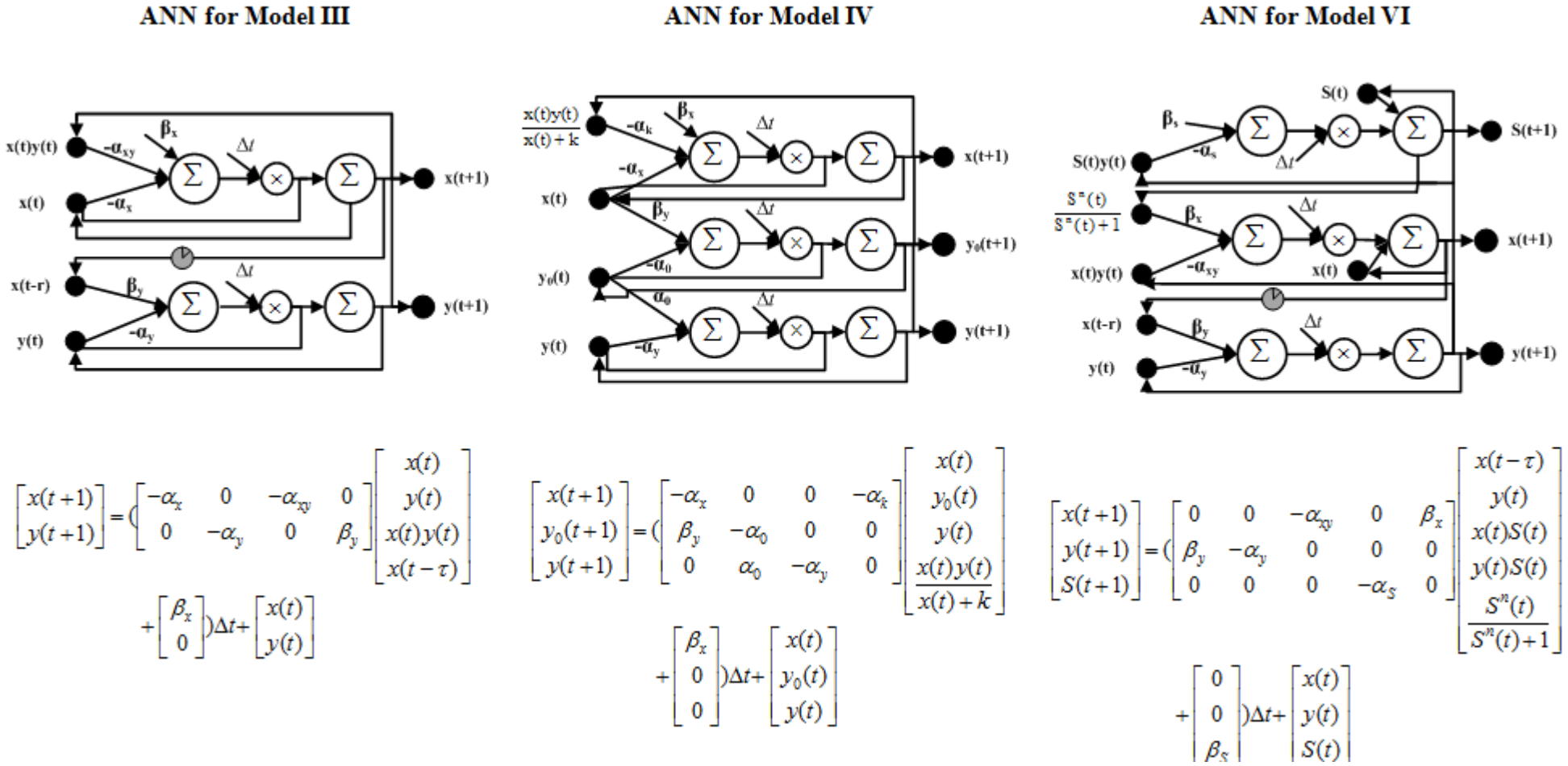

$$\begin{bmatrix} x(t+1) \\ y(t+1) \end{bmatrix} = \left(\begin{bmatrix} -\alpha_x & 0 & -\alpha_{xy} & 0 \\ 0 & -\alpha_y & 0 & \beta_y \end{bmatrix} \begin{bmatrix} x(t) \\ y(t) \\ x(t)y(t) \\ x(t-\tau) \end{bmatrix} + \begin{bmatrix} \beta_x \\ 0 \end{bmatrix} \right) \Delta t + \begin{bmatrix} x(t) \\ y(t) \end{bmatrix}$$

$$\begin{bmatrix} x(t+1) \\ y_0(t+1) \\ y(t+1) \end{bmatrix} = \left(\begin{bmatrix} -\alpha_x & 0 & 0 & -\alpha_k \\ \beta_y & -\alpha_0 & 0 & 0 \\ 0 & \alpha_0 & -\alpha_y & 0 \end{bmatrix} \begin{bmatrix} x(t) \\ y_0(t) \\ y(t) \\ \frac{x(t)y(t)}{x(t)+k} \end{bmatrix} + \begin{bmatrix} \beta_x \\ 0 \\ 0 \end{bmatrix} \right) \Delta t + \begin{bmatrix} x(t) \\ y_0(t) \\ y(t) \end{bmatrix}$$

$$\begin{bmatrix} x(t+1) \\ y(t+1) \\ S(t+1) \end{bmatrix} = \left(\begin{bmatrix} 0 & 0 & -\alpha_{xy} & 0 & \beta_x \\ \beta_y & -\alpha_y & 0 & 0 & 0 \\ 0 & 0 & 0 & -\alpha_S & 0 \end{bmatrix} \begin{bmatrix} x(t-\tau) \\ y(t) \\ x(t)S(t) \\ y(t)S(t) \\ \frac{S^n(t)}{S^n(t)+1} \end{bmatrix} + \begin{bmatrix} 0 \\ 0 \\ \beta_S \end{bmatrix} \right) \Delta t + \begin{bmatrix} x(t) \\ y(t) \\ S(t) \end{bmatrix}$$

Figure 7-5 Architecture of the developed recurrent ANNs and the corresponding mathematical form for the representation of Models III, IV and VI .

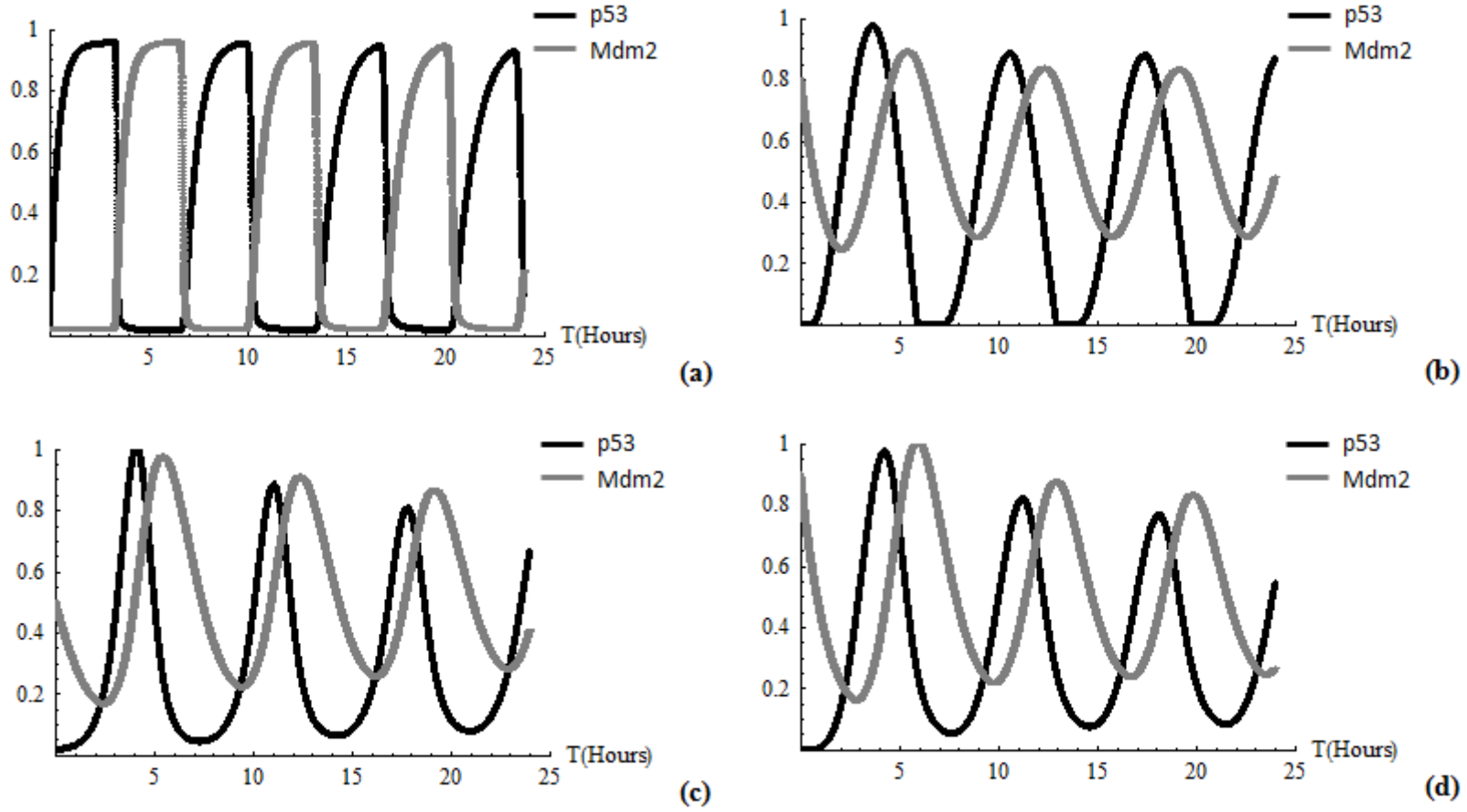

Figure 7-6 Numerical solutions of ODE-based Models III-VI showing oscillations in p53 and Mdm2 levels undergo oscilation in response to DNA damage stresses: (a) Model III, (b) Model IV, (c) Model V and (d) Model VI.

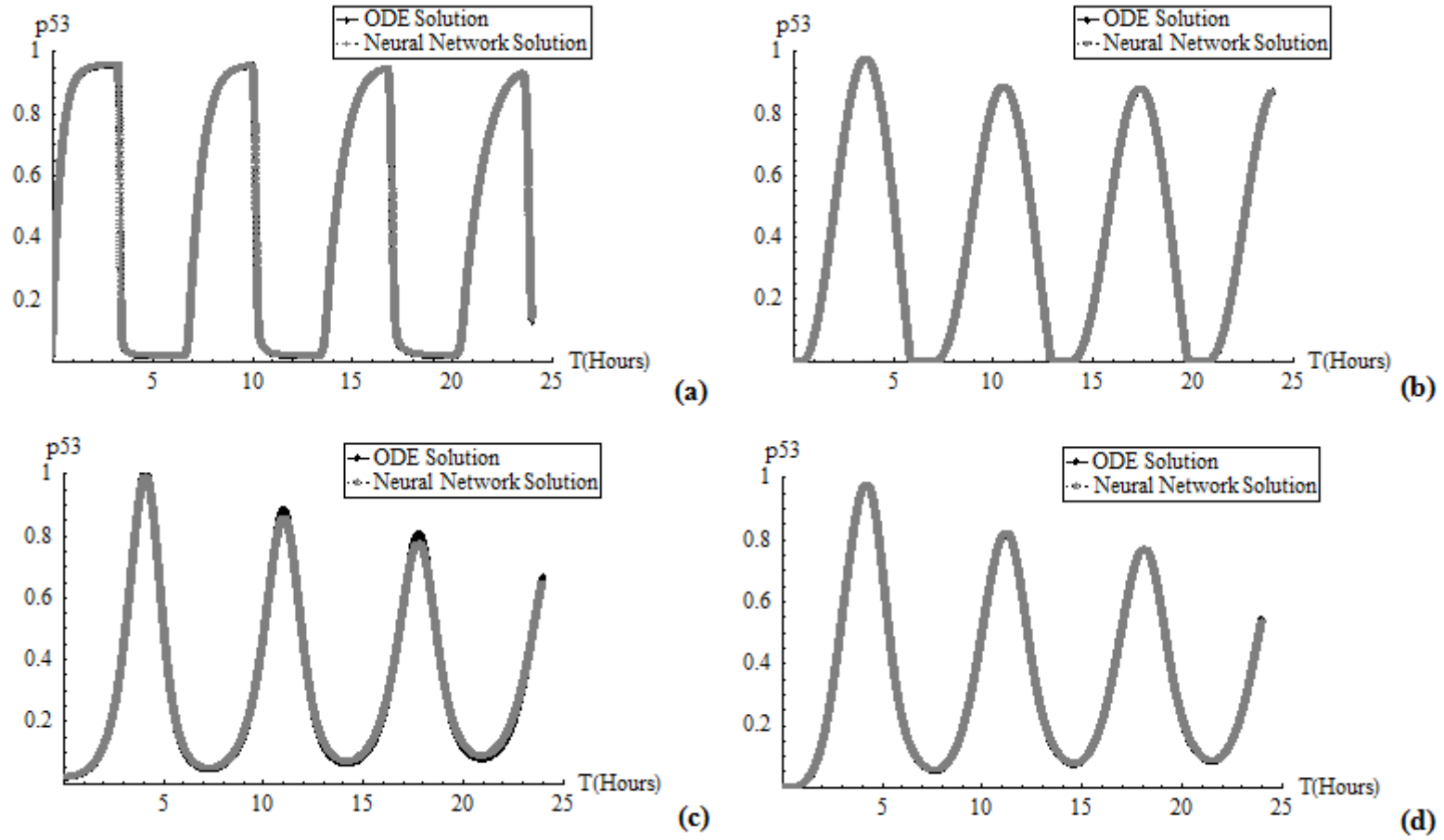

Figure 7-7 The predicted p53 concentration from ANNs for the four different models superimposed on the solutions from the corresponding ODEs: (a) Model III, (b) Model IV, (c) Model V and (d) Model VI. A perfect agreement between the two solutions is seen.

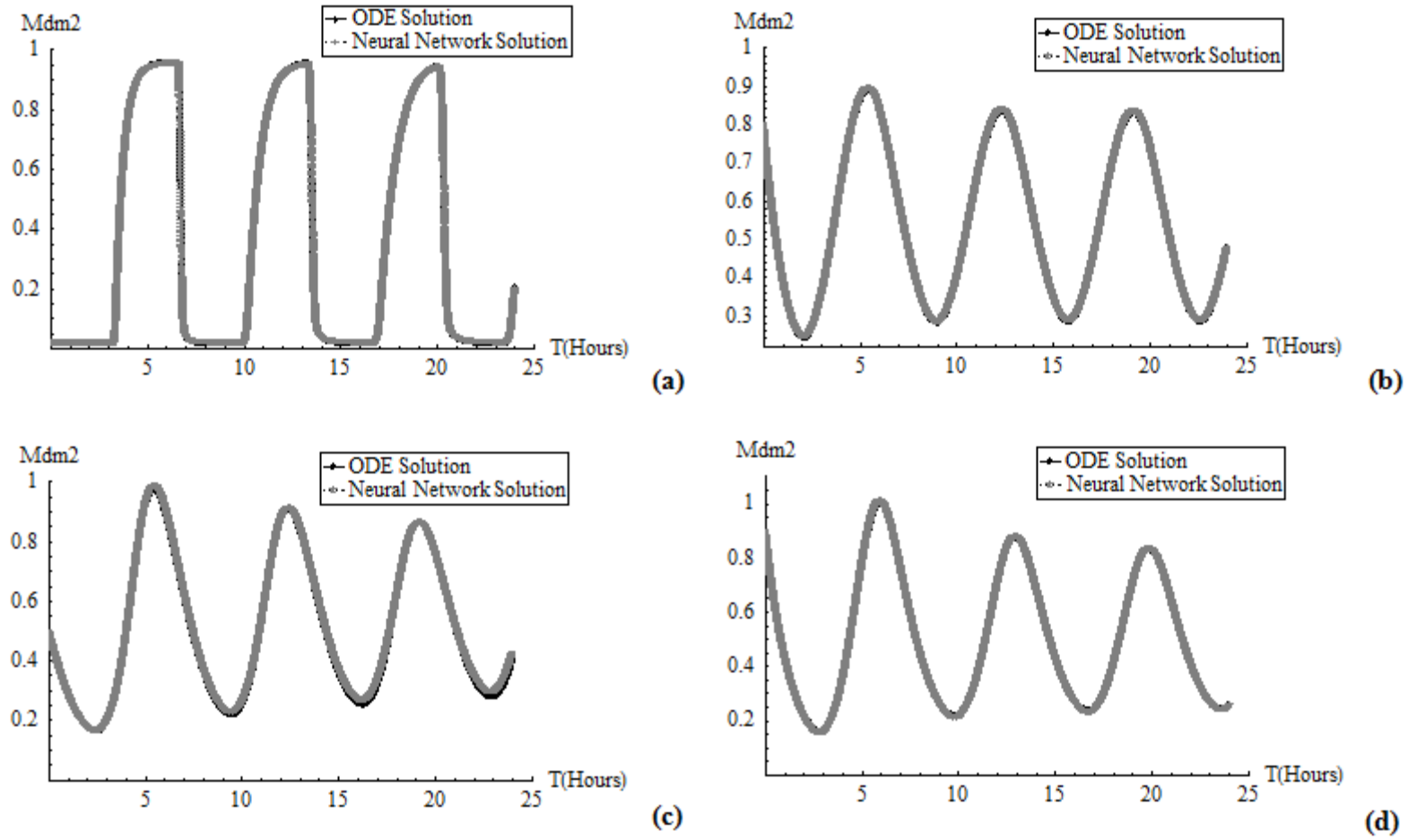

Figure 7-8 The predicted Mdm2 concentration from ANNs for the four different models superimposed on the solutions from the corresponding ODEs: (a) Model III, (b) Model IV, (c) Model V and (d) Model VI. A prefect agreement between the two solutions can be seen.

We extracted the weights from the developed ANNs and compared them with the kinetic constants used in the ODEs. All weights perfectly match the corresponding kinetic constants, as shown in Table 7-2. All these results reveal that the developed ANNs are successful in parameter estimation based on very small dt. However, very small dt does not currently represent accurately possible measurements in a real system. In fact, realistic experiments generally record the change of chemical species in constant time intervals like a few minutes (this time interval is referred to as Δt in the ANNs). For the p53-Mdm2 oscillation system here, the constant time interval for the real experiments is about 0.3 hours [Geva-Zatorsky et al., 2006]. Compared to Δt used in the developed ANNs, the realistic constant time interval is much larger. We retrained the ANN models with the data for a larger time interval of 0.3 hours but the results did not agree well with the corresponding results from ODEs. Therefore, a new question arose as to whether it was possible to develop ANNs to estimate the chemical kinetic parameters for reactions in the p53-Mdm2 oscillation system for a larger time interval (dT)? The answer to this question is "Yes" but certain modifications are needed to the original ANN. The modified ANN is still based on a small Δt; however, we needed to be made to install a "switch" into the ANN before the final output of the network was calculated. This is the same recurrent neural network involving feedback as before but with a timer switch as represented in the right hand side of Figure 7-9 and the structure of this network is shown in Figure 7-9 where the right hand side implements the above described switch.

In this kind of ANN, there are two output layers: one is the inner output layer whose output is used as input into the next time step; and the other is the final output layer whose output is the network output that is used for the error calculation and weight update. The following equation represents the network output:

$$Z(n) = X(t+1) = X(t+dT), \qquad \text{for } n = \frac{\sum \Delta t}{dT}, \quad n = 1, 2, 3, 4, 5, ...n \ , \tag{7-12}$$

where Z is the final output of the network, X is the inner output of the network, n is the n^{th} final output. The purpose of this switch is to accumulate the results of the inner output layer over the time interval dT before deciding that the network can enter the final output layer. The network can only enter the final output layer when the summation of the small time intervals Δt equals the large time interval dT at which point error calculations and weight updates are made. Figures 7-10 and 7-11 illustrate the behaviour of p53 and Mdm2 obtained from the modified ANNs superimposed on the ODE solutions. The results indicate that the

Table 7-2 The comparison of model parameters between ODE and ANN based on a small Δt .

Parameters	ODE				ANN			
	III	**IV**	**V**	**VI**	**III**	**IV**	**V**	**VI**
α_0	-	$0.8\pm20\%$	$1.1\pm25\%$	-	-	**0.796**	**1.11**	-
α_x	**0**	**0**	-	-	**0**	**0**	-	-
α_y	**24**	$0.8\pm25\%$	$0.9\pm30\%$	$0.7\pm20\%$	**24.97**	**0.798**	**0.91**	**0.72**
α_{xy}	**120**	-	$3.7\pm50\%$	$1.4\pm20\%$	**118.25**	-	**3.68**	**1.36**
β_x	**2.3**	$0.9\pm35\%$	-	$0.9\pm60\%$	**2.27**	**0.9**	-	**0.88**
β_y	**24**	$1.1\pm55\%$	$1.5\pm60\%$	$1.0\pm10\%$	**24.89**	**1.11**	**1.51**	**1.0**
α_s	-	-	-	$2.7\pm30\%$	-	-	-	**2.75**
β_S	-	-	-	$0.9\pm25\%$	-	-	-	**0.91**
α_k	-	$1.7\pm20\%$	-	-	-	**1.7**	-	-
Γ	-	-	$2.0\pm25\%$	-	-	-	**1.99**	-

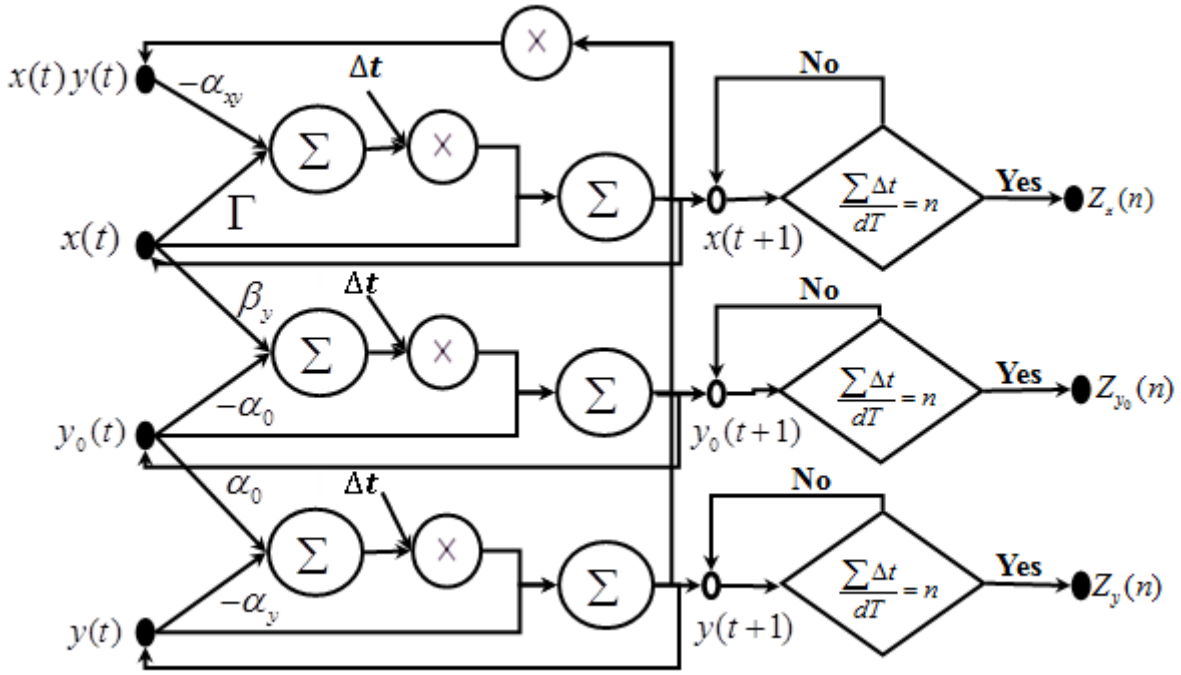

Figure 7-9 Architecture of the developed ANN for Model V of the p53-Mdm2 oscillation system based on the larger time interval (dT) given in Eq. (7-12).

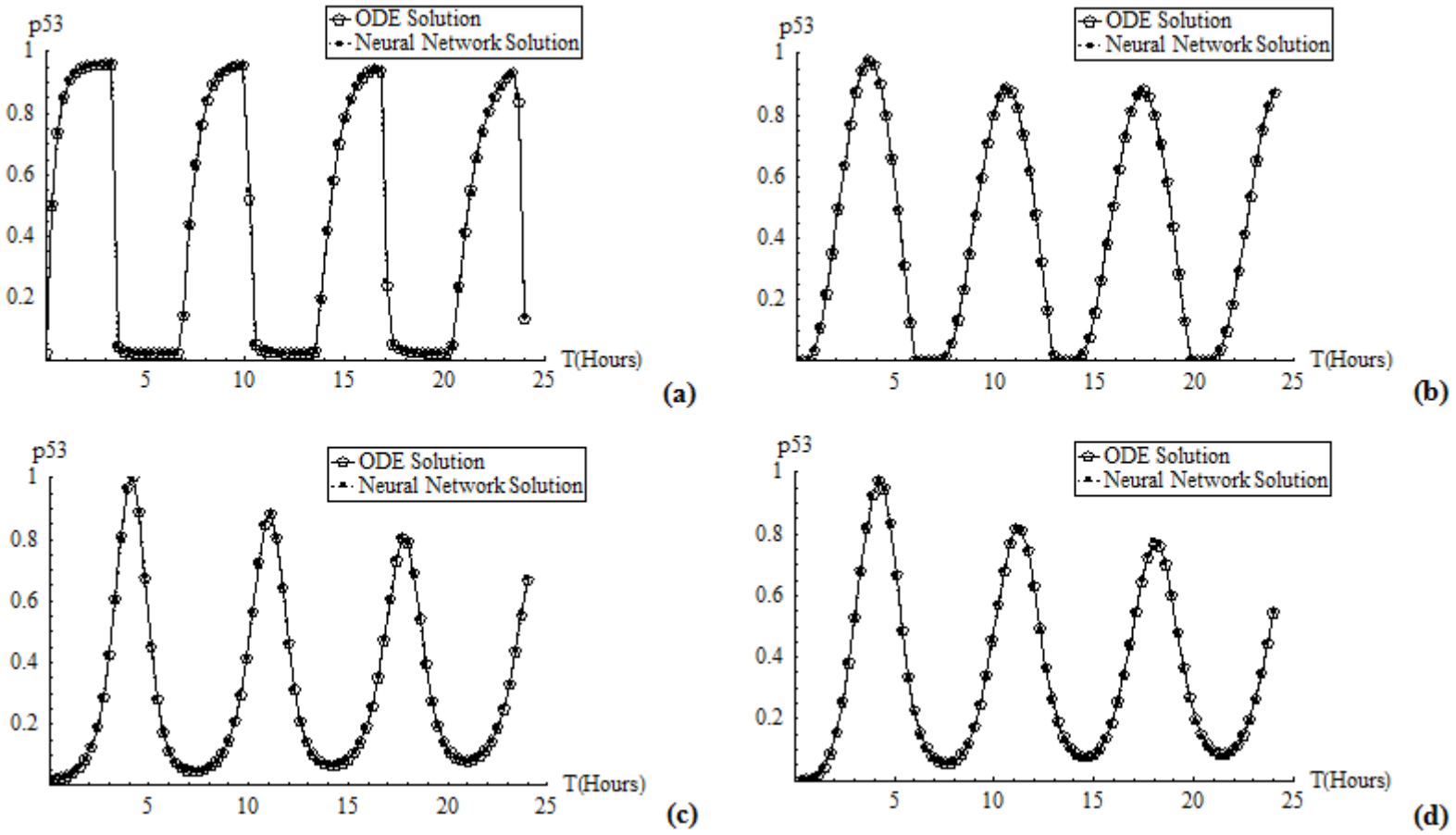

Figure 7-10 The aproximated p53 concentration derived from ANNs for the four different models based on a large *dT* (0.3 hours) superimposed on the corresponding ODE solutions: (a) Model III, (b) Model IV, (c) Model V and (d) Model VI. A perfect agreement can be seen in the model outcomes.

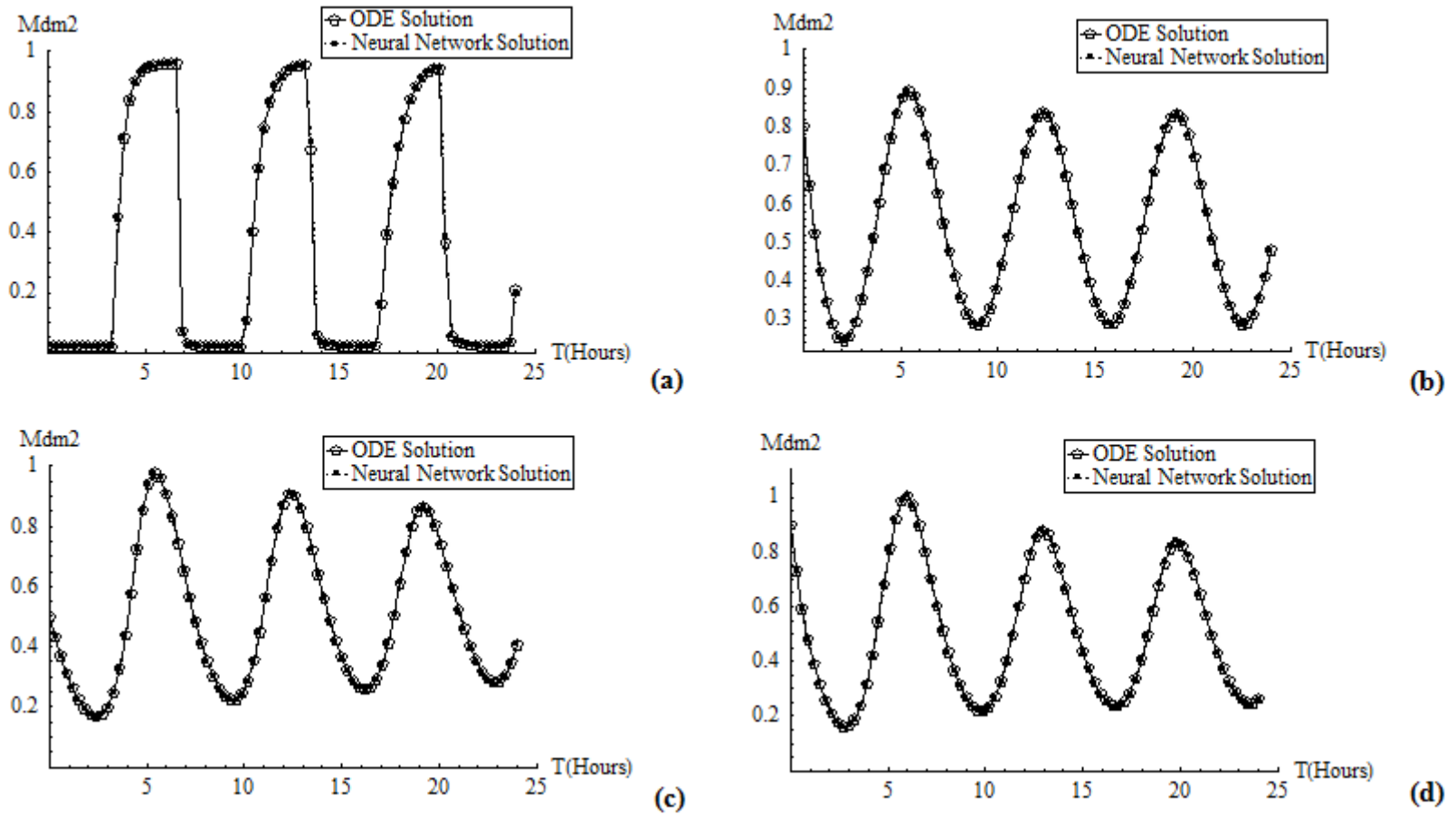

Figure 7-11 The aproximated Mdm2 concentration derived from ANNs for the four different models based on a large *dT* (0.3 hours) superimposed on the corresponding ODE solutions: (a) Model III, (b) Model IV, (c) Model V and (d) Model VI. A perfect agreement can be seen in the model outcomes.

ANN outcomes agree with the ODE solutions in representing the behaviour of p53 and Mdm2. We also compared the model parameters calculated based on the larger time interval dT with the corresponding kinetic constants in the ODE based models as shown in Table 7-3. The results indicate that the estimated constants are in almost perfect agreement with the corresponding kinetic constants used in the ODEs.

7.4 Robustness of the P53-Mdm2 System Based on the Developed ANNs

We define robustness here as the ability to sustain oscillatory behaviour in the p53-Mdm2 system. The robustness of the p53 oscillation system with respect to various perturbations in the model parameters can be achieved by the autocorrelation function which measures the degree of periodicity of time evolution for a given variable. For the constant parameter set obtained from training, we can compute the autocorrelation function. Based on the autocorrelation function, we can calculate the time corresponding to a 50% decrease in the initial correlation values, called the half-life of the correlation, under this particular condition. Meanwhile, we also compute the periods for this system (time interval between a pair of successive peaks) as well as their mean value, called the "mean period".

In terms of the robustness of the p53-Mdm2 oscillation system, we define the ratio of the half-life and the mean period (HoMP) as a measure of the robustness of this system in the presence of various levels of perturbations in its model parameters (See Appendix E for the details of HoMP calculation). In general, molecular fluctuations reduce the half-life of autocorrelation functions and diffuse the phase of the oscillations [Baras, 1997; Baras, et al., 1990; Gonze et al., 2002]. This is the resaon why we use HoMP as a measure of the robustness of the p53-Mdm2 oscillation system. Here, we assume that the system is robust if the system can keep HoMP for various internally or/and externally caused perturbations the same as that (HoMP = 4) under the reference parameter values. We tested the robustness of the ANN-based p53 systems for Model VI. We generated perturbations by changing model parameters to investigate the robustness of the system. The following section discusses the results for the robustness of the p53 oscillation system for Model VI in response to changes in model parameters made in two different ways: the individual parameter changes and the simultaneous parameter changes with different ranges.

Table 7-3 A comparison of model parameters between ODE and ANN based on a larger time interval dT ·

Parameters	ODE				ANN			
	III	**IV**	**V**	**VI**	**III**	**IV**	**V**	**VI**
α_0	-	$0.8\pm20\%$	$1.1\pm25\%$	-	-	**0.8**	**1.1**	-
α_x	**0**	**0**	-	-	**0**	**0**	-	-
α_y	**24**	$0.8\pm25\%$	$0.9\pm30\%$	$0.7\pm20\%$	**24.96**	**0.8**	**0.9**	**0.7**
α_{xy}	**120**	-	$3.7\pm50\%$	$1.4\pm20\%$	**118.27**	-	**3.68**	**1.43**
β_x	**2.3**	$0.9\pm35\%$	-	$0.9\pm60\%$	**2.27**	**0.9**	-	**0.9**
β_y	**24**	$1.1\pm55\%$	$1.5\pm60\%$	$1.0\pm10\%$	**24.97**	**1.1**	**1.5**	**1.0**
α_s	-	-	-	$2.7\pm30\%$	-	-	-	**2.7**
β_S	-	-	-	$0.9\pm25\%$	-	-	-	**0.9**
α_k	-	$1.7\pm20\%$	-	-	-	**1.7**	-	-
Γ	-	-	$2.0\pm25\%$	-	-	-	**2**	-

7.4.1 The Robustness of the P53-Mdm2 System in Response to Individual Parameter Changes

To investigate the robustness of the system in response to individual parameter changes, we changed only one parameter at a time within the $\pm 50\%$ range in 10% intervals and calculated HoMP values for these 11 cases. The purpose is to investigate the influence of the change in the value of a parameter in disrupting the oscillatory behaviour of the p53-Mdm2 system. Figures 7-12 (a) and (b) show the results of the influence of individual parameter changes on HoMP for p53 and Mdm2, respectively, indicating that the behaviours of p53 and Mdm2 have quite similar trends; the value of HoMP increases with increases in the parameter values, but all parameters allow the system to reach its original HoMP value of 4.0 beyond -20% of the parameter value. Therefore, the system is robust with respect to parameter changes around the original values up 50% (original value is represented by the 6^{th} increment in Figures 7-12 (a) and (b)). This reveals that the robustness of the p53-Mdm2 system is not susceptible to perturbations in the individual parameters of the model in this range, which is in good agreement with the model sensitivity analysis results reported by Geva-Zatorsky et al. [2006] who state that Models IV-VI can generate sustained or weakly damped oscillation over a broad range of parameters.

One parameter, α_s (Mdm2-dependent signal inactivation rate), was different from the other parameters in that the HoMP for -50% of α_s was significantly lower than the original HoMP (Specifically, about 50% of the original HoMP as shown in Figures 7-12 (a) and (b)). Therefore, we compared the behaviour of p53 and Mdm2 under a 50% reduced parameter value and the reference value of α_s (see Figures 7-12 (c) and (e)). For -50% of α_s, both p53 and Mdm2 concentrations reach a fixed point with time making the whole system stable. In this case, we represent the behaviour of p53-Mdm2 for only 48 hours. This is the reason why the exact fixed stable point cannot be seen in Figures 7-12 (c) and (d). For a lager time range, the system will reach a fixed stable point. However, for the reference values of α_s, the concentrations of p53 and Mdm2 each comprise an oscillator that follows a cyclical path in phase space called a limit cycle that keep the whole system stable (Figures 7-12 (e) and (f)). This type of stability in the system exists for all parameter perturbations beyond -20% of parameter values. In terms of the intermediate value of HoMP (3 in this case) for -40% of α_s, the behavious of p53 and Mdm2 are shown in Appendix F.

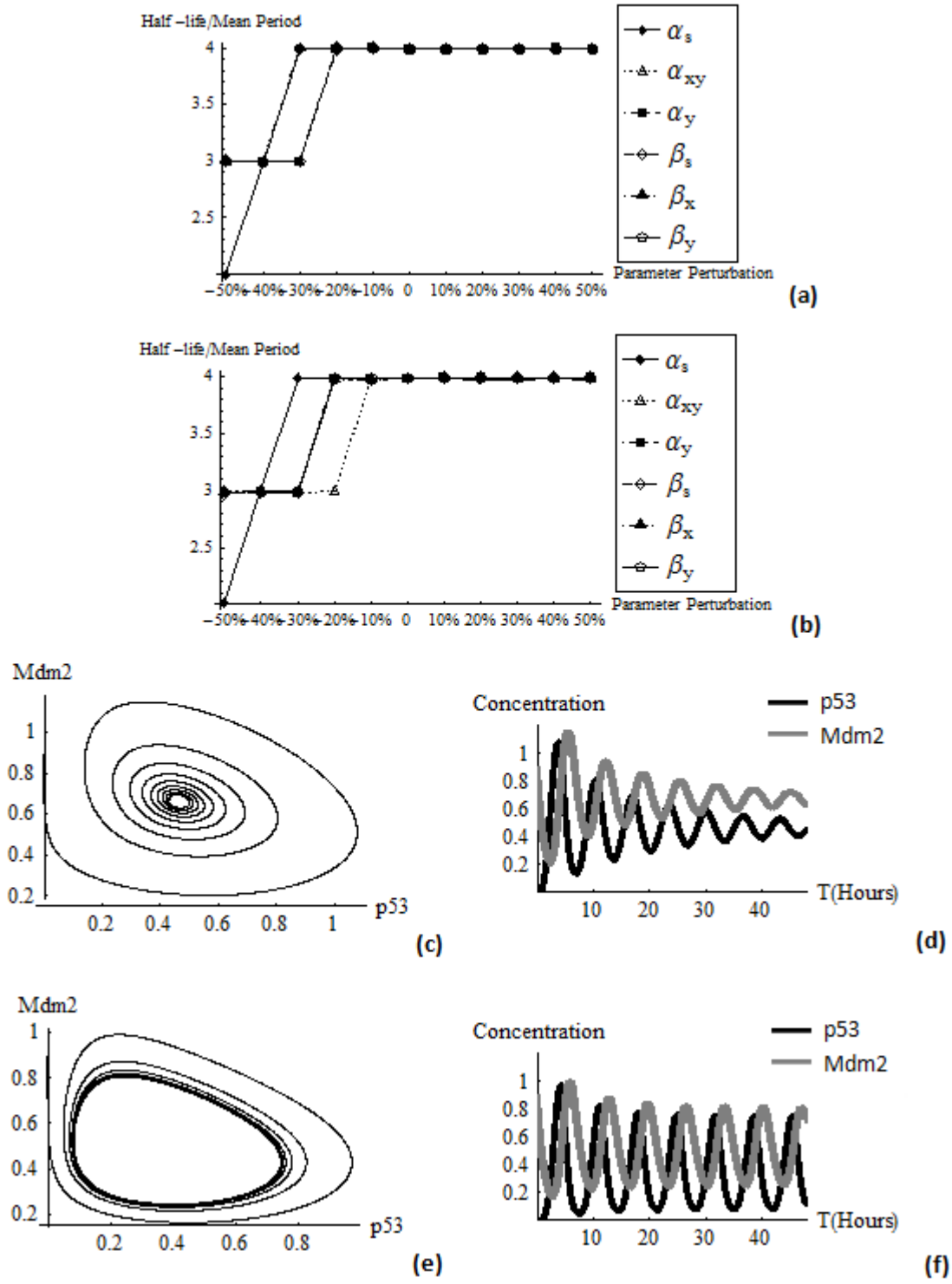

Figure 7-12 The analytical results from the proposed ANN model based on local sensitivity analysis (a and b): The influence of individual parameter changes on HoMP based on the behaviours of p53 and Mdm2, respectively. (c and e): Phase plane trajectories of p53 and Mdm2 under 50% reduced parameter value for α_s and the reference value for α_s, respectively. (d and f): Temporal performances of p53 and Mdm2 under the 50% reduced parameter value for α_s and the reference value for α_s, respectively.

7.4.2 The Robustness of the P53-Mdm2 System in the Presence of Various Levels of Perturbations to All Paramters (GSA)

In Chapter 4, we discussed why it was important to analyze the system's behaviour in response to simultaneous variation in parameters. In this investigation, we randomly generated 1000 samples of parameter vectors for the model parameters in three defined levels: reference values $\pm 10\%$; reference values $\pm 30\%$ and reference values $\pm 50\%$. Figure 7-13 illustrates the distribution of HoMP from the behaviours of p53 (Figure 7-13 (a, c and e)) and Mdm2 (Figure 7-13 (b, d and f)) under the three defined levels of parameter range, respectively. According to Figure 7-13, the p53-Mdm2 system is very robust for $\pm 10\%$ perturbation in all parameters (HoMP is almost equal to 4, which means that the half-life is close to four times the mean period of the p53-Mdm2 oscillation) as revealed by the behaviour of both p53 and Mdm2. With increases in perturbation of the model parameters, the robustness of the system becomes more susceptible and sensitive, which means that the p53-Mdm2 system generates less oscillatory behaviour when the parameters are examined within a range of $\pm 30\%$ to $\pm 50\%$. However, these may represent fixed stable points similar to that shown in Figure 7-12 (c). We also compute the mean of HoMP for 1000 samples under the three parameter ranges, and the results are given in Figure 7-13 (g). It shows that the robustness of the system as measured by HoMP in the presence of different parameter perturbations decreases with the severity of perturbations but the system stays more robust compared to the case of individual parameter perturbations presented in the previous section. For example, HoMP in Figure 7-13 (g) is above 2.8.

7.5 Summary

We have demonstrated that ANNs can be successfully developed to represent the p53-Mdm2 system and to solve the parameter estimation problem in the traditional ODE system. The ANN estimates of parameters agree with the kinetic constants used in the ODE-based models. More importantly, we investigated the robustness of the p53-Mdm2 system by studying the influence of individual parameter changes on HoMP which indicated the propensity to disrupt the oscillatory behaviour of the p53-Mdm2 system.

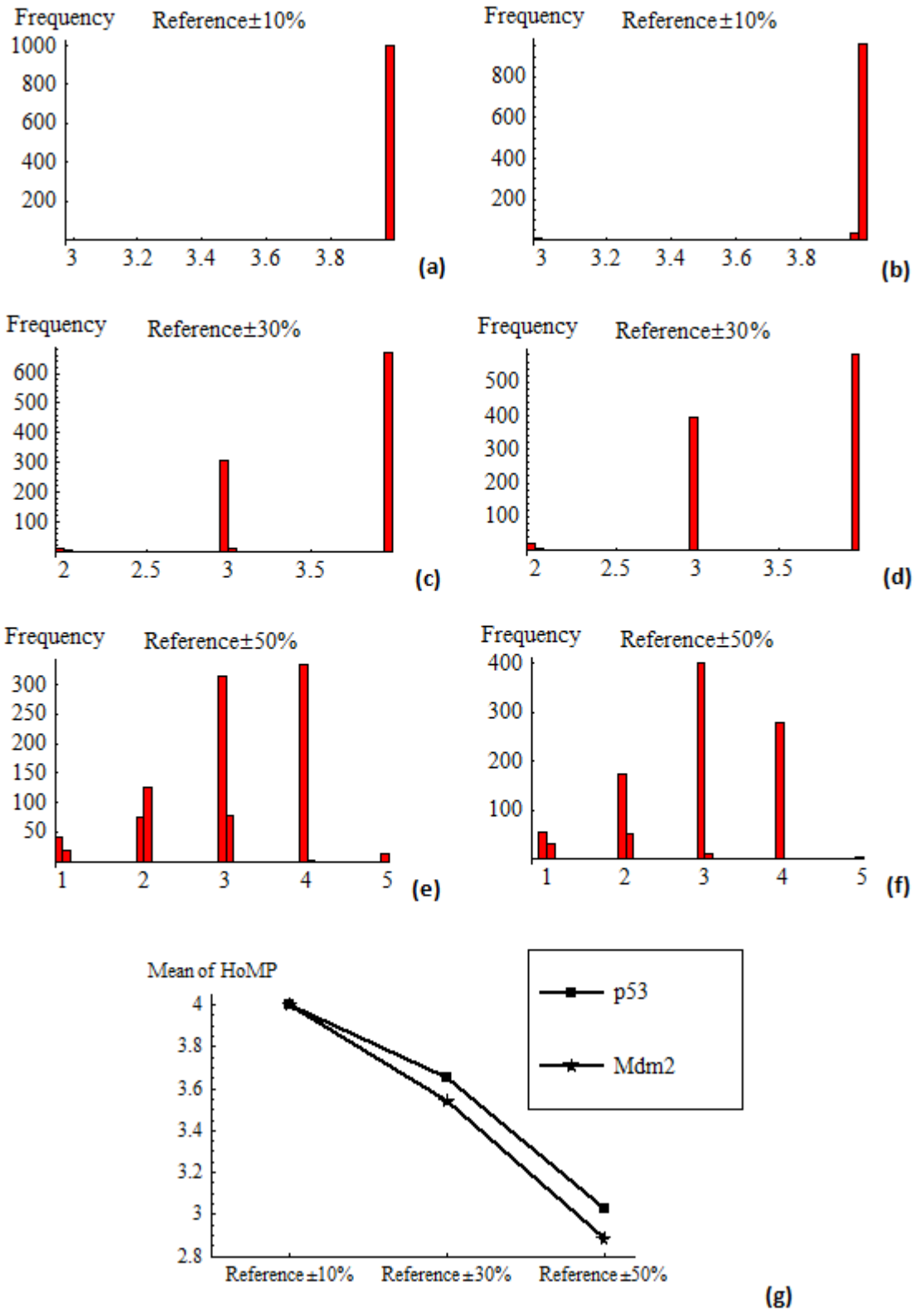

Figure 7-13 The analytical results from the proposed ANNs based on GSA. (a, c and e): The distribution of HoMP based on the behaviour of p53 under three defined parameter ranges. (b, d and f): the distribution of HoMP based on the behaviour of Mdm2 under three defined parameter ranges. (g): the mean HoMP for 1000 samples under three parameter ranges as a measure of the robustenss of the p53-Mdm2 oscillation system.

The developed recurrent ANNs representing Models III-VI proposed by Geva-Zatorsky et al. [2006] showed a good agreement with results from the ODE solutions for small Δt . Furthermore, the modified recurrent ANN accurately represented p53-Mdm2's behaviour for larger time steps (0.3 hours) that are representative of time scales in experimental measurements. These results demonstrated that the ANN technique can be used for representating real biological networks and parameter estimation of mathematical models for these real biological networks. These two aspects are novel contributions of the thesis to the field of computational systems biology.

In terms of the investigation of the robustness of the p53-Mdm2 oscillation system, the values of HoMP, used as a measure of the system's robustness in the presence of various levels of perturbations in model parameters, revealed that HoMP (HoMP = 4) was not affected by the changes in parameter values in the range [-20%, 50%], indicating that the proposed ANN suggested a sustained or weakly damped oscillation over a broad range of parameters. This agreed with Geva-Zatorsky et al.'s [2006] observations from the corresponding ODE models. Furthermore, parameter α_s (Mdm2-dependent signal inactivation rate) with a -50% change made a significant contribution to adjusting the stability of the system. For this condition, the system remained at a stable fixed point to keep the whole system stable instead of entering a limit cycle. Results of the investigation of the robustness of the p53-Mdm2 system based on simultaneously changing model parameters within $\pm 50\%$ range indicated that HoMP decreased with increased range of perturbations in the model parameters but the HoMP is more resilient to change than when individual parameter varies.

Chapter 8: Conclusions and Future Directions

The overall theme of this thesis was to integrate our knowledge of mathematics, biology and ANN techniques to study, model and gain insights into biological networks. The main objective of this research was to investigate a mathematical model for the G1/S cell-cycle checkpoint pathway incorporating the DNA-damage signal transduction pathway in cell division as well as the implementation of an ANN technique for the p53-Mdm2 oscillation system. Analytical approaches were developed for the G1/S checkpoint pathway and the p53-Mdm2 oscillation system, depending on the level of detail of the systems and the particular research questions asked. The simulated results from our approaches have indicated that they can be successful in gaining novel insights into the behaviour of these two biological systems. We now give a general overview of what we have achieved and the contribution of these achievements and future directions that can follow from the current work.

8.1 General Overview

The first focus of the current work was to investigate the robustness and the behaviour of the critical proteins under parameter perturbations of the G1/S checkpoint pathway with different levels of DNA-damage. To fulfil this goal, we first used a mathematical model for this system based on a model developed by Iwamoto et al. [2008], consisting of 28 ODEs with 75 kinetic parameters (Chapter 3). Then, to characterise the dynamic behaviours and the robustness of the system in the presence of various levels of perturbations in the kinetic parameters, we identified the critical proteins (E2F and CycE in this case) of the system as our biomarkers and proposed an analytical approach including Local Sensitivity Analysis (LSA), Global Sensitivity Analysis (GSA) and statistical Type II error (Chapter 4).

Finally, the resulting model was extensively tested and compared with the experimental data (Chapter 5). We summarised the findings of the model in the following three aspects. (1) We extensively tested the influence of individual kinetic parameters on the chosen biomarkers in the G1/S transition and the response of the cells to different intensities of DNA-damage: kinetic parameters related to p27 and CycE were the most significant factors affecting the

behaviour of the chosen biomarkers under no DNA-damage situation. In response to a DNA-damage situation, the kinetic parameters related to p21 and p53 became more important than for the normal cells. All these findings demonstrated the ability of the model to correctly predict experimental outcomes. (2) We used an analytical approach to GSA and Type II error: we focused on investigating the probability of accurately distinguishing healthy cells from defective cells on four defined levels of parameter range. The simulation results indicated that the percentage of damaged cells passing as healthy cells became very large (more than 38%) when the level of change of parameters exceeded $\pm 20\%$. This had a good qualitative agreement with experimental findings which stated that a large number of damaged cells undergo proliferation without being caught at DNA damage checkpoints. (3) We used two different approaches to analyze the robustness of the G1/S checkpoint: one was based on different thresholds of biomarkers, and the other was based on the mathematical definition of robustness. Results revealed from the behaviour of the two biomarkers were that the probability of damaged cells passing as healthy cells was not affected by the changes in peak time up to $\pm 20\%$, indicating the robustness of the G1/S checkpoint under parameter perturbations in response to different DNA-damage situations. The results based on the mathematical definition indicated that the robustness of the G1/S checkpoint pathway decreased with the increased intensity of the DNA-damage signal.

The second focus of the current research was to validate whether the mathematical model incorporating G1/S checkpoint pathway and DNA damage signal transduction pathway can highlight cellular senescence and formulate scenarios for adjusting the threshold for senescence to evaluate its efficacy and outcomes (Chapter 6). We started with the biological definition and some experimental observations. The purpose was to define critical factors (such as CDK2 and Skp2) in triggering cellular senescence in order to develop a hypothesis based on the proposed model. In our research, we analyzed the cellular senescence through lowering the critical trigger - CDK2. To do this, we focused our investigation on the behaviour of two important proteins (E2F and CycE) for several reduced CDK2 levels under two DNA-damage conditions by calculating the probability of DNA-damaged cells passing the G1/S checkpoint. A comparison of the values of the probability (β) under the normal CDK2 level and low CDK2 levels revealed that reducing CDK2 levels can reduce the percentage of damaged cells passing the G1/S checkpoint; in particular, a 50% reduction of CDK2 achieved a 65% reduction in the percentage of damaged cells passing the checkpoint.

We then analyzed the relationship between CDK2 and its corresponding CKIs in order to help find other effective ways to bring forward cellular senescence. Results showed that the degradation rate of p21 and the initial concentration of p27 can be effectively used to lower CDK2 levels to lower the senescence threshold. Specifically, p27 was the most effective in lowering the percentage of damaged dells passing the G1/S checkpoint and CDK2 and p21 had similar effects according to the behaviour of E2F, while CycE behaviour indicated that CDK2 and p27 had similar effects with p21 having a smaller influence. However, both E2F and CycE revealed that simultaneous variation of CDK2 and CKIs produced a dramatic reduction in damaged cells passing G1/S; CDK2/p27 combination almost totally arrested the passage of damaged cells through the checkpoint. These model findings can be validated by biologists in order to ascertain the real efficacy of these targets for treating cancer.

In addition, the same approaches as before were used to analyze the robustness of CDK2 in triggering cellular senescence. Results from different thresholds of biomarkers indicated that the percentage (β) of damaged cells passing G1/S checkpoint was not affected by the perturbation in their PT up to ±20% indicating the robustness in lowering the senescence bar through reduced CDK2. The results from the mathematical approach revealed that the robustness of CDK2 in triggering cellular senescence increased with the reduced CDK2 levels for the DNA-damage situation.

The final focus of the current thesis was to implement an ANN approach for simulating the p53-Mdm2 oscillation system as well as analysing the robustness of this system (Chapter 7). We first described the behaviour of p53-Mdm2 negative feedback loop under normal and DNA-damage conditions. Then, we described why we use ANN approach instead of the traditional approach using ODEs, and described how to develop ANNs for biological systems. Specifically, the incremental learning approaches used in ANNs made it possible for them to solve the most difficult parameter estimation problem in a mathematical model. More importantly, the structure of the proposed ANNs can directly represent the relationship of the chemical species involved in reactions in the simulated biological network. We developed and validated ANNs to represent four different mathematical models of the p53 and Mdm2 oscillation system proposed by Geva-Zatorsky et al., [2006]. Results from the ODE solutions and the proposed ANNs indicated that the proposed ANNs can successfully represent the behaviour of the p53-Mdm2 oscillation systems and accurately solve the parameter estimation problem. Finally, we used the developed ANNs to investigate the robustness of the p53-

Mdm2 oscillation system. According to the analytical results from LSA on HoMP, the measure of robustness of the system, the p53-Mdm2 oscillation system was very robust. The system can generate sustained or weakly damped oscillations over a broad range of parameters. Furthermore, α_s (Mdm2-dependent signal inactivation rate) played an important role in changing the stable configuration of the system from remaining in a limit cycle giving rise to oscillations to entering a stable fixed point with decreasing values of α_s. The GSA of the developed ANNs revealed that the ANN can generate stable and sustained oscillations when parameter variation was within a range of $\pm 10\%$; however, the robustness of the system became very sensitive with larger perturbations of the parameters. The results revealed from the mean of HoMP for the p53-Mdm2 model indicated that the robustness of the system decreased as expected from the behaviour of both p53 and Mdm2 in response to increased parameter perturbations. However, HoMP was more resilient to simultaneous parameter change, which is more realistic biologically.

8.2 Contributions

The contribution of this thesis spanned two topics through modelling and analysis of two systems:

- Advanced our understanding of the G1/S transition incorporating the DNA-damage transduction pathway by building and validating models incorporating current knowledge;
- Analyzed the influence of the kinetic parameters associated with the *in silico* biomarkers based on the mathematical model of the G1/S transition under different levels of DNA-damage situations, and identified the most significant kinetic parameters for the chosen biomarkers through the developed LSA approach;
- Evaluated the probability of DNA-damaged cells passing as healthy cells in the presence of various levels of perturbation in the key kinetic parameters of the *in silico* biomarkers associated with the mathematical model based on a combination of GSA and Type II error approach;
- Formulated a mathematical expression for defining the robustness of the protein signaling networks;
- Confirmed that the mathematical model of the G1/S transition incorporating DNA-damage signal transduction pathway can highlight cellular senescence;

- Demonstrated the potential of lowering the bar for triggering cellular senescence in cells based on the model's analytical results;
- Developed ANNs for the p53-Mdm2 oscillation system and solved the parameter estimation problem faced by the current mathematical models for biological networks.

8.3 Future Directions

The work described in this thesis suggested several directions for future work.

- As discussed in Section 2.2, there are two different ways to inhibit the activity of CycE/CDK2 in order to delay the G1/S transition in response to DNA-damage situation: one is based on the p53-p21 pathway and the other is based on the Chk2-Cdc25A pathway. The current model only focuses on the p53-p21 pathway. However, the Chk2-Cdc25A pathway plays an equally important role in controlling cell cycle progression as well as cell cycle arrest under DNA-damage situations. Therefore, it is important to extend the existing model to this pathway. The purpose of this is to extend our understanding of how cells control themselves in response to DNA damage through these two pathways.

- In terms of the DNA-damage transduction pathway, the current model revealed that the damage signal directly affects the activity of p53. In fact, the DNA-damage signal first activates both ATM and ATR. The activated ATM and ATR then promote the synthesis of p53 and Chk2 (in Chapter 2). The G1/S checkpoint pathway then combines with the p53-p21 pathway and Chk2-Cdc25A pathway for the cell cycle arrest. Therefore, it is necessary to establish the mathematical model to simulate the dynamic behaviour of the reactions among the DNA-damage signal, ATM/ATR, p53 and Mdm2. Furthermore, the equation denoting the DNA-damage signal should take a cellular mechanism of damage repair into account; however, it currently just uses a rate with a constant repair value. In fact, the DNA-damage repair is a complicated process. In our study, we do not incorporate into our model: (1) specific DNA-damage repair pathways to reflect the fact that different types of damage can be repaired by different pathways [Friedberg, 1995], and (2) the direct and indirect important role that p53 may play in DNA-damage repair processes [Smith et al., 1995]. Future work therefore could focus on these directions.

- The current model mainly focuses on the dynamic behaviour of the G1/S transition incorporating the DNA-damage transduction signal. Although the reconstructed model has a good predictive performance of the G1/S transition, it cannot represent the dynamic behaviour of the whole cell cycle regulation process. In order to have a deep understanding of cell cycle regulation in response to DNA-damage situations, a model that combines G1/S and G2/M transitions should be developed. Thus, we can develop two sub-models: one is the G1/S model and the other is the G2/M model. The details of the G2/M transition are shown in Chapter 2, and the differential equations can be assumed to follow chemical reactions involved in the G2/M transition.

- In Chapter 6, we demonstrated that the G1/S model can highlight cellular senescence through lowering the critical trigger - CDK2 and then investigated the potential of lowering the bar for triggering cellular senescence in oncogenically primed cells. Most results from the model have not been validated by realistic experimental observations; therefore, it is necessary to set up some real biological experiments as evidence for ascertaining the effectiveness of the targets. Meanwhile, these established experiments can help us optimize or advance the current model in order to better understand the behaviour of cellular senescence.

- In Chapter 7, we developed ANNs to simulate the p53-Mdm2 oscillation system. The developed ANN requires the estimations for initial weight values and time increments (dt) for each model. Small random values can be confidently used for initial weights; however, time increments need to be selected carefully depending on the temporal behaviour of the p53 and Mdm2. We do not have a precise benchmark to confirm whether the proposed neural network is the most optimum with the highest possible accuracy but ANNs were developed to mimick the ODEs models which they did with excellent accuracy. The proposed ANNs could represent the ODEs for this network with just linear activation functions (linear neurons) and a simple learning algorithm was able to estimate parameter values with remarkable accuracy. However, more powerful activation functions and learning algorithm have the potential to represent more complex chemical reactions that may be more realistic for biological systems. Therefore, there is much scope for improving and optimizing the developed neural networks in the future.

- The investigation of the mathematical model for the G1/S checkpoint pathway as well as the p53-Mdm2 oscillation system was based on deterministic simulations in the current study. However, investigating the stochastic properties of the biological network is another critical concept in systems biology. In terms of the stochastic simulations, we needed to focus on three questions: (1) What are the origins and consequences of intrinsic noise? (2) How do the chemical species in individual cells change under the different levels of extrinsic noise? (3) What is the difference between the deterministic and stochastic simulations of the dynamic behaviour of the system in order to gain more insights into the real system? We believe that it is worthwhile to tackle these issues as the answers will give us insights into the dominant reactions that drive the system's dynamics and therefore allow us to determine the most responsible chemical species that control the whole process.

8.4 Conclusions

Although the study of highly dynamic, interacting and complex biological systems is a challenging topic, it is becoming a critical focus in the current biological research. Furthermore, it is very difficult to understand the dynamics and functions of the underlying biological and biochemical processes in the complicated biological networks just from *in vitro* experiments. However, the mathematical modelling and simulation-based approaches have the potential to study, explore and understand such processes. More importantly, the mathematical model based on chemical kinetic theory of reactions invovled in the biological network played a crucial and reliable role in revealing the complexities of the simulated system. In this thesis, we have shown how the model developed can be used to investigate and understand the dynamic behaviour of the G1/S checkpoint pathway in response to DNA-damage signals; how the G1/S model can explore the potential to trigger cellular senescence in oncogenically primed cells and how ANN can be developed to represent properties of the p53-Mdm2 oscillation system. More importantly, we highlighted how ANN can accurately represent the biological networks and solve the parameter estimation problem of the traditional ODEs.

Although our investigation concentrated on a small subset of a specific problem in the G1/S checkpoint pathway as well as the DNA-damage signal pathway of cell cycle regulation, there

is indeed a large array of challenging and exciting biological phenomena in cell cycle regulation that require exploration. We believe that the success of the mathematical models presented in the thesis will encourage more biologists and mathematicians to look beyond the difficulties of interdisciplinary work and to investigate the benefits of integrated approaches in systems biology. Therefore, there are more opportunities to explore and provide valuable insights into the dynamic behaviour of these diverse biological systems.

References

Aderem, A., (2005). Systems biology: Its practice and challenges, Cell, 121, 511-513.

Aguda, B. D. & Tang. Y. (1999). The kinetic origins of the restriction point in the mammalian cell cycle. Cell Proliferation, 32(5), 321-335.

Allman, E. S., & Rhodes, J. A. (2004). Mathematical models in biology: an introduction. New York: Cambridge University Press.

Alon, U. (2003). Biological networks: the tinkerer as an engineer. Science, 301, 1866-1877.

Andreassen, P. R., Ho, G. P. H., & D'Andrea, A. D. (2006). DNA damage responses and their many interactions with the replication fork. Carcinogenesis, 27(5), 883-892.

Arkin, A. P., (2001). Synthetic cell biology. Curr Opin Biotechnol **12**(6): 638-44.

Avkin, S., Sevilya, Z., Toube, L., Geacintov, N., Chaney, S. G., Oren, M., & Livneh, Z., (2006). p53 and p21 Regulate Error-Prone DNA Repair to Yield a Lower Mutation Load., 22(3), 407-413.

Barak, Y., Juven, T., Haffner, R. & Oren, M. (1993). Mdm2 expression is induced by wild type p53 activity. EMBO J., 12, 461-468.

Baras, F., Pearson, J. E., & Mansour, M. M., (1990). Microscopic simulation of chemical oscillations in homogeneous systems. J. Chem. Phys., 93(8), 5747-5750.

Baras, F., (1997). In Stochastic Dynamics. In Lecture Notes in Physics (LNP484), eds. Schimansky-Geier, L. & Poeschel, T., 167–178.

Bartek, J., & Lukas, J., (2001). Mammalian G1- and S-phase checkpoints in response to DNA damage. Current Opinion in Cell Biology, 13(6), 738-747.

Bartek J., & Lukas J., (2001). Pathways governing G1/S transition and their response to DNA damage. FEBS Letters, 490(3), 117-122.

Batchelor, E., Mock, C.S. Bhan, I., Loewer, A., & Lahav, G., (2008). Recurrent initiations: a mechanism for triggering p53 pulses in response to DNA damage. Mol. Cell, 30, 277-289.

Beck, H., Nahse, V., Larsen, M. S. Y., Groth, P., Clancy, T., Lees, M., et al. (2010). Regulators of cyclin-dependent kinases are crucial for maintaining genome integrity in S phase. Journal of Cell Biology, 188(5), 629-638.

Bertalanffy, L. V. (1950). An outline of general system theory. British journal for the philosophy of science, 1, 134-165.

Black K., (2007). Australasian business statistics. Milton: John Wiley & Sons Australia. 3rd edn.

Bloom J., & Pagano M., (2003). Deregulated degradation of the cdk inhibitor p27 and malignant transformation. Seminars in Cancer Biology, 13(1), 41-47.

Boutros, R., Dozier, C., & Ducommun, B., (2006). The when and wheres of CDC25 phosphatases. Current Opinion in Cell Biology, 18(2), 185-191.

Branzei, D., & Foiani, M., (2007). Interplay of replication checkpoints and repair proteins at stalled replication forks. DNA Repair, 6(7), 994-1003.

Campaner, S., Doni, M., Hydbring, P., Verrecchia, A., & Bianchi, L., (2010). Cdk2 suppresses cellular senescence induced by the c-myc oncogene. Nat Cell Biol., 12(1), 54-59.

Chini, C. C. S., & Chen, J., (2003). Human Claspin Is Required for Replication Checkpoint Control. J. Biol. Chem., 278(32), 30057-30062.

Ciliberto, A., Petrus, M. J., Tyson, J. J., & Sible, J. C., (2003). A kinetic model of the cyclin E/Cdk2 developmental timer in *Xenopus laevis* embryos. Biophysical Chemistry, 104(3), 573-589.

Ciliberto A., Novak B., & Tyson J., (2005). Steady states and oscillations in the p53/Mdm2 network. Cell Cycle, 4(3), 488-493.

Collado, M., Blasco, M. A., & Serrano, M., (2007). Cellular senescence in cancer and aging. Cell 130, (2), 223-233.

Collado M., & Serrano M., (2010). Senescence in tumours: evidence from mice and humans. Nat Rev Cancer, 10(1), 51-57.

Cooper, G., (2000). The Cell: A Molecular Approach. Sinaeur Associates, Inc.

Coqueret O., (2003). New roles for p21 and p27 cell-cycle inhibitors: a function for each cell compartment? Trends in Cell Biology, 13(2), 65-70.

Covert, M. W., & Palsson, B. O., (2002). Transcriptional regulation in constraintsbased metabolic models of *Escherichia coli*. J Biol Chem., **277**(31), 28058-64.

Dang, T., Bao, S., & Wang, X.-F. (2005). Human Rad9 is required for the activation of S-phase checkpoint and the maintenance of chromosomal stability. Genes to Cells, 10(4), 287-295.

Dart, D. A., Adams, K. E., Akerman, I., & Lakin, N. D. (2004). Recruitment of the Cell Cycle Checkpoint Kinase ATR to Chromatin during S-phase. J. Biol. Chem., 279(16), 16433-16440.

Dasika, G. K., Lin, S. C., Zhao, S., Sung, P., Tomkinson, A., & Lee, E. Y. (1999). DNA damage-induced cell cycle checkpoints and DNA strand break repair in development and tumorigenesis. Oncogene, 18, 7883-7899,

Denicourt, C., & Dowdy, S.F., (2004). Cip/Kip proteins: CDKs inhibitors. Genes Dev., 18, 851–855.

Desany, B. A., Alcasabas, A. A., Bachant, J. B., & Elledge, S. J. (1998). Recovery from DNA replicational stress is the essential function of the S-phase checkpoint pathway. Genes Dev., 12(18), 2956-2970.

Dickson, M.A., & Schwartz, G.K., (2009). Development of cell-cycle inhibitors for cancer therapy. Curr Oncol., 2009; 16(2): 36–43.

Dulic V., Kaufmann W.K., Wilson S.J., Tisty T.D., Lees E., Harper J.W., Elledge S.J., & Reed S.I., (1994). p53-dependent inhibition of cyclin-dependent kinase activities in human fibroblasts during radiation-induced G1 arrest. Cell, 76(6), 1013-1023.

Dyson N., (1998). The regulation of E2F by pRB-family proteins. Genes & Dev., 12, 2245-2262

Enders, G. H., Johnson, N., & Shapiro, G. I. (2010). Targeting Cyclin-Dependent Kinases for Cancer Therapy. In Cell Cycle Deregulation in Cancer (pp. 167-185): Springer New York.

Fausett,L.A. (1994). Fundamentals of Neural Networks: Architectures, Algorithms and Applications. US, Prentice Hall.

Foster, I., (2008). Cancer: a cell cycle defect. Radiography, 14 (2), 144–149.

Freeman, S., (2002). Cell Division. Biological Science. Upper Saddle River, NJ: Prentice Hall, 155-174

Fridman, J. S., & Lowe, S. W., (2003). Control of apoptosis by p53. Oncogene, 22(56), 9030-9040.

Friedberg, E. C., (1995). DNA repair and Mutagenesis. Washington, DC, American Society for Microbiology, 2nd ed.

Fuss, H., Dubitzky, W., Downes, C. S., & Kurth, M. J. (2005). Mathematical models of cell cycle regulation. Brief Bioinform., 6(2), 163-177.

Gardner, R. D., & Burke, D. J. (2000). The spindle checkpoint: two transitions, two pathways. Trends in Cell Biology, 10(4), 154-158.

Ge, H., Walhout, AJ.M., & Vidal, M., (2003). Integrating 'omic' information: a bridge between genomics and systems biology. Trends Genet., 19, 551-560.

Geva-Zatorsky, N., Rosenfeld, N., Itzkovitz, S., Milo, R., Sigal, A., Dekel, E., Yarnitzky, T. Liron, Y., Polak P., Lahav G., & Alon U. (2006). Oscillations and variability in the p53 system, Mol. Syst. Biol., 2.

Giordano, A., & Galderisi, U., (2010). Short Introduction to the Cell Cycle. In Cell Cycle Regulation and Differentiation in Cardiovascular and Neural Systems (pp. 3-14): Springer New York.

Gonze, D., Halloy, J., & Goldbeter, A. (2002). Robustness of circadian rhythms with respect to molecular noise. Proc. Natl. Acad. Sci., U.S.A., 99(2), 673-678.

Gutierrez, G. J., Tsuji, T., Cross, J. V., Davis, R. J., Templeton, D. J., Jiang, W., et al. (2010). JNK-mediated Phosphorylation of Cdc25C Regulates Cell Cycle Entry and G2/M DNA Damage Checkpoint. Journal of Biological Chemistry, 285(19), 14217-14228.

Haberichter, T., Madge, B., Christopher, R. A., Yoshioka, N., Dhiman, A., Miller, R., et al. (2007). A systems biology dynamical model of mammalian G1 cell cycle progression. Mol Syst Biol., 3.

Hagan, M.T.,& Demuth, H.B., Beale, M.H. (1995). Neural network design. UAS, PWS Pub.

Hanahan, D. & Weinberg, R. (2000). The hallmarks of cancer. Cell, 100(1), 57-70.

Harper, J. W., Burton, J. L., & Solomon, M. J. (2002). The anaphase-promoting complex: it's not just for mitosis any more. Genes Dev., 16(17), 2179-2206.

Harris S.L., & Levine A.J., (2005). The p53 pathway: positive and negative feedback loops. Oncogene, 24, 2899-2908.

Hartwell L.H., & Kastan M.B., (1994). Cell cycle and cancer. Science, 266, 1821-1828.

Hassoun, M.H. (1995). Fundamentals of artificial neural networks. Cambridge: MIT Press.

Hatzimanikatis, V., Lee, K. H., Renner, W. A., & Bailey, J. E. (1995). A mathematical model for the G1/S transition of the mammalian cell cycle. Biotechnology Letters, 17, 669-674.

Hatzimanikatis, V., Lee, K. H. & Bailey, J. E. (1999). A mathematical description of regulation of the G1-S transition of the mammalian cell cycle. Biotechnology and Bioengineering, 65(6), 631-637.

Haupt S., Berger M., Goldberg Z., & Haupt Y., (2003). Apoptosis - the p53 network. J Cell Sci., 116(20), 4077-4085.

Haup, Y., Maya, R., Kazaz, A., & Oren, M., (1997). Mdm2 promotes the rapid degradation of p53. Nature, 387(6630), 296-299.

Hayflick, L., & Moorhead, P. S., (1961). The serial cultivation of human diploid cell strains. Experimental Cell Research, 25(3), 585-621.

Haykin, S., (1994). Neural networks: a comprehensive foundation. New York: McMillan.

Haykin, S., (1999). Neural networks: a comprehensive foundation. Prentice Hall. 2nd ed.

Heath, A.P., & Kavraki, L.E., (2009). Computational challenges in systems biology. Computer science reviews, 3, 1-17.

Helin K., (1998). Regulation of cell proliferation by the E2F transcription factors. Current Opinion in Genetics and Development, 8(1), 28-35.

Hertz, J.A., Krogh, A., & Palmer R.G., (1991). Introduction to the theory of neural computation. Redwood City, California: Addison-Wesley Publishing.

Hiebert, S.W., Chellappan, S.P., Horowitz, J.M., & Nevins, J.R., (1992).The interaction of RB with E2F coincides with an inhibition of the transcriptional activity of E2F. Genes & Development, 6(2), 177-185.

Hill, A. V., (1910). The possible effects of the aggregation of the molecules of haemoglobin

on its oxygen dissociation curve. J Physiol, 40, 4-7.

Hopfield, J. J., (1982). Neural Networks and Physical Systems with Emergent Collective Computational Abilities. Proc. Natl. Acsd. Sci., U.S.A. 79, 2554.

Horn, H.F. & Vousden, K. (2007). Coping with stress: multiple ways to activate p53. Oncogene, 26, 1306-1316.

Ideker, T., Galitski, T., & Hood,L., (2001). A new approach to decoding life: Systems biology, Annu. Rev. Genom. Hum. Genet., 2, 343-372.

Ikeda M.A., Jakoi L., & Nevins J.R., (1996). A unique role for the Rb protein in controlling E2F accumulation during cell growth and differentiation. Proc. Natl. Acad. Sci., USA, 93, 3215-3220.

Iliakis G., Wang Y., Guan J., & Wang H., (2003). DNA damage checkpoint control in cells exposed to ionizing radiation. Oncogene, 22(37), 5834-5847

Iwamoto, K., Hamada, H., Eguchi, Y., & Okamoto, M. (2011). Mathematical modelling of cell cycle regulation in response to DNA damage: Exploring mechanisms of cell-fate determination. Biosystems, 103(3), 384-391.

Iwamoto, K., Tashima, Y., Hamada, H., Eguchi, Y., & Okamoto, M., (2006), Mathematical Modelling of G1/S Phase in the Cell Cycle with Involving the p53/Mdm2 Network.

Iwamoto, K., Tashima, Y., Hamada, H., Eguchi, Y., & Okamoto, M., (2008). Mathematical modelling and sensitivity analysis of G1/S phase in the cell cycle including the DNA-damage signal transduction pathway. Biosystems, 94(1-2), 109-117.

Jin, S., & Levine, A.J., (2001). The p53 functional circuit. Journal of Cell Science, 114, 4139-4140.

Karlsson-Rosenthal, C., & Millar, J. B. A., (2006). Cdc25: mechanisms of checkpoint inhibition and recovery. Trends in Cell Biology, 16(6), 285-292.

Kelly, T. J., & Brown, G. W., (2000). Regulation of chromosome replication. Annual Review of Biochemistry, 69(1), 829-880.

Kennedy M.P., & Chua L.O., (1998). Neural networks for nonlinear programming. IEEE trans. Circuits syst., CAS-35 (5). 554-562.

Keyomarsi K., & Herliczek T.W., (1997). The role of cyclin E in cell proliferation, development and cancer. Prog Cell Cycle Res., 3, 171-191.

Kim, J.-E., McAvoy, S. A., Smith, D. I., & Chen, J., (2005). Human TopBP1 Ensures Genome Integrity during Normal S Phase. Mol. Cell. Biol., 25(24), 10907-10915.

Kitano, H., (2002). Systems Biology: a brief overview. Science, 295, 1662-1664.

Kitano, H., (2004a). Biology robustness. Nat. Rev. Geget., 5, 826-837.

Kitano, H., (2004b). Cancer as a robust system: implications for anticancer therapy. Nat Rev Cancer, 4, 227-235.

Kitano, H., (2007). Towards a theory of biological robustness. Mol Syst Biol., 3.

Kitano, H., & Oda, K. (2006). Robustness trade-offs and host-microbial symbiosis in the immune system. Mol. Syst. Biol., 2, 0022.

Klipp, E., & Liebermeister, W., (2006). Mathematical modelling of intracellular signalling pathways. BMC Neuroscience, 7(Suppl 1), S10.

Kobayashi, M., Hirano, A., Kumano, T., Xiang, S.-L., Mihara, K., Haseda, Y., et al., (2004). Critical role for chicken Rad17 and Rad9 in the cellular response to DNA damage and stalled DNA replication. Genes to Cells, 9(4), 291-303.

Kohn, K. W., (1998). Functional capabilities of molecular network components controlling the mammalian G1/S cell cycle phase transition. Oncogene, 16, 1065-1075.

Kubbutat, M.H., Jones, S.N. & Vousden, K.H.,(1997), Regulation of p53 stability by Mdm2. Nature, 387(6630), 299-303.

Lahav G., Rosenfeld N., Sigal A., Geva-Zatorsky N., & Levine A.J., (2004). Dynamics of the p53-Mdm2 feedback loop in individual cells. Nat. Genet, 36,147-150.

Lane, D.P., (1992), Cancer. p53, guardian of the genome. Nature, 358(6381), 15-16.

Lapenna, S., & Giordano, A. (2009). Cell cycle kinases as therapeutic targets for cancer. Nat. Rev. Drug. Discov., 8(7), 547-566.

Leone G., DeGregori J., Jakoi L., Cook J.G., & Nevins J.R., (1999). Collaborative role of E2F transcriptional activity and G1 cyclin dependent kinase activity in the induction of S phase. Proc. Natl. Acad. Sci., USA, 96, 6626-6631.

Lev Bar-Or R., Maya R., Segel L.A., Alon U., Levine A.J., & Oren M., (2000). Generation of oscillations by the p53-Mdm2 feedback loop: A theoretical and experimental study. Proc. Natl. Acad. Sci., USA, 97(21), 11250-11255.

Li G., & Ho V.C., (1998). p53-Dependent DNA repair and apoptosis respond differently to high- and low-dose ultraviolet radiation. British Journal of Dermatology, 139(1), 3-10.

Ling, H., Kulasiri, D., and Samarasinghe, S.: ‘Robustness of G1/S checkpoint pathways in cell cycle regulation based on probability of DNA-damaged cells passing as healthy cells’, Biosystem, 2010, 101, (3), pp. 213-22.

Lin, H.-K., Chen, Z., Wang, G., Nardella, C., & Lee, S.-W., (2010). Skp2 targeting suppresses tumorigenesis by Arf-p53-independent cellular senescence. Nature, 464(7287), 374-379

Liu, W.-F., Yu, S.-S., Chen, G.-J., & Li, Y.-Z. (2006). DNA Damage Checkpoint, Damage Repair, and Genome Stability. Acta Genetica Sinica, 33(5), 381-390.

Lukas J., Petersen B.O., Holm K., Bartek J., & Helin K., (1996). Deregulated expression of E2F family members induces S-phase entry and overcomes p16INK4A-mediated growth suppression. Mol. Cell. Biol., 16(3), 1047-1057.

Lupardus, P. J., Byun, T., Yee, M.-c., Hekmat-Nejad, M., & Cimprich, K. A. (2002). A requirement for replication in activation of the ATR-dependent DNA damage checkpoint. Genes Dev., 16(18), 2327-2332.

Mailand, N., Falck, J., Lukas, C., Sylju, aring, sen, R. G., et al. (2000). Rapid Destruction of Human Cdc25A in Response to DNA Damage. Science, 288(5470), 1425-1429.

Malumbres, M., & Barbacid, M., (2009). Cell cycle, CDKs and cancer: a changing paradigm. Nat. Rev. Cancer, 9(3), 153-166.

Malumbres, M., & Carnero. A., (2003). Cell cycle deregulation: a common motif in cancer. Progress in cell cycle research, 5, 5-18.

Malumbres, M., & Barbacid, M. (2009). Cell cycle, CDKs and cancer: a changing paradigm. Nat. Rev. Cancer, 9(3), 153-166.

Ma, L., Wagner, J., Rice, J.J., Hu, W., Levine, A.J., & Stolovitzky G.A. (2005). A plausible model for the digital response of p53 to DNA damage. Proceedings of the National Academy of Sciences, USA, 102, 14266-14271.

Maren, A. Harston, C., & Pap, R. (1990). Handbook of neural computing applications. California: Academic Press.

Matsuoka, S., Huang, M., & Elledge, S. J. (1998). Linkage of ATM to cell cycle regulation by the Chk2 protein kinase. Science, 282(5395), 1893-1897.

McKay M.D., Beckman R.J., & Conover W.J., (2000). A comparison of three methods for selecting values of input variables in the analysis of output from a computer code. Technometrics, 42(1),55-61.

Mesarovic, M.D., (1968). Systems theory and biology. NY: Springer-Verlag.

Michaelis, L., & Menten M. I. (1913). Die Kinetik der Invertinwirkung. Biochemische Zeitschrift, 49, 333-69.

Molinari M., (2000). Cell cycle checkpoints and their inactivation in human cancer. Cell Proliferation, 33(5), 261-274.

Monk, N. A., (2003). Oscillatory Expression of Hes1, p53 and NF-_B driven by transcriptional time delays, Current Biology, 13, 1409-1413.

Morgan, D.O. (2007). The cell cycle: principles of control. United Kingdom: Oxford University Press

Murray, A. W., & Hunt, T. (1993). The cell cycle: an introduction. New York: W.H. Freeman.

Musacchio, A., & Hardwick, K. G. (2002). The spindle checkpoint: structural insights into dynamic signalling. Nat. Rev. Mol. Cell Biol., 3(10), 731-741.

Novák, B., & Tyson, J. J. (2003). Modelling the controls of the eukaryotic cell cycle. Biochem. Soc. Trans., 31(Pt 6), 1526-1529.

Novák, B., & Tyson, J. J. (2004). A model for restriction point control of the mammalian cell cycle. Journal of Theoretical Biology, 230(4), 563-579.

Nyberg, K. A., Michelson, R. J., Putnam, C. W., & Weinert, T. A. (2002). Toward maintaining the genome: DNA damage and replication checkpoints. Annual Review of Genetics, 36(1), 617-656.

Obaya A.J., & Sedivy J.M., (2002). Regulation of cyclin-Cdk activity in mammalian cells. Cellular and Molecular Life Sciences, 59, 126-142.

Obeyesekere, M. N., Knudsen, E. S., Wang, J. Y. J. & Zimmerman, S. O. (1997). A mathematical model of the regulation of the G1 phase of Rb +/+ and Rb -/- mouse embryonic fibroblasts and an osteosarcoma cell line. Cell Proliferation, 30(3-4), 171-194.

Obeyesekere, M. N., Zimmerman, S. O., Tecarro, E. S., & Auchmuty, G. (1999). A model of cell cycle behaviour dominated by kinetics of a pathway stimulated by growth factors. Bulletin of Mathematical Biology, 61, 917-934.

Ohtani K., (1999). Implication of transcription factor E2F in regulation of DNA replication. Front. Biosci. 4, d793-d804.

Ohtani K., DeGregori J., & Nevins J.R., (1995). Regulation of the cyclin E gene by transcription factor E2F1. Proc. Natl. Acad. Sci., USA, 92(26),12146-12150

Ohtsubo, M., Theodoras, A. M., Schumacher, J., Roberts, J. M., & Pagano, M. (1995). Human cyclin E, a nuclear protein essential for the G1-to-S phase transition. Mol. Cell. Biol., 15(5), 2612-2624.

Oltvai, Z.N., & Barabasi, A.L. (2002). Systems biology. Life's complexity pyramid, Science 298(5594), 763-764.

Petermann, E., & Caldecott, K. W. (2006). Evidence that the ATR/Chk1 pathway maintains normal replication fork progression during unperturbed S phase. Cell Cycle, 5(19), 2203-2209.

Petersen, L., Hasvold, G., Lukas, J., Bartek, J., & Syljuåsen, R. G. (2010). p53-dependent G1 arrest in 1st or 2nd cell cycle may protect human cancer cells from cell death after treatment with ionizing radiation and Chk1 inhibitors. Cell Proliferation, 43(4), 365-371.

Peng, C.-Y., Graves, P. R., Thoma, R. S., Wu, Z., Shaw, A. S., & Piwnica-Worms, H., (1997). Mitotic and G2 Checkpoint Control: Regulation of 14-3-3 protein binding by phosphorylation of Cdc25C on Serine-216. Science, 277(5331), 1501-1505.

Pierce, B. A. (2005). Genetics: a conceptual approach (2nd ed.). New York: W.H. Freeman.

Poehlmann, A., & Roessner, A. (2010). Importance of DNA damage checkpoints in the pathogenesis of human cancers. Pathology - Research and Practice, 206(9), 591-601.

Pritchard, L., & Kell, D. B., (2002). Schemes of flux control in a model of *Saccharomyces*

cerevisiae glycolysis. Eur J Biochem., 269**[**16]: 3894-904.

Proctro, C.J., & Gray, D.A. (2008). Explaining oscillations and variablity in the p53-Mdm2 system. BMC Systems Biology, 2(75).

Qu, Z., Weiss, J. N., & MacLellan, W. R. (2003). Regulation of the mammalian cell cycle: a model of the G1-to-S transition. Am. J. Physiol. Cell Physiol., 284(2), C349-364.

Ramalingam, S., Honkanen, P., Young, L., Shimura, T., Austin, J., Steeg P.S., & Nishizuka, S., (2007). Quantitative Assessment of the p53-Mdm2 feedback loop using protein lysate microarrays. Cancer Research, 67(13), 6247-6252

Rand D.A., (2008). Mapping global sensitivity of cellular network dynamics: sensitivity heat maps and a global summation law. J. R. Soc., Interface, 5 (Suppl 1), S59-S69.

Reed S., (1997). Control of the G1/S transition. Cancer Surv., 29, 7-23

Rieder, C. L., Cole, R. W., Khodjakov, A., & Sluder, G. (1995). The checkpoint delaying anaphase in response to chromosome monoorientation is mediated by an inhibitory signal produced by unattached kinetochores. J. Cell Biol., 130(4), 941-948.

Robert, J., Vekris, A., Pourquier, P. & Bonnet, J., (2004). Predicting drug response based on gene expression. Crit. Rev. Oncology/Haematology. 51, 205-227.

Rojas, R. (1996). Neural Networks: A systematic introduction. Berlin: Springer-Verlag.

Samarasinghe, S. (2006). Neural networks for applied sciences and engineering: from fundamentals to complex pattern recognition. Boca Raton, FL: Auerbach.

Samuel, B., & Basile, G., (2007). Analysis of a minimal model for p53 oscillations. Jounal of Theretical Biology, 249, 235-245.

Sanchez, Y., Wong, C., Thoma, R. S., Richman, R., Wu, Z., Piwnica-Worms, H., et al. (1997). Conservation of the chk1 checkpoint pathway in mammals: linkage of DNA damage to Cdk regulation through Cdc25. Science, 277(5331), 1497-1501.

Serrano, M., (2010). Cancer: a lower bar for senescence. Nature, 464(7287), 363-364.

Sherr, C.J., (1994). G1 phase progression: cycling on cue. Cell, 79, 551–555.

Sherr C.J., & Roberts J.M., (1999). CDK inhibitors: positive and negative regulators of G1-phase progression. Genes & Dev., 13, 1501-1512.

Shu K.X., Li B., & Wu L.X., (2007). The p53 network: p53 and its downstream genes. Colloids and Surfaces B: Biointerfaces, 55(1), 10-18.

Skibbens, R.V., & Hieter. P. (1998). Kinetochores and the checkpoint mechanism that monitors for defects in the chromosome segregation machinery. Annu. Rev. Genet., 32, 307–337.

Smith, M.L., Chen, L-T., Zhan, Q., O'Connor, P.M., & Fornace, A.J., (1995). Involvement of the p53 tumor suppressor in repair of u.v.-type DNA damage. Oncogene, 10, 1053-1059.

Smits, V. A. J., Klompmaker, R., Arnaud, L., Rijksen, G., Nigg, E. A., & Medema, R. H. (2000). Polo-like kinase-1 is a target of the DNA damage checkpoint. Nat. Cell Biol., 2(9), 672-676.

Smits, V. A. J., & Medema, R. H. (2001). Checking out the G2/M transition. Biochimica et Biophysica Acta (BBA) - Gene Structure and Expression, 1519(1-2), 1-12.

Sogo, J. M., Lopes, M., & Foiani, M. (2002). Fork Reversal and ssDNA Accumulation at Stalled Replication Forks Owing to Checkpoint Defects. Science, 297(5581), 599-602.

Srivastava, N., Gochhait, S., de Boer, P., & Bamezai, R. N. K. (2008). Role of H2AX in DNA damage response, human cancers. Mutation Research/Reviews in Mutation Research, 681(2-3), 180-18.

Stelling, J., Gilles, E. D., & Doyle, F. J., (2004). Robustness properties of circadian clock architectures. Proceedings of the National Academy of Sciences of the United States of America, 101(36), 13210-13215.

Stelling J., Sauer U., Szallasi Z., Doyle Iii F.J., & Doyle J., (2004). Robustness of cellular functions. Cell, 118(6), 675-685.

Stein, G. S., & Pardee, A. B. (2004). Cell cycle and growth control: biomolecular regulation and cancer (2nd ed.). Hoboken, NJ: Wiley-Liss.

Strogaz, S. H. (2000). Non-linear Dynamics and Chaos. Perseus Books, Reading, MA.

Sudakin, V., Chan, G. K. T., & Yen, T. J. (2001). Checkpoint inhibition of the APC/C in HeLa cells is mediated by a complex of BUBR1, BUB3, CDC20, and MAD2. J. Cell Biol., 154(5), 925-936.

Tao Q., Cao J.D., Xue M.S., & Qiao H. (2001). A high performance neural network for solving nonlinear programming problems with hybrid constraints. Phys. Lett., 288(2), 88-94.

Tashima, Y., Hanai, T., Hamada, H., & Okamoto, M. (2003). Kinetics Behavior of G1-to-S Cell Cycle Phase Transition Model. Genome Informatics, 14, 607-608.

Tashima, Y., Hanai, T., Hamada, H., & Okamoto, M. (2004). Simulation for detailed mathematical model of G1-to-S cell cycle phase transition. Genome Informatics, 9.

Tashima, Y., Hamada, H., Okamoto, M. & Hanai, T., (2008). Prediction of key factor controlling G1/S phase in the mammalian cell cycle using system analysis. Journal of bioscience and bioengineering, 106(4), 368-374.

Tessema, M., Lehmann,U., Kreipe, H.,(2004). Cell cycle and no end. Virchows Archiv, 444, 313-323.
Trewavas, A., (2006), A brief history of systems biology, Plant. Cell. 18(10), 2420-2430.

Toledo, F., & Wahl, G. M., (2006). Regulating the p53 pathway: *in vitro* hypothesis, in *vivo veritas*. Nature Review Cancer, 6, 909-923.

Tyson, J. J., Novak, B., Odell, G. M., Chen, K., & Dennis Thron, C. (1996). Chemical kinetic theory: understanding cell-cycle regulation. Trends in Biochemical Sciences, 21(3), 89-96.

van Vugt, M. A. T. M., Smits, V. A. J., Klompmaker, R., & Medema, R. H. (2001). Inhibition of polo-like kinase-1 by DNA damage occurs in an ATM-/ATR-dependent fashion. J. Biol. Chem., M101831200.

Vermeulen, K., Van Bockstaele, D.R., Berneman, Z.N., 2003. The cell cycle: a review of regulation, deregulation and therapeutic targets in cancer. Cell Prolif., 36, 131–149.

Vijg J., & Dollé M.E.T., (2002). Large genome rearrangements as a primary cause of aging. Mechanisms of Ageing and Development, 123(8), 907-915.

Vlach, J., Hennecke, S., & Amati, B., (1997). Phosphorylation dependent degradation of the cyclin-dependent kinase inhibitor p27Kip1. EMBO J., 16, 5334–5344.

Vogelstein, B., Lane, D., & Levine, A.J., (2000). Surfing in p53 network. Nature, 408, 307-310.

Waage, P. G., C. M. (1864). Forhandlinger: Videnskabs-Selskabet i. Christiana 35.

Wagner, J., Ma,L., Rice, J. J., Hu, W., Levine, A. J., & Stolovitzky, G. A. (2005). p53-Mdm2 loop controlled by a balance of its feedback strength and effective dampening using ATM and delayed feedback, IEE Systems Biology, 152(3), 109-118.

Walter, J., & Newport, J. (2000). Initiation of eukaryotic DNA replication: origin unwinding and sequential chromatin association of Cdc45, RPA, and DNA polymerase α. molecular Cell, 5(4), 617-627.

Wiener, N. (1948). Cybernetics, or, Control and communication in the animal and the machine. New York, Wiley.

Wolkenhauer, O., (2001). Systems biology: the reincarnation of systems theory applied in biology? Brief Bioinform., 2(3), 258-70.

Wu, T., Zhang, X., Huang, X., Yang, Y., & Hua, X. (2010). Regulation of Cyclin B2 Expression and Cell Cycle G2/M Transition by Menin. Journal of Biological Chemistry, 285(24), 18291-18300.

Wu, X., Bayle, J.H., Olson, D., & Levine, A.J., (1993). The p53-mdm-2 autoregulatory feedback loop. Gene Dev., 7, 1126-1132.

Xia, Y. S., & Wang, J., (1998). A general methodology for designing globally convergent optimization neural networks. IEEE Ttans. Neural Netw., 9(6), 1331-1343.

Xie, S., Wu, H., Wang, Q., Cogswell, J. P., Husain, I., Conn, C., et al. (2001). Plk3 Functionally Links DNA Damage to Cell Cycle Arrest and Apoptosis at Least in Part via the p53 Pathway. J. Biol. Chem., 276(46), 43305-43312.

Yang, Y.; Lee. K.S., Xiang, C., & Lin, H., (2009). Biological mechanisms revealed by a mathematical model for p53-Mdm2 core regulation. IET Syst Biol., 3(4), 229-238.

Yarbro, J. W., (1992). Mechanism of action of hydroxyurea. Sem. Oncol., 19, 1-10.

Yuh, C. H., Bolouri, H. et al., (2001). Cis-regulatory logic in the endo16 gene:switching from a specification to a differentiation mode of control. Development, 128(5), 617-29.

Zacharie, W., & K. Nasmyth. (1999). Whose end is destruction: cell division and the anaphase-promoting complex. Genes Dev., 13, 2039–2058.

Zerfass-Thome, K., Schulze, A., Zwerschke,W., Vogt, B., Helin, K., Bartek, J., Henglein, B., & Jansen-Durr, P., (1997). p27KIP1 blocks cyclin E-dependent transactivation of cyclin A gene expression. Mol. Cell Biol., 17, 407–415.

Zou, L., Cortez, D., & Elledge, S.J., (2002). Regulation of ATR substrate selection by Rad17-dependent loading of Rad9 complexes onto chromatin. Genes Dev., 16, 198-208.

Zou, L., & Elledge, S. J. (2003). Sensing DNA Damage through ATRIP Recognition of RPA-ssDNA Complexes. Science, 300(5625), 1542-1548.

Zimmerman, B. T., & Ebrary, Inc. (2004). Understanding breast cancer genetics. Jackson: University Press of Mississippi.

Appendices:

Appendix A: The sequential order ODEs for the G1/S model

$$\frac{dx_0}{dt} = k_1 + k_4 x_5 - (k_2 x_0 + k_3 x_0 x_3) \quad \text{(A-1)}$$

$$\frac{dx_1}{dt} = k_5 x_{21} + k_8 x_6 - (k_6 x_1 + k_7 x_1 x_4) \quad \text{(A-2)}$$

$$\frac{dx_2}{dt} = k_9 x_{26} + k_{12} x_8 - (k_{10} x_2 + k_{11} x_2 x_4) \quad \text{(A-3)}$$

$$\frac{dx_3}{dt} = k_4 x_5 + k_{13} x_5 - (k_3 x_0 x_3) \quad \text{(A-4)}$$

$$\frac{dx_4}{dt} = k_8 x_6 + k_{12} x_8 + k_{14} x_9 + k_{15} x_8 + k_{16} x_6 + k_{17} x_7^2 - (k_7 x_1 x_4 + k_{11} x_2 x_4) \quad \text{(A-5)}$$

$$\frac{dx_5}{dt} = k_3 x_0 x_3 + k_{19} x_{15} + k_{21} x_{11} - (k_4 x_5 + k_{13} x_5 + k_{18} x_5 x_{14} + k_{20} x_5 x_{10} + k_{44} x_5 x_{18}) \quad \text{(A-6)}$$

$$\frac{dx_6}{dt} = k_7 x_1 x_4 + k_{23} x_7 - (k_8 x_6 + k_{16} x_6 + k_{22} x_6 x_7) \quad \text{(A-7)}$$

$$\frac{dx_7}{dt} = k_{22} x_6 x_7 + k_{25} x_{12} + k_{27} x_{16} - (k_{23} x_7 + k_{24} x_7 x_{10} + k_{26} x_7 x_4 + k_{17} x_7^2) \quad \text{(A-8)}$$

$$\frac{dx_8}{dt} = k_{11} x_2 x_4 + k_{29} x_9 - (k_{12} x_8 + k_{15} x_8 + k_{28} x_8 x_9) \quad \text{(A-9)}$$

$$\frac{dx_9}{dt} = k_{28} x_8 x_9 + k_{31} x_{13} + k_{33} x_{17} - (k_{14} x_9 + k_{29} x_9 + k_{30} x_9 x_{10} + k_{32} x_9 x_{14}) \quad \text{(A-10)}$$

$$\frac{dx_{10}}{dt} = k_{34} + k_{21} x_{11} + k_{25} x_{12} + k_{31} x_{13} - (k_{20} x_5 x_{10} + k_{24} x_7 x_{10} + k_{30} x_9 x_{10} + k_{35} x_7 x_{10} + k_{36} x_9 x_{10}) \quad \text{(A-11)}$$

$$\frac{dx_{11}}{dt} = k_{20} x_5 x_{10} - k_{21} x_{11} \quad \text{(A-12)}$$

$$\frac{dx_{12}}{dt} = k_{24} x_7 x_{10} - k_{25} x_{12} \quad \text{(A-13)}$$

$$\frac{dx_{13}}{dt} = k_{30}\,x_9\,x_{10} - k_{31}\,x_{13} \tag{A-14}$$

$$\frac{dx_{14}}{dt} = k_{37} + k_{19}\,x_{15} + k_{27}\,x_{16} + k_{33}\,x_{17} + k_{38}\,x_{24} - (k_{39}\,x_{14} + k_{18}\,x_5\,x_{14} + k_{26}\,x_7\,x_{14} + k_{32}\,x_9\,x_{14}) \tag{A-15}$$

$$\frac{dx_{15}}{dt} = k_{18}\,x_5\,x_{14} - k_{19}\,x_{15} \tag{A-16}$$

$$\frac{dx_{16}}{dt} = k_{26}\,x_7\,x_{14} - k_{27}\,x_{16} \tag{A-17}$$

$$\frac{dx_{17}}{dt} = k_{32}\,x_9\,x_{14} - k_{33}\,x_{17} \tag{A-18}$$

$$\frac{dx_{18}}{dt} = k_{40} + \frac{k_{41}}{1 + k_{42}\,x_{23}} - (k_{43}\,x_{18} + k_{44}\,x_5\,x_{18}) \tag{A-19}$$

$$\frac{dx_{19}}{dt} = k_{45}\,x_{21}\,x_{23} - (k_{46}\,x_5\,x_{19} + k_{47}\,x_{11}\,x_{19} + k_{48}\,x_{15}\,x_{19}) \tag{A-20}$$

$$\frac{dx_{20}}{dt} = k_{46}\,x_5\,x_{19} + k_{47}\,x_{11}\,x_{19} + k_{48}\,x_{15}\,x_{19} - (k_{49}\,x_7\,x_{20} + k_{50}\,x_9\,x_{20}) \tag{A-21}$$

$$\frac{dx_{21}}{dt} = k_{52} + k_{51}\,x_{21} + k_{49}\,x_7\,x_{20} + k_{50}\,x_9\,x_{20} - (k_{53}\,x_{21} + k_{45}\,x_{21}\,x_{23} + k_{54}\,x_9\,x_{21}) \tag{A-22}$$

$$\frac{dx_{22}}{dt} = k_{49}\,x_7\,x_{20} + k_{50}\,x_9\,x_{20} - k_{55}\,x_{22} \tag{A-23}$$

$$\frac{dx_{23}}{dt} = k_{56} + \frac{k_{58}}{1 + k_{59}\,x_{18}} + k_{55}\,x_{22} - (k_{57}\,x_{23} + k_{45}\,x_{21}\,x_{23}) \tag{A-24}$$

$$\frac{dx_{24}}{dt} = k_{60} + k_{61}\,signal - (degradation\,x_{24}\,x_{25} + k_{62}\,x_{24}) \tag{A-25}$$

$$\frac{dx_{25}}{dt} = k_{63} + \frac{k_{66}\,x_{27}^9}{k_{65}^9 + x_{27}^9} - k_{64}\,x_{25} \tag{A-26}$$

$$\frac{dx_{26}}{dt} = k_{68}\,x_{21} - k_{69}\,x_{26} \tag{A-27}$$

$$\frac{dx_{27}}{dt} = \frac{k_{70}\,x_{24}\,signal}{1 + k_{71}\,x_{24}x_{25}} - k_{67}\,x_{27} \tag{A-28}$$

Appendix B: The details of the behaviour of the key proteins in G1/S transition under different DNA-damage situations

As mentioned in Section 4.1, proteins (E2F, CycE and CycA) are the important factors in G1/S transition while proteins (p53 and p21) are the significant indicators for the DNA-damage signal and for blocking the cell cycle progression into the S phase. Therefore, we investigate the behaviour of these notable chemical species under normal and two different DNA-damage situations as shown in Figure B-1. For the normal cell, the concentration of p53 and p21 are kept at low levels. We focus on the dynamical behaviour of E2F, CycE, CycA and p27 in Figure B-1 (a). Based on the biological theory and experimental findings, p27 maintains the high concentration during the G0 phase and the early G1 phase [Sherr, 1994]. However, the level of p27 decreases in the G1 phase or later due to the degradation of p27 caused by the activation of CycE/CDK2 [Vlach et al., 1997; Zerfass-Thome et al., 1997]. As a result, the concentration of E2F increases with the decrease in the concentration of p27. The reason is that the activation of E2F can promote the synthesis of CycE and CycA, and the increased level of CycE can promote the activation of CycE-CDK2 for p27 degradation. Although the activation of E2F promotes the synthesis of CycE and CycA, the expression of CycA is delayed compared to that of CycE [Ohtsubo et al., 1995]. It means that there is a discrepancy in peak time between CycE and CycA. All these results are shown in Figure B-1 (a), which indicates that the dynamical behaviour of these chemical species revealed from the model in normal condition is in qualitative agreement with the biological theory and experimental findings.

For the DNA-damage situations, the damaged signal can trigger the activation of p53. The activated p53 can promote the accumulation of p21 as one of the CDK inhibitors, resulting in the arrest of cell cycle progression [Dulic et al., 1994]. Therefore, the delays in these chemical species (E2F, CycE and CycA) cause discrepancies in their PTs compared to healthy cells. The comparison of the PT of proteins (E2F, CycE and CycA) between Figure B-1 (a) and Figure B-1 (b and c) is a good agreement with the experimental observations. More importantly, we also analyse the concentration of E2F, p21 and p53 under three difference intensities of DNA-damage signal as shown in Figure B-2. According to Figure B-2, it can be seen that the level of p53 and p21 is very low in normal cells. More importantly, the concentration of p21 under the low-level DNA-damage is larger than that under the high-level

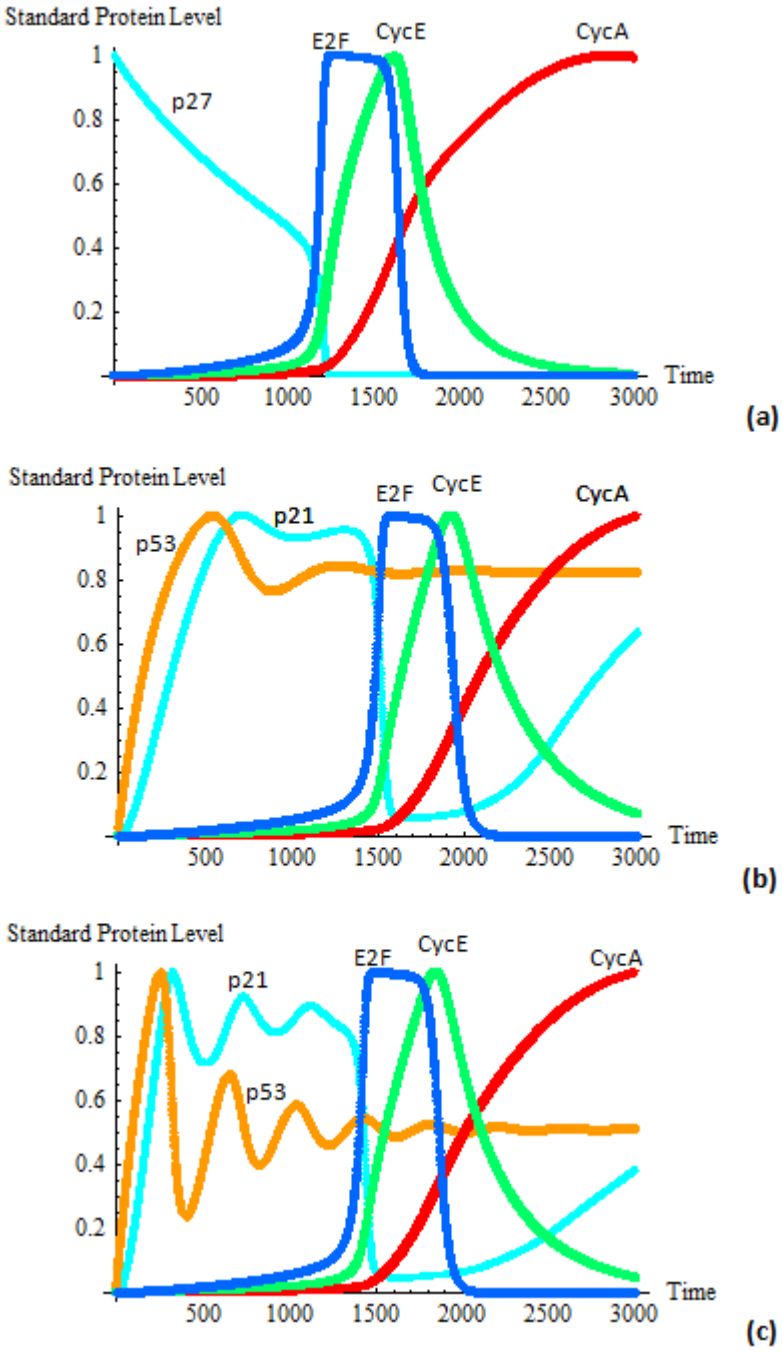

Figure B-1 Time course of the key chemical species in the G1/S transition under different DNA-damage situations: (a) Normal Cell, (b) Low DNA-damage and (c) High DNA-damage (Standard Protein Level = $\frac{C(t)}{Max(C(t))}$, where $C(t)$ denotes the concentration of the chemical specie and $Max(C(t))$ is the maximum level in the time range).

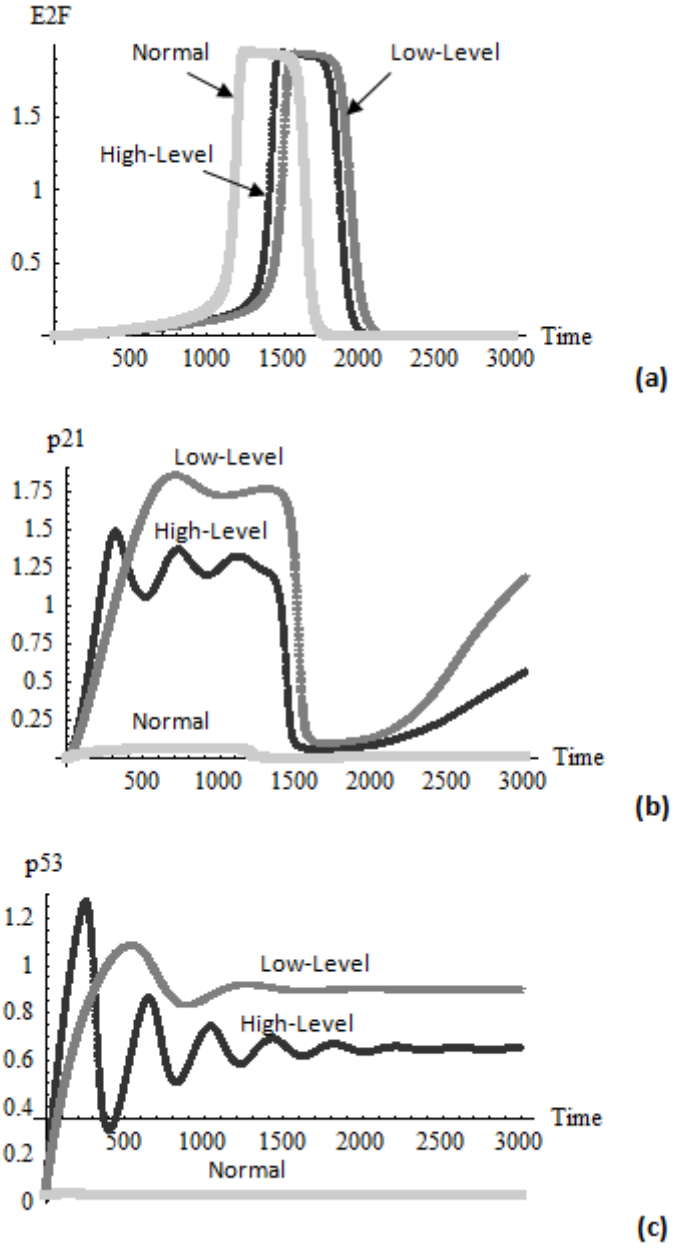

Figure B-2 Time course of E2F, p21and p53 under different DNA-damage situations: (a) E2F, (b) p21 and (c) p53.

DNA-damage. This is reflected in the fact that both damage situations cause delays in E2F reaching the peak time but the low-level DNA-damage results in a slightly larger delay than the high-level DNA-damage. The larger delay for low DNA-damage allows a cell to arrest cell cycle and attempt repair; wheras, smaller delay for high DNA-damage reflects the alternative path of apoptosis/senescence taken by the cell requiring less time delay. As a result, the model results related to the dynamical behaviour of both p21 and E2F qualitatively support the experimental findings and the biological theory that the synthesis of p21 is mainly enhanced and induced after the low-level DNA-damage [Li and Ho, 1998].

Appendix C: The details of the effectiveness of CKIs alone and simultaneous variation of CDK2/CKIs on lowering senescence bar under parameter range ±50%

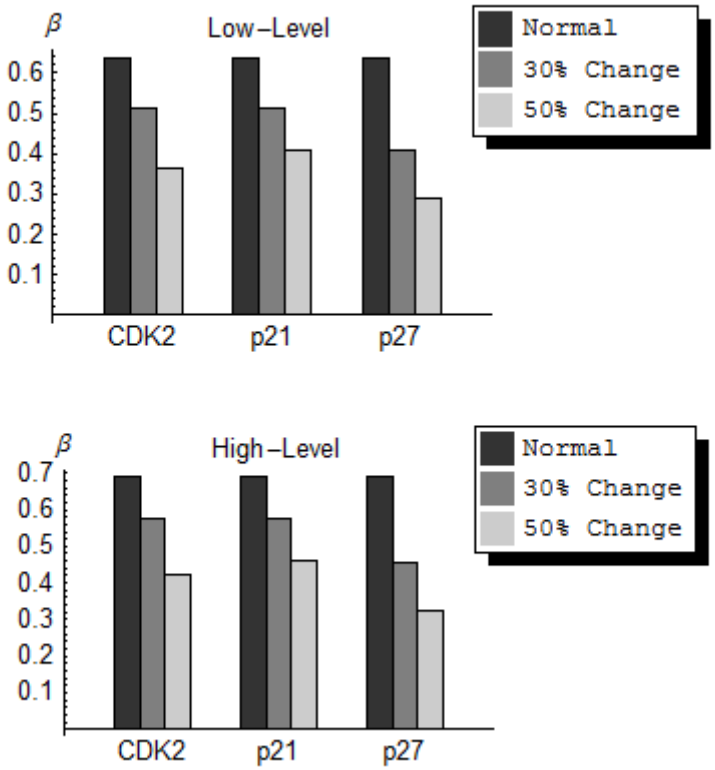

Figure C-1 The probability β of a damaged cell passing the G1/S checkpoint in response to only changing CDK2 or CKIs (i.e. p21 degradation rate and p27 initial condition) for three different ranges of normal, 30% and 50% - specifically, CKD2 or p21 degradation rate reduced or p27 initial condition increased by 0%, 30% and 50%, respectively - using the behaviour of E2F for parameter range ±50% under different DNA-damage conditions: low level DNA-damage and high level DNA-damage.

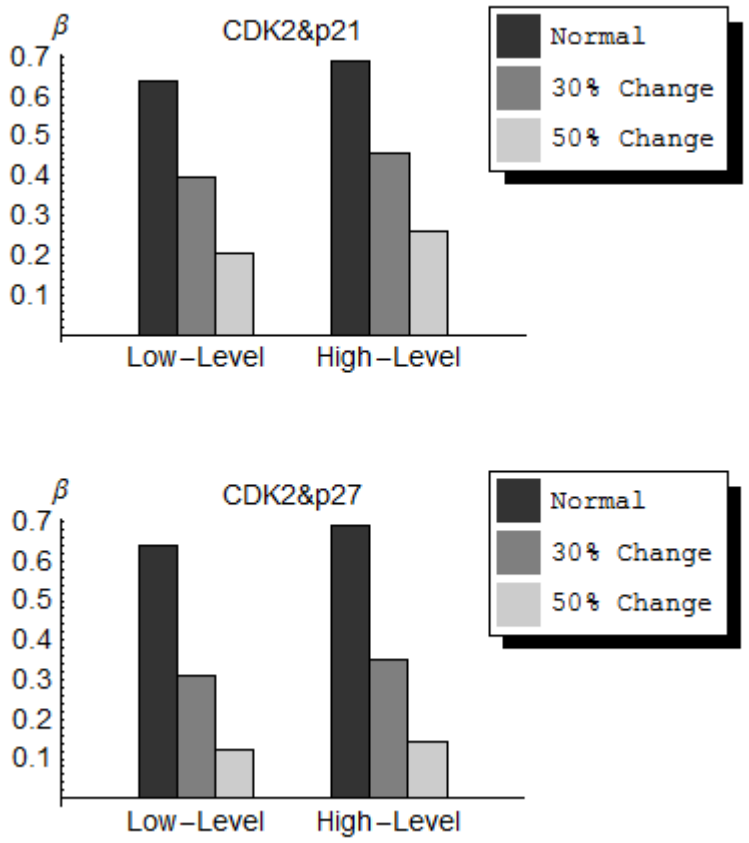

Figure C-2 The probability β of a damaged cell passing G1/S in response to simultaneously changing CDK2 and CKIs (i.e. p21 degradation rate and p27 initial condition) for three different ranges of normal, 30% and 50% - specifically, CKD2 and p21 degradation rate both reduced by 0%, 30% and 50%, respectively, or CDK2 reduced and p27 initial condition increased by 0%, 30% and 50%, respectively- using the behaviour of E2F for parameter range ±50% under two different DNA-damage conditions.

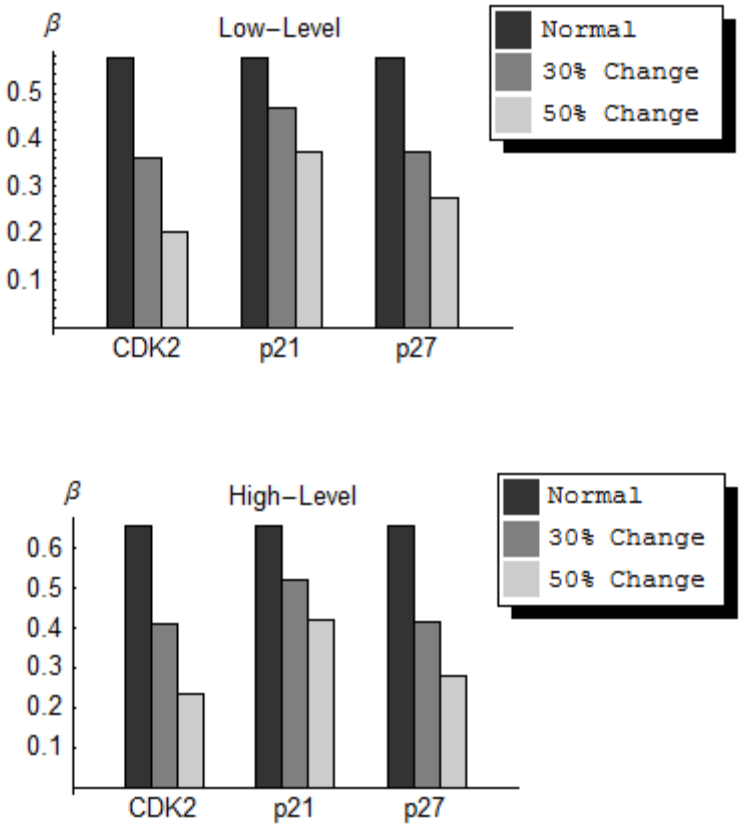

Figure C-3 The probability β of a damaged cell passing the G1/S the checkpoint for only changing CDK2 or CKIs (i.e. p21 degradation rate and p27 initial condition) for three different ranges of normal, 30% and 50% - specifically, CKD2 or p21 degradation rate reduced, or p27 initial condition increased by 0%, 30% and 50%, respectively - using the behaviour of CycE for parameter range ±50% **under different DNA-damage conditions: low level DNA-damage and high level DNA-damage.**

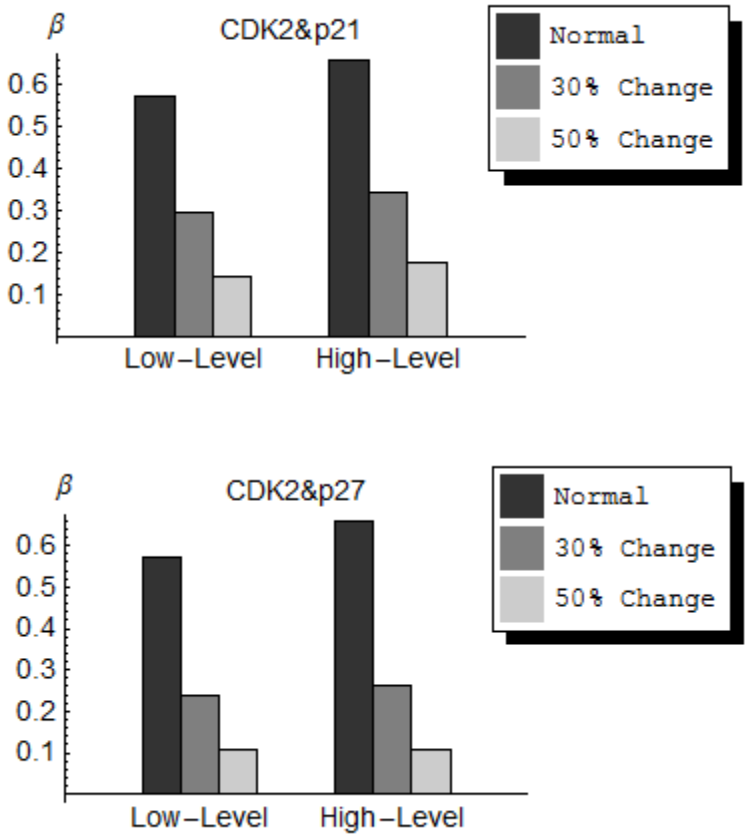

Figure C-4 The probability β of a damaged cell passing G1/S in response to simultaneously changing CDK2 and CKIs (i.e. p21 degradation rate and p27 initial condition) for three different ranges of normal, 30% and 50% - specifically, CKD2 and p21 degradation rate both reduced by 0%, 30% and 50%, respectively, or CDK2 reduced and p27 initial condition increased by 0%, 30% and 50%, respectively - using the behaviour of CycE for parameter range ±50% under two different DNA-damage conditions.

Appendix D: The details of mathematical models for the p53-Mdm2 oscillation system

Table D-1 Description of variables and parameters in the four models for the p53-Mdm2 oscillation system [Geva-Zatorsky et al., 2006].

Model variables and parameters	Description
x	nuclear p53
y_0	Mdm2 precursor
y	nuclear Mdm2
S	active signal
α_0	Mdm2 maturation rate
α_x	Mdm2-independent p53 degradation rate
α_y	Mdm2 degradation rate
α_{xy}	Mdm2-dependent p53 degradation rate
α_s	Mdm2-dependent signal inactivation rate
α_k	saturating p53 production rate inactivation rate
β_x	p53 product rate
β_y	p53-depdendent Mdm2 production rate
β_S	constant activation rate of signal (when damage is present)
τ	delay in Mdm2 accumulation
Γ	linear p53 production rate
k	P53 threshold for degradation by Mdm2
n	cooperativity of signal

Table D-2 Parameter values and Initial conditions of the four models for the p53-Mdm2 oscillation system [Geva-Zatorsky et al., 2006].

Common parameters	**III**	**IV**	**V**	**VI**
α_0	-	$0.8 \pm 20\%$	$1.1 \pm 25\%$	-
α_x	0	0	-	-
α_y	24	$0.8 \pm 25\%$	$0.9 \pm 30\%$	$0.7 \pm 20\%$
α_{xy}	120	-	$3.7 \pm 50\%$	$1.4 \pm 20\%$
β_x	2.3	$0.9 \pm 35\%$	-	$0.9 \pm 60\%$
β_y	24	$1.1 \pm 55\%$	$1.5 \pm 60\%$	$1.0 \pm 10\%$
τ	3.3	-	-	$0.9 \pm 25\%$
Initial conditions				
x	0.02	0	0.02	0
y_0	-	0.1	0.2	-
y	0.02	0.8	0.5	0.9
S	-	-	-	0
Particular parameters	$k = 0.0001$	$\Gamma = 2.0 \pm 25\%$	$n = 4$	
	$\alpha_s = 2.7 \pm 30\%$	$\beta_S = 0.9 \pm 25\%$	$\alpha_k = 1.7 \pm 20\%$	

Appendix E: The details of HoMP calculation

In this research, HoMP is the ratio of the half-life and the mean period as a measure of the robustness the p53-Mdm2 oscillation system in respose to various levels of perturbations in the model parameters. The half-life of the correlation is the time corresponding to a 50% decrease in the intial correlation value indicated by the autocorrelation function. Now, we give a summary of how to generate the autocorrelation function and the mean period.

In stastistics, autocorrelation can be considered as the correlation of a time series with its own past and future values. The most important factor in autocorrelation is autocorrelation coefficients, which measure the correlation between the given time series and a time-shifted version of itself. Furthermore, the autocorrelation function is a set of autocorrelation coefficients [Black, 2007]. Now, we take the calculation of the first-order autocorrelation as an example. The first-order autucorrealtion means that the lag is one time unit, and represents the correlation coefficient of the first N-1 observations and the next N-1 observations. The autocorrelation coefficent of x_t and x_{t+1} can be written by

$$R_1 = \frac{\sum_{t=1}^{N-1}(x_t - \overline{x}_{(1)})(x_{t+1} - \overline{x}_{(2)})}{\left[\sum_{t=1}^{N-1}(x_t - \overline{x}_{(1)})^2\right]^{1/2}\left[\sum_{t=2}^{N}(x_t - \overline{x}_{(1)})^2\right]^{1/2}} \quad \text{(E-1)}$$

where R is the autocorrelation coefficient, $\overline{x}_{(1)}$ represents the mean of the first N-1 observations, $\overline{x}_{(2)}$ denotes the mean of the next N-1 observations and N is the length of the given time series.

If N becomes very large, the difference between the following contents can be ignored: one is the difference between $\overline{x}_{(1)}$ and $\overline{x}_{(2)}$; the other is difference between the summations over observations from 1 to N-1 and from 2 to N. Therefore, Eq. (E-1) can be simplified as

$$R_1 = \frac{\sum_{t=1}^{N-1}(x_t - \overline{x})(x_{t+1} - \overline{x})}{\sum_{t=1}^{N-1}(x_t - \overline{x})^2}, \quad \text{(E-2)}$$

where $\bar{x} = \frac{\sum_{t=1}^{N} x_t}{N}$.

According to Eq. (E-2), we can generalize the mathematical formula of the autocorrelation coefficient at lag j:

$$R(j) = \frac{\sum_{i=1}^{N-j} (x_i - \bar{x})(x_{i+j} - \bar{x})}{\sum_{i=1}^{N-1} (x_i - \bar{x})^2}, \quad j = 1, 2, 3, \cdots N-1. \tag{E-3}$$

Once the autocorrelation function is generated, we can calcualte the half-life of the correlation, a time period for 50% decrease in the initial correlation value (See Figure E-1). Meanwhile, we also calculate the periods for the p53-Mdm2 system (time interval between a pair of successive peaks) as well as their mean value, called the "mean period". Therefore, HoMP can be computed based on the equation given below:

$$\text{HoMP} = \frac{\text{Half-life}}{\text{Mean Period}}. \tag{E-4}$$

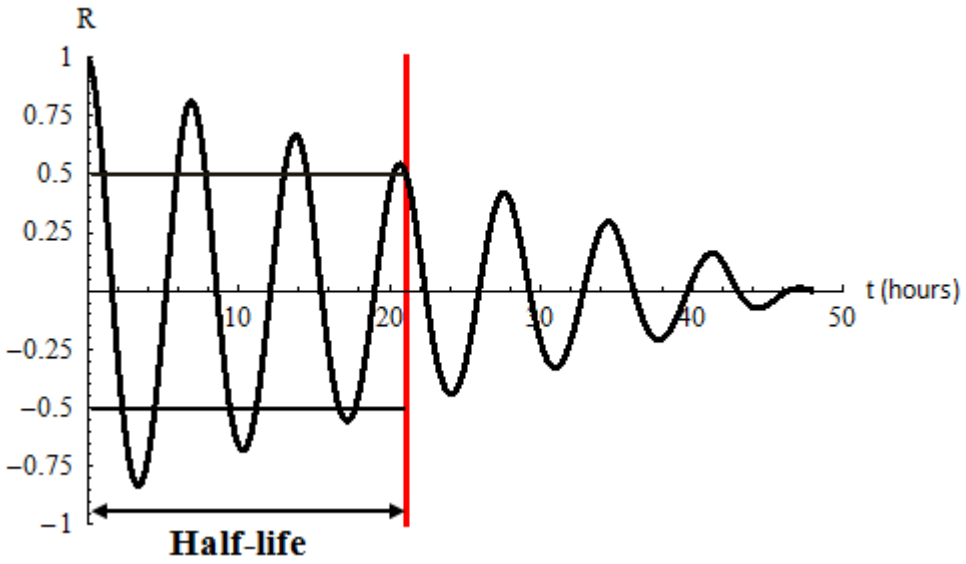

Figure E-1 Time evolution of the autocorrelation function, with indication of half-life, for the oscillation based on the behaviour of p53 for a time-length of 48 hours. The red line denotes the 50% decrease in the initial correlation value.

Appendix F: The behaviours of p53 and Mdm2 when HoMP equals 3

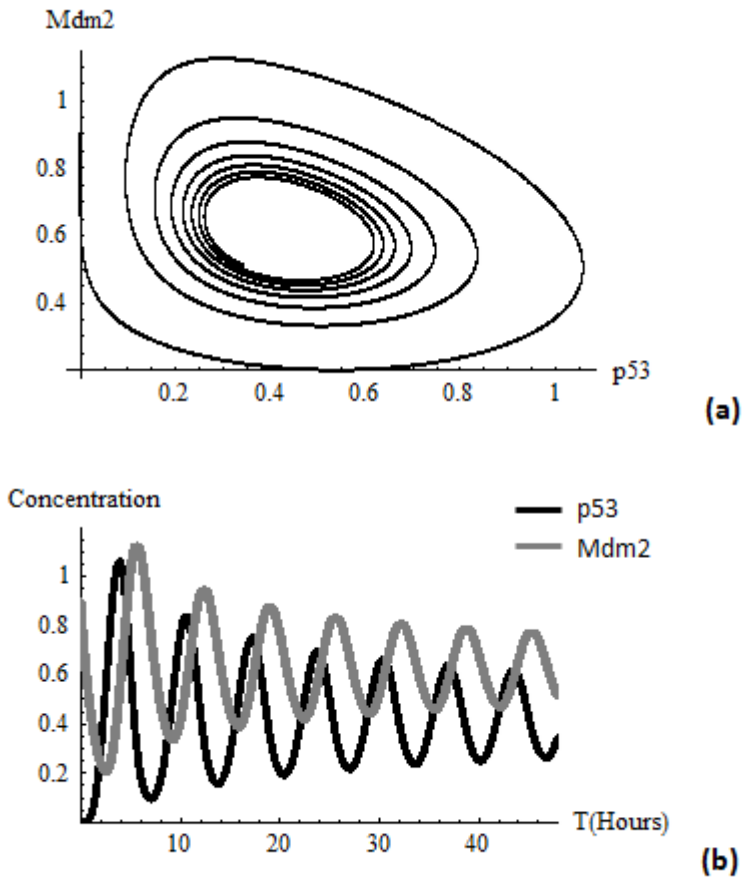

Figure F-1 The behaviours of p53 and Mdm2 when HoMP equals 3 for 40% reduced parameter values for α_s : (a) phase plane trajectories and (b) temporal performances of p53 and Mdm2.